Investigating the use of sodium metasilicate to improve the flotation performance of altered PGE ores

Andrea Molifie

A thesis submitted to the Faculty of Engineering and the Built Environment, University of Cape Town, in fulfillment of the requirements for the degree of

Doctor of Philosophy

at

Centre for Minerals Research

Department of Chemical Engineering

University of Cape Town

2021

Plagiarism declaration

I, **Andrea Molifie**, hereby declare that the work on which this thesis is based is my original work (except where acknowledgements indicate otherwise) and that neither the whole work nor any part of it has been, is being, or is to be submitted for any other degree in this or any other university. I authorise the University to reproduce for the purpose of research either the whole or any portion of the contents in any manner whatsoever.

Signed by candidate

Signature: _____ Date: 1 October 2021

Acknowledgements

I am grateful to the following people, institutions, and companies for having played important roles in this project:

- To my primary supervisor, **A/Prof Belinda McFadzean** and my co-supervisors **A/Prof Megan Becker** and **Mr Stefan Geldenhuys,** thank you very much for being incredible supervisors. Thank you for placing me on the right path whenever I strayed from the aim of this project, for your open-door policy, for stepping into the laboratory with me, for caring about my well-being, and for shaping and editing the thesis. I can truly say that I did not walk this difficult journey alone, but that you accompanied me during an important Chapter in my life. I could not have asked for better supervisors. We made a great team!
- The **University of Cape Town** for being an excellent university and for accepting me to do my PhD. Also thank you to the **Centre for Minerals Research** for having a body of people who are warm and helpful. Thank you to all Staff at the CMR, including our laboratory manager, Shireen Govender and our technical and laboratory staff; Monde Bekaphi, Kenneth Maseko, Refilwe Moalosi and Nqobile Dingilizwe, for helping with sample preparation, handling of chemicals and with equipment. Thank you, Monde, for the flotation training, and for being very patient when I spilled slurry all over the floor on my first try
- To the **QEMSCAN staff** including A/Prof Megan Becker, Keshree Pillay and Lorraine Nkemba for helping with sample preparation, the QEMSCAN analysis and interpretation. Thank you Keshree for not only running my QEMSCAN and XRD samples, but also for all the runs, hikes and fun talks. Thank you to Lorraine for being a mentor and for your hard work in the sample preparation laboratory. Thank you to our previous QEMSCAN operator, Gaynor Yorath, for patiently teaching me how to run the QEMSCAN and to use the iDiscover software, which greatly helped me to do this project
- Members of the **Flotation Group** including Prof Cyril O'Connor, A/Prof Kirsten Corin, Mrs Jenny Wiese and the students for all the feedback which contributed to this work
- **Staff at** the **CMR** and **other research unit**s including Malibongwe Manono for always being willing to give advice on the work, Gary Groenmeyer for your amazingly positive talks in the laboratory, Mehdi Safari for your inputs regarding this work, Jason Waters for helping with rheology, Sandeeran Govender for allowing me to use the rheometer and zetasizer whenever I needed to use it, and Miranda Waldron for your help with the Raman analysis. Thank you to Jody Miller from Stellenbosch University for helping me with the decisions to enrol in honours and a

NRF internship, which thereafter led me to do this PhD

- This work is based on the research supported in part by the **National Research Foundation of South Africa** (Grant numbers: 114547 and 120170), the **South African Minerals to Metals Research Institute (SAMMRI),** the **Department of Science and Innovation** (DSI) and the **Department of Chemical Engineering.** Thank you for providing financial assistance towards the research of this work and to my personal funding. Thank you to Heather Sundström, late Bongiwe Ndamane and the rest of your teams for managing my finances throughout the duration of my studies at UCT. Thank you to the SAMMRI members, including Mpho Ramonotsi, Jeremy Mann, Jules Aupiais, Victor Ross and Prof Cyril O'Connor for all your input into this work
- **Pilanesberg Platinum Mines** and **Mpho Ramonotsi** for facilitating the site visit, providing the ores, all the feedback regarding this work and your contribution toward assay costs
- My parents, **Willie Molifie** and **Mary Molifie**, for teaching me how to be a strong and independent woman and for helping me to guide my academic path up to this very moment: a PhD. Thank you for implanting a dream into my mind, when I was a little girl, that I can do anything I set my mind to. So, I chose to become a geologist, which you fully supported
- My sisters, **Melanie Molifie** and **Tiffany Molifie**, for being my best friends and supporters in everything I do. Thank you for your love, patience, and sacrifice during my studies
- My partner, **Andani Mulelu**, for being incredibly supportive during my PhD journey. Thank you for listening to all of my talks about rheology and flotation, for your kind and positive personality, and for making life so easy while I focused on being in the laboratory and writing my thesis
- My **peers at the CMR**, including CK, Sarah, Audrey, Mathew, Dandré, Dineo, Noli, Sophia, Tanaka, Shoki and Everjoice for being not only very friendly, but also for giving input into the experiments I conducted. Thank you Everjoice for the feedback on the final document
- My **extended family** and **friends** including my very supportive aunts (Rhonda, Lena and Dawn), uncles (Malcolm, Isak and Joey) and my close friend Martha for praying for me and giving me all the advice and encouragement throughout my studies, and
- Last, and most importantly, thank you **God** my **Heavenly Father** and my **Saviour Jesus Christ**, for being with me and holding my hand every step of the way.

List of publications and presentations

Molifie, A., McFadzean, B., Becker, M., Geldenhuys, S. 2021. Investigating the use of sodium metasilicate to improve the flotation performance of altered PGE ores. *In Proceedings of the XXVIIIth International Mineral Processing Congress*. 18-22 October 2020. Cape Town, South Africa.

Molifie, A., McFadzean, B., Becker, M., Geldenhuys, S. 2019. Investigating the use of sodium metasilicate to improve the flotation performance of altered PGE ores. *SAIMM Minerals Research Showcase*. 11-12 November 2019. Cape Town, South Africa.

Synopsis

Currently, many near-surface Southern African platinum group element (PGE) ores are low grade and have some degree of ore alteration. A type of alteration undergone by some of the rock forming minerals is mineral hydration which produces secondary minerals such as the phyllosilicates serpentine and talc. The abundance of these minerals is detrimental to the flotation process and results in three major problems during froth flotation. The first problem is due to the presence of serpentine slimes which can coat valuable minerals and decrease recoveries. The second problem is due to the flocculation of minerals which can increase pulp viscosity and also negatively impact recoveries, and the third problem is due to naturally floating gangue (NFG) which can lower the concentrate grades. The main NFG mineral in Southern African PGE ores is talc. Mitigation strategies commonly target each problem individually which can be very costly for a plant operation. It was identified that the dispersant, rheology modifying, and depressant effects of sodium metasilicate could be used to combat these three major problems and that this could potentially occur simultaneously under favourable conditions. Quantitative evaluation of minerals by scanning electron microscopy (QEMSCAN) analysis revealed that the main PGE ore under investigation constitutes 33.6 weight percent (wt.%) alteration minerals (19.2 wt.% serpentine, 5.0 wt.% talc and 9.4 wt.% other). The flotation performance using this ore was expected to be problematic.

To determine whether sodium metasilicate could improve the flotation response of altered PGE ores, batch flotation experiments were conducted at various sodium metasilicate dosages ranging between 0 g/t (no sodium metasilicate added) to 2000 g/t sodium metasilicate. These experiments revealed that sodium metasilicate significantly improved the Pt and Pd recoveries and grades at high dosages (>1000 g/t sodium metasilicate). The enhancements in recovery were postulated to be due to the dispersant effect of sodium metasilicate, which removed the slimes off platinum group minerals (PGMs) and base-metal sulphides (BMS), and also due to the rheology modifying effect which lowered the pulp viscosity and improved fluid flow and therefore gas dispersion. Grade improvements were attributed to sodium metasilicate's depressant effect, which depressed talc. To decouple whether it was in fact the dispersant, rheology modifying and depressant effects of sodium metasilicate which combated slime coating, rheology and NFG issues, respectively, various experiments were conducted.

Firstly, the dispersant effect of sodium metasilicate was decoupled by performing microflotation and zeta potential experiments. In terms of microflotation experiments, the floatability of chalcopyrite (used as a PGM proxy) in the presence of serpentine slimes was explored. This revealed that the presence of serpentine slimes had a severely detrimental impact on recovery during batch flotation. Zeta potential measurements indicated that slime coatings were due to the electrostatic attraction between oppositely charged serpentine and chalcopyrite. The addition of high sodium metasilicate dosages restored

chalcopyrite floatability to nearly 100% in the presence of serpentine slimes, which was analogous to the improvement in PGM recovery during sodium metasilicate addition in batch flotation tests.

Secondly, the rheology modifying effect of sodium metasilicate was decoupled by conducting rheology, batch flotation at decreasing solids concentrations, and particle settling experiments. The rheology experiments indicated that the pulp viscosity was reduced when adding increasing dosages of sodium metasilicate. The results indicated that sodium metasilicate is a rheology modifier and that high sodium metasilicate dosages lowered the pulp viscosity. To determine whether a reduction in the viscosity of the pulp corresponded with improved PGE recoveries, the solids concentration in batch flotation tests was decreased in order to decrease viscosity. Decreasing solids concentrations, which corresponded to decreasing viscosities, resulted in higher PGE recoveries. This series of experiments indicated that the addition of sodium metasilicate could reduce the pulp viscosity that, in turn, increased PGM recovery. This was due to improved fluid flow and gas dispersion due to a lower pulp viscosity. Higher viscosities, when no sodium metasilicate was added, were attributed to the aggregation of minerals (mainly involving serpentine, talc and orthopyroxene). These minerals were dispersed when adding increasing sodium metasilicate dosages and this was reflected by much slower particle settling rates at high sodium metasilicate dosages.

Thirdly, the depressant effect of sodium metasilicate was decoupled by performing QEMSCAN concentrate analyses and microflotation experiments. The QEMSCAN concentrate analyses conducted on batch flotation concentrates at low and high sodium metasilicate dosages revealed that the higher dosage lowered the recovery of both liberated and unliberated talc. Unliberated talc mainly consisted of talc associated with orthopyroxene. Talc microflotation experiments confirmed that sodium metasilicate depressed talc and that high sodium metasilicate dosages were most effective for the depressant effect of sodium metasilicate. The depressant effect of sodium metasilicate was suggested to occur via two different mechanisms depending on pH: through ligand exchange directly onto the surface of talc below pH 10 and by a bridging cation mechanism above pH 10.

Froth stability tests indicated that the froth was much more stable in the absence of sodium metasilicate, which was due to the absence of stabilizing NFG reporting to the froth as well as increased drainage due to the lowered slurry viscosity. The dispersant effect of sodium metasilicate dispersed aggregated particles in the froth, which corresponded with improved froth drainage and a decrease in froth stability. This was confirmed by QEMSCAN which revealed that the amount of liberated hydrophilic minerals reporting to the concentrate decreased with increasing sodium metasilicate concentration.

Since it was found that the addition of sodium metasilicate substantially modified the pH of the slurry, tests were conducted to decouple the effects of pH from those of the sodium metasilicate species. These found that, even though an increase in pH could also decrease the serpentine surface charge and thereby reduce electrostatic attraction between it and the valuable minerals, not all the beneficial effects of sodium

metasilicate could be attributed to pH. It was confirmed that, when sodium metasilicate was present in solution, these species adsorbed to the mineral surface and were responsible for both the decrease in surface charge and the decrease in talc floatability. An increase in pH alone had no effect on talc floatability.

A final part of this work evaluated sodium metasilicate against other well-known methods of combating some of the problems associated with altered ores. Sodium metasilicate was evaluated against ultrasonication which is a well-known mechanical method, and carboxymethyl cellulose (CMC) which is a well-known chemical method. Ultrasonication significantly improved PGE recoveries, but PGE grades were poor, indicating that it targeted mainly the slime cleaning aspect of the alteration mineral problem, but not the rheology and NFG problem. Using CMC did not significantly improve either recovery or grade. It was, therefore, clear that sodium metasilicate is the superior method over these two methods, because its dispersant, rheology modifying, and depressant effects could be effective simultaneously at high dosages to improve both recovery and grade. The outcomes of this work are currently being implemented at a number of South African PGM mineral processing concentrators.

Statement of originality

The novelty of this sodium metasilicate investigation centres on the application of sodium metasilicate to the flotation processing of a PGM ore, which has not been previously published. In addition, this investigation is novel in that it decouples the various mechanisms by which sodium metasilicate acts, viz as a dispersant, rheology modifier and depressant to improve the recovery and grade simultaneously.

The following points summarize the original contributions from the sodium metasilicate investigation:

- Utilising sodium metasilicate's dispersant, rheology modifying and depressant effects to combat slime coating, rheology and NFG issues present within an altered PGE ore simultaneously
- Determining the impact of serpentine slimes on PGE recovery and the role of sodium metasilicate's dispersant effect in PGE recovery enhancement
- Determining the role of sodium metasilicate's rheology modifying effect to reduce the pulp viscosity of altered PGE ores for recovery enhancement
- Determining whether sodium metasilicate's depressant effect can depress NFG to improve concentrate grade in altered PGE ores.

Table of Contents

List of Figures

List of Tables

Abbreviations and acronyms

BMA	Bulk Mineralogical Analysis
BSE	Back-Scattered Electron
BIC	Bushveld Igneous Complex
BMS	Base-Metal Sulphide
CMC	Carboxymethyl Cellulose
DLVO	Derjaguin-Landau-Verwey-Overbeek
ECD	Equivalent Circle Diameter
EDS	Energy-Dispersive X-ray Spectrometers
g/t	Grams Per Ton
ICP-OES	Inductively Coupled Plasma – Optical Emission Spectrometry
i.e.p	Iso-Electric Point
J_g	Superficial Gas Velocity
NFG	Naturally Floating Gangue
PGE	Platinum Group Element
PGM	Platinum Group Mineral
PMA	Particle Mineral Analysis
PPM	Pilanesberg Platinum Mines
PSD	Particle Size Distribution
p.z.c	Point of Zero Charge
QEMSCAN	Quantitative Evaluation of Minerals by Scanning Electron Microscopy
RLS	Rustenburg Layered Suite
SEM	Scanning Electron Microscopy
SHMP	Sodium Hexametaphosphate
SIBX	Sodium Isobutyl Xanthate
SIP	Species Identification Protocol

SS	Sodium Silicate
TMS	Trace Mineral Search
UG2	Upper Group 2 Chromitite
Vol.%	Volume Percent
Wt.%	Weight Percent
XPS	X-ray Photoelectron Spectroscopy
XRD	X-ray Diffraction
XRF	X-ray Fluorescence Spectrometry

Glossary

Alteration	A change in the mineral chemical composition or crystallography due to a change in chemical or physical conditions
Association	A measure of the surface area in contact between different minerals
Feldspathic	Containing feldspar
Grain	Discrete areas of a specific mineral host within a particle
Harzburgite	An ultramafic rock consisting mostly of olivine and low Ca pyroxene such as enstatite
Liberated	Mineral grains having '> 90 area %'
Locked	Mineral grains having 'area % < 30'
Mesh-textured	A serpentine texture composed of a lattice work of longitudinal cross-fibre serpentine veins which encloses olivine cores
Middlings	Mineral grains having '90 ≥ area % > 30'. This is commonly divided into High Grade Middlings: '90 ≥ area % > 60', and Low Grade Middlings: '60 ≥ area % > 30'
Particle	A rock fragment consisting of multiple mineral grains
Pegmatoidal	Having an exceptionally coarse-grained texture
Peridotite	A group of ultramafic rocks consisting mainly of olivine, which can also contain pyroxene
Pyroxenite	A group of ultramafic rocks consisting mainly of ferromagnesian silicates such as enstatite and ferrosilite (orthopyroxene), as well as diopside and augite (clinopyroxene)
Relict	A mineral or rock that remained unaltered when surrounding minerals or rock have been altered by a geological event
Serpentinization	Hydrothermal alteration of ultramafic rocks which alters ferromagnesian silicates present in the rock, such as olivine and pyroxene, to serpentine minerals
Unliberated	Mineral grains having '90 ≥ area % > 0'

Chapter 1: Introduction

The purpose of the introduction is to provide the context, motivation, and importance of this work. The background of this work is provided in Section 1.1. This is followed by the problem statement in Section 1.2, the major objectives (Section 1.3), the thesis scope and limitations (Section 1.4), and lastly, the thesis layout (Section 1.5).

1.1. Background

Many near-surface platinum group element (PGE) orebodies contain alteration minerals, due to the retrograde hydrothermal alteration of olivine and pyroxenes in ultrabasic rocks, thus resulting in the formation of hydrated Mg- and/or Fe-bearing phyllosilicate minerals such as serpentine or talc (Kirjavainen & Heiskanen, 2007: 630). Ore alteration is often accompanied by low grade PGEs, with PGEs being primarily hosted within fine-grained platinum group minerals (PGMs). This requires fine-grinding to liberate the PGMs, but alteration minerals present in the ore can also be finely milled in the process due to their soft nature. It has been recognized that processing ores containing significant alteration minerals can have serious processing consequences which have forced many Southern African operations to leave ores *in situ,* to process them at the expense of significant PGE losses, to blend altered ores with less altered ores for processing, or to stockpile them until a new metallurgical process is in place to improve beneficiation (Oberthür et al., 2013: 192; Becker, Wiese & Ramonotsi, 2014: 25; Sefako, Sekgarametso & Sibanda, 2017: 798). Figure 1.1 illustrates that the presence of alteration minerals occurs in many Southern African PGE ores, which are in relatively high quantities in some ores (between 3.5 wt.% and 40 wt.% in the ores illustrated in Figure 1.1). Exploring alternative methods of processing such complex ores have in recent years become the subject of many investigations to improve the flotation responses of such ores, but the problem with processing altered ores remains, especially when an operating concentrator is already in place (Sefako, Sekgarametso & Sibanda, 2017: 799; Yu, Ma, et al., 2017: 32; Wang & Li, 2020: 11). Therefore, there is a continuous need to explore viable options.

Phyllosilicate minerals can have three major impacts on a flotation performance. The first two impacts are caused by fine-grained phyllosilicates which can i) form hydrophilic slime coatings on the valuable minerals which impede collector adsorption and ii) phyllosilicate slime flocculation and the presence of fines can increase the pulp apparent viscosity which leads to poor gas dispersion (Edwards, Kipkie & Agar, 1980: 35; Shabalala et al., 2011: 1452). This can result in reduced valuable mineral recoveries. The third problem is caused by the reporting of liberated and composite particles of talc to the froth, which can significantly reduce concentrate grades due to its hydrophobic nature (Wiese, Harris & Bradshaw, 2010: 1013). Talc is the main naturally floating gangue (NFG) mineral in Southern African PGE ores. Previous studies determined that slime coatings can be mitigated by either mechanical or chemical

cleaning such as using ultrasonication or dispersants such as sodium hexametaphosphate (SHMP), respectively (Celik, 1989: 1164; Long, Huang & Xiao, 2019: 11). The higher viscosity of ores can be mitigated by diluting the ore or using rheology modifiers (Andreola et al., 2006: 1108; Gao et al., 2018: 5). Lastly, NFG can be combated by using depressants to depress talc (McFadzean et al., 2011: 465). However, no study has integrated and addressed these three problems within a single ore together, and a single method of combating all three problems has not been investigated. These problems are common in ores containing phyllosilicate minerals (including NFG) and fine-grained valuable minerals that require fine grinding to achieve liberation. Some PGE ores in South Africa contain these major ore problems. Therefore, mitigating these major ore problems can enhance the flotation performance of altered PGE ores. Alteration minerals do not only cause problems during froth flotation, but downstream processes can also be negatively impacted. The presence of MgO, which is a major constituent in gangue such as serpentine, talc, and orthopyroxene, can cause serious furnace operational problems. This is due to an increase in the liquid temperature and slag viscosity which requires furnace operations to occur at much higher temperatures (Jung, Decterov & Pelton, 2006: 228). It is, therefore, critical to reduce the MgO

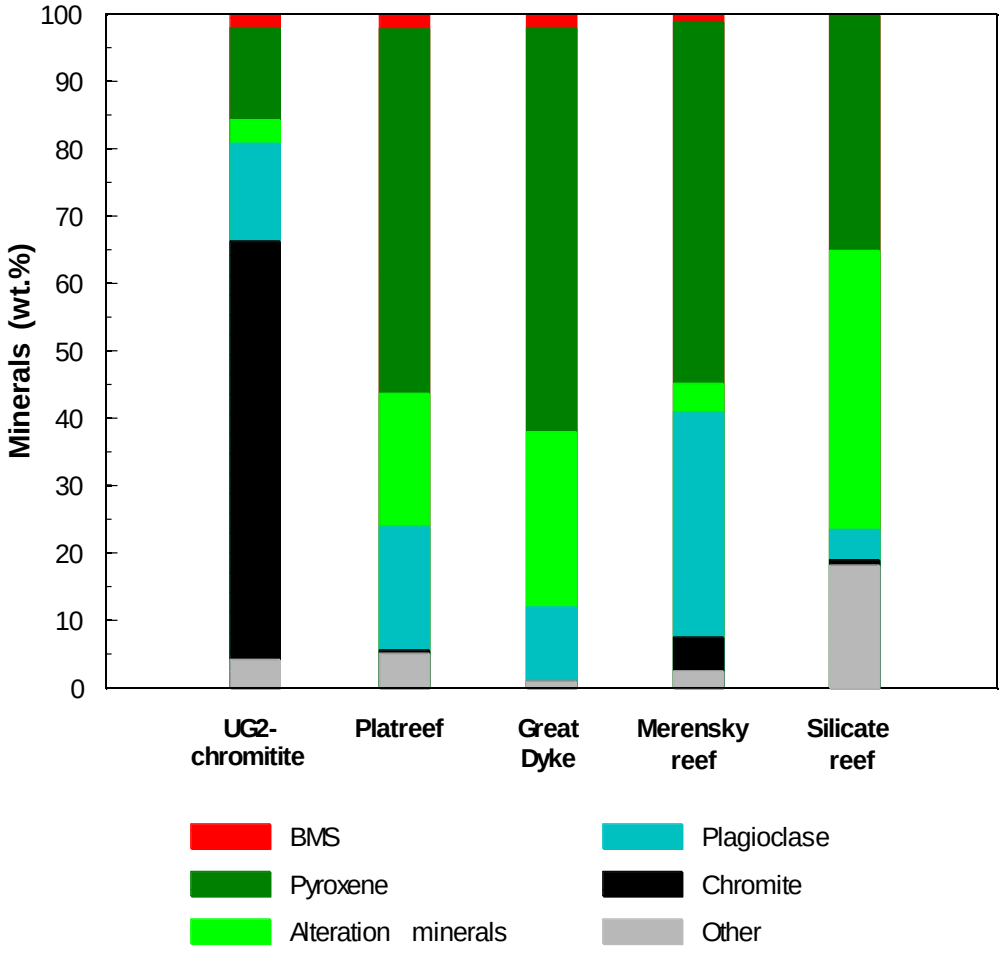

Figure 1.1: Bulk mineralogies in typical Southern African PGE ores. Information was gathered from the following sources: Solomon et al. (2011: 1371), Corin, Bezuidenhout and Connor (2012: 101), Becker et al. (2013: 94) and Becker, Wiese and Ramonotsi (2014: 28).

grade in the concentrate to reduce the amount of MgO reporting to the smelter.

Sodium silicate is a well-known chemical reagent that is mainly used in non-sulphide flotation for its dispersant, rheology modifying and depressant effects (Fuerstenau, Gutierrez & Elgillani, 1968: 319; Garrido, Gainza & Pereira, 1988: 330; Andreola et al., 2006: 1108; Silva et al., 2012: 208). The individual effects of sodium silicate have mainly been studied in non-sulphide ore investigations, however, due to its complex speciation, there is still room to understand its mechanisms and to investigate it during the processing of sulphide ores (Phair, Van Deventer & Smith, 2001: 151; Feng et al., 2012: 12092). There is minimal published research using sodium silicate in sulphide ore flotation (Edwards, Kipkie & Agar, 1980: 38; Feng et al., 2012: 12091), and even less in the public domain in the context of Southern African PGE ores (Bulatovic, 2003: 936). Investigating these three effects of sodium silicate could prove promising in mitigating the three major problems of altered ores simultaneously: i) the dispersant effect of sodium silicate could mitigate slime coating issues, ii) the rheology modifying effect of sodium silicate could mitigate pulp rheology issues, and iii) the depressant effect of sodium silicate could mitigate NFG issues.

The overarching objective of this study is to decouple the multiple effects of sodium metasilicate (a specific type of sodium silicate) by addressing the slime coating, higher viscosity and NFG problems within altered South African PGE ores.

1.2. Problem statement

Many PGE ores suffer from alteration, the extents of which are variable between different ore bodies. The observed consequence of this alteration is a decline in PGE recovery and concentrate grades. Therefore, alternative strategies to process these ores are critical. There is a need for these strategies to address multiple aspects for enhanced flotation performances and to depend less on multiple reagents or mechanical solutions to enhance flotation performances. Studies have shown some preliminary promise in this regard, however, little is known about the mechanisms behind the effects of sodium metasilicate in a PGE ore.

1.3. Objectives

This study sets out to determine how the dispersant, rheology modifying, and depressant effects of sodium metasilicate impacts the recovery and grade of altered PGE ores. Sodium metasilicate was the reagent of choice due to its known dispersant, rheology modifying and depressant properties, its readily availability and low cost. Each effect is first studied individually using a series of specific methods aimed to decouple the effects before integrating the effects through a discussion. The integration of these effects allows an understanding of how a single method can be used to overcome three major challenges faced by altered ores simultaneously to enhance the flotation response in terms of both recovery and concentrate grade. The capability of sodium metasilicate is also assessed against other methods known in the literature to combat ores of similar issues, placing sodium metasilicate's capability into perspective.

This study offers a foundation upon which further studies can investigate sodium metasilicate to mitigate complex issues in low grade and mineralogically complex altered ores. It is anticipated that in doing so, there is improved confidence in sodium metasilicate's capability to improve flotation performances of various PGE ore deposits at plant scale. Due to current processing issues of altered ores, this work serves as a contribution towards the knowledge of improving the processing response of such ores.

1.4. Scope and limitations

The use of sodium metasilicate in overcoming the three main problems associated with altered ores simultaneously in altered PGE ores is the focus of this work. This only includes problems associated with hydration hydrothermal alteration. The work is limited to investigating sodium metasilicate on two Merensky reef-Pseudo reef ore blends from Pilanesberg Platinum Mines (PPM) and not other PGE ore types, such as pure Merensky reef, Upper Group 2 (UG2) chromitite or Platreef. One of the ores, referred to as 'Ore 1', will form part of the main sodium metasilicate investigation, as illustrated in Figure 1.2 which illustrates the flow of this work. The ore will then be characterised in terms of both crushed and milled material, where the crushed material is not representative of the ore and, therefore, only gives a sense of the mineralogical characteristics of some of the rock types in the blend. The characterisation will include a bulk mineralogy of the other PGE ore, referred to as 'Ore 2'. The sodium metasilicate batch flotation investigation will then be performed at a standard solids concentration, collector dosage, frother dosage, air flow rate and other physical cell parameters, where the only changing variable will be the sodium metasilicate dosage. The use of sodium metasilicate is limited to one type and modulus of sodium silicate. This work will acknowledge some other issues which may cause processing issues, such as the association between PGM and gangue or relative amounts of fine particles, but the focus of this work is not to further liberate PGMs or to physically remove fine gangue particles.

Special emphasis will be placed on decoupling the mechanisms of sodium metasilicate's dispersant, rheology modifying and depressant effects to mitigate the three main problems (Figure 1.2). In terms of the dispersant effect, techniques were chosen to determine the interaction of serpentine both with PGMs and base-metal sulphides (BMS) at the sodium metasilicate dosages applicable to this work. The BMS was used as a PGM proxy due to the inability to obtain pure PGMs and the BMS response was interpreted to be an estimate of the PGM response. This work then decoupled the rheology modifying effect of sodium metasilicate and thereafter decoupled the depressant effect. One of the important highlights of the depressant effect was to determine whether sodium metasilicate is a depressant of talc, which was not previously determined. Once the sodium metasilicate effects were understood and decoupled, this knowledge was then applied to understand the sodium metasilicate batch flotation responses.

This work will then evaluate sodium metasilicate's performance against chosen mechanical and chemical methods well-known to mitigate some of the problems associated with altered PGE ores (Figure 1.2). This is limited to comparing batch flotation responses only, and not to discuss the individual responses of

these methods. Finally, sodium metasilicate batch flotation experiments will be performed on Ore 2 to assess whether the same sodium metasilicate responses were observed using another altered PGE ore. This research only focuses on flotation, and downstream effects of concentrate handling are beyond the scope of this work.

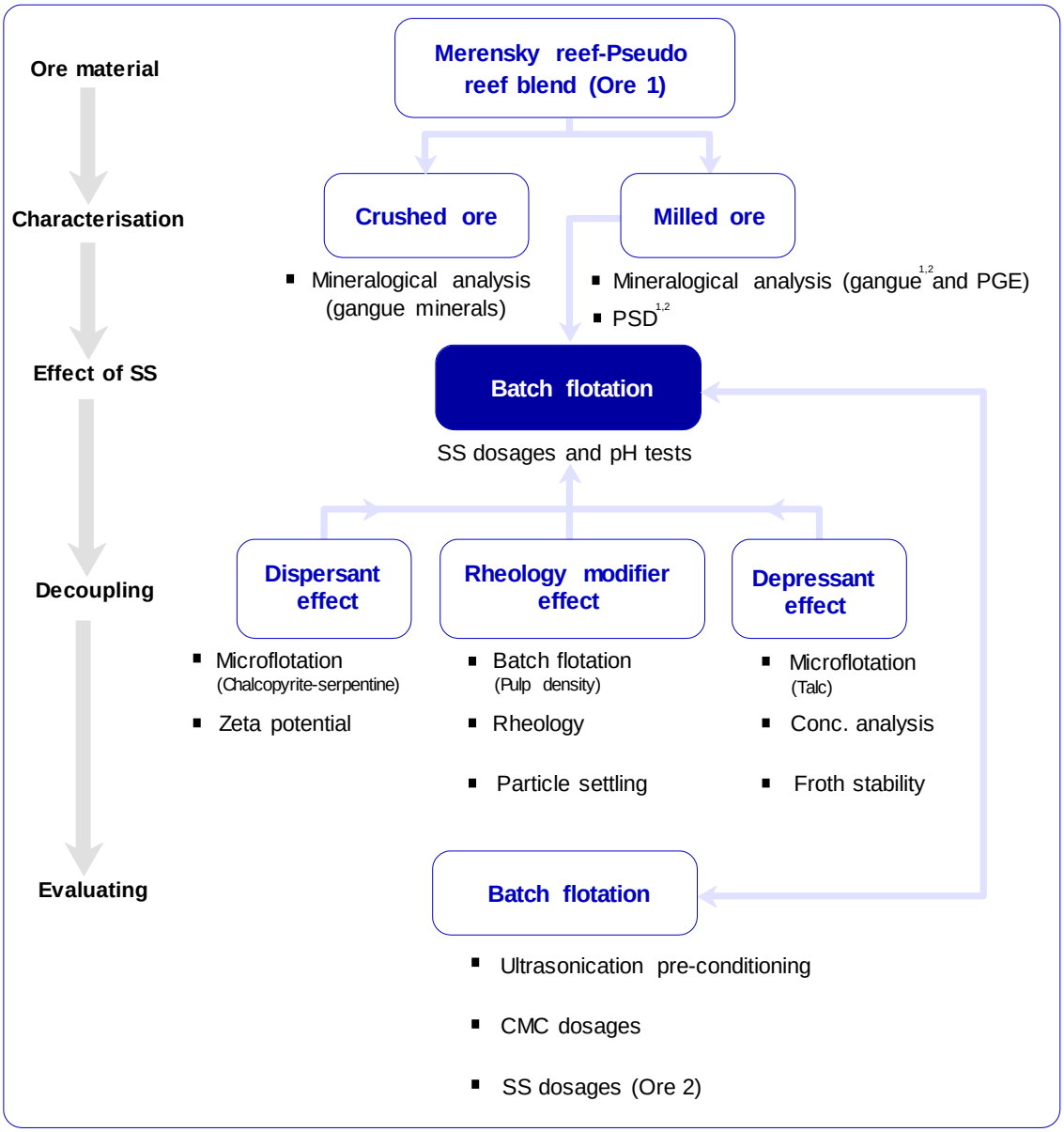

1- Ore 1 SS- Sodium metasilicate
2- Ore 2

Figure 1.2: Flow of the work covered in this project.

1.5. Thesis layout

The body of this thesis is assembled into seven chapters. A short background, the problem statement, overall objectives, the scope and limitations, and the thesis layout is presented in this chapter (Chapter 1). Chapter 2 provides a critical literature review of important topics applicable to this work, a critical synthesis, the study hypotheses, and key questions. The materials and methods are detailed in Chapter 3. Chapter 4 presents the results of the experimental work in answer to the key questions, whereas Chapter 5 is a discussion of the results. Conclusions and recommendations for future work are summarized in Chapter 6. The reference list is provided in Chapter 7. In addition, an appendix containing calculations, some additional material, as well as links to the electronic raw datasets are provided at the end of the thesis.

Chapter 2: Literature review

This literature review chapter is aimed at providing existing relevant research relating to the topics covered in this thesis. The review begins with the assemblage and characteristics of PGE ores (Section 2.1), a froth flotation overview (Section 2.2), dispersants and depressants (Section 2.3), major problems due to phyllosilicate minerals (Section 2.4), a critical synthesis (Section 2.5), hypotheses (Section 2.6), and the key questions (Section 2.7).

2.1. Assemblage and characteristics of PGE ores

2.1.1. Setting and PGE mineralization

There is great interest in the layered Bushveld Igneous Complex (BIC) in South Africa as it contains the world's largest PGE resources (Cawthorn, 1999: 489). The BIC is divided into a number of 'suites', namely the Rustenburg Layered Suite (RLS), Lebowa Granite Suite and Rashoop Granophyre Suite (Hatton & Schweitzer, 1995: 579). The RLS is further subdivided into zones, where the critical zone contains four important layers host to economic PGE mineralisation known as the Platreef, Merensky reef, UG2 chromitite reef, and the recently discovered Flatreef. The mafic-ultramafic Merensky reef varies in lithology and PGE mineralization in the Western and Eastern Limbs of the BIC. The "normal" lithology of the Merensky reef dips evenly, is pegmatoidal (feldspathic) pyroxenite dominant and is interlayered with a pegmatoidal feldspathic harzburgite at the base (Kinloch & Peyerl, 1990: 537; Osbahr et al., 2013: 213). Ultramafic rocks include peridotites such as dunite, harzburgite and lherzolite, and pyroxenite, such as orthopyroxenite and clinopyroxenite. Olivine and lesser pyroxenes are the main constituents of peridotites. The hanging wall is 1.5 to 3.5 m thick and consists of either feldspathic pyroxenite or norite, whereas the footwall is a 5 m thick anorthosite layer (Osbahr et al., 2013: 213). The PGE mineralized units of the reef, including the feldspathic pyroxenite, norite, anorthosite and pegmatoidal pyroxenite are commonly sandwiched between two mineralized chromitite stringers (Schwellnus, Hiemstra & Gasparrini, 1976: 251; Osbahr et al., 2013: 215).

The lithology of the Merensky reef varies depending on location, as determined by drill core logging (Wilson, Lee & Brown, 1999: 660). For the most part, lithologies generally have characteristics of the normal Merensky reef, but can contain other units, such as harzburgite, dunite or sulphide stringers (Osbahr et al., 2013: 215), structural differences such as potholes which are evident in the Brakspruit or Amandelbult sections (Kinloch & Peyerl, 1990: 539), or varying thicknesses. In the Swartklip Sector in the northwest BIC between the Merensky reef and UG2 chromitite, there is an occurrence of ultramafic cumulate layers of feldspathic harzburgite known as the Pseudo reef which resembles an inverted sequence of the normal Merensky reef (Mitchell, Henckel & Mason-Apps, 2019: 119; Mitchell, Scoon & Sharpe, 2019: 151). The Pseudo reef is divided into an upper Pseudo reef and lower Pseudo reef which are

separate cyclic units on the basis that the lower Pseudo reef generally has a lower olivine-orthopyroxene ratio. The upper- and lower Pseudo reefs are separated by a chromitite layer, and they have different mineralogical characteristics (Scoon & De Klerk, 1987: 58). The upper Pseudo reef consists of pegmatoidal pyroxenite, feldspathic harzburgite, leuconorite, anorthosite and thin chromitite stringers. The lower Pseudo reef consists of olivine pyroxenite, pegmatoidal feldspathic harzburgite or orthopyroxenite which is characterised by coarse euhedral olivine (Scoon, 1987: 390; Scoon & De Klerk, 1987: 58; Viring & Cowell, 1999: 195; Molifie, 2016: 14; Mitchell, Henckel & Mason-Apps, 2019: 130; Mitchell, Scoon & Sharpe, 2019: 147). The upper- and lower Pseudo reefs are often separated by the central Pseudo reef unit, also known as the "Tarentaal harzburgite", which contains mainly harzburgite (Mitchell, Scoon & Sharpe, 2019: 151). Profiles of the Pseudo reef unit and the overlying Merensky reef footwall unit in the Pilanesberg, Union and Amandelbult sections in the Swartklip Sector are illustrated in

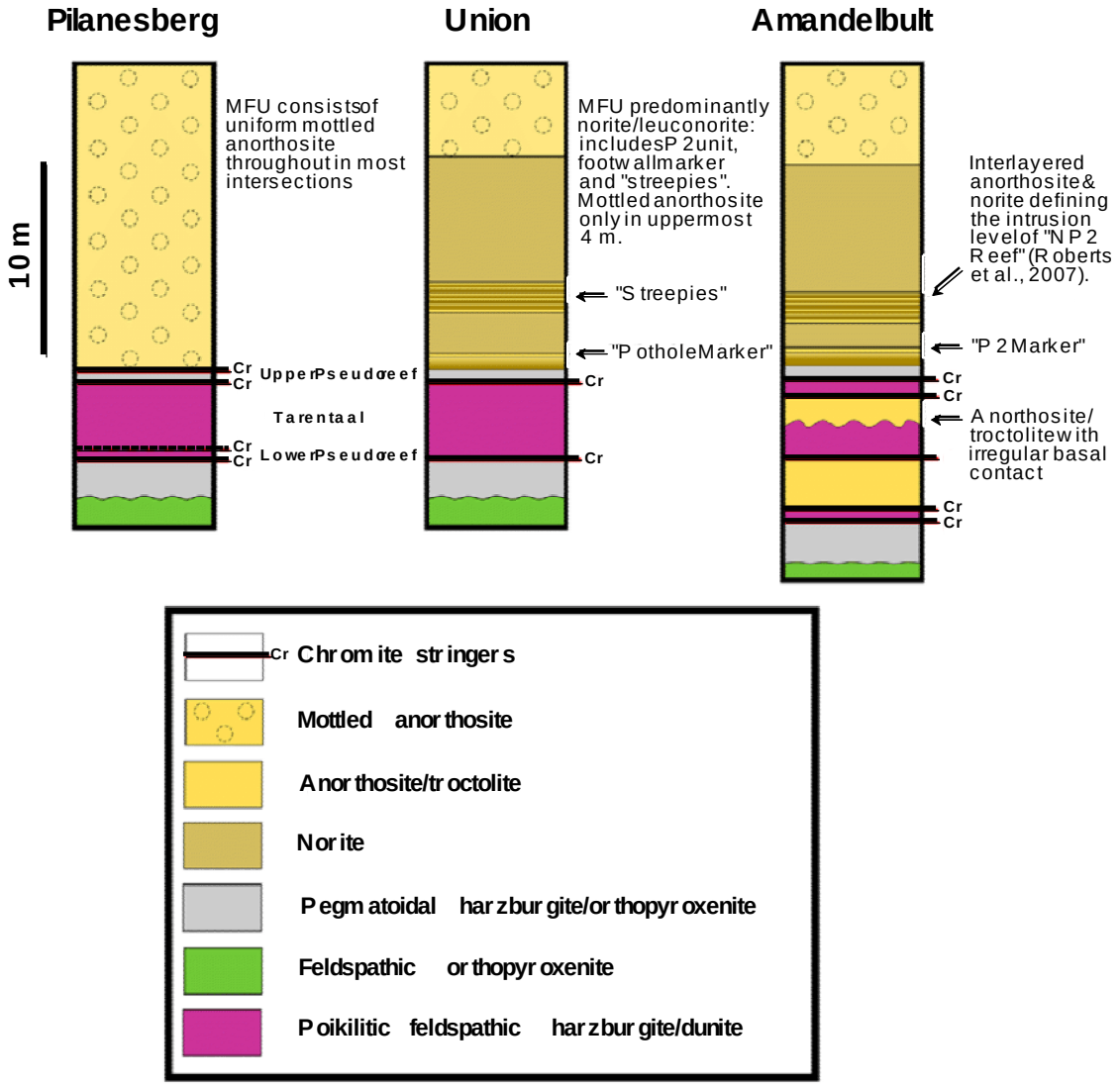

Figure 2.1: Representative profiles of the Pseudo Reef Unit and the overlying Merensky Footwall Unit (MFU) in the Pilanesberg, Union and Amandelbult sections of the Swartklip Sector, modified from Mitchell, Scoon and Sharpe (2019: 153).

Figure 2.1. This shows that the Pseudo reef unit stratigraphy varies in different sections. The Merensky reef footwall and upper Pseudo reef of the Pilanesberg section are separated by a thin chromitite stringer, but this is absent in Union and Amandelbult sections. The Amandelbult section is further distinguished by anorthosite intervals within the central Pseudo reef unit (Mitchell, Henckel & Mason-Apps, 2019: 129; Mitchell, Scoon & Sharpe, 2019: 151).

Although the PGM speciation and PGE distribution with depth and along strike of the Merensky reef is relatively well-known, fewer published studies have reported the speciation and distribution in the Pseudo reef unit (Scoon & De Klerk, 1987: 69; Scoon & Teigler, 1994: 1105; Mitchell, Henckel & Mason-Apps, 2019: 130). Economic PGE mineralization in the normal Merensky reef and Pseudo reef unit have commonly been found to be confined to the area of the chromitite stringers and the surrounds (Scoon & Teigler, 1994: 1105; Osbahr et al., 2013: 214). The average grade of the Merensky reef is between 5 to 7 g/t PGE and the Pseudo reef unit between 1 to 3 g/t 3PGE + Au (Viring & Cowell, 1999: 205; Cawthorn et al., 2002: 317). Similar to other reefs in the critical zone, a significant proportion of PGEs are hosted within discrete PGMs. Different theories have been proposed to explain the enrichment of PGEs and other precious metals. Some authors suggested that PGEs were able to crystallize from the magma as PGMs and accumulated on top of a crystal pile (Kinloch, 1982: 548; Campbell, Naldrett & Barnes, 1983: 138). Others have theorized that a magmatic fluid containing PGEs precipitated PGMs as the fluid ascended (Vermaak & Hendriks, 1976: 1249; Boudreau & Meurer, 1999: 177). Due to sulphide liquid fractionation and weathering processes, PGEs can occur in BMS through solid solution substitution (Godel, Barnes & Maier, 2007: 1579; Dare, Barnes & Prichard, 2010: 775). Of all PGEs that do not exist in discrete PGMs, Pd was found to be the main metal of interest as it can largely occur by solid solution substitution in pentlandite in the Merensky reef and Pseudo reef unit (Godel, Barnes & Maier, 2007: 1575; Osbahr et al., 2013: 223, 2014: 223; Molifie, 2016: 29). This is due to Pd partitioning into monosulphide solid solution or the diffusion of intermediate solid solution at early and late magmatic stages, respectively (Osbahr et al., 2013: 230). Weathering processes can also mobilize Pd and redistribute it in the exogenic environment through hydrothermal fluids, especially when the PGE carriers are altered. This is generally indicated by Pt/Pd ratios of the feed material, where ratios between 2 to 5 are typical of altered ores, and 1.3 to 1.7 typical of pristine/normal ores (Locmelis, Melcher & Oberthür, 2010: 96; Oberthür et al., 2013: 199). Evidence of re-distributed PGEs in the Pseudo reef unit through weathering processes have also been noted, as PGEs were found to occur, through solid solution substitution, in silicate gangue including plagioclase, talc and amphibole. A similar observation was made for some hydrothermally altered Great Dyke ores in Zimbabwe (Locmelis, Melcher & Oberthür, 2010: 101; Oberthür et al., 2013: 198; Molifie, 2016: 43).

Some mines such as PPM process the Merensky reef and Pseudo reef unit, at various pre-determined ratios, which are collectively called "Silicate reef". A PGM analysis performed on a Silicate reef feed

indicated that the major PGE species were PGE alloys (30 area %), PGE sulphides (26 area %) with lesser PGE arsenides (15 area %) and PGE tellurides (7 area %) (Becker, Wiese & Ramonotsi, 2014: 28). However, this depends on the sampling statistics and mining cut as PGE arsenides (36 area %), PGE alloys (26 area %) and PGE sulphides (24 area %) were abundant in the Silicate reef from an earlier study (Becker, Ramonotsi & Petersen, 2012: 3). On average between the two Silicate reef studies, at a common grind of 80% passing 75 μm, 60.7% of PGMs were liberated, 15.6% were locked in gangue, 15.2% were attached to gangue, and 6.5% were associated with Fe-oxides (Becker, Ramonotsi & Petersen, 2012: 6; Becker, Wiese & Ramonotsi, 2014: 28). Typical Merensky reef contains approximately 1 wt.% BMS which includes pyrrhotite, pentlandite and chalcopyrite (Becker et al., 2009: 248; Dzvinamurungu et al., 2013: 77). The BMS content in the Silicate reef was found to be much lower: 0.2 wt.% (Becker, Wiese & Ramonotsi, 2014: 28). In the Merensky reef, there is a striking association of the BMS with PGMs (Rose et al., 2011: 1393; Solomon et al., 2011a: 1373). The association between BMS and PGMs has also been observed in the Silicate reef, however, only 3.3% of PGMs were associated with BMS in the feed (Becker, Ramonotsi & Petersen, 2012: 3). This association appears to be much less in the Silicate reef compared to their association within the Merensky reef, which has been recorded to be as high as 89% in previous work (Schouwstra, Kinloch & Lee, 2000: 36).

2.1.2. Hydration hydrothermal alteration

Peridotites are thermodynamically stable in deeper crustal levels where temperatures and rock pressures are high, but the displacement of the rocks to shallower levels exposed the rocks to lower temperatures and hydrothermal fluids. This caused the units to become unstable and vulnerable to weathering processes such as mineral hydration reactions. Various chemico-physical parameters drive hydration reactions including temperature, fluid characteristics, upwelling rate, deformation or the fluid/rock ratio (Wenner & Taylor, 1973: 220; Viti, Mellini & Rumori, 2005: 502; McCollom & Bach, 2009: 862). Hydration reactions of near-surface peridotites in the presence of hydrothermal fluids, and at suitable chemico-physical parameters, have commonly been observed to alter some of the rock forming minerals to secondary minerals. These minerals commonly include serpentine along with minor talc, magnetite, awaruite, amphibole, chlorite and brucite (Johannes, 1968: 312; Eggleton & Boland, 1982: 14; Mével, 2003: 834; Viti, Mellini & Rumori, 2005: 497). The presence of these secondary minerals have been associated with peridotites within the Merensky reef and Pseudo reef unit (Zingg, 1996: 20; Becker et al., 2009: 248; Becker, Wiese & Ramonotsi, 2014: 28; Molifie, 2016: 20). These secondary minerals are commonly mineralogically and chemically distinct from their primary counterparts. For example, the granular and stubby habits of olivine and pyroxene can be altered to serpentine and talc, respectively, which have platy habits. These alteration minerals are known as phyllosilicates, where "phyllo" is a Greek term that means platy or leaf. The altered minerals also have different compositions to their primary counterparts. Examples of hydration reactions of olivine producing serpentine, brucite and magnetite are provided in

Equation 2.1 (McCollom & Bach, 2009: 857), pyroxene to serpentine in Equation 2.2 (Rouméjon et al., 2014: 726), and orthopyroxene to talc in Equation 2.3 (Iyer et al., 2008: 80).

$$Mg_{1.8}Fe_{0.2}SiO_4 + 1.37H_2O \rightarrow 0.5Mg_3Si_2O_5(OH)_4 + 0.3Mg(OH)_2 + 0.067Fe_3O_4 + 0.067H_2 \quad \textit{Equation 2.1}$$

Olivine (Fo_{90}) Serpentine Brucite Magnetite

$$3(Mg, Fe)SiO_3 + 2H_2O \rightarrow (Mg, Fe)_3Si_2O_5(OH)_4 + SiO_2(aq) \quad \textit{Equation 2.2}$$

Pyroxene Serpentine

$$5Mg_2Si_2O_6 + 2H_2O \rightarrow 2Mg_3Si_4O_{10}(OH)_2 + 2Mg_2SiO_4 \quad \textit{Equation 2.3}$$

Orthopyroxene Talc olivine

A type of hydration reaction responsible for the secondary minerals under investigation in this work is called "serpentinization". Serpentinization reactions undergo various stages which indicate the "degree" or extensiveness of serpentinization. Figure 2.2 illustrates textures of ultrabasic rock at an increasing degree of serpentinization. Petrographic mineral textures showing evidence of various stages of serpentinization have been gathered by various authors including that within the BIC (Zingg, 1996: 33; Li, Ripley & Merino, 2004: 176; Ningthoujam et al., 2012: 131; Rouméjon et al., 2014: 708). In the early serpentinization stage, most of the relict olivine or orthopyroxene grains are visible and there are fine thread-like serpentine veins or veinlets branching from olivine, mainly trans granularly, through other minerals (Ningthoujam et al., 2012: 131). Depending on the extensiveness of alteration, the alteration minerals may range in size, however, it is common for minor alteration minerals such as talc to be fine-grained (Zingg, 1996: 25). With an increasing degree of serpentinization, olivine and pyroxene grains start disappearing and are replaced by mesh textures. Secondary veins have also been observed to overlap the primary veins developed in the early stage. Relict olivine occupies the mesh cores and serpentine rims are either pseudo-columnar or polygonal in texture. Pyroxenes mainly have unaltered cores and are less altered than olivine (Rouméjon et al., 2014: 708). In the final stage of serpentinization, olivines and pyroxenes are nearly completely altered and there are well-developed serpentinized mesh textures (and others), such as seen for mesh-textured lizardite after olivine and orthopyroxene. At this stage, it is difficult to recognize any of the primary minerals (Ningthoujam et al., 2012: 131).

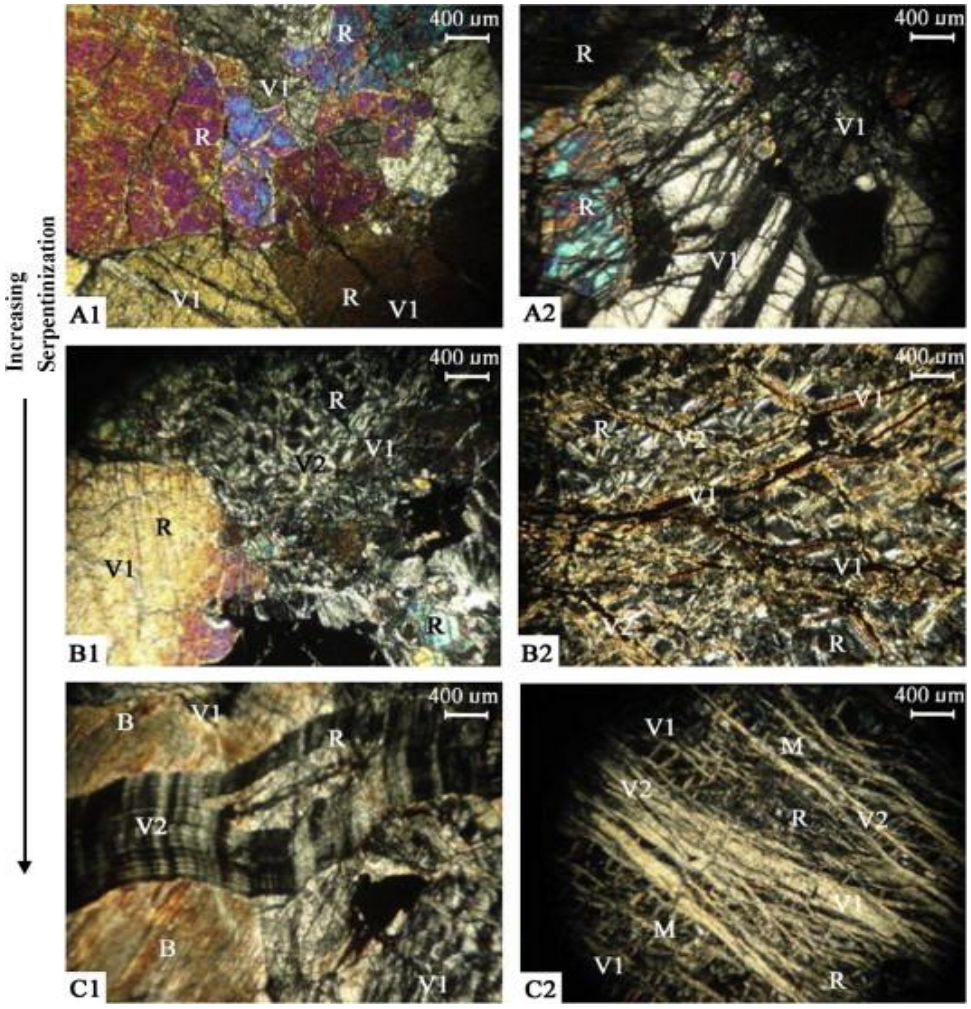

Figure 2.2: Cross polarised light photomicrographs showing the increasing degree of serpentinization and development of veins in ultramafic rock. R – relict of olivine and pyroxene, V1 – primary veins, V2 – secondary veins, B – bastite and M – mesh, taken from Ningthoujam et al. (2012: 132).

There are three serpentine phyllosilicate polymorphs namely lizardite, antigorite and chrysotile, all of which have the same general formula: $Mg_3Si_2O_5(OH)_4$. The polymorphs have different structural configurations, with lizardite being platy, chrysotile being tabular and antigorite having a ridged structure. The polymorphs consist of one magnesium oxide (brucite) octahedral sheet and one silicate tetrahedral sheet in a 1:1 arrangement, as illustrated in the crystal structure schematic of lizardite (Figure 2.3). The inner OH group forms weak hydrogen bonds attaching the next brucite octahedral sheet whereas the tetrahedral and octahedral sheets are held together by iono-covalent bonds (Mellini, 1982: 591; Benco & Smrcok, 1998: 1; Auzende et al., 2006: 272). The mineral is forced to solve lateral dimension mismatches due to dissimilarities in the brucite octahedral and silicate tetrahedral layers (Tartaj et al., 2000: 179). For lizardite, which is the expected serpentine polymorph present within the ores investigated in this study, this is overcome by the substitution of Si^{4+} with Al^{3+}, instead of Fe^{3+}, which will result in an overall positive surface charge of serpentine (Tartaj et al., 2000: 179; Feng et al., 2013: 1125). The observation of

positive serpentine zeta potentials at various pH's confirms the substitution of Si^{4+} with Al^{3+} (Martinez & Zucker, 1960: 926; Feng et al., 2013: 1125; Cao et al., 2017: 624). Similarly to many other phyllosilicates, lizardite is anisotropic, as it contains a positive basal face charge, which is the octahedral sheet, and negative edge plane charges, which is the tetrahedral sheet (Gillery, 1959: 147; Alvarez-Silva et al., 2010: 407, 2010: 385; Ndlovu et al., 2011: 1318; Ndlovu, 2013: 111). The overall charge of lizardite is dependent on the solution chemistry (Feng et al., 2012: 12093; Feng et al., 2013: 1125; Zhou & Feng, 2015: 432; Lu et al., 2019: 39).

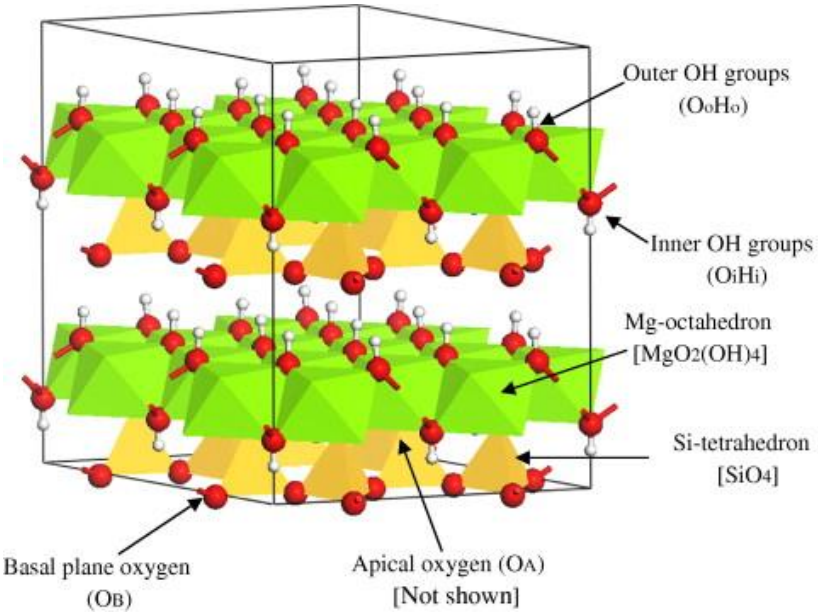

Figure 2.3: Crystal structure of lizardite - 1T showing the 1:1 layer of one octahedral and one tetrahedral sheet with the inner and outer OH groups, taken from Hossain et al. (2011: 1726).

Another phyllosilicate of interest to this work is the mineral talc, which has the general formula $Mg_3Si_4O_{10}(OH)_2$. Talc is of interest because pyroxene in the BIC has experienced some degree of alteration to talc and is the most common NFG mineral in these ores (Lotter et al., 2008: 906; Becker et al., 2009: 248; Jasieniak & Smart, 2009: 175). Talc has a 2:1 structural arrangement which consists of a brucite octahedral sheet sandwiched between two silicate tetrahedral sheets, as illustrated in the crystal structure schematic (Figure 2.4). Similarly to lizardite, the layers are bonded by weak van der Waals forces through OH groups whereas atoms within the layers are held together by iono-covalent groups. Talc consists of a basal plane which contains hydrophobic -Si-O-Si- non-polar inert links and edge planes which contain hydrophilic -SiOH and -MgOH groups (Fuerstenau, Lopez-Valdivieso & Fuerstenau, 1988: 162; Mälhammar, 1990: 68). The basal plane of talc generally has no charged groups along its surface, whereas the edge plane contains Mg^{2+} and OH^- charged ions, and is dependent on the solution chemistry (Khraisheh et al., 2005: 198; Burdukova et al., 2007: 341). Not all talc samples consist of fully

compensated Si-O tetrahedral basal planes, as substitution of Si^{4+} with Al^{3+} and Ti^{3+} ions can cause a proton deficiency in the outer tetrahedral layers, as observed for New York talc (Burdukova et al., 2007: 340). This can cause the basal plane of talc to have a negative surface charge. This is significant because the type of talc which will be used in this work is New York talc. Therefore, the talc used in this work is expected to have a negative surface charge. Talc's basal plane occupies 90% of its surface area (Morris, Fornasiero & Ralston, 2002: 212).

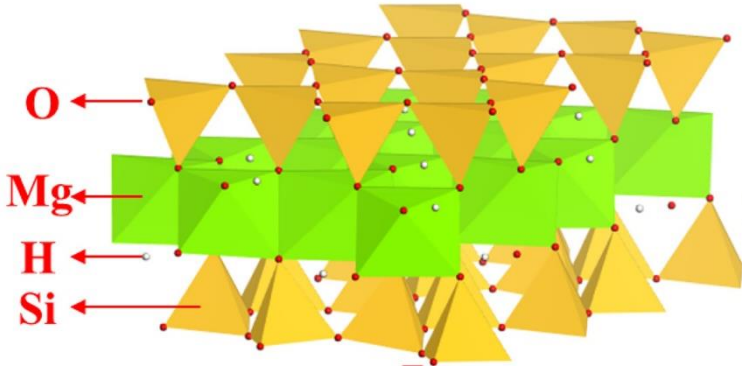

Figure 2.4: Schematic representation of talc's crystal structure, modified from Yi et al. (2019: 27).

2.2. A froth flotation overview

Since the introduction of froth flotation in the early 1900s, much research effort has gone into optimizing the process. Froth flotation is heavily dependent on the surface chemistry of minerals where valuable minerals need to be rendered hydrophobic and gangue minerals hydrophilic for an optimum separation efficiency. The efficiency is mainly determined by the amount of minerals recovered by true flotation by virtue of their hydrophobicity, whereas recovery of non-sulphide gangue depends on the amount of water entering the froth and concentrate launder which is an indicator of entrainment. The flotation process requires a pulp phase, where a suitable physical and chemical environment is needed to enhance gas dispersion, bubble-particle collisions and attachment, and ultimately bubble-particle transportation into the froth phase, while entrained particles are drained from the froth phase back into the pulp phase. The froth phase structure and stability need to be suitable for the transport of valuable minerals to the concentrate launder. The hydrophobicity of minerals can be selectively induced with collectors or activators, whereas selective hydrophilicity of floatable gangue can be induced with depressants (Wiese, Harris & Bradshaw, 2005a: 797, 2010: 1013; Tadie et al., 2015: 49). Frothers are used to adjust the air-water interfacial properties, produce stable bubbles, and reduce the surface tension, which all aid in the attachment of hydrophobic particles (Comley et al., 2002: 90; Corin & Wiese, 2014: 134). Dispersants may be added to disperse minerals in the pulp which can also modify pulp rheology (Edwards, Kipkie & Agar, 1980: 40; Andreola et al., 2006: 1108). Physical cell parameters, such as the impeller, and air flow are responsible for suspending the slurry in the cell and to disperse air, which is dependent on factors

including impeller speed and pulp viscosity (Bakker, Meyer & Deglon, 2009: 949, 2010: 970; Shabalala et al., 2011: 1451).

2.2.1. Entrainment

During froth flotation, fine or ultrafine hydrophobic and/or hydrophilic minerals can be unselectively dragged by liquid films between air bubbles, and enter the froth phase with water, which is known as mechanical entrainment (Warren, 1985: 33). Entrainment is significant for particles below 50 μm in size, although many other studies have determined this to be below 30 μm (Smith & Warren, 1989: 126; Maachar & Dobby, 1992: 171; Savassi et al., 1998: 245; Wang & Peng, 2013: 312). The Plateau borders in the froth are particularly important as they hold the most water in the froth, which is the medium for particle transfer to the concentrate (Neethling & Cilliers, 2002: 125). Particles attached to the bubble lamella move with the bubbles, whereas unattached particles flow with the water in the plateau borders. Therefore, there is a direct correlation between recovered solids by entrainment and recovered water to the concentrate - an increase in recovered water leads to an increase in recovered solids, which in turn reduces grade (Warren, 1985: 43; Laplante, Kaya & Smith, 1989: 150). An increase in the mass of solids recovered also correlates with increasing valuable mineral recoveries (Hadler, Smith & Cilliers, 2010: 999; Dzingai, 2017: 59). A higher recovery, therefore, also means a greater recovery of gangue minerals, which reduces grade. An optimum separation efficiency can therefore shift the recovery-grade curve into a zone of significantly improved performance.

2.2.2. Froth characteristics

The froth stability can be influenced by a great number of factors including particle characteristics (e.g. quantity, size, shape, or degree of hydrophobicity), chemical conditions (pH, frother type, frother concentration, or Eh) or cell characteristics (e.g. air flow rate or solids concentration) (Johansson & Pugh, 1992: 9; Schwarz & Grano, 2005: 159). One of the major contributing factors to froth stability is the effects of particles, as they are known to stabilize the liquid films which separate the bubbles in the froth by forming coherent shells around the bubbles (Johansson & Pugh, 1992: 20; Farrokhpay, 2011: 3). This depends on particle size - smaller particles, typically smaller than the film thickness, give a higher packing efficiency which produces a more homogenous layer, and therefore greater froth stability which also prevents coalescence (Flynn & Woodburn, 1987: 133; Aktas, Cilliers & Banford, 2008: 69). Particles coarser than the film thickness can otherwise bridge and rupture the films. This also shows in studies that correlated an increase in froth stability with a reduction in particle size (Tang et al., 1989: 502). Overall, a froth that is 'too stable' can recover substantial amounts of entrained gangue which lowers grade without valuable recovery losses, whereas a froth that is 'too unstable' upgrades the concentrate but will result in valuable recovery losses (Wiese, Harris & Bradshaw, 2010: 1012). Therefore, there is an optimum froth stability to enhance recovery and grade.

Apart from particle size, the contact angle between air bubbles and the surface of minerals, which may also be indicative of the hydrophobicity of the minerals, can indicate how the minerals impact froth stability. The froth stability can be increased when the contact angle is less than the degree of wetting but can otherwise be reduced when the contact angle is greater than the degree of wetting. Strongly hydrophobic particles, having a contact angle of about 82°, can significantly destabilize the froth. The greatest froth stability can be achieved for moderately hydrophobic particles which have a contact angle of about 60° (Johansson & Pugh, 1992: 12; Ata, Ahmed & Jameson, 2003: 263). Ata, Ahmed and Jameson (2003: 263) compared hydrophobic glass spheres, having contact angles of 50°, 66° and 82°, to recovered water. The study by Ata, Ahmed and Jameson (2003: 263) observed that the water recovered, which was representative of the froth stability, increased from 50° to 60° contact angles, and then decreased at 82°. With the effects of particles on froth stability demonstrated in practice, Schreithofer et al. (2011: 37) observed that the presence of solids consisting of mixed pyroxene and oxidized chalcopyrite also contributed towards the destabilization of the froth, while unaltered chalcopyrite stabilized the froth in a system with added carboxymethyl cellulose (CMC).

Froth stability can be measured by either dynamic or static tests. In dynamic tests, a dynamic equilibrium occurs between rates of its formation and decay after the air is turned on, whereas in static tests, the rate of foam formation is zero, where the foam is allowed to form, and then allowed to collapse without further agitation or air supply input (Bikerman, 1965: 59; Barbian, Ventura-Medina & Cilliers, 2003: 1114). One commonly used method to quantify froth stability was proposed by Bikerman (1965: 59). The method can be expressed by the following equation:

$$\Sigma = \frac{V_f}{Q} = \frac{H_{max}A}{Q} \qquad \textbf{\textit{Equation 2.4}}$$

Where '$\sum$' is the dynamic froth stability, 'V_f' is the foam volume, 'Q' is the gas volumetric flowrate, 'H_{max}' the total foam height, and 'A' the cross-sectional area of the column (Bikerman, 1965: 59).

This method passes a flow of air or nitrogen gas through a column containing frother and water (for a 2-phase system) or frother, solids and water (for a 3-phase system). The froth height increases with time until an equilibrium height is reached. Barbian, Ventura-Medina and Cilliers (2003: 1114) proposed that it is more useful to show the rate of growth in terms of the froth height, which is characteristic of exponential growth, or an initial rapid growth, followed by slow growth towards the equilibrium height. The froth height varies with time according to the equation:

$$H(t) = H_{max}(1 - e^{\frac{t}{\tau}}) \qquad \textbf{\textit{Equation 2.5}}$$

Where 'H(t)' is the froth height as a function of time (t), 'H_{max}' is the equilibrium height, and 'τ' the characteristic average bubble lifetime (Barbian, Ventura-Medina & Cilliers, 2003: 1114).

2.2.3. Effect of pH

Pulp pH can play a significant role in pulp and froth characteristics which can significantly impact both recovery and grade. The pH can impact bubble-particle interactions, froth stability, pulp viscosity or the formation of hydrophobic films on mineral surfaces (Farrokhpay & Zanin, 2012: 495; Sheni, Corin & Wiese, 2018: 17). It is therefore important to acknowledge how pH impacts recovery and grade, especially when chemical reagents can impact froth or pulp processes. The natural pH of the pulp during PGE flotation is commonly around pH 9, which is also the pH where xanthate, a collector commonly used in the PGE industry, is stable (xanthate absorption is high and its decomposition low) and PGE recoveries are highest (Mustafa et al., 2004: 363; Muzenda et al., 2011: 3). Lime is often used to adjust the pH to greater values where needed, but lime can cost twice as much as collectors which indicates that the choice of pH modifiers is both an economic and technical decision. However, operating at pH's that are too high is avoided as this has been observed to have a detrimental impact on PGE recovery (Muzenda et al., 2011: 3). Investigators observed that with increasing pH, the froth stability was reduced, which suggests that poor PGE recoveries at high pH's could also be due to low froth stability and lower quantities of recovered solids (Farrokhpay & Zanin, 2012: 495). Contrary to these findings, Sheni, Corin and Wiese (2018: 17) demonstrated that increasing pH from 9 to 11 corresponded with increasing froth stability and recovered solids. In addition to pH having an impact on the froth phase, it was also demonstrated to have an impact on the rheological properties of a pulp (Johnson et al., 1999: 2846; Morris et al., 1999: 34). Common to these studies, the yield stress increased until about pH 9, where it reached a peak, and then decreased with a further increase in pH. Therefore, this indicates that pH can significantly impact the flotation process and any effects by chemical additive which also adjust the pH should be decoupled.

2.3. Dispersants and depressants

2.3.1. Sodium silicate and other dispersants/depressants

Sodium silicate is a well-known industrial chemical which, in minerals processing, is commonly used as a depressant of silicate minerals or a dispersant/deflocculant of clays or iron-bearing minerals (Garrido, Gainza & Pereira, 1988: 330; Andreola et al., 2006: 3; Ma, 2011a: 234; Rao et al., 2011: 520). The reagent is well-known in non-sulphide flotation although fewer studies have investigated sodium silicate in sulphide ore flotation (Edwards, Kipkie & Agar, 1980: 37; Feng et al., 2012: 12091), and even less are available in the public domain that has investigated its effects in the context of PGE ores (Bulatovic, 2003: 936). Although sodium silicate is well-known, its mechanisms, however, are poorly understood.

Sodium silicate, $m Na_2O \cdot n SiO_2$, is a general name encompassing various ratios of sodium oxide to silicon dioxide, where n:m is referred to as the sodium silicate modulus. These include sodium metasilicate,

$Na_2O{\cdot}SiO_2$, which is a more alkaline silicate, as well as silicates with higher sodium oxide contents such as sodium squisilicate ($1.5Na_2O{\cdot}SiO_2$) or sodium orthosilicate ($2Na_2O{\cdot}SiO_2$). The modulus can easily be manipulated by the addition of a sodium-based pH modifier, such as NaOH. Moduli between 1.6 and 4 are commercially available and commonly found in aqueous form, called "waterglass". Unfortunately, many studies do not specify the type of sodium silicate used, as its modulus is known to impact separation efficiency. However, it can be assumed that the general name, sodium silicate, refers to sodium metasilicate which is most commonly available. In addition to varying moduli, the effect of SS to depress or disperse minerals is also impacted by the SiO_2 concentration, pH, and temperature (Irannajad, Ejtemaei & Gharabaghi, 2009: 770; Amorós et al., 2010: 35; Park & Jeon, 2010: 1368; Feng et al., 2012: 12093; Silva et al., 2012: 209). In this study, "SS" will refer to the general name sodium silicate. It should be noted that the type of SS used in this work is sodium metasilicate.

The dissolution of SS undergoes complex hydrolysis reactions which can generate a suite of different SS species, which are mainly dependent on SS concentration and pH. Some SS dissolution reactions are shown in Equation 2.6 and Equation 2.7. The SS species include a colloidal silicate such as SiO_2, monomeric species, such as $Si(OH)_4$, $SiO(OH)_3^-$, $SiO_2(OH)_2^{2-}$, $HSiO_3^-$, SiO_3^{2-} and H_2SiO_3, and polymeric species, such as $Si_2O_3(OH)_4^{2-}$, $Si_4O_6(OH)_6^{2-}$, $Si_2O_2(OH)_5^-$ and $Si_3O_5(OH)_5^{3-}$. It is accepted that below pH 9.4, the prevailing SS component in solution is $Si(OH)_4$, between pH 9.4 and 12.6, the prevailing component is $SiO(OH)_3^-$, and above pH 12.6, the prevailing component is $SiO_2(OH)_2^-$, as illustrated in the species distribution diagram in Figure 2.5 (Furlong, Sing & Parfitt, 1979: 415; Phair, Van Deventer & Smith, 2001: 151; Feng et al., 2012: 12092; Bo et al., 2015: 47). Decreasing the pH from 10 to 7, for example, changes the prevailing silica species from $SiO(OH)_3^-$ to $Si(OH)_4$ (Furlong, Sing & Parfitt, 1979: 415). Apart from the SS species being dependent on solution pH, SS has been observed to be a pH modifier (Amorós et al., 2010: 35; Park & Jeon, 2010: 1369). Increasing SS concentration increases solution pH, which is typically in the pH 5 to 11 range due to the amount of OH^- ions dissolved into solution (Amorós et al., 2010: 35; Park & Jeon, 2010: 1369).

The following reactions shows the dissolution of SS (Park & Jeon, 2010: 1369; Fedorockova et al., 2015: 276):

$$Na_2SiO_3 + 2H^+ + H_2O \leftrightarrow Si(OH)_4 + 2Na^+ \qquad \textbf{\textit{Equation 2.6}}$$

$$Na_2SiO_3 + 2H_2O \leftrightarrow H_2SiO_3 + 2Na^+ + 2OH^- \qquad \textbf{\textit{Equation 2.7}}$$

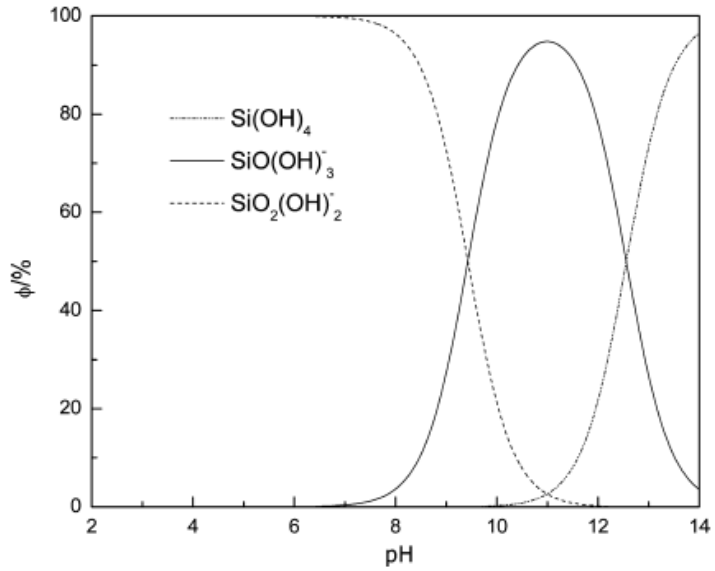

Figure 2.5: Distribution coefficients of various species of SS as a function of pH, taken from Feng et al. (2012: 12092).

Silva et al. (2012: 210) observed that at pH 7, the $Si(OH)_4$ species adsorbed onto quartz occurred by sharing of electron pairs, but the depression of quartz did not occur above pH 10. The authors observed that the pH range which favoured the depressant effect of SS was between pH 5 and 8 (Silva et al., 2012: 210). Various other authors found that when $SiO(OH)_3^-$ prevailed, which Figure 2.5 illustrates to be between about pH 9.5 to 12.5, the dispersant effect of SS was prominent (Feng et al., 2012: 12092; Bo et al., 2015: 47; Han, Liu & Chen, 2016: 409). The adsorption between SS and kaolinite was studied by density functional theory simulation (Han, Liu & Chen, 2016: 404). The species $Si(OH)_4$ and $SiO(OH)_3^-$ mainly adsorbed onto the basal plane Al-terminated surface of kaolinite by the hybridization of O atoms and H atoms between $Si(OH)_4$ and the kaolinite surface. In addition to the same mechanism of hybridization between $SiO(OH)_3^-$ and the surface, electrostatic forces also occurred. Figure 2.6 illustrates the adsorption of $Si(OH)_4$ and $SiO(OH)_3^-$ species on the Al-terminated surface of kaolinite (Han, Liu & Chen, 2016: 403). The O atom on $SiO(OH)_3^-$ has an unpaired electron, which was compensated by transfer of more electrons by Al-terminated surface. The $SiO(OH)_3^-$ species easily adsorbed onto the kaolinite surface and were more stable compared to $Si(OH)_4$.

In the context of rheology, a dispersant denotes all reagents capable of adjusting the viscosity and yield stress of a suspension and these will be referred to as 'rheology modifiers', even though the effect of rheology modifiers is the same as that of dispersants. Sodium silicate has also been recognized as a rheology modifier, although the species involved have not properly been investigated, it is expected that the same species serving as dispersants would behave as rheology modifiers (Andreola et al., 2006: 1108; Amorós et al., 2010: 37; Zhang, Chen & Liu, 2017: 9; Xia et al., 2018: 2908).

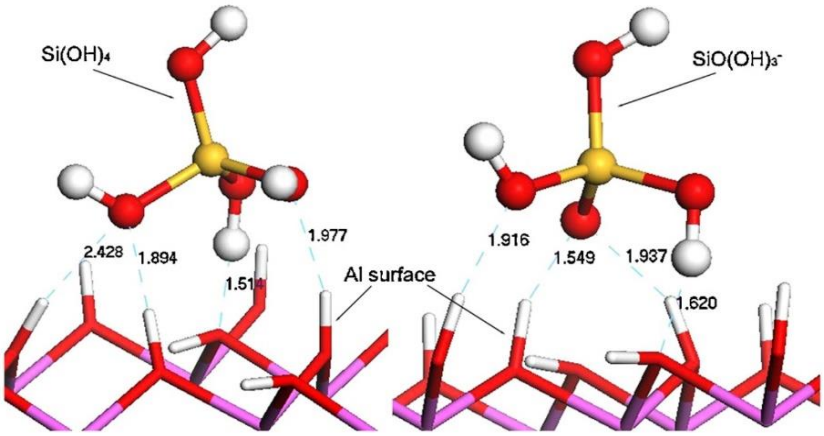

Figure 2.6: Adsorption of the monomeric $Si(OH)_4$ and $SiO(OH)_3^-$ SS species onto Al-terminals on the basal plane of kaolinite, taken from Han, Liu and Chen (2016: 403).

No published literature has studied the use of SS in terms of dispersant, rheology modifying or depressant effects in the Southern African PGE industry. Polysaccharides such as modified guar gum and CMC are the most used gangue depressants in the PGE industry. There are very limited investigations of the use of SS as a depressant of NFG (Witney & Yan, 1997: 147), but both CMC and guar gum have been extensively studied as talc depressants and were found to adsorb onto talc by either hydrogen bonding or chemical interaction. The adsorption of CMC has also been found to have dispersant effects which have been used to disperse minerals during flotation, however, it is better known and used as a depressant in the Southern African PGE industry (Edwards, Kipkie & Agar, 1980: 40; Wellham, Elber & Yan, 1992: 389; Bremmell, Fornasiero & Ralston, 2005: 210). It was proposed that CMC, for example, adsorbs on the basal plane by hydrophobic bonding and on edge planes by hydrogen bonding (Steenberg & Harris, 1984: 89). Depressants like CMC and guar gum have been shown to play an important role in depressing talc and have been extensively studied (Khraisheh et al., 2005: 200; Wiese, Harris & Bradshaw, 2010: 1011; McFadzean et al., 2011: 465; Manono, Corin & Wiese, 2019: 220).

2.4. Major problems due to phyllosilicate minerals

2.4.1. Slime coatings

In the context of this work, "slimes" refer to fine serpentine particles (-10 μm) which are susceptible to coating valuable minerals. This is the same definition of slimes used in other studies, where it is referred to as fine-grained minerals (clays such as kaolinite or illite, or silicates such as quartz), which may either slime coat valuables, increase pulp viscosity, or are liable to entrainment (Bandini, Prestidge & Ralston, 2001: 487; Jorjani et al., 2011: 754; Forbes, Davey & Smith, 2014: 136; Liu & Peng, 2014: 216). Slimes are hydrophilic minerals that form a hydrophilic "armour" on valuable mineral surfaces. Valuable mineral particles coated with hydrophilic slimes will decrease the hydrophobicity of the valuable and prevent or reduce collector adsorption which hinders its attachment to rising air bubbles (Edwards, Kipkie & Agar,

1980: 41). The interaction between pyrite and lizardite in the presence of a sodium sulphide (Na_2S) activator below and above pH 10 is illustrated in Figure 2.7 (Yang et al., 2020: 1).

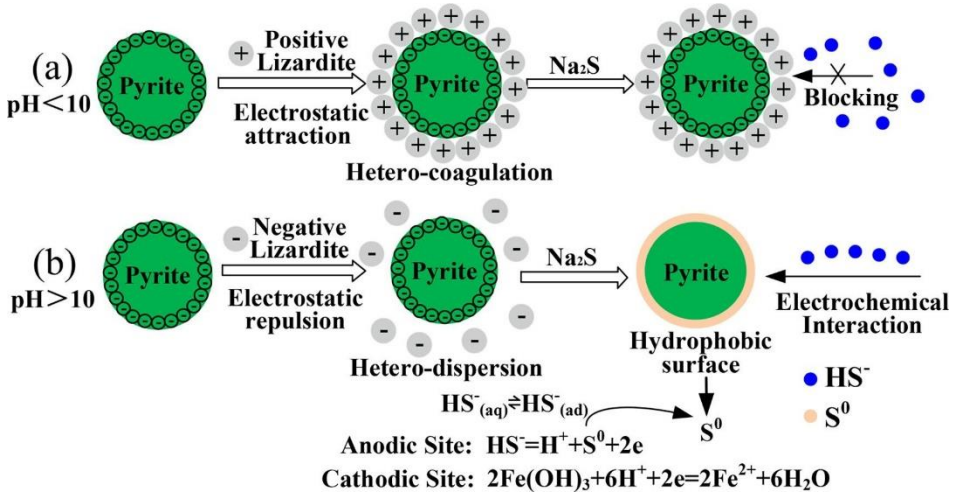

Figure 2.7: The interaction between pyrite and lizardite in the presence of a sodium sulphide (Na_2S) activator, taken from Yang et al. (2020: 1).

Below pH 10, lizardite slimes coated the surface of pyrite due to electrostatic attraction which hindered the activator adsorption. Above pH 10, lizardite slimes are detached from the surface of pyrite due to an electrostatic repulsion which allowed the adsorption of the main component of the Na_2S (HS^-) to adsorb onto the surface of pyrite (Yang et al., 2020: 3). This is an indication that pH can govern slime coating and whether reagents, such as collectors or activators, are adsorbed onto mineral surfaces.

The following sections give insight into the causes and detection of slime coatings, the effect of slime coatings and SS on recovery, zeta potential measurements and the effect of SS, and other slime mitigating methods.

Causes and detection of slime coatings

Differences in the surface electrical properties of slimes can have marked impacts on its ability to slime coat as surface charge can impact particle-particle interactions. The surface charge of serpentines is developed either by the ionization or dissolution of OH^- or Mg^{2+} or inherited by the adsorption of other ions (Martinez & Zucker, 1960: 925). For example, the serpentine polymorph chrysotile was found to have a greater positive zeta potential and a faster electrophoretic mobility compared to lizardite due to greater exposure of Mg^{2+} ions on chrysotile because it dissolved more OH^- ions compared to lizardite (Martinez & Zucker, 1960: 926; Edwards, Kipkie & Agar, 1980: 35). A reduction in pH also exposed more Mg^{2+} due to the dissolution of OH^- (Martinez & Zucker, 1960: 925). The greater positive charge of chrysotile resulted in a poorer floatability of pentlandite due to the stronger electrostatic attraction between pentlandite and chrysotile compared to using lizardite at equivalent pH 9 experiments (Martinez

& Zucker, 1960: 926). This suggests that the greater exposure of Mg^{2+} on the surface of serpentine, the larger the positive surface charge of serpentine and the poorer the floatability of the BMS. Conversely, a negative zeta potential of serpentine at high pH's could indicate greater exposure of OH^- ions on the surface of serpentine. The influence of Mg^{2+} was further investigated by Feng et al. (2013: 1125) who observed that the zeta potential magnitude and sign were largely negative when Mg^{2+} was leached from serpentine, but its zeta potential was restored to positive values with added Mg^{2+}. This reduction in zeta potential when serpentine was leached was also observed by Feng et al. (2012: 71).

The suspension pH has a significant impact on surface charge which governs whether slime coating or dispersion within a suspension occurs. At the same pH, if the slime is positively charged and the valuable mineral negatively charged, slime coating can occur. Contrary to this, if the slime and valuable have the same surface charge, slime coatings can be removed from valuable minerals. Manipulating pulp pH to remove slime coatings has been explored by a few authors (Vergouw et al., 1998: 612; Bandini, Prestidge & Ralston, 2001: 492; Oats, Ozdemir & Nguyen, 2010: 417; Yang et al., 2020: 2). This suggests that slime dispersion at high pH's, above the iso-electric point (i.e.p), might remove slime coatings from BMS, where the i.e.p refers to the activity of the potential determining ions (base 10) at zero zeta potential (Alvarez-Silva et al., 2010: 405). This is where both the BMS and slime have the same negative charge sign and is likely to have an electrostatic repulsion. However, many serpentine slimes investigations determined the serpentine i.e.p value to be between 9 and 12, which indicates that the charge of serpentine above the i.e.p is negative, like that of BMS. However, the effect of pH (above the i.e.p) on slime dispersion has not been acknowledged (Feng et al., 2013: 1125; Lu et al., 2019: 38).

The consequences of slime coatings are often detected before determining what the causes of slime coatings are. Poor flotation recoveries using altered ores may infer slime coatings, but poor recoveries might be due to other causes including changes in pulp rheology or froth stability (Adeyinka et al., 2009: 432; Farrokhpay & Bradshaw, 2012: 04606). This makes identifying slime coatings difficult, and even more so in low grade ores where the quantity of gangue far exceeds that of valuable minerals. Fortunately, there are indirect methods, and more accurately, direct observations to identify slime coatings. Once slime coatings are identified, a suitable mitigation method (or methods) can be put in place to overcome slime coatings.

Visual evidence of slime coatings has been provided by a few scanning electron microscopy- energy-dispersive x-ray spectrometers (SEM-EDS) investigations, including serpentine slime coatings of BMS (Edwards, Kipkie & Agar, 1980: 39; Song et al., 2006: 914; Oats, Ozdemir & Nguyen, 2010: 418; Peng & Bradshaw, 2012: 288). These can sometimes provide interesting characteristics of slimes, as determined by Peng and Bradshaw (2012: 288). The SEM images revealed that serpentine slime characteristics, as noted for lizardite, in deionized water were evenly distributed on the pentlandite surface, whereas in borehole water, the slimes on the surface of pentlandite are irregularly distributed. The irregular distribution of

slimes on pentlandite under two types of electron imagery is illustrated in Figure 2.8.

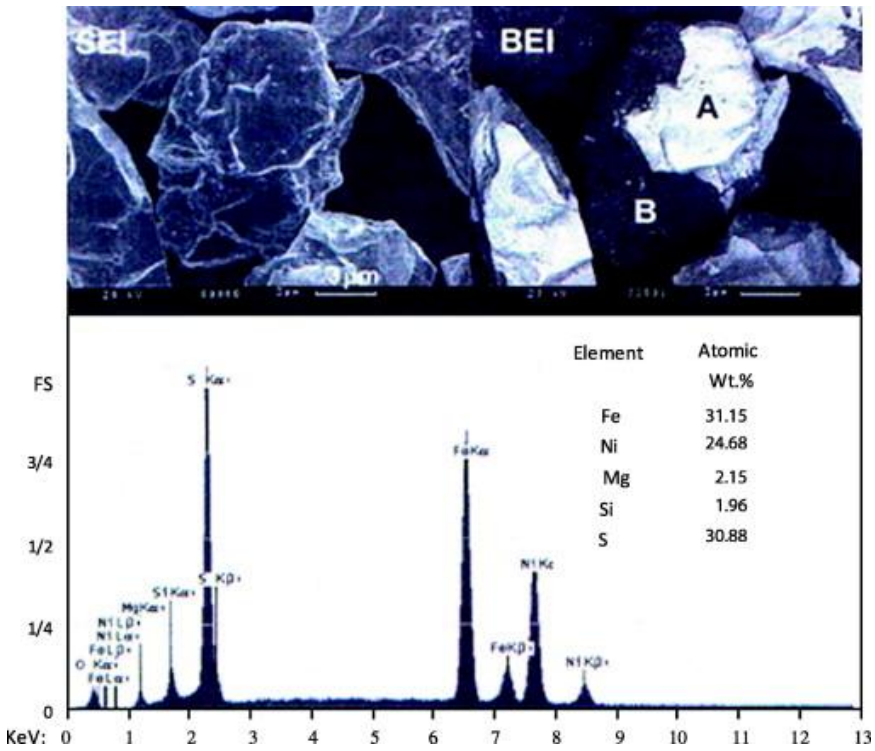

Figure 2.8: SEM image (top) and EDS (bottom) of pentlandite surfaces with attached lizardite particles in borehole water: 10% pentlandite mixed with 90% lizardite, taken from Peng and Bradshaw (2012: 287).

The accompanying EDS analysis of the pentlandite particle detected the mineral identities of both lizardite and pentlandite, which indicated the presence of lizardite slimes on the surface of pentlandite. This indicates that SEM coupled with EDS could identify slimes, but this is not an *in-situ* method as slimes could be inadvertently attached through the sample preparation process, as emphasized by Yu et al. (2017: 28). Using cryogenic-SEM could be useful as it flash-freezes slurry solutions and has successfully demonstrated slime coatings on clay samples (Wang, Peng & Vink, 2013: 4872). However, this method is impractical when using low grade ore slurries but may prove useful when dealing with synthetic solutions, such as the same sample used during microflotation or zeta potential experiments.

Microflotation and zeta potential are commonly paired indirect and direct methods, respectively, which can collectively be interpreted to determine whether valuable minerals are prone to slime coatings (Feng et al., 2012: 12093; Peng & Bradshaw, 2012: 289; Feng, Lu & Luo, 2015: 1242; Long, Huang & Xiao, 2019: 11; Yang et al., 2020: 3). Placed in the context of a realistic ore system, this has often been used to identify whether minerals of interest are subjected to slime coatings (Alvarez-Silva et al., 2016: 70). Zeta potential measurements performed on binary mineral mixtures can detect whether one mineral is slime coated by the other on the basis that each mineral possesses very different surface charges. The absence of slime

coating will result in a bimodal zeta potential distribution whereas slime coated particles will result in the zeta potential of the slime coated phase only (Xu et al., 2003: 184; Forbes, Davey & Smith, 2014: 139; Chen, Zhao & Song, 2017: 63; Liang et al., 2017: 5). In a serpentine-pentlandite mixture, pentlandite showed a positive zeta potential between pH 3 to 10 compared to it having a negative zeta potential without serpentine present (Alvarez-Silva et al., 2016: 69).

Effect of slime coatings and SS on recovery

The degree to which slimes coat valuable minerals may have two negative impacts: i) a low coverage of slimes on the valuable may not hinder the floatability of the valuable but this may reduce concentrate grade, and ii) an extensively covered valuable mineral can be rendered hydrophilic, as it takes on the characteristics of the coated phase, and hinders the recovery of the valuable mineral as it prevents the adsorption of collectors and/or air bubbles (Bandini, Prestidge & Ralston, 2001: 490; Tabatabaei et al., 2014: 29; Wang, Peng, Nicholson, et al., 2015: 50). Most serpentine slime investigations are related to BMS recovery investigations for good reason: serpentine is a common gangue mineral component in complex sulphide-bearing ores (Wellham, Elber & Yan, 1992: 382; Bremmell, Fornasiero & Ralston, 2005: 207; Peng & Bradshaw, 2012: 284; Feng et al., 2013: 1123). Therefore, many authors have made reference to the influence of serpentine on BMS recovery and in addition to this reasoning, BMS and serpentine are both common minerals associated with PGE deposits in South Africa (Bulatovic, 2003: 932; Becker et al., 2009: 248; Becker, Wiese & Ramonotsi, 2014: 28).

The occurrence of serpentine slimes is closely related to the size of the serpentine particles which in turn impacts the recovery of valuables. The particle size of serpentine was demonstrated to impact the floatability of BMS, such as pyrite, where a reduction in serpentine particle size correlated with a lower pyrite recovery (Feng, Lu & Luo, 2015: 2; Liu et al., 2018: 4). In both cases, serpentine in the -10 μm size class had the most detrimental impact on pyrite recovery, as illustrated in Figure 2.9. The recovery of pyrite in the presence of -10 μm serpentine was also found to be increasingly reduced with increasing pH, indicating that the negative impacts of slimes within alkaline ore slurries could be problematic (Feng et al., 2012: 12091; Liu et al., 2018: 4; Feng et al., 2019: 488).

Studies agree that increasing serpentine slime concentrations can further reduce the recovery of BMS (Edwards, Kipkie & Agar, 1980: 36; Bremmell & Addai-Mensah, 2005: 209; Peng & Bradshaw, 2012: 286; Feng et al., 2019: 488; Chen et al., 2021: 7). For example, with increasing serpentine slime concentration, as shown for lizardite, the recovery of pentlandite decreased from a maximum recovery of 78% to 39% when 0.11 g/L serpentine was used (Bremmell, Fornasiero & Ralston, 2005: 209). Many studies observed that very low serpentine slime concentrations relative to BMS had significant impacts on recoveries (Edwards, Kipkie & Agar, 1980: 36; Bremmell & Addai-Mensah, 2005: 209; Peng & Bradshaw, 2012: 286; Cao et al., 2017: 624; Feng et al., 2019: 488). An example of this was presented by Edwards, Kipkie and Agar (1980: 36), who demonstrated that serpentine to pentlandite in a 1:20 ratio drastically reduced

pentlandite recovery from 80% to 20%. This may indicate that ores containing serpentine slimes at low concentrations can have significant impacts on PGE recoveries.

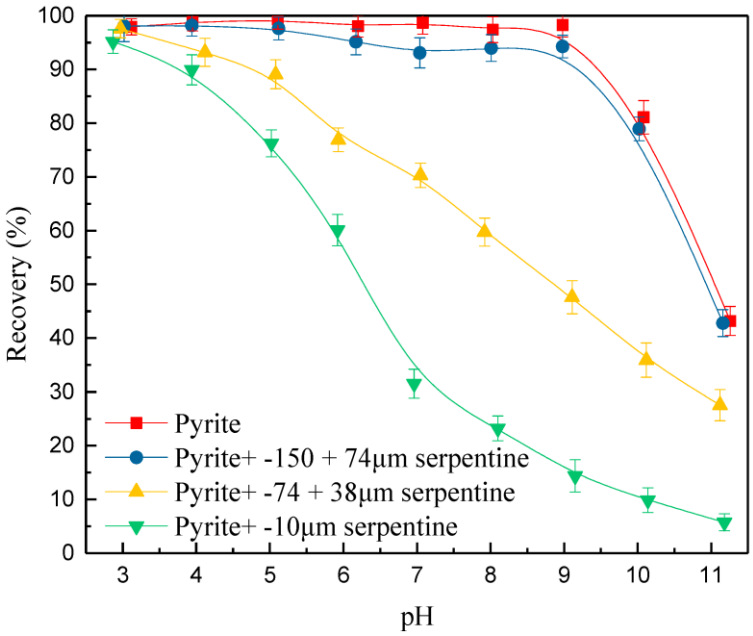

Figure 2.9: Effect of serpentine with different particle sizes on the flotation of pyrite as a function of pulp pH (potassium butyl xanthate = 3.75 × 10^{-5} mol/L, methyl isobutyl carbinol (MIBC) = 2 × 10^{-4} mol/L), taken from Liu et al. (2018: 4).

In terms of its dispersant effect, SS studies have mainly investigated dispersing clay slimes such as the dispersion of bentonite, kaolinite, illite or montmorillonite from coal, mineral sands or iron oxide minerals (Li et al., 2005: 4755; Oats, Ozdemir & Nguyen, 2010: 415; Ma, 2011b: 234), but its use as a dispersant of serpentine slimes from BMS are rare (Edwards, Kipkie & Agar, 1980: 37; Feng et al., 2012: 12091). A good example of the effect of SS on the flotation of BMS, as demonstrated for pyrite from pH 3 to 11, was presented by Feng et al. (2012: 12091). Without SS, the floatability of pyrite with added serpentine slimes steadily decreased with increasing pH from pH 3 to 11, as indicated in Figure 2.10. The introduction of SS restored pyrite recovery in the pH range of 6.2 to 11. Alkaline pH's were observed to be most successful for pyrite recovery in the presence of lizardite and SS.

Many studies observed high SS dosages to be much more effective at dispersing slimes than lower dosages (Al-Thyabat, 2009: 290; Ma, 2011: 234; Feng et al., 2012: 12091; Li et al., 2019: 4). Through x-ray photoelectron spectroscopy (XPS) analysis, Feng et al. (2012: 12092) have demonstrated that increasing SS concentrations increased the amount of SS adsorbed onto the positively charged surface of lizardite. This indicates that a higher concentration of SS onto the slime can result in a stronger slime dispersion, as similarly observed by Ma (2011: 237) in the case of kaolinite. The study further found increased concentrations of silicon and oxygen, and decreasing concentrations of Mg^{2+}, on the surfaces of lizardite

by XPS analysis. This confirms the adsorption of negatively charged SS species onto Mg^{2+} ions on the surface of lizardite. The same study also concluded that $SiO(OH)_3^-$ species were the reason that the pyrite floatability was restored at this pH.

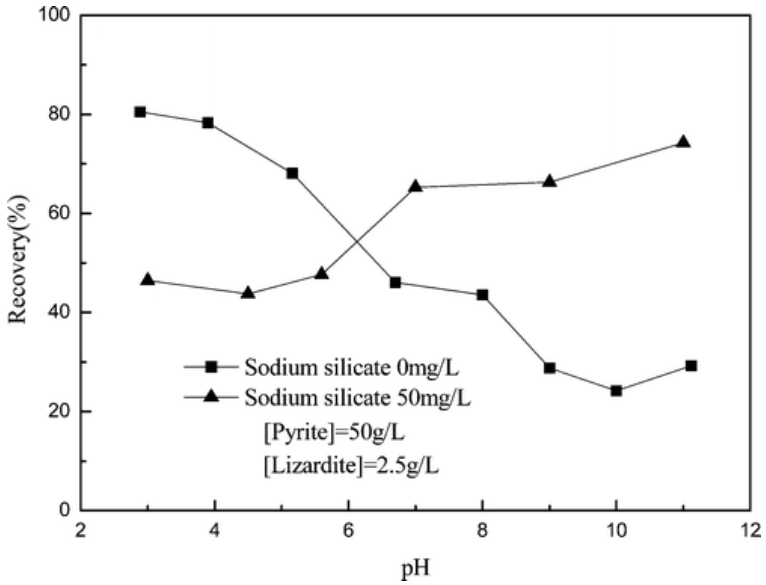

Figure 2.10: Recovery of pyrite as a function of pH (potassium amyl xanthate = 1×10^{-4} M; MIBC = 1×10^{-4} M), taken from Feng et al. (2012: 12091).

Published literature where SS was used as a dispersant in PGE flotation is very rare (Bulatovic, 2003: 936). In the study of Bulatovic (2003: 936), 300 g/t SS was used in the rougher flotation of a high-chromium PGE ore from the Panton Sill deposit in Australia. Using SS improved PGE recovery only marginally (by 1.9%). While there might be unpublished SS research on PGE deposits, no published literature has explored the use of SS in Southern African PGE deposits. This work is therefore the first to do so.

Zeta potential measurements and the effect of SS

An electrical double layer surrounds a particle when it is immersed in a liquid solution, which is electrically inhomogeneous. Reaction equilibria including adsorption, protonation and deprotonation homogenizes the surface charge creating an electric field. Counter-ions are attracted to the particle whereas co-ions are repelled. The distribution of surrounding ions forms two layers: a) a Stern layer where attractive ions are tightly bound to the particle, and b) a diffuse layer where weakly attractive and repelled ions exist. In the diffuse layer, there is a conceptual boundary called the slipping plane where all ions within the boundary are very likely to travel with the particle when it moves in solution, whereas ions beyond the boundary will not. The potential at this boundary is known as the zeta potential and it is this value that is of great interest in mineral surface chemistry analyses. The zeta potential value is not the actual charge at the surface of the mineral; however, its value gives great insight into the electrostatic interactions and colloidal stabilities between minerals.

A common method for measuring the electrophoretic mobility of particles within an electric field is laser doppler electrophoresis. This method is commonly used by the Malvern Zetasizer Nano instrument. A folded capillary cell is commonly used during measurements, where nanometer sized particles move to the electrode of opposite charge on either end of the cell. The electrophoresis method determines the displacement of the particles (Δx) during a specific length of time (Δt) within an electric field applied to the aqueous suspension. The particle velocity is the ratio of $\Delta x / \Delta t$, which is then divided by the magnitude of the applied voltage gradient to calculate the electrophoretic mobility. Modern equipment, such as the Malvern Zetasizer, automatically calculates the electrophoretic mobility by dividing the particle velocity by the voltage gradient. The instrument then applies the electrophoretic mobility to the Henry equation to determine the zeta potential, as expressed in Equation 2.8.

$$U_E = \frac{2\varepsilon Z f(\kappa\alpha)}{3\eta} \qquad \textit{Equation 2.8}$$

Where 'U_E' is the electrophoretic mobility, 'Z' the zeta potential, 'ε' the dielectric constant, 'η' the dynamic viscosity and $f(\kappa\alpha)$ Henry's function (Hunter, 2001: 206). The folded capillary cell is commonly paired with the Smoluchowski approximation which is valid for a thin double layer when the Debye length ($1/\varkappa$) is smaller than the radius of the particle (α). Although Smoluchowski application works well with isotropic spherical minerals, measuring anisotropic minerals are much more complicated due to their irregular surface charge. In the case of anisotropic minerals, such as phyllosilicates, the zeta potential measurement depends on the plane being measured and have been characterised by having different i.e.p and the point of zero charge (p.z.c) values (Alvarez-Silva et al., 2010: 407, 2010: 385; Ndlovu et al., 2011: 1318; Ndlovu, 2013: 111). The p.z.c refers to the activity of the potential determining ions (base 10) at zero surface charge (Alvarez-Silva et al., 2010: 405). Differences in the p.z.c and i.e.p values are due to differences in drag experienced by the plane and edges of the particle during measurement, which gives discrepancies in the electrophoretic mobility readings. However, serpentine zeta potential measurements have previously shown good estimated readings, which could successfully be applied in the context of slime coating, especially when pairing the zeta potential measurements with microflotation (Feng et al., 2012: 12093; Peng & Bradshaw, 2012: 289; Feng, Lu & Luo, 2015: 1242; Long, Huang & Xiao, 2019: 11; Yang et al., 2020: 3).

Now that a brief overview of zeta potential was provided, the rest of the literature in this section will focus on the application of zeta potential to understand slime coatings. Serpentine slime coatings are primarily governed by the sign and magnitude of the surface charge of the serpentine slimes and the valuable minerals. The surface charge of minerals can be inferred by zeta potential measurements which can then be interpreted to determine the interaction between serpentine and valuable minerals, such as BMS, in a liquid suspension. Natural variations of physical and chemical properties of the different serpentine polymorphs, such as chrysotile and lizardite, are the cause for their differences in zeta potential

(Martinez & Zucker, 1960: 925). For this reason, lizardite will be the serpentine mineral of interest seeing as this is the expected serpentine mineral type within the ore used in this study. However, not many studies investigated the effects of lizardite. Therefore, some references to the general name 'serpentine' will be used in the case where the type of serpentine was not mentioned in the literature.

Zeta potential findings can be used to quantitatively calculate the Derjaguin-Landau-Verwey-Overbeek (DLVO) interaction energy between serpentine and BMS (Bremmell, Fornasiero & Ralston, 2005: 211; Long, Huang & Xiao, 2019: 11). The theory determines the aggregation and dispersion of colloidal particles by summing the van der Waals interaction and the electrostatic double-layer interaction. An extended DLVO theory also considers the addition of hydration and hydrophobic interactions which proves more accurate when considering anisotropic fine particles (Derjaguin & Churaev, 1992: 230; Yao et al., 2016: 85). Researchers used the DLVO theory to determine the interaction energies between serpentine slimes and BMS, both with and without SS (Bremmell, Fornasiero & Ralston, 2005: 211; Feng et al., 2012: 12093; Li et al., 2019: 5; Long, Huang & Xiao, 2019: 9). At pH 9 in 10^{-3} M KNO_3 solutions, an attractive interaction occurred between serpentine and pyrite at specific apparent separation distances, as indicated between serpentine and pyrite in Figure 2.11 (Feng et al., 2012: 12093). Once SS was added, the attractive force between serpentine slimes and BMS was no longer observed due to the repulsive force between the minerals.

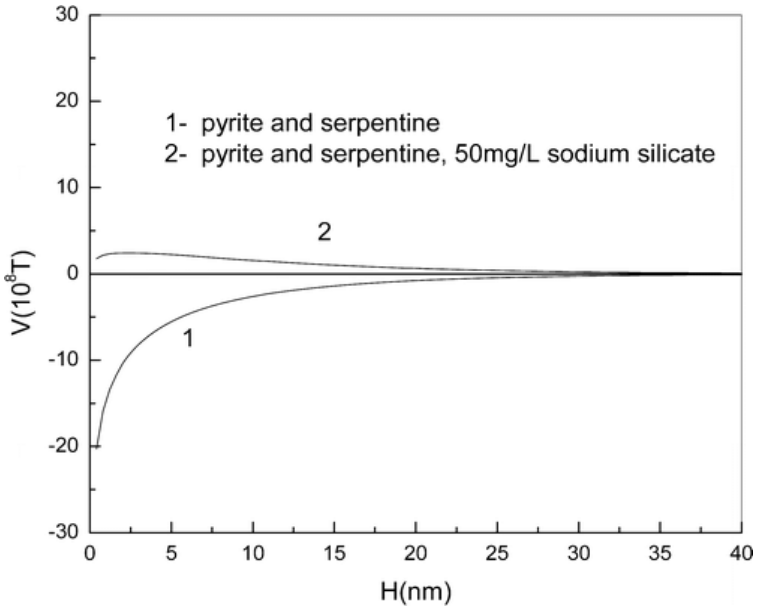

Figure 2.11: Total potential energy interaction between pyrite and lizardite as a function of particle distance, taken from Feng et al. (2012: 12093).

DLVO energy calculations are useful in quantitatively understanding the interaction between serpentine slimes and BMS, but the zeta potential of minerals are also good indicators of the likely interactions between serpentine and BMS. The zeta potential of lizardite in the absence and presence of SS, which have commonly been analyzed in KNO_3 and KCl electrolytes, have been determined in various studies

(Martinez & Zucker, 1960: 925; Bremmell & Addai-Mensah, 2005: 211; Feng et al., 2012: 12092; Feng et al., 2013: 1125; Zhou & Feng, 2015: 432; Lu et al., 2019: 39). The zeta potential of lizardite has been recorded to be positive for most of the pH range, where it decreased with increasing pH until it reached an i.e.p at alkaline pH's, as demonstrated in Figure 2.12.

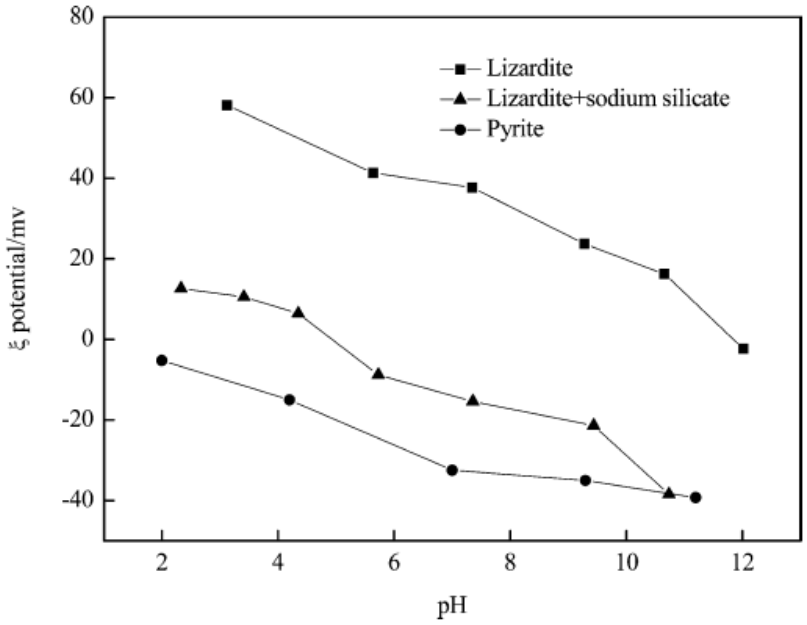

Figure 2.12: Zeta potential of lizardite and pyrite particles as a function of pH, taken from Feng et al. (2012: 12093).

At pH 9, where most PGE flotation occurs, the zeta potential of lizardite was commonly found to fall between +15 and +30 mV. In experiments with added SS, the zeta potential of lizardite effectively changed from positive to negative values. For example, as demonstrated in Figure 2.12, the zeta potential of lizardite was +25.6 mV without SS, and -21.2 mV with SS in solution. Inductively coupled plasma - optical emission spectroscopy (ICP-OES) and XPS experiments revealed that SS species adsorbed onto lizardite which explained the zeta potential shift of lizardite from a positive to negative value. Due to the same zeta potential signs between lizardite and pyrite, an electrostatic repulsion between lizardite and pyrite was created. Therefore, SS could remove slimes from the surface of pyrite. It is common for BMS to have negative zeta potentials, similarly to what was observed for pyrite in Figure 2.12. For example, the zeta potential of chalcopyrite was found to occur between -10 mV and -50 mV at pH 9 (Liu et al., 2010: 544; Petrus et al., 2012: 120; Hirajima et al., 2014: 105; October et al., 2019: 442; Zeng et al., 2020: 5). Most studies that investigated the interaction between lizardite and BMS did not report whether SS influenced the zeta potential of BMS, however, some studies observed reducing chalcopyrite zeta potentials with increasing SS dosages, which indicates that SS species were able to adsorb onto chalcopyrite (Xia et al., 2018: 2908; Li et al., 2019: 5). The adsorption of SS onto BMS is of no real

concern as this can only induce more negative zeta potentials. It is therefore most important for the zeta potential of lizardite to be shifted from positive to low negative values similarly to that of the BMS.

Once the interaction between slimes and valuables minerals has been determined, both with and without SS, it can be used to interpret microflotation findings. Studies observed that an electrostatic attraction between lizardite and BMS corresponded with a reduction in BMS recovery because the slimes coating the BMS hindered collector adsorption (Feng et al., 2012: 12093). However, the electrostatic repulsion created by SS restored the BMS recovery due to the ability of the collector to adsorb onto the cleaned BMS surface. This has not only been observed for SS, but other dispersants such as CMC and SHMP which have also shown similar results (Bremmell, Fornasiero & Ralston, 2005; Long, Huang & Xiao, 2019: 11). This indicates that dispersants can play an important role in altering the zeta potential of lizardite. Therefore, to improve recoveries, the zeta potential of serpentine needs to be shifted from positive to negative values to create an electrostatic repulsion between serpentine slimes and BMS.

Platinum-group minerals closely follow the measured zeta potential of BMS and therefore it can be extrapolated from the literature that the dispersant effect of SS will also improve the PGM flotation response even though the PGM behaviour has not been directly measured. The zeta potentials of sperrylite, cooperite and moncheite were -13 mV, -5 mV and -18 mV at pH 9 respectively, which resemble similar values to that of BMS such as chalcopyrite at pH 9 (Shackleton, 2007: 86; Shackleton, Malysiak & O'Connor, 2007a: 34, b: 1237). These are common PGMs found within the Silicate reef, as mentioned in Section 2.1.1. These negative zeta potentials infer the possibility that positively charged phyllosilicate slimes can have an electrostatic attraction to negatively charged PGMs, which can hinder collector adsorption and have a problematic effect on PGM recoveries. The reversal of serpentine's charge sign in SS solutions is therefore also expected to improve the PGM floatability, similarly to the observation of BMS.

Other slime mitigating methods

Slime coatings can be mitigated by using mechanical methods to remove fine particles from the system using hydrocyclones or by ultrasonicating the pulp (Celik, 1989: 1164; Tao et al., 2007: 245; Oats, Ozdemir & Nguyen, 2010: 415). Chemical methods can also remove slime coatings, such as the use of dispersants or novel clay binders, where clay binders can agglomerate and remove clays from valuable mineral surfaces (Wellham, Elber & Yan, 1992: 389; Tao et al., 2007: 245; Yu, Ma, et al., 2017: 33). While clay binders and removing fines from the ore before flotation proved successful in some investigations, this may prove impractical in ore systems where slimes have similar particle sizes to valuables, which is typically the case in PGE ores due to the fine grain sizes of PGMs. In cases where slimes and valuable minerals have similar grain sizes, using ultrasonication and dispersants to mitigate the effects of slime coatings are better options.

Various studies reported that ultrasonic treatment either before or during batch flotation increased valuable mineral recoveries by removing fine particles from the surfaces of minerals (Celik, 1989: 1163; Djendova & Mehandjiski, 1992: 209; Aldrich & Feng, 1999: 703). Ultrasonication can also facilitate floatability by forming microbubbles on the hydrophobic mineral surface which enhances bubble-particle attachment (Celik, 1989: 1165; Ross, Singh & Pillay, 2019: 134). Some studies relating to the removal of fine- or ultrafine particles from sulphide minerals for recovery improvement using ultrasonication methods were previously investigated (Celik, 1989: 1163; Aldrich & Feng, 1999: 703; Misra, Raichur & Lan, 2003: 95; Videla et al., 2016: 91). Common to these studies is the use of an ultrasonication preconditioning step before flotation by either submerging the mineral slurry directly into an ultrasonication bath or placing a beaker containing the slurry into the bath. This method resulted in significant recovery improvements which was commonly attributed to the cleaning of either fine or oxidized particles which facilitated the adsorption of the collector.

The ultrasonic vibroacoustic waves emanating from ultrasonic transducers generate bubbles due to a pressure drop in each wave cycle, known as acoustic cavitation. At the initial stages of ultrasonication, the bubbles oscillate along waves, but soon deviate from this regime after a few wave cycles, as outlined by Videla et al. (2016: 90). Under immense elevated pressure due to the difficulty in bubble expansion under compressing inertial forces, the bubbles collapse which generates a microjet of fluid near the surfaces of minerals. This force can remove fine particles or other contaminants from the mineral surface. Slurries can be ultrasonicated either within an ultrasonication bath, where ultrasonic waves emanate from transducers that are positioned at the bottom of the bath, or by the insertion of a probe placed into the slurry, where waves emanate from the horn tip. Schematics of laboratory ultrasonic bath and probe equipment are illustrated in Figure 2.13 (Mason, 2003: 99). Probes are very useful for ultrasonicating ores at high power (e.g. 500 W) and intensities (e.g. 0.5 to 2 kW/cm^2), but this is only effective at small slurry volumes (50 to 200 ml), whereas baths can accommodate larger slurry volumes, but the intensities of baths are often low.

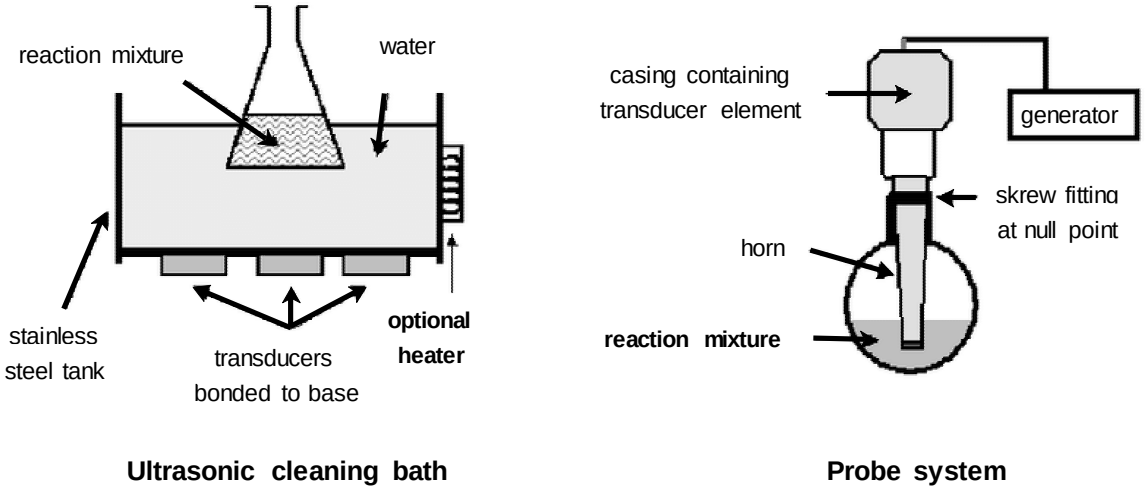

Figure 2.13: Schematic diagrams of common laboratory ultrasonic equipment, modified from Mason (2003: 99).

Most of the studies made use of an ultrasonic bath, but the use of probes has also been documented in flotation studies (Feng & Aldrich, 2004: 4423; Chen et al., 2020: 5; Hassanzadeh et al., 2021: 5). Hydrodynamic cavitation devices (HCDs), which use nano-bubbles and microbubbles to float fines and ultra-fines, have found commercial applications in recent years (Oliveira, Azevedo & Rubio, 2018; Ross, Singh & Pillay, 2019). The Mach HCD reactor is a device that can aid the removal of surface oxidation and slime coatings from valuable mineral surfaces by exposing the feed to intensive inter-particle attritioners (Ross, Singh & Pillay, 2019: 138). The use of this device has shown great promise in improving the selectivity of PGM recovery at South Africa PGE operations (Ross, Singh & Pillay, 2019: 138).

In Section 2.4.1, it was highlighted that SS is effective at removing slime coatings from the surfaces of valuable minerals by inducing an electrostatic repulsion between the valuable minerals and slimes. However, other reagents such as CMC have also been used to disperse MgO-bearing slimes from the surfaces of BMS (Edwards, Kipkie & Agar, 1980: 37; Wellham, Elber & Yan, 1992: 389; Pietrobon et al., 1997: 779; Bremmell, Fornasiero & Ralston, 2005: 209). Using CMC was found to remove surface slime coatings from pentlandite by modifying the surface charge of serpentine slimes (Edwards, Kipkie & Agar, 1980: 37). Common to these studies is the ability of CMC to mitigate slimes and improve pentlandite recovery. For example, Bremmell, Fornasiero and Ralston (2005: 209) reported the pentlandite recovery to be enhanced by as much as 15% in the presence of lizardite and CMC. This corresponded with a change in serpentine's zeta potential from positive to negative values and the confirmation that a repulsive force between the minerals occurred between pentlandite and lizardite in the presence of CMC, as determined by zeta potential and DLVO interaction energy calculations, respectively.

2.4.2. Rheology issues

An introduction to rheology

Rheology is the study of the flow behaviour of complex multiphase fluids. Rheological parameters, such as yield stress and apparent viscosity, is measured experimentally by measuring the shear stress at pre-defined shear rates within a device typically referred to as a rheometer or viscometer. The resulting plot often referred to as a "rheogram" or "flow curve" is then used to determine common rheological parameters such as yield stress and apparent viscosity. Yield stress is the y-intercept of the rheogram which is at a zero-shear rate, whereas the apparent viscosity is the slope of the line (for straight line rheograms) or the slope of the straight line that is tangent to the curve at a particular value of shear rate (for curved rheograms). Yield stress and apparent viscosity define the flow characteristics of the fluid which are directly related to the degree of particle aggregation. Suspensions can show either Newtonian or non-Newtonian behaviour, where non-Newtonian behaviour includes plastic, Bingham plastic, Pseudo plastic and dilatant behaviour, as illustrated in Figure 2.14 (Farrokhpay, 2012: 273). Most mineral slurries exhibit non-Newtonian behaviour. Newtonian behaviour is characterised by a linear increase in shear stress as a function of shear rate indicating a constant viscosity throughout the entire shear range. For fluids

exhibiting non-Newtonian behaviour, the viscosity changes as a function shear rate. The viscosity of non-Newtonian fluids is usually referred to as the apparent viscosity and is usually determined with the use of a mathematical model.

The Bingham and Casson mathematical models are often applied to estimate the apparent viscosity or yield stress to support measurements performed at low shear rates (Khalili-Garakani et al., 2011: 257). The equations for these models are shown below:

Bingham Model:

$$\tau = \tau_B + \eta_{pl} D \qquad \textit{Equation 2.9}$$

Casson Model:

$$\tau^{\frac{1}{2}} = \tau_B{}^{\frac{1}{2}} + \left(\eta_{pl} D\right)^{\frac{1}{2}} \qquad \textit{Equation 2.10}$$

Where 'η_{pl}' is the plastic viscosity, 'D' is the shear rate, 'τ_B' is the yield stress, and 'τ' is the shear stress.

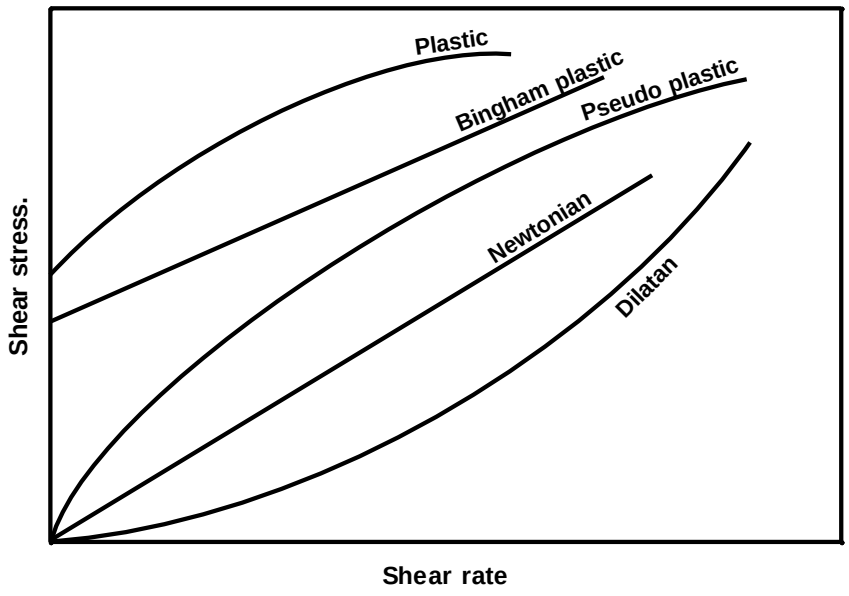

Figure 2.14: Schematic diagram of shear rate as a function of shear stress showing the characteristics of different fluids including Newtonian and non-Newtonian (plastic, Bingham plastic, pseudo plastic and Dilatan), modified from Farrokhpay (2012: 273).

Effect of rheology on flotation

An important factor impacting the rheology of a mineral suspension is the pulp solids concentration. Some investigations compare viscosity or yield stress in terms of solids concentrations, which is the concentration of solids by wt.% in the slurry, whereas others report this in terms of pulp density, which is the pulp mass: pulp volume ratio. Understanding these factors and the subsequent interactions within a typical flotation system will greatly improve the understanding of managing the flotation response of an ore. Ores containing phyllosilicate minerals can be termed 'rheologically complex' because of their propensity to higher pulp viscosities.

The apparent viscosity generally increases with increasing solids concentration which indicates that the slurry concentration within the flotation cell impacts the rheology (Bakker, Meyer & Deglon, 2009: 946; Mueller, Llewellin & Mader, 2010: 1216; Shabalala et al., 2011: 1449; Genovese, 2012: 5; Becker et al., 2013: 95; Ndlovu et al., 2014: 197). There is often a critical concentration point, known as the 'inflection point', after which the viscosity increases exponentially, and significant inter-particle interactions occur. The lower the concentration of solids at which the inflection point occurs, the more rheologically complex the pulp (Becker et al., 2013: 95). Minerals such as chrysotile have major consequences on the apparent viscosity and yield stress at low solids concentrations, whereas orthopyroxene and plagioclase had minimal influence on these parameters even at high concentrations (Becker et al., 2013: 96). This indicates that the type and concentration of minerals can have pronounced impacts on the rheological properties of a slurry (Becker et al., 2013: 96). Thus, it may be problematic for operators who intend to run their flotation circuits at high solids concentrations to improve plant throughput by accommodating high tonnages, reducing water consumption, and maximizing residence times.

Some studies have correlated increasing pulp densities to increasing recoveries (Sarghini, 1966: 140; Luo et al., 2016: 134). Common reasons for this are reduced turbulence, good selectivity, and a good chance of particle-particle and bubble-particle collision and adhesion. However, this depends on the ore system as many other investigators reported that lower pulp densities increased flotation kinetics and recovery (Mehrotra & Kapur, 1974: 217; Lins & Adamian, 1993: 273; Chen et al., 2017: 43). For a 1:1 sulphide ore to serpentine blend, the Cu and Ni recoveries improved significantly when the pulp density was lowered from 40- to 20 wt.% (Gao et al., 2018: 7). This was attributed to less friction between particle-particle and bubble-particle aggregates. Furthermore, the study found that an increase in pulp density increased the apparent viscosity, as illustrated in Figure 2.15. This was attributed to greater friction and deteriorated mobility in the pulp. This infers that operating at a lower solids concentration will correspond with a lower pulp viscosity. Some studies correlated rheology findings directly to flotation recoveries (Patra et al., 2012: 25; Zhang & Peng, 2015: 12; Chen et al., 2017: 44). These studies observed that mineral recoveries were reduced with increasing apparent viscosities or yield stresses. For example, Patra et al. (2012: 12) found that an increase in yield stress corresponded with a decreasing Cu recovery with the addition of chrysotile.

It was noted that increasing pulp viscosities or yield stresses resulted in reduced recoveries as cell hydrodynamics were impacted (Bakker, Meyer & Deglon, 2009: 949, 2010: 970; Shabalala et al., 2011: 1452). Therefore, a reduction in solids concentration can reduce the rheological complexity and improve recoveries.

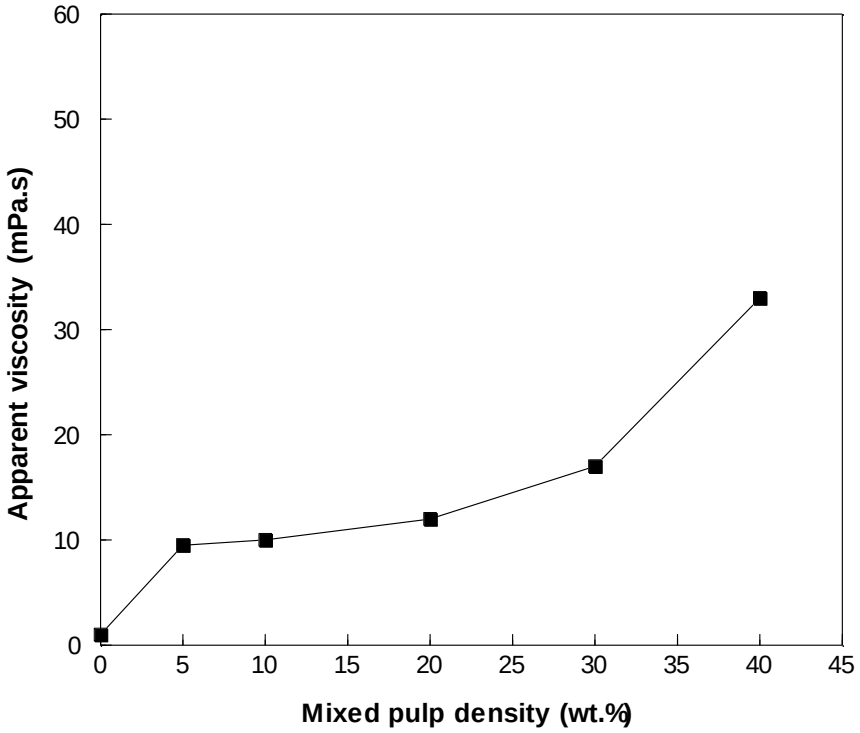

Figure 2.15: Apparent viscosity as a function of pulp density at the shear rate of 100 s^{-1}, modified from Gao et al. (2018: 6).

High yield stress slurries are known to form a 'cavern' around the impeller, which is characterised by mobile slurry in which the fluid is mixed or agitated, whereas the slurry surrounding the cavern remains stagnant and unmixed as the shear stress is not great enough to overcome the yield stress (Moore, Cossor & Baker, 1995: 2472; Wilkens et al., 2005: 5270; Bakker, Meyer & Deglon, 2010: 969). The cavern has local power intensities and small bubbles, but bubbles here rise directly overhead and gas dispersion throughout the cell is inhibited at an increased solids concentration. Reduced gas dispersion corresponds with reduced particle mobility, bubble-particle interactions, and bubble-particle mobility, which are all critical for enhanced recoveries. Bakker, Meyer and Deglon (2009: 949) demonstrated that velocity contours in a tank containing 60 wt.% slurry were confined to the impeller region, whereas the contours in water were detected throughout the cell. This indicates that the turbulent zone and gas dispersion is extremely inhibited at high solids concentrations, and is expected to be enhanced at lower solids concentrations (Bakker, Meyer & Deglon, 2009: 949; Shabalala et al., 2011: 1452). Since increasing solids concentrations are known to correspond with increased rheological complexity, authors have noted that increasing the pulp viscosity would decrease the turbulent energy dissipation (Schubert, 1999: 263). This is

detrimental for bubble-particle attachment in the bulk cell, as high energy dissipation rates are needed for attachment and ultimate recovery of valuable minerals. A lower solids concentration is, therefore, expected to expand the turbulent zone in the flotation cell, improve gas dispersion and enhance recoveries as particle mobility, bubble-particle interaction and bubble-particle mobility is improved.

Lower solids concentrations of the pulp have been observed to correspond with lower entrainment and improved grades (Gao et al., 2018: 8; Bahrami et al., 2019: 414). Gao et al. (2018: 8) observed that at the baseline condition (0 mg/L SHMP), a 40 wt.% pulp density resulted in a greater silicon recovery within a fine-grained serpentine-bearing ore compared to a lower pulp density. The silicon recovery was representative of serpentine in the synthetic ore which consisted of 50 wt.% sulphides and 50 wt.% serpentine. Fine-grained serpentine was, therefore, recovered more easily when the pulp density was higher compared to when it was lower. Other studies observed that particle entrainment increased with increasing pulp viscosity (Kirjavainen, 1992: 7; Chen et al., 2017: 45). For example, Chen et al. (2017: 45) found that as the concentration of amorphous silica increased up to 30 vol.%, so did the slurry viscosity and degree of entrainment. This can be attributed to a change in froth characteristics as an increase in entrainment hinders liquid drainage in the froth (Ata, Ahmed & Jameson, 2004: 901). Therefore, operating at a lower solids concentration and a lower pulp viscosity can reduce the recovery of minerals by entrainment.

Pulp viscosity has generally been found to increase with decreasing particle size, at a constant solids concentration, indicating that particle size has a significant impact on the pulp rheological behaviour (Kawatra & Eisele, 1988: 254; Zhou, Scales & Boger, 2001: 2913; Tangsathitkulchai, 2003: 42; Olhero & Ferreira, 2004: 73). The surface area which binds water molecules increased, thus the effective solids concentration also increased (Kawatra & Eisele, 1988: 254). Electroviscous effects are more important for finer particles as the effective volume fraction is increased due to the larger double layer for smaller particles and that there is a larger extension of the double layer interaction due to a shorter particle mean distance (Zhou, Scales & Boger, 2001: 2913). Shear thickening behaviour and particle aggregation are other consequences of fine particles in the pulp (Mueller, Llewellin & Mader, 2010: 1223). Schubert (1999: 263) demonstrated that in pulps containing fine minerals, the local energy dissipation rate can be increased by adding a dispersant.

Effect of phyllosilicates and particle interactions on rheology

The dominance of certain phyllosilicates can greatly impact rheology based on their morphology or shape, surface charge, or concentration (Ndlovu et al., 2011: 1319; Becker et al., 2013: 96; Ndlovu et al., 2014: 197; Zhang & Peng, 2015: 12). According to a proposed phyllosilicate mineral classification, suspensions containing chrysotile, which has a fibrous morphology, will result in a high yield stress and viscosity, whereas non-phyllosilicates such as quartz have the least impact on pulp rheology (Ndlovu et al., 2011: 1320). This correlates with studies that demonstrated that rod and platy morphologies have greater

impacts on the rheological complexity than minerals of spherical shapes, where its effect on rheology typically decreases in the order of rods, plates, grains and spheres (Collins, Napier-Munn & Sciarone, 1974: 105; Burdukova et al., 2008: 2175; Ndlovu, 2013: 176). Orthopyroxene and plagioclase have minor influences on pulp rheology between a concentration of 5- and 40 vol.% and this was mainly explained by their stubby and tabular shape. The platy minerals talc and vermiculite, on the other hand, significantly increased the apparent viscosity and yield stress of the fluid (Becker et al., 2013: 96).

Lizardite has rarely been the focus of a rheology study within minerals processing. A few studies interested in lizardite shear deformation determined the shear stress of lizardite as a function of normal stress (Reinen, Weeks & Tullis, 1994: 327; Behnsen & Faulkner, 2012: 54; Viti et al., 2018: 5). The studies agreed that shear stress increased with normal stress and the trend was found to be similar to kaolinite and illite (Behnsen & Faulkner, 2012: 54). In other areas of research, as shown previously, the effect of lizardite is well established. On the other hand, the effects of talc on rheology have received much attention, especially since low concentrations of talc are known to have a strong impact on the rheological properties of suspensions (Burdukova et al., 2008: 2172; Becker et al., 2013: 96).

Phyllosilicates are typically anisotropic which indicates that they have different basal face and edge plane charges which are commonly indicated by differences in their i.e.p and p.z.c values, as previously mentioned (Alvarez-Silva et al., 2010: 407, 2010: 385; Ndlovu et al., 2011: 1318; Ndlovu, 2013: 111). The charge signs and magnitude on these surfaces are dependent on pH, salt type and concentration of the solution in which the phyllosilicate is present. Charges may arise from either an isomorphic substitution, lattice defects or incongruent dissolution. For example, the overall positive charge on lizardite is suggested to be due to incongruent dissolution and not due to isomorphic substitution which would otherwise have caused a proton deficiency in the outer tetrahedral layer, as previously mentioned (Feng et al., 2013: 1125). Gillery (1959: 147) confirmed that the octahedral basal plane of lizardite was positively charged, and the tetrahedral layer was negatively charged which is exposed at the edge after comminution. Edges are typically smaller than faces which is indicative of phyllosilicates having a higher lateral extent (Johnson, Russell & Scales, 1998: 128). The charge of the greatest surface area, which is generally positive for lizardite, largely contributed to the overall positive charge as indicated by zeta potential measurements at pH values below the i.e.p (Feng et al., 2013: 1125; Feng, Lu & Luo, 2015: 4; Lu et al., 2019: 38). As mentioned in Section 2.1.2, talc is also anisotropic, where the basal plane of talc has been determined to be negatively charged for New York talc, whereas the edge charge is pH-dependent.

Due to the anisotropic nature of phyllosilicates, they can form low-density aggregates known as "house of cards" configurations (Luckham & Rossi, 1999: 56). There are three modes of particle interactions which are face-face (FF), edge-face (EF), and edge-edge (EE). The EF and EE association leads to 3D house of cards structures which can lead to rheologically complex suspensions, as demonstrated in Figure 2.16. The FF association results in lamellar aggregate structures and these have low yield stresses. The aggregation or

flocculation of the same mineral type are referred to as "homo-aggregation". The likelihood of homo-aggregates can be estimated by considering the p.z.c and the i.e.p of minerals, and the charge of the face and edge surfaces at specific pH's.

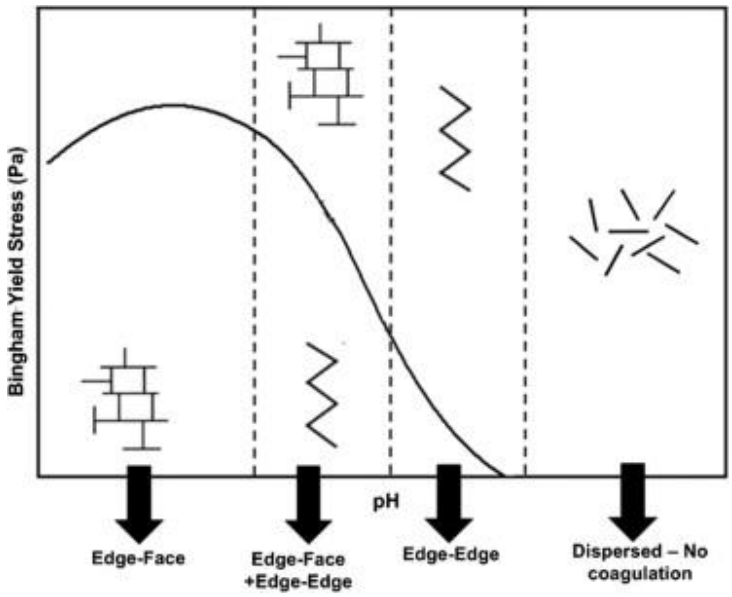

Figure 2.16: Schematic illustrating the effect of pH on the Bingham yield stress with regards to the particle association in a layered clay mineral, modified from Rand and Melton (1977: 310) in Ndlovu et al. (2011: 58).

Increasing divergence in the p.z.c and i.e.p values indicates that the mineral increasingly deviates from isotropic behaviour, with the same p.z.c and i.e.p values being indicative of mineral isotropy. In addition, a higher p.z.c value compared to the i.e.p indicates that the face carries a negative charge. Moreover, a lower p.z.c compared to the pH of interest indicates that the overall charge of the mineral is negative, whereas a higher p.z.c is indicative of an overall positive charge (Ndlovu et al., 2011: 1319, 2014: 196). For lizardite, i.e.p values, as determined by zeta potential, are typically between pH 9 and 12, whereas the p.z.c values, as determined by potentiometric titration have been reported to be around pH 4.3 (Alvarez-Silva, Mirnezami, et al., 2010: 407; Alvarez-Silva, Uribe-salas, et al., 2010: 387; Feng, Lu, Feng & Li, 2012: 12093; Feng et al., 2013: 1125; Feng, Lu & Luo, 2015: 4; Lu et al., 2019: 38). However, the values for the lizardite p.z.c reported by Alvarez-Silva et al. (2010: 407, 2010: 387) are much lower than what is typically expected for lizardite, because the zeta potential of lizardite at pH 9 has been reported to be positive (Feng et al., 2012: 12093; Feng, Lu & Luo, 2015: 4), and the p.z.c is much lower (around 4.3) compared to pH 9, which otherwise indicates that the overall charge should have been negative. The i.e.p values for lizardite in the studies by Alvarez-Silva et al. (2010: 407, 2010: 388), have been reported to be 3.3 to 4.0, which are much lower compared to the i.e.p values for lizardite in other studies, as mentioned. This indicates that the p.z.c information in the Alvarez-Silva et al. (2010: 407, 2010: 387) studies cannot be used in the interpretation of results in this work, due to the large discrepancies in the i.e.p values to that reported in other work. Knowing that the overall charge of lizardite at pH 9 is positive, it can be assumed that the

p.z.c of lizardite is above 9, but below the value of the i.e.p because the basal plane of lizardite is known to be positively charged (Gillery, 1959: 147). In the case of New York talc, the i.e.p has been measured to be between 2.2 and 2.5, whereas the p.z.c, as determined by potentiometric titration, is between 7.7 and 8.4, which corresponds with a negatively charged basal plane of talc (Burdukova et al., 2007: 341; Ndlovu et al., 2014: 194).

Considering pH 9, which is the pH at which flotation processes are commonly operated, studies have estimated that p.z.c values close to the pH of interest indicate that both positive and negative charges are present and would result in homo- aggregation, whereas p.z.c values very dissimilar to the pH of interest will indicate that it is less likely for both positive and negative charges to occur (Ndlovu et al., 2011: 1319). In the study conducted by Ndlovu et al. (2011: 1319), pH 9 was found to be very different to the p.z.c of muscovite, which occurs at pH 4.6. It is, therefore, less likely for muscovite particles to contain both positive and negative charges, and if these opposite charges do exist on muscovite, this difference would be small due to fairly similar i.e.p (at pH 5.6) and p.z.c values of muscovite (Ndlovu et al., 2011: 1318). Due to this, and knowing that the overall charge of muscovite is negatively charged as determined by a comparison of the p.z.c and pH 9 in Ndlovu et al. (2011: 1319), the possible modes of muscovite particle interaction at pH 9 would be i) particle dispersion due to negative face and edge charges which would result in a very low yield stress, ii) EE aggregation due to near neutral edge charges and weakly negative face charges, which would result in low yield stresses, and iii) both dispersion and EE aggregation due to low heterogeneity of muscovite, which is expected to result in very low yield stresses (Ndlovu et al., 2011: 1319). For talc, pH 9 is close to the estimated p.z.c values reported in the literature (7.7 to 8.4), which indicates that there is a close balance between positive and negative charges of faces and edges on the surfaces of talc, which is likely to result in a combination of both EE and EF aggregation (Burdukova et al., 2007: 341; Ndlovu et al., 2014: 196). The expected p.z.c of lizardite is also close to pH 9, which suggests that there will also be a close balance between positive and negative charges on the faces and edges of lizardite. However, unlike talc which has very different i.e.p and p.z.c values, these values are expected to be very similar for lizardite, which infers that it is likely that lizardite faces are weakly positive, or even be neutral. It is, therefore, likely for a combination of EE and EF aggregation to occur in the case of lizardite.

Numerous studies found serpentine able to aggregate with other silicate minerals which is known as hetero- aggregation. Hetero- aggregation between serpentine and other silicates such as quartz, olivine or pyroxenes can occur due to an electrostatic attraction between serpentine and the other silicates for most of the pH range (Feng, Feng & Lu, 2012: 13; Feng, Lu & Luo, 2015: 5; Yang et al., 2018: 4). At pH 9, it was found that the degree of hetero- aggregation between serpentine and the other silicates was the greatest, but this was very low at low and high pH extremes. Another study found serpentine-pyroxene and serpentine-olivine aggregates possible, but this was dependent on pH (Yang et al., 2018: 4). At pH 9,

the degree of hetero- aggregation for both serpentine-pyroxene and serpentine-olivine was high, but this was very low at higher pH's. This corresponded with zeta potential measurements and DLVO calculations which revealed that pyroxene and olivine zeta potentials were smaller than -30 mV at pH 9, which had an electrostatic attraction to positively charged serpentine, and that this attraction was diminished at pH 11 on account of their same charges and repulsive energies.

Knowing how phyllosilicates and their interactions impact rheology, it is important to consider how SS impacts rheology. Sodium silicate was able to lower the viscosity of suspensions in some rheology investigations (Andreola et al., 2006: 1108; Amorós et al., 2010: 37; Zhang, Chen & Liu, 2017: 9; Xia et al., 2018: 2906). In one such study, the shear stress was found to rapidly increase with increasing shear rate at a low SS dosage, which was attributed to the formation of house of cards structures due to the electrostatic attraction between edge and face charges of kaolinite (Figure 2.17). However, at a higher dosage, the adsorption of SS species changed edge and basal plane charges from slightly positive to negative values at pH 6.2 which allowed substantially lower shear stresses with increasing shear rates to be measured (Amorós et al., 2010: 38). In another study, the hetero- aggregation between fluorite and quartz became weakened with an increasing SS modulus, as reflected by a reduction in shear yield stress (Zhang, Chen & Liu, 2017: 9). This indicates that particles of similar charges approaching each other will experience an increasing repulsive force due to the extension of the double layer. These studies demonstrate that SS can reduce the rheological complexity of a suspension on the basis that it disperses aggregates.

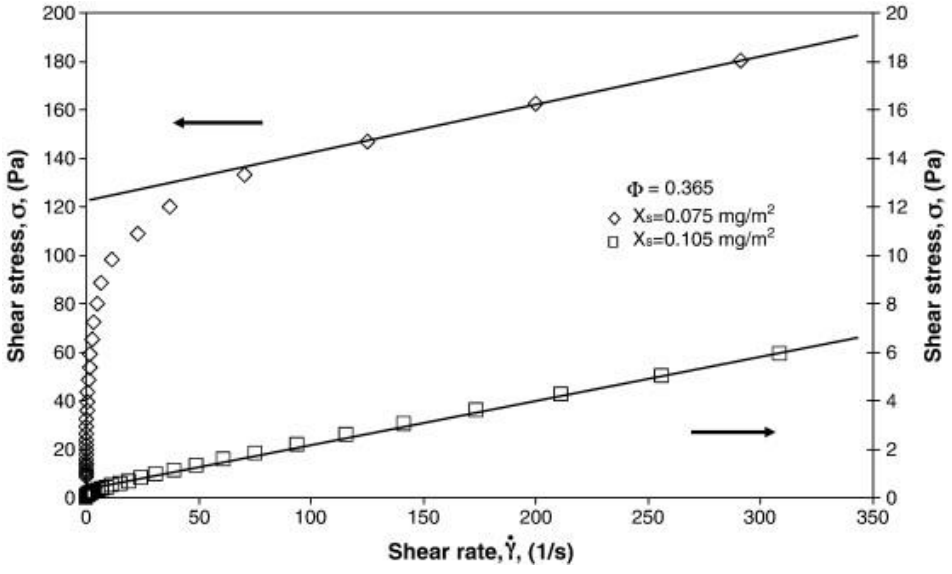

Figure 2.17: Bingham plot for suspensions at volume fraction ϕ = 0.365. Effect of sodium silicate (denoted 'X_s' in the study) addition, taken from Amorós et al. (2010: 38).

2.4.3. Gangue recovery and mitigating strategies

Effect of talc recovery and depression during flotation

Talc has a disproportionate effect on the flotation process as even low quantities of its recovery relative to the feed mass can reduce grade due to the recovery of liberated or composite talc particles, or it can stabilize the froth which leads to increased recovery of entrained gangue (Wiese, Harris & Bradshaw, 2008: 480; Becker, Wiese & Ramonotsi, 2014: 27). Microflotation studies performed on pure talc demonstrated that talc recovery without depressant addition was high and its recovery was unaffected by a change in pH (Beattie et al., 2006a: 245, b: 601; Feng et al., 2012: 70). This is due to talc's natural hydrophobicity, as mentioned in Section 2.1.2. For example, Feng et al. (2012: 70) found the talc recovery to be approximately 90% at all pH's. Other studies recognized that due to talc's natural hydrophobicity, it can enter the froth ahead of slower floating minerals, stabilize the froth, increase the quantity of recovered solids and, therefore, decrease concentrate grade (Wiese, Harris & Bradshaw, 2010: 1012; Farrokhpay, Ndlovu & Bradshaw, 2018: 273). These studies demonstrated that talc's recovery could have serious consequences on concentrate grades and the use of depressants is critically needed to depress talc in order to improve concentrate grades.

The polymers CMC, guar gum and starches, which differ in molecular structure, chemical composition, molecular weight and charges, have commonly been investigated as talc depressants at varying reagent dosages, molecular weights or degrees of substitution (Laskowski, Liu & Connor, 2007: 60; McFadzean et al., 2011: 465). All depressants significantly depressed talc and have also been observed to correlate with an improvement in concentrate grade (Shortridge et al., 2000: 222; Wiese, Harris & Bradshaw, 2008: 474; Becker, Wiese & Ramonotsi, 2014: 27). In one such study, low molecular weight CMC and guar gum were found to reduce the quantity of floatable gangue (by 19 g at 100 g/t CMC), which became increasingly reduced with increasing dosages (Wiese, Harris & Bradshaw, 2008: 475). Studies have also demonstrated that increasing depressant dosages, and reducing talc recovery, reduced the quantity of recovered solids (Beattie et al., 2006a: 245). This indicates that depressants can depress talc and improve concentrate grade.

Mineralogical studies found that composite talc-orthopyroxene particles mainly constituted NFG in the Merensky reef (Lotter et al., 2008: 907; Becker et al., 2009: 251; Jasieniak & Smart, 2009: 175). The association between talc and orthopyroxene usually manifests as talc rims on orthopyroxene particles, sometimes referred to as rimming, where these talc rims impart naturally floating behaviour to the orthopyroxene, even at low concentrations of talc (Lotter et al., 2008: 907; Becker et al., 2009: 254). In Becker et al. (2009: 248), the absence of guar gum recovered a significantly greater quantity of orthopyroxene and talc (>19 g and 4.3 g, respectively) from the 1 kg feed compared to the addition of depressant (<0.8 g and 0.1 g for orthopyroxene and talc, respectively), which demonstrates the importance of depressant addition during flotation. Both liberated and unliberated talc are able to report to the concentrate. This indicates that the recovery of composite talc-orthopyroxene particles without a suitable

depressant can greatly increase the recovery of overall MgO on account of talc's natural hydrophobicity. The term 'naturally floating gangue' is usually given to these minerals in magmatic Ni-Cu ores due to their natural hydrophobic nature.

It is well documented that depressants such as CMC and guar gum can reduce talc recovery; however, the use of SS as a talc depressant has rarely been studied. The depressant behaviour of SS is well established in the context of silicate minerals (Irannajad, Ejtemaei & Gharabaghi, 2009: 770; Silva et al., 2012: 209; Arantes & Lima, 2013: 158). A study by Irannajad, Ejtemaei and Gharabaghi (2009: 770) highlighted a reduction in quartz recovery of nearly 28% with an increase in SS dosage from 0 g/t to 2000 g/t SS at a pH of 11. A study by Witney and Yan (1997: 147) demonstrated the ability of SS to improve nickel grade, using a nickel sulphide ore containing NFG, while the MgO grade remained unaffected. In the study, MgO was representative of a few Mg-bearing silicates including 26.6 wt.% talc. This study demonstrated an increase in Ni grade from 8.5% to 9.5% at increasing SS dosages from 500 g/t to 1000 g/t SS, while the MgO grade at the same dosage range remained the same (12%). However, the study by Witney and Yan (1997: 147) only demonstrated this in an image and did not interpret the results. The MgO results infer that SS did not depress talc in this dosage range, however, this cannot be confirmed because the MgO assay represented various other minerals in addition to talc and many other factors, such as entrainment, could have impacted the MgO grade. It is therefore unclear whether SS can be used to depress talc.

Silva et al. (2012: 210) demonstrated that the adsorption of the monomeric $Si(OH)_4$ species depressed quartz between pH 5 and 8. This was attributed to the sharing of electron pairs between silicon sites on the surfaces of quartz and oxygen sites of the $Si(OH)_4$ species. However, contrary to findings by Irannajad, Ejtemaei and Gharabaghi (2009: 770), the depression effect of SS was absent at a high pH due to the strong electrostatic repulsion between quartz and SS. Other studies have also confirmed the adsorption of $Si(OH)_4$ directly onto the surfaces of minerals below pH 10, but the direct adsorption of SS diminished above pH 10 (Furlong, Sing & Parfitt, 1979: 415; Phair, Van Deventer & Smith, 2001: 151). It is suggested that talc will respond similarly to quartz because both quartz and the basal plane of talc have similar structures, and both minerals have very low negative zeta potentials at alkaline pH's: approximately -70 mV for quartz and approximately -30 mV for talc (Fuerstenau, Lopez-Valdivieso & Fuerstenau, 1988: 164; Martinovic, Bradshaw & Harris, 2005: 152; Feng, Lu & Luo, 2015: 4). Since SS at high dosages can adjust the pH to high alkaline values, it is important to recognize whether SS can depress talc at high pH. Irannajad, Ejtemaei and Gharabaghi (2009: 770) demonstrated that both concentration and pH need to be high (<1500 g/t SS and around pH 11) to effectively depress quartz. Low dosages, even when the pH is high, is insufficient for quartz depression.

The influence of cations on depressant adsorption

Bridging polyvalent cations, such as Zn^{2+}, Al^{3+}, $Mg^{2+,}$ and Ca^{2+}, have previously been found to enhance the adsorption of depressants such as CMC and guar gum onto talc, as well as the adsorption of SS onto silicate minerals (Liu & Laskowski, 1989: 105; Bogusz et al., 1997: 443; Parolis, Groenmeyer & Harris, 2005: 13; Manono, Corin & Wiese, 2012: 234, 2019: 220, 2020; Tohry & Dehghani, 2016: 31; O'Connor et al., 2018: 6). This is because polyvalent cations have been observed to significantly lower the magnitude of talc's zeta potential (-18 mV at pH 9 in a 10^{-2} M KNO_3 electrolyte solution), which improved the adsorption of depressants onto talc and quartz (Feng et al., 2012: 69). The adsorption of polysaccharides onto talc in the presence of metal hydroxyl species, which occur at high pH's, occurs via a bridging cation mechanism (Laskowski, Liu & Connor, 2007: 66; Liu et al., 2015: 43, 2019: 26). In a study performed by Tohry and Dehghani (2016: 31), polyvalent cations enhanced the depression of quartz at an alkaline pH in SS solutions. The SS-$CaCl_2{\cdot}2H_2O$ mixture was more effective at depressing quartz, which was followed by the SS-$MgCl_2{\cdot}6H_2O$ mixture. This was attributed to the ability of the cations to activate the quartz surface, as similarly observed in other investigations (e.g. Ye & Matsuoka, 1993: 133). These divalent cation metal hydroxyl species served as bridging cations between SS and quartz and, therefore, can potentially serve as bridging cations between SS and talc. Moreover, SS is known to interact with Ca^{2+} and Mg^{2+} as adsorption studies have previously observed the interaction between SS and calcite or serpentine, respectively (Feng et al, 2012: 12092; Chen et al., 2019: 352).

Previous work indicated that divalent cations are much better at depressing talc than monovalent cations, such as K^+ and Na^+, in depressant solutions (Parolis, Groenmeyer & Harris, 2005: 13; Manono, Corin & Wiese, 2019: 223). Monovalent cations have been correlated with slower settling times, less positive zeta potentials, lower concentrations of CMC adsorption, higher talc recoveries, and ultimately lower concentrate grades, compared to using divalent cations (Parolis, Groenmeyer & Harris, 2005: 13; Parolis et al., 2008: 111; Manono, Corin & Wiese, 2019: 220, 2020: 5). This is because monovalent cations have insufficient charge suppression to overcome the repulsion between anionic depressants and the negative charge of talc to allow sufficient adsorption of the depressants (Parolis et al., 2008: 111). This suggests that the Na^+ dissolved into solution when SS is added may play either a minor or no role in enhancing talc's depression with SS. An absence of SS's depressant effect at high pH's infers that the Na^+ dissolved into solution when SS was added did not serve as bridging cations for SS adsorption onto quartz, and is, therefore, not expected to serve as bridging cations in the case of talc.

Although various authors determined the influence of cations individually, others determined the influence of multiple cations on talc depression in the presence of depressants (Manono, Corin & Wiese, 2012: 234, 2019: 220). During froth flotation at plant scale, salts containing divalent and monovalent cations can be sourced from the interaction between water and the ore (e.g. dissolution) and introduced by residual reagents. A source of cations commonly added to laboratory-scale batch flotation experiments, to

mimic these cation concentrations in solution, are synthetic plant water salts. Some studies determined how synthetic plant water impacts talc recovery (Manono, Corin & Wiese, 2012: 234, 2019: 220). Using synthetic plant water obtained a lower talc recovery compared to using Na^+ in CMC solutions (Manono, Corin & Wiese, 2019: 221). The synthetic plant water experiment corresponded with higher talc settling rates and slightly less negative talc zeta potentials compared to using Na^+, although the adsorption of depressant using synthetic plant water was lower than using Na^+ (Manono, Corin & Wiese, 2012: 234, 2019: 220). This suggests that the synthetic plant water present in the flotation system may serve as bridging cations to improve the adsorption of depressants onto talc, and importantly the adsorption of SS onto talc.

Studies demonstrated that with decreasing pH, increasing concentrations of Mg^{2+} dissolved from talc's lattice, which can re-adsorb onto the basal plane of talc as $Mg(OH)_2$ species at alkaline pH's (Bremmell & Addai-Mensah, 2005: 388; Liu et al., 2019: 26). The concentration of Mg^{2+} ions dissolved into solution from 15- and 45 wt.% suspensions are illustrated in Figure 2.18. This indicates that Mg^{2+} ions are able to dissolve from talc into solution, which is significant at pH up to 8.5. Liu et al. (2019: 24) studied the depression of talc at various acid/base pH's in the presence of various CMC dosages by microflotation, adsorption density and zeta potential measurements. Increasing the pulp pH from natural (pH 7.5) to pH 12 and thereafter to pH 8.5 reduced the recovery of talc by 40% at 60 mg/L, as CMC was able to adsorb onto talc. A similar result was obtained when the pH was adjusted from natural to pH 8.5. The biggest talc depression occurred when the pulp was adjusted from neutral to pH 4 and then up to pH 8.5, which reduced talc recovery by 70% due to a greater adsorption affinity of the CMC onto talc. According to the

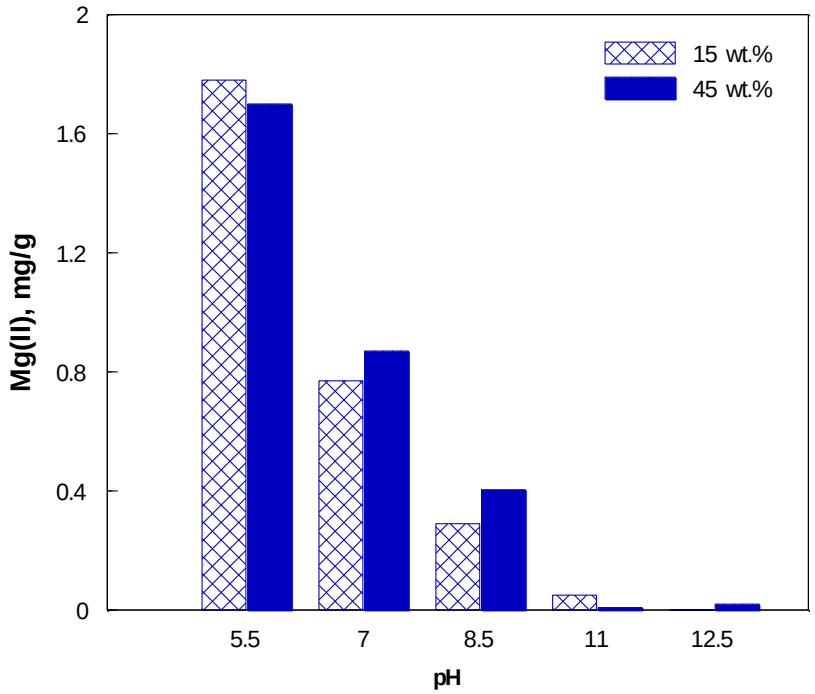

Figure 2.18: Concentration of Mg^{2+} ions dissolved into solution from 15 and 45 wt.% talc suspensions as a function of pH, measured with ICP-OES, modified from Bremmel and Addai-Mensah (2005: 388).

Mg ion species diagram, Mg^{2+} dominate in solution below approximately pH 10 and $Mg(OH)_2$ dominate above approximately pH 10 (Liu et al., 2015: 43, 2019: 26) This indicates that Mg^{2+} dissolution below approximately pH 10 will re-adsorb onto talc's surface as hydrolysis $Mg(OH)_2$ species by electrostatic attraction once the pH is raised above pH 10, which will allow better adsorption of CMC (Bremmell & Addai-Mensah, 2005: 388; Liu et al., 2019: 26). This indicates that Mg^{2+} ions dissolved into solution can serve as bridging cations when $Mg(OH)_2$ species are re-adsorbed onto the basal planes of talc at high pH's.

Effect of talc on froth stability and entrainment

Talc is fast-floating and enters the froth ahead of slower-floating valuable minerals. There it has been reported to stabilize the froth and increase gangue entrainment, which will inevitably lower concentrate grades (Wiese, Harris & Bradshaw, 2010: 1012; Farrokhpay, Ndlovu & Bradshaw, 2018: 273). Section 2.2.3 described that the highest froth stability is obtained for moderately hydrophobic particles which have a contact angle of about 60°. Talc's contact angle falls in the moderately hydrophobic range as it is typically between 50° and 74° (Douillard et al., 2002: 347; Ata, Ahmed & Jameson, 2003: 263; Choi et al., 2020: 3). This indicates that its recovery can greatly stabilize the froth. Farrokhpay, Ndlovu and Bradshaw (2018: 273) demonstrated that the froth half-life was 7- and 35 seconds when 0% and 7% talc was used, respectively. This indicates that the presence of talc stabilized the froth which corresponded with a reduction in copper grade from approximately 19% without added talc to approximately 2% when 7% talc was used. Wiese, Harris and Bradshaw (2010: 1013) observed that without the addition of a depressant, NFG contents as high as 6% to 8% can be recovered during batch flotation experiments. The quantity of talc in the ore was about 1.2% (Wiese, Harris & Bradshaw, 2005b: 190). This demonstrates that large quantities of talc can enter the froth and have a major impact on the froth characteristics. Photographs of the froth at various talc concentrations showed that increasing the talc content resulted in a dull, sticky froth due to the attachment of particles in the bubble lamellae (Farrokhpay, Ndlovu & Bradshaw, 2018: 274). This indicates that the recovery of NFG can stabilize the froth and increase the recovery of minerals by entrainment.

The recovery of minerals by entrainment was effectively reduced with the use of depressants (Wiese, Harris & Bradshaw, 2010: 1017). The addition of CMC or guar gum depressed talc, which reduced the froth stability and lowered the quantities of recovered solids and water. This indicates that using depressants can substantially improve concentrate grades by not only depressing talc, but by lowering the recovery of entrained minerals.

2.5. Critical synthesis

A schematic showing the effect of no added SS and added SS on the three major problems in altered ores is illustrated in Figure 2.19. The presence of phyllosilicate alteration minerals is known to have a

detrimental effect on flotation for three distinct reasons. Firstly, due to the difference in surface charge, phyllosilicate minerals can coat the surface of valuable minerals, defined as slime coating, which hinders collector adsorption and bubble-particle interactions, as illustrated in Figure 2.19(a). Secondly, it is well documented that phyllosilicate minerals form aggregates and significantly alter the flow behaviour of the slurry leading to poor gas dispersion and a decrease in bubble-particle collection efficiency, as illustrated in Figure 2.19(b). Lastly, NFG such as talc are commonly associated with major minerals such as orthopyroxene. The recovery of such talc composite particles can significantly decrease the concentrate grade, as illustrated by the schematic in Figure 2.19(c). A suitable SS dosage and pH is expected to combat the three challenges mentioned by adsorbing onto phyllosilicate slimes and creating an electrostatic repulsion between the slimes and PGMs, as illustrated in Figure 2.19(d). Secondly, SS will disperse aggregates which will improve gas dispersion and increase bubble-particle collection efficiency, as illustrated in Figure 2.19(e). Lastly, SS will depress talc which will not only depress talc, but other gangue minerals in the pulp, as illustrated in Figure 2.19(f).

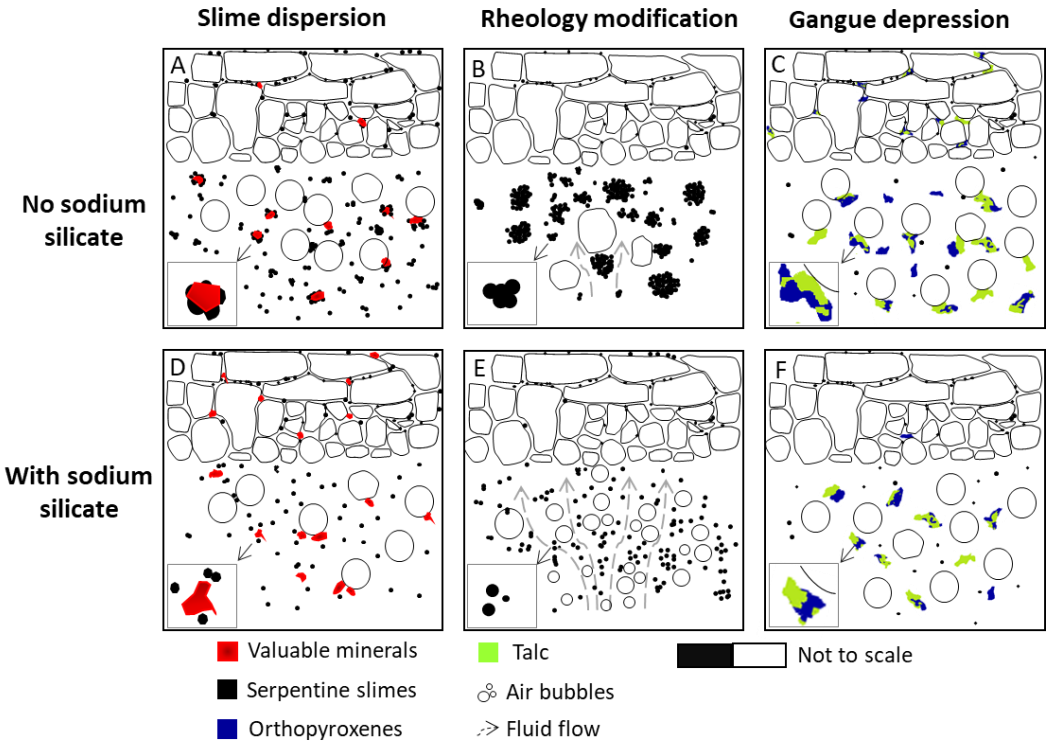

Figure 2.19: Effect of no added SS (A to C) and added SS at suitable conditions (D to F) on the three major problems in altered ores.

2.6. Hypotheses

Based on the critical review of the literature, the following three hypotheses relating to SS's dispersant, rheology modifying, and depressant effects are proposed:

Hypothesis one:

Sodium metasilicate will act as a dispersant and remove surface phyllosilicate slime coatings from PGMs and BMS by adsorbing onto the phyllosilicate slime particles, thus creating an electrostatic repulsion between PGMs/BMS and slimes.

Hypothesis two:

Sodium metasilicate will reduce the viscosity and yield stress of the pulp because its rheology modifying effect will disperse aggregated phyllosilicate alteration minerals in the pulp which will result in better gas dispersion and bubble-particle collisions and therefore improve flotation recoveries.

Hypothesis three:

Sodium metasilicate will depress talc because anionic SS species will adsorb onto talc. The depression of talc, especially when occurring in composite particles, will improve PGE concentrate grade.

2.7. Key questions

The following key questions have been formulated to test hypotheses 1 to 3:

1. **How does the *dispersant* effect of SS improve PGE *recovery*, and how can this knowledge be utilized to provide an optimum PGE *recovery*?**
    - How are the recovery of PGEs influenced by SS addition?
    - How are the floatability of PGMs (proxy) and BMS influenced by the presence of slimes and SS addition?
    - How are the zeta potentials of PGMs (proxy), BMS and slimes influenced by SS addition?
    - How are the recoveries of PGEs affected by the addition of CMC, and ultrasonication which are known chemical and mechanical methods of slime dispersions? How does this compare to SS?
    - How does pH influence PGE recovery?
2. **How does the *rheology modifying* effect of SS improve PGE *recovery,* and how can this knowledge be utilized to provide an optimum PGE *recovery* ?**

- How does solids concentration impact PGE recovery?
- How are the rheological properties of the slurry influenced by SS addition?
- How are particle settling rates effected by SS addition?

3. **How does the *depressant* effect of SS improve PGE *grade*, and how can this knowledge be utilized to provide an optimum PGE *grade*?**

    - How is concentrate PGE grade influenced by SS addition?
    - What are the mineralogy and texture chracteristics of talc in the feed and concentrate?
    - How is talc flotation impacted by SS addition?
    - How is froth stability impacted by SS addition?
    - How are the grade of PGEs in the concentrate affected by the addition of CMC, which is a chemical method known to depress talc? How does this compare to SS?
    - How does pH influence PGE concentrate grade?

Chapter 3: Materials and Methods

This section outlines the details of the materials and methods selected to achieve the main objectives of this work. Information relating to the ores and reagents used in this study and their preparation is given in Section 3.1. Section 3.2 focuses on information relating to the characterisation of the ores and single mineral samples. This is followed by the flotation experiments in Section 3.3 which includes information on the batch flotation and microflotation experiments. Details of the froth stability experiments are provided in Section 3.4. This is followed by information on the rheology measurements in Section 3.5, and finally the zeta potential information in Section 3.6.

3.1. Ores and reagents used

3.1.1. Ore information and preparation

Two PGE ores, each weighing approximately 400 kg, were sampled from the open pit at PPM for this study. Images of the mined ores at PPM are provided in Appendix B. Approximately 200 kg of each ore was used for this work and the rest was stored for future work. The mine is situated north-west of the Pilanesberg Alkaline Complex, on the farm Tuschenkomst in the North West Province of South Africa. The mine processes the 'Silicate reef' which is a local term used by the mine describing a blend of the lower Merensky reef, upper Pseudo reef, Pseudo reef and the lower Pseudo reef units. The mine also processes the UG2 chromitite reef, but this takes place in a separate processing stream. Both ores used in this work are Silicate reef ores - the first ore will be referred to as "Ore 1" and the second ore will be referred to as "Ore 2". Ore 1 was mined at a depth of 20 m and consists of less altered material with little Merensky reef, Pseudo reef unit and anorthosites, according to PPM terminology. Ore 2 was mined 500 m southwest of Ore 1 at a depth of 30 m. This ore constitutes mainly oxidized material with some dilution of dyke, Merensky reef footwall and unaltered silicates and is a slightly lower grade ore. At the time that this study commenced, Ore 1 was being actively mined at PPM, however, Ore 2 remained *in situ* due to its mineralogical complexity and low grade. Due to Ore 1 having a higher PGE grade and a lower mineralogical complexity compared to Ore 2, this ore would be the primary ore of investigation, whereas Ore 2 would only be used during selected experiments.

The mine processed the ores by pre-crushing them which was thereafter packaged into drums and sent off to the Centre for Minerals Research (CMR) at the University of Cape Town (UCT). Once the ores arrived at UCT, they were laid out to dry on drying pans for a week. The dried ores were then individually crushed to 100% passing 3 mm using a jaw crusher. The oversized fraction (+3 mm) was further jaw crushed until is passed through the 3 mm aperture screen. The ores were then manually blended using a spade and riffled to 30 kg samples. Each 30 kg sample was further riffled into two and finally split using a 10-way Dickie and Stockler rotary splitter to approximately 3.6 kg samples. The samples were bagged in

these masses as these were the required masses to obtain 35 wt.% solids during the 8 L batch flotation experiments. Calculations for these masses are provided in Appendix A.

A milling curve was produced with a targeted grind of 60% passing 75 μm on both ores. The grind was chosen as this was the primary grind at PPM at the time this project commenced, and the goal was to "mimic" a similar particle size distribution (PSD). Approximate 3.6 kg bags of each ore were milled for 20, 30, and 40 minutes using a 3 kg stainless steel rod mill. The mill was charged with 22 stainless steel rods, having the dimensions 6 × 25 mm, 8 × 20 mm and 6 × 16 mm, the ore sample and synthetic plant water to obtain a mill slurry density of 66 wt.%. The composition of the synthetic plant water is provided in Table 3.1 and calculations performed to determine the volume of synthetic plant water required for the milling experiments are shown in Appendix A. The synthetic plant water mimics the major ion concentrations to that found in industrial flotation concentrators treating PGE ores. The milled product was thereafter filtered, and a quarter of the milled cake wet screened through a 75 μm aperture screen. Both the +75 μm and -75 μm samples were dried and weighed, and a milling curve set up to determine the time required to obtain the targeted grind. The milling curves for both ores are provided in Figure 3.1. This demonstrates that both ores have similar milling curves and to obtain 60% passing 75 μm required 30 minutes of milling for both ores. The feeds are, therefore, likely to have similar PSDs after 30 minutes of grinding.

Table 3.1: Synthetic plant water salts used to make up the solution.

Inorganic salt	**Chemical formula**	**Concentration (g/L)**
Magnesium sulphate	$MgSO_4 \cdot 7H_2O$	0.615
Magnesium nitrate	$Mg(NO_3)_2 \cdot 6H_2O$	0.107
Calcium nitrate	$Ca(NO_3)_2 \cdot 4H_2O$	0.236
Calcium chloride	$CaCl_2$	0.147
Sodium chloride	NaCl	0.356
Sodium carbonate	Na_2CO_3	0.030

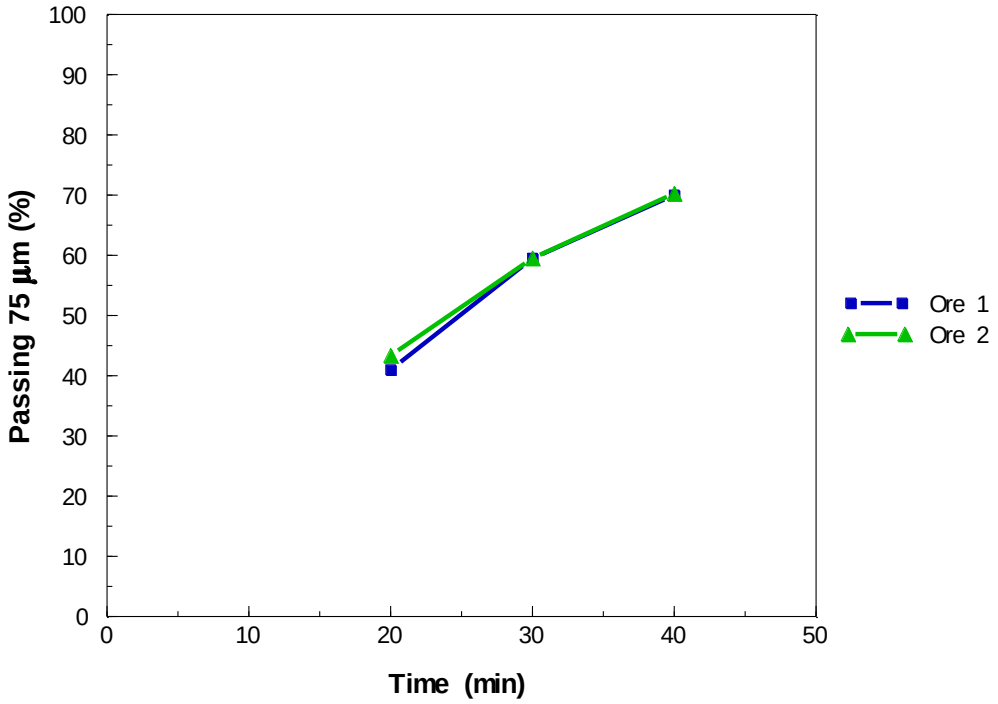

Figure 3.1: Milling curves for the ores used in this study to determine the required target grind to obtain 60% passing 75 µm.

3.1.2. Reagents

Information on the reagents used during the experiments are shown in Table 3.2. The collector, frother types and dosages, as indicated, were chosen as they closely resembled the reagent suite used on the primary rougher at PPM at the time the project commenced. The mine also trialed SS at a very low dosage at the time this study commenced. The SS used for this work is sodium metasilicate (modulus 1) which was provided by Sigma-Aldrich in pellet form, whereas the collector, frother, CMC depressant, pH modifiers, buffer and the electrolyte were supplied by Senmin International (Pty) Ltd. The pH modifier and buffer were used only when pH maintenance was required, where it was added dropwise to obtain the targeted pH. Instances where a buffer was required with SS involved zeta potential measurements at low SS dosages only, as high dosages were observed to have a buffering effect. For all zeta potential measurements and talc microflotation experiments with SS, pH modifiers were required to obtain the desired pH. Some error in this can therefore be expected as NaOH is expected to have slightly influenced the SS modulus. However, this error is not expected to be large, as very minimal strengths and quantities were added.

The collector and SS were freshly prepared daily using tap water, whereas all other reagents which required dilution were prepared using distilled water and stored in a cool dry area. All reagents used during zeta potential measurements were added to the sample using a 0.45 µm Millipore syringe filter to avoid the

interference of small particles or undissolved reagent. This exact sample of CMC used (FinnFix300) was characterised by Dzingai (2017: 33) in the Polymer Characterisation Laboratory at UCT and found to have a molecular weight of 251 000 g/mol, a purity of 97.6%, insoluble content of 1.4%, polydispersity of 7.0 and a degree of substitution of 0.7.

Table 3.2: Details of the reagents, dosages and experimental conditions used.

Reagent type	Name	Experiment type	Dosage/Conc.	Add Seq (min)	Conditioning (min)
Collector	Sodium isobutyl xanthate	Batch flotation	140 g/t at 1%	0-5	5
Frother	SENFROTH F200	Batch flotation	22 g/t (neat)	"last reagent"	1
Dispersant/ Depressant	Sodium metasilicate ($Na_2O{\cdot}SiO_2$). Modulus (*n:m*) ration of 1.	All experiments	0- to 2000 g/t (batch) and 0- to 1064 mg/L (micro floats) at 1%	0-5	5
	Carboxymethyl cellulose (FinnFix300)	Batch flotation	0- to 300 g/t at 1%	5-7	2
pH Modifier	Hydrochloric acid (HCl)	All experiments excl. rheology	0.1- to 1 M (conc.)	0	-
	Sodium hydroxide (NaOH)		0.1- to 1 M	0	-
Buffer	Sodium tetraborate ($Na_2[B_4O_5(OH)_4]{\cdot}8H_2O$)	All experiments excl. rheology	0.1- to 1 M	0	-
Electrolyte	Potassium nitrate (KNO_3)	Zeta potential	10^{-3} M	0	-

3.2. Characterisation

3.2.1. QEMSCAN and validation

Quantitative evaluation of minerals by scanning electron microscopy (QEMSCAN) experiments were performed using a FEI FEG QEMSCAN 650F equipped with two Bruker XFlash 6130 EDS set to operate at an accelerating voltage of 25 kV and a beam current of 10 nA. An image of the QEMSCAN is provided in Appendix B. Minerals in the samples were identified using a combination of EDS and back-scattered electron (BSE) brightness. The BSE brightness was calibrated using a quartz standard at a BSE of 42, copper at a BSE of 130 and gold at a BSE of 232. The QEMSCAN bulk mineralogical analysis (BMA) routine was performed on two representative unsized milled feed samples for both ores. This mode of analysis uses rapid line scans to determine the bulk mineralogies of the samples. To prepare for this analysis, representatively split 1 g aliquots of each sample was mixed in graphite powder and epoxy

resin and cured in 30 mm × 10 mm cylindrical block molds. Each sample block then underwent a series of grinding and polishing steps until a 1 μm diamond finish, and finally dried in an oven set to a temperature beneath 60°C. The samples were then carbon coated using a Quorum Q150T E coater to diffuse electrons from the sample surface once it is run in the QEMSCAN. Prior to QEMSCAN analysis, the samples were stored under vacuum to degas. A summary of the QEMSCAN experiments are provided in Table 3.3, and all raw QEMSCAN data used to set up QEMSCAN related graphs are provided in Appendix B.

Table 3.3: QEMSCAN experimental details.

Measurement	Sample	Information gained	Field size (μm)	Point spacing (μm)
Bulk mineralogical analysis (BMA)	Unsized Ore 1 and 2 feeds	Bulk mineralogy	700	3
Trace mineral search (TMS)	Unsized Ore 1 feed	PGM speciation, liberation and association, grain size distribution, BSE and false-colour imagery	500	0.8
Particle mineral analysis (PMA)	Unsized Ore 1 feed, unsized 215 g/t and 2000 g/t SS batch flotation first concentrates	Liberation and associations, grain size distribution, false-colour imagery	700	3
Field image (FI)	Six selected coarse particles	Bulk mineralogies, grain size distribution, false-colour imagery and ESD	1500	15

The QEMSCAN trace mineral search (TMS) method was used to search for discrete PGMs in the Ore 1 unsized feed. The TMS was done to determine the species types, the PGM associations and liberation data as well as the PGM grain size distribution. Equivalent circle diameter (ECD) is a 2-D size descriptor which have been used to determine the PGM grain size in μm. Additionally, PGM BSE imagery was captured, and false-colour PGM particle images were used as part of the associations and liberation statistics. The TMS analysis required a total of 24 sample blocks, which was prepared using the same method as the BMA analysis. Each block was then reground and polished to perform another TMS analysis on a fresh surface. The samples were then reground and polished a third time to analyze another layer. This was done to obtain a total of over 100 PGM particles over 84 polished surfaces in total for an acceptable PGM statistical analysis.

A particle mineral analysis (PMA) was performed on two representative unsized feed samples, and two representative unsized 215 g/t and 2000 g/t SS first concentrate samples. Sample preparation for QEMSCAN involves the same method to that of the BMA and TMS analyses. The PMA analysis was done to determine the talc and serpentine association and liberation data and grain size distribution in the

unsized feed and concentrate samples. The ECD size descriptor was used to determine the grain sizes of talc and serpentine. In addition, images of false-colour talc particles in the feed were also taken, and orthopyroxene and serpentine associations as well as the bulk mineralogies in the -50 μm virtually sized fractions were also determined. Mineral masses for the SS batch flotation first concentrate analyses were calculated based on the mineral proportions determined by QEMSCAN PMA on the unsized first concentrate as well as the batch flotation concentrate mass. Appendix B shows the mineral proportions determined through PMA and the Ore 1 batch flotation masses, and Appendix A shows an example of how the mineral masses have been determined.

Prior to Ore 1 being jaw crushed at the CMR, six coarse rock particles, which visually displayed mineralogical and textural differences, were selected to be run on the QEMSCAN using the field image analysis method. This involved a sample preparation method slightly differently to the unsized feed and concentrate samples. Each rock sample was cut and embedded in epoxy resin using 30 mm × 10 mm cylindrical block molds. This was followed by grinding and polishing steps until a 1 μm diamond polishing finish. The samples were then dried, carbon coated and then placed into the vacuum. The analysis provided bulk mineralogy and false-colour imagery.

Once samples were run in the QEMSCAN, the QEMSCAN FEI iDiscover™ software was used to check the data, perform pre-processing, define categorizers, classify or re-classify minerals, and obtain the reported statistics. A mineral library known as a species identification protocol (SIP) list, consisting of mineral criteria which includes "must have" and "may have" elemental concentrations, peak intensity ranges, x-ray count rates and BSE brightness, was used. The x-ray spectra and BSE data are collectively used to match each measured point to a mineral species when the mineral criteria assigned to each mineral have been met. Pre-customized SIP lists were chosen based on the sample types, which were further refined in this project for a more accurate mineral identification. To support the accuracy of mineral identification of the bulk mineralogies, x-ray diffraction (XRD) analyses were performed on the same samples, and x-ray fluorescence (XRF) spectrometry assays were used to validate all QEMSCAN bulk mineral measurements. Representatively split Ore 1 and 2 feed samples, as well as the 215 g/t and 2000 g/t SS first concentrate samples, weighing 10 g each, were micronized and sent for XRD analysis using a Malvern Panalytical Aeris benchtop XRD equipped with a Co tube. The minerals were identified using Bruker EVA software and thereafter, Rietveld refinement was performed using the Bruker Topas software to obtain quantification data. Crystal structure information, which was needed for mineral quantification, was sourced from the Crystallographic Open Database. X-ray diffractograms and quantitative XRD data for the samples are provided in Appendix B. There is good parity between the major minerals determined by XRD and QEMSCAN within the Ore 1 and 2 feeds, as well as the concentrate samples. The XRF analysis was used to give more confidence in the QEMSCAN data. A Panalytical Axios Wavelength dispersive XRF spectrometer was used. The major oxides for the Ore 2 feed, as well as the 215 g/t and

2000 g/t SS concentrate samples were analyzed by XRF, whereas the CuO content in the Ore 2 feed, batch flotation and microflotation samples were analyzed by microwave digestion followed by ICP-OES at an external ISO 9001 accredited laboratory (Scientific Services). All major oxides in the Ore 1 feed were analyzed by XRF in the Department of Chemical Engineering at UCT. Prior to XRF analysis, the loss of ignition was measured and thereafter the major oxides were determined. This data was imported into the iDiscover software and, where required, the QEMSCAN data processed to match the back calculated QEMSCAN assay to the measured XRF chemical assay. The assay reconciliation which compares the QEMSCAN and XRF chemistry assays are illustrated in Figure 3.2. This indicates that there are close similarities between the QEMSCAN and XRF assays between the samples. Raw XRF data is provided in Appendix B.

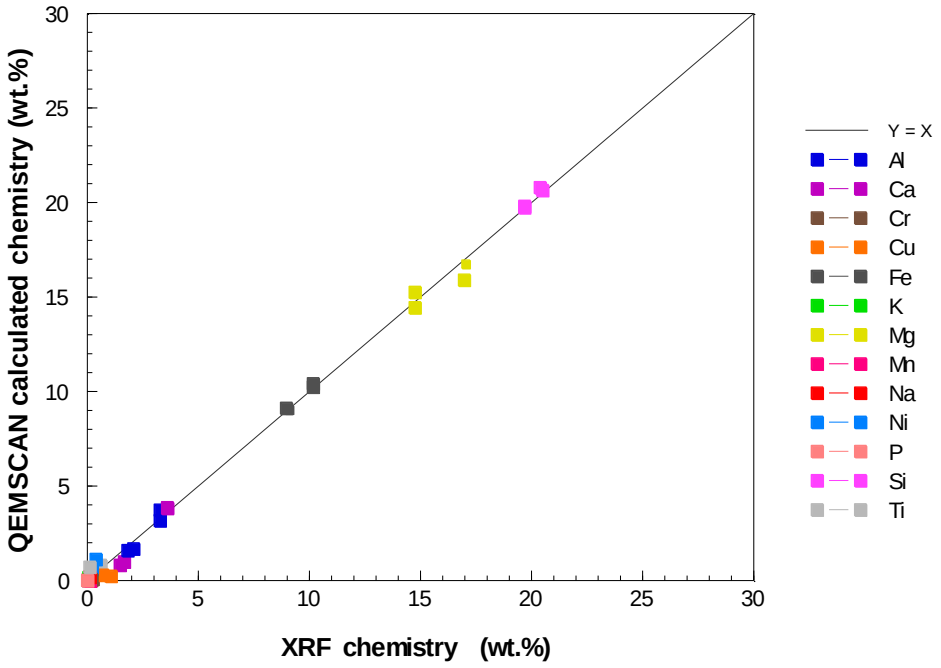

Figure 3.2: Assay reconciliation for the unsized Ore 1 and 2 feeds, and the unsized 215 g/t and 2000 g/t SS first concentrate samples.

3.2.2. PGE feed assays

Representative unsized and sized feed samples were sent for PGE fire assays and ICP-OES at Quality Laboratory Services in Rustenburg. The PGEs assayed on the unsized Ore 1 and 2 feeds, as well as the +53 µm, +10/-53 µm and -10 µm size fractions on the Ore 1 feed were Pt, Pd, Rh, Ru and Ir (and Au). The assays were used to determine the PGE distribution in the Ore 1 feed by size (6E PGE grades incl. Au) in both ores, and also the Pt/Pd ratios in both ores. Results of the PGE assays and calculations for the PGE distribution are provided in Appendix A.

3.2.3. Single minerals

Single minerals of importance to this investigation are talc, chalcopyrite and serpentine. Both talc and chalcopyrite samples were supplied by Ward's Natural Science Establishment NY, whereas serpentine samples were supplied by Sargent Welch. The samples were manually hammered, and the visually purest pieces of mineral samples were pulverized for a maximum of five seconds. The talc sample was wet screened using a mixture of water and a weak acetone solution to the +38/-53 μm size fraction. The acetone solution was used to prevent the clumping of talc during screening and allowed to evaporate when the sample was left to dry. The chalcopyrite sample was dry screened to -38 μm (for zeta potential experiments) and +38/-75 μm (for microflotation experiments). The serpentine sample was dry screened to -10 μm, whereas chalcopyrite was dry screened to the -38 μm and +38/-75 μm size fractions. A magnet was then passed through each of the samples to pick out some of the magnetic minerals present in the samples, and then lightly brushed to remove excess fine minerals attached to the magnetic minerals. Images of the serpentine samples are provided in Appendix B.

A representative sample of each mineral was analyzed by XRD to determine the purity of the samples. The serpentine sample was analyzed using a Bruker D8 Advanced powder diffractometer equipped with a LynxEye detector with Co tube. The data was processed and refined using the same Bruker software mentioned earlier. The talc and chalcopyrite samples were analyzed using the same machine used to analyze the feed and concentrate samples mentioned earlier and have also been processed and refined using Bruker software. The XRD data for each mineral showing the quantity of minerals present in each sample is shown in Appendix B. The talc sample contained 68.3 wt.% talc, 31.0 wt.% magnesite and <1 wt.% dolomite, the chalcopyrite sample was virtually 100 wt.% pure, and the serpentine sample contained 83.1 wt.% lizardite, 12.7 wt.% maghemite, 3.6 wt.% chlorite and <1 wt.% biotite.

3.2.4. Raman analysis

Raman microscopy is a suitable technique for the identification of various serpentine types and has therefore been used to identify the type of serpentine present in the 'pure' serpentine and the Ore 1 samples. The analysis was performed on a rock fragment of the pure serpentine sample, whereas serpentine in a coarse rock taken from the Ore 1 crushed rock stockpile (Figure 4.6d) was chosen to be representative of the serpentine in Ore 1. Previous Raman work performed on different serpentine types have indicated that Raman spectra in the low wavelength region (130 to 1200 cm^{-1}) are similar between the different serpentine types, but there are characteristic Raman signatures for each serpentine mineral in the high wavelength region (3600 to 3750 cm^{-1}), due to inner and outer hydroxyl vibrations (Groppo et al., 2006: 325; Schwartz et al., 2013: 202; Petriglieri et al., 2015: 956; Tarling et al., 2018: 1982). Raman peaks in the high wavelength region will, therefore, be observed to positively identify the type of serpentine in the samples, whereas serpentine peaks in the low wavelength region will confirm that the sample is in fact serpentine (Schwartz et al., 2013: 202; Petriglieri et al., 2015: 956; Tarling et al., 2018: 1982). Raman

analysis was performed using a Witec Confocal Raman Microscope (alpha300) at UCT, which collects Raman spectra with a high throughput UHTS300 spectrometer VIS-NIR equipped with a thermoelectrically cooled charge-coupled device (CCD) camera. The microscope is also equipped with 10x, 50x, and 100x Zeiss objectives, a video system for optical observation of the sample, and a 532 nm excitation laser module, which is connected to a powerful software-computer system. The laser input power varied between 5 and 30 mV as needed to obtain suitable spectra between samples. A total of 2 different spots were analyzed on the pure serpentine sample, and 6 spots on the Ore 1 sample.

The Raman spectra for serpentine in the pure serpentine and Ore 1 samples in the low and high wavelength regions are illustrated in Figure 3.3. Low wavelength Raman spectra for both samples show peaks at 130 cm^{-1}, 230 cm^{-1}, 386/8 cm^{-1} and 690 cm^{-1}, which are in good agreement with serpentine minerals analyzed in other studies (Groppo et al., 2006: 325; Schwartz et al., 2013: 202; Petriglieri et al., 2015: 953). Two intense peaks were identified in the high wavelength region. For both samples, the main

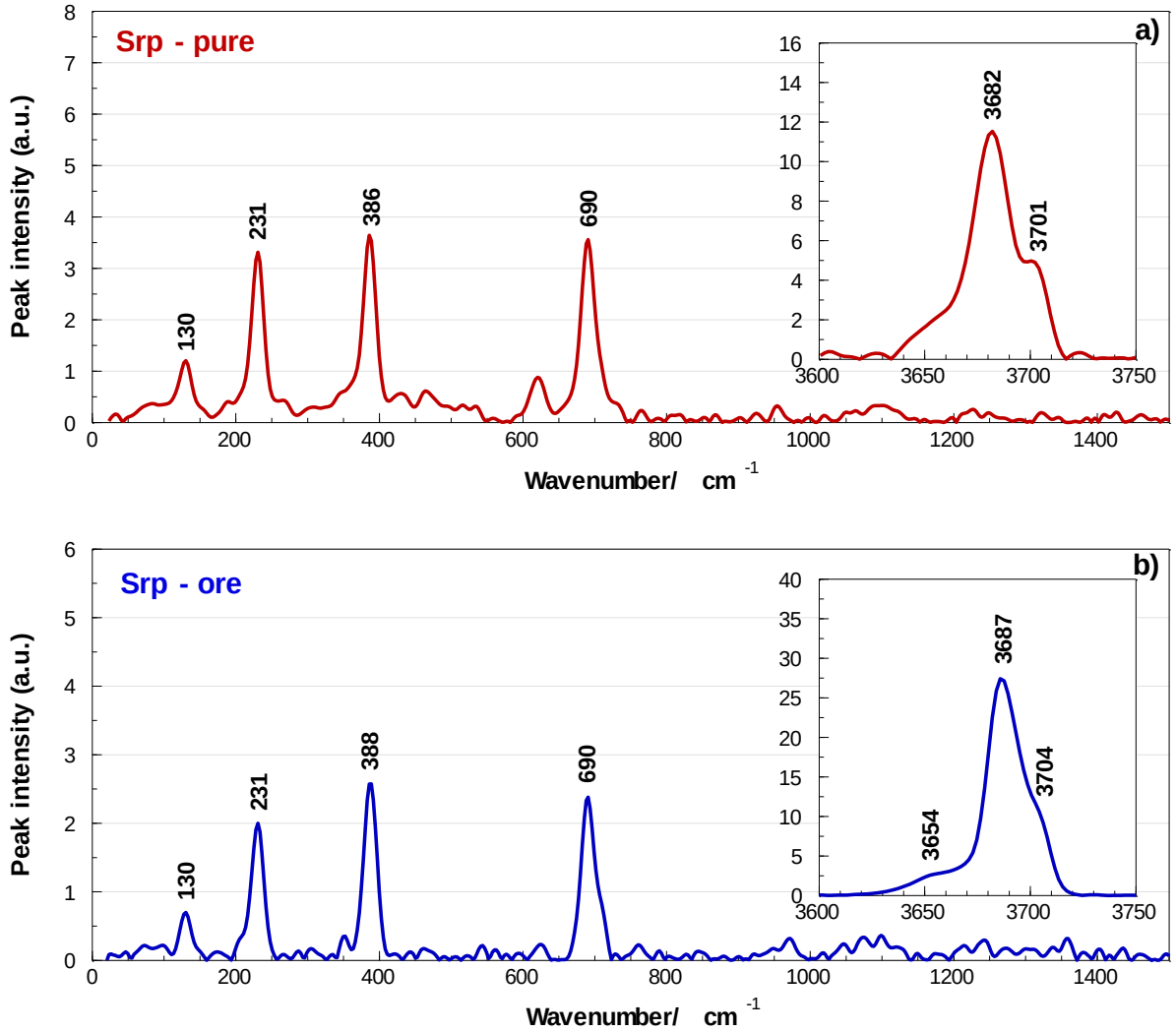

Figure 3.3: Raman spectra in the low and high wavelength regions of lizardite in the pure serpentine and Ore 1 samples. Serpentine is denoted by 'Srp', and arbitrary units by 'a.u.'.

peak for serpentine in the pure serpentine and Ore 1 samples are displayed at 3682 cm^{-1} and 3687 cm^{-1}, in Figure 3.3a and Figure 3.3b respectively, and there are shoulder peaks to the right of the main peak at 3701 cm^{-1} and 3704 cm^{-1}, respectively. This is specifically characteristic of lizardite and confirms that the serpentine type in these samples is lizardite and not antigorite or chrysotile (Schwartz et al., 2013; Petriglieri et al., 2015: 955). The Raman and XRD analyses, therefore, both agree that the sample is lizardite. This also confirms that the serpentine in the coarse rocks (e.g. Figure 4.6d), as determined by QEMSCAN, is lizardite.

3.2.5. Particle size distribution

The PSD of the Ore 1 and 2 milled feeds were determined by laser diffraction using the Malvern Mastersizer 2000, which is suitable for size analysis of particles between 0.2- to 2000 μm. Raw data for the PSD analysis is provided in Appendix B.

3.3. Flotation experiments

3.3.1. Batch flotation

Batch flotation tests on the ores were conducted using an 8 L Modified Leeds flotation cell at the CMR. Images of the batch flotation cell is provided in Appendix B. The choice for using this cell was due to the masses required for the PGE assay of the concentrates (approximately 50 g). The standard procedure for these tests is similar to that outlined in Wiese, Harris & Bradshaw, (2005b: 191). The freshly milled feed was carefully transferred into the batch flotation cell and topped with synthetic plant water to obtain 35 wt.% solids by mass. The impellor was set to a speed of 1200 rpm and the slurry was allowed to mix thoroughly for 5 minutes. The reagents and dosages were then added in sequence and conditioned for various times, as shown in Table 3.2. The air flow was switched on and maintained at 11 L/min and the froth height was maintained at 2 cm. The water added to maintain the 2 cm froth height was recorded. The reagent addition and conditioning procedure varied depending on the type of experiment conducted. For example, SS experiments dosages were performed at various dosages, as indicated in Table 3.2, which required the addition of the collector and SS simultaneously. The reagents were then allowed to condition for 5 minutes. Thereafter, the frother was added and allowed to condition for a further 1 minute before the air valve was opened. On the other hand, CMC was added after the collector and allowed to condition for 5 minutes. Dosages for the CMC experiments performed are shown in Table 3.2. The concentrates (C1-C4) were collected by scraping the froth every 15 seconds for a duration of 2, 4, 6 and 8 minutes which totaled 20 minutes of flotation time. Once the experiment was complete, the tailings sample was drained and filtered using a filter press, oven dried and weighed. The concentrate samples were initially weighed to obtain the masses of the concentrate pan consisting of concentrate sample and water, thereafter, filtered and in turn, dried, and weighed. This allowed the solids and water recovered during the process to be determined. The experiment was then duplicated, and in some cases triplicated, to gain the

required concentrate masses. It should be noted that the baseline batch flotation experiments are referred to as '0 g/t', unless otherwise indicated. This indicates that experiments were performed using collector and frother only. All batch flotation raw data are provided in Appendix B, including the Cu and Ni results. The Cu and Ni results follow very similar trends to that of Pt and Pd. Therefore, these results were not presented in the main text.

Batch flotation error and assay preparation

Due to the large concentrate masses required for the PGE assays, the number of experiments planned for this project, the cost and the strict time duration of this project, each concentrate of the repeat experiments was added together and representatively split for assays. For example, dried and weighed C1 samples were thoroughly mixed, representatively split using a small 10-way rotary splitter until a 50 g sample was split from the sample. This was the procedure for C2-C4 as well. The tailings samples were also blended, split to 150 g using a combination of large and small rotary splitters, and sent for assays.

It was assumed that the error inherent in the batch flotation procedure would be far higher than the error inherent in the assay procedure. Therefore, the error for duplicate or triplicate solids and water recoveries are reported in this study and were deemed to be acceptable if they were less than 10 standard error percent (Std. Err %). The exact value of these errors can be viewed in Appendix B. It is evident that in most cases, the error was far less than 10%. Any experiments with an error above 10% were repeated. Error bars illustrated on graphs represent the standard error (not the %) between an experimental run and the repeat(s).

Ultrasonication preconditioning

Ultrasonication tests were primarily performed for preconditioning prior to the batch flotation experiments. A summary of the ultrasonication experiments is shown in Table 3.4. The ultrasonication tests were performed using a Eumax UD300SH-10LQ ultrasonication bath which had the dimensions 300 × 240 × 150 mm (see photograph in Appendix B). The bath bottom was lined with six transducers, each producing 40 kHz frequency and 50 W of power. The milled slurry was transferred to the bath and topped with synthetic plant water to the 10 L mark. An overhead Heidolph impeller stirrer was positioned at the center of the bath and set to 250 rpm, which was visually enough to hold the slurry in suspension without slurry overflow, spattering or settling of the sample. The collector dosage was added and the slurry was then sonicated for preconditioning times of 5, 10, 15, and 20 minutes. The choice of collector addition at this point stemmed from the analogy that collector adsorption could take place the moment slime removal from valuable minerals occurred, especially since transportation of the slurry to the flotation cell occurred after sonication, which might otherwise have led to the reformation of slime coatings. The sonicated slurry was then transferred to the flotation cell, allowed to mix and followed the batch flotation procedure. In terms of reagents, the mixed slurry only required the addition and conditioning of the frother.

Table 3.4: Summary of ultrasonication experiments.

Ultrasonication method	Instrument	Transducers	Frequency (kHz)	Power (W)	Precondition time (min)
Bath	Eumax UD300SH-10LQ	6	40 each	40 each	5 to 20
Probe	Omnic Sonic Ruptor 400	1	20	20	20

An additional preconditioning ultrasonication test was performed using an Omnic Sonic Ruptor 400 Ultrasonic probe (Appendix B). The homogenizer probe was used to compare the recovery analyses relative to the ultrasonication bath. The titanium probe tip has a diameter of 25.4 mm and length of 12.4 mm. The probe tip produced 400 W power, 2 kW/cm^2 intensity and 20 kHz frequency. The probe was positioned centrally and at a depth of 10 cm overhead into the flotation cell and turned on for the first 20 minutes of the slurry collector conditioning step. The probe was then removed from the cell before the frother was added to the system and flotation experiments were carried out. All ultrasonication experiments were performed with Ore 1 only.

Solids concentration measurements

Batch flotation experiments were performed at various solids concentrations including 15 wt.%, 25 wt.%, 30 wt.% and 35 wt.%. The procedure began by allowing the 35 wt.% slurry in the flotation cell to mix thoroughly, and thereafter to representatively drain specific slurry volumes from the cell using a pump set to a low flow rate. The cell was then topped with synthetic plant water to the 8 L mark. Calculations showing the volume of slurry needed to be pumped from the flotation cell for solids concentration experiments are shown in Appendix A.

Chalcopyrite-serpentine flotation

Batch flotation experiments were performed using a 500 ml bench mini flotation cell to understand the floatability of chalcopyrite in the presence of serpentine slimes. An image of the mini flotation cell is provided in Appendix B. Only two experiments and their repeats were performed. Firstly, batch flotation experiments were conducted using pure chalcopyrite and thereafter a chalcopyrite-serpentine mixture was floated in a 1:2 ratio. A 12 g sample was used for each experiment. For the chalcopyrite flotation, 12 g of chalcopyrite was weighed and placed in a glass beaker which was filled to 100 ml. The sample was then ultrasonicated for a duration of 5 minutes before being transferred to the flotation cell and topped to the 500 ml mark. The impeller speed was set to 100 rpm and the slurry was allowed to mix for 2 minutes. The sample was dosed with 140 g/t collector and allowed to condition for a further 2 minutes, which was proceeded by the addition and conditioning of the frother. The air flow rate was set to 1.8 L/min, which was calculated based on the superficial gas velocity (J_g) in the 8 L batch flotation cell. These calculations

are provided in Appendix A. The froth height was maintained at a height of 2 cm. The concentrates (C1-C4) were collected by scraping the froth every 15 seconds for a duration of 2, 4, 6 and 8 minutes which totaled 20 minutes of flotation time. Finally, the tailings and concentrate samples were weighed, filtered, dried and the dry sample re-weighed.

The 1:2 ratio experiment followed a similar procedure to that of chalcopyrite, but the sample preparation differed. Chalcopyrite and serpentine samples were weighed to 4 g and 8 g, respectively. Each sample was placed in a glass beaker which was filled to 100 ml. Each sample was sonicated for 5 minutes and thereafter slowly mixed using a magnetic stirrer. The mixed sample was then placed into the 500 ml cell and the flotation procedure was carried out. The dried concentrate and tailing samples were analyzed by microwave digestion followed by ICP-OES at an external ISO 9001 accredited laboratory, as previously mentioned, to determine the Cu content from which the recovery could be calculated.

3.3.2. Microflotation

Talc analysis

Talc microflotation tests were conducted using a microflotation cell designed by Bradshaw & O'Connor, (1996: 444) at UCT. A picture of the microflotation cell is provided in Appendix B. A 2 g talc sample was mixed with 50 ml of distilled water in a glass beaker using a magnetic stirrer for a duration of 5 minutes. The mixture was then dosed with SS solution according to the dosages shown in Table 3.5, and the pH adjusted to equivalent pH's to that in the SS batch experiments, and the buffer used where required. The 0 g/t experiment was performed at natural pH. These microflotation dosages were chosen as they represent similar liquid SS concentrations in the batch flotation cell. The sample was then ultrasonicated in an ultrasonication bath for 5 minutes before being transferred to the microflotation cell.

The microflotation cell was topped using distilled water to a total volume of 365 ml and the pump turned on to flow in an anticlockwise direction at 60 rpm. Once the sample within the cell had settled into the pulp zone, a Hamilton syringe needle, connected to an external pump speed set to 2.0 rpm, was inserted into the base of the cell which injected a stream of air at a flowrate of 7 ml/min. The needle was withdrawn from the base after 2, 4, 6 and 8 minute intervals, totaling 20 minutes of flotation time. The concentrates (C1-C4) were then drained and washed out from the concentrate launder at various intervals. The concentrates and tailings samples were dried and weighed. All tests were conducted in duplicate. An additional experiment was performed using 100 mg/L CMC to compare the depressant effects of SS and CMC on the floatability of talc. The CMC experiment, and the duplicate, followed the same procedure to that outlined for SS. All microflotation raw data is provided in Appendix B.

Table 3.5: Dosages used for batch- and microflotation tests, where dosages in the same column are common in terms of their liquid concentrations.

Batch cell SS dosage (g/t)	0	215	700	1000	1500	2000
Microfloat equivalent SS dosage (mg/L)	0	120	270	530	800	1064
pH	Nat	10.3	10.5	11.0	11.3	11.7

Chalcopyrite-serpentine analysis

The analysis was performed using the same microflotation cell and a similar procedure to the talc experiments, however, the sample preparation for these tests differed. Table 3.6 shows the samples and experimental conditions for the experiments.

Table 3.6: Samples and experimental conditions for the chalcopyrite-serpentine microflotation.

Sample	Chalcopyrite to serpentine ratio	Sample mass used (g)	SS dosage (g/t)	pH
Chalcopyrite	-	3	0	9
Serpentine and chalcopyrite	1:2	3	0	9
Serpentine and chalcopyrite	2:1	3	0	9
Serpentine and chalcopyrite	1:2	3	2000	11.7
Serpentine and chalcopyrite	1:2	3	0	11.7

The pure +38/-75 μm chalcopyrite sample was weighed and mixed with 50 ml of distilled water in a glass beaker using a magnetic stirrer. The sample was dosed with 140 g/t collector and allowed to condition for 5 minutes. The pH was then adjusted using HCl, NaOH and a buffer for pH maintenance where required. Once the pH was stable, the sample was ultrasonicated for a duration of 5 minutes before being transferred to the microflotation cell. The procedure for samples involving serpentine differed. Depending on the ratio, chalcopyrite and serpentine were weighed and mixed with 20 ml of distilled water. Each sample was sonicated before being mixed using a magnetic stirrer. The samples were then dosed with collector and in the case where SS was used, the SS was added simultaneously with the collector. The sample was then allowed to condition for 5 minutes before the pH was adjusted. The sample was then transferred to the microflotation cell. The microflotation cell procedure was the same to that using talc.

The concentrate and tailing samples were then weighed and analyzed by microwave digestion followed by ICP-OES at an external ISO 9001 accredited laboratory, as previously mentioned, to determine the Cu content from which the recovery could be calculated.

3.4. Froth stability

The standard froth column, which has a height of 1 m and a diameter of 100 mm, has been used for the froth stability experiments. An image of the column used in this work and all froth stability raw data is provided in Appendix B. Both 2-phase and 3-phase froth stability experiments were conducted using this column.

In terms of 3-phase experiments, the column was set up by fitting a pore 4 frit into the base of the column. The choice of the frit size was to disperse fine air bubbles throughout the column. An overhead stirrer was used to hold particles in the slurry in suspension and to prevent clogging of the glass frit once the slurry was present in the column. The stirrer was kept on for the duration of the experiment. A bucket containing the feed slurry at 35 wt.% solids was thoroughly mixed using an overhead stirrer. The slurry was made up of freshly milled feed and filled to 8 L with synthetic plant water. Once mixed, the slurry was pumped into the cell through an inlet valve near the base of the column and filled to the 200 mm mark. The slurry was then dosed with reagents and conditioned in the same manner as the SS 8 L batch flotation experiments, as shown in Table 3.2. This included the use of a collector, frother and SS. In the case of the baseline experiment, experiments were conducted without SS addition. The air flow was turned on and the froth rise recorded every 5 seconds until the maximum froth height was recorded. At the end of the experiment, the air flow was turned off and the froth allowed to collapse completely. The air flow was then turned on and the experiment repeated. All experiments were triplicated.

In terms of 2-phase experiments, the synthetic plant water was added into the column at the top of then allowed to mix using the overhead impeller. The procedure for reagent dosing, reagent conditioning times, and the rest of the procedure were kept the same to that of the 3-phase experiments.

3.5. Rheology measurements

3.5.1. Rheology

Rheology measurements were performed on Ore 1 using an AR1500EX TA rheometer in the Analytical Laboratory at UCT. An image of the rheometer and rheology raw data is provided in Appendix B. These experiments aimed to understand the apparent viscosity (Pa.s) of the ore and how this was influenced by high SS dosages and a finer grind. The tests were conducted at various solids volume concentrations between 10- and 40 vol.%. Increments of 5 vol.% were used where rapid increases in the viscosities occurred.

Sample preparation involved determining the sample mass, volume of distilled water and volume of 1% SS solution to obtain the required solids contents. To determine this, sample densities were performed on the ore feeds using a Micromeritics AccuPyc II 1340 instrument at the UIS Analytical Services (Pty) Ltd in Centurion. The calculations for the sample mass, volumes of SS solution and water required to obtain the various solids % used are provided in Appendix A. Once the sample, water and reagents were mixed in a

glass beaker, the mixture was then transferred into the rheometer cup and the standard vaned rotor geometry spindle attached to the rheometer was lowered into the sample. The TA Instruments Operating Software was used to set the conditions for the experiments. The conditioning step included the pre-shear rate, pre-shear time duration and equilibration time to be set up. These settings varied depending on the solids concentration used. A higher shear was applied for higher solids concentrations to suspend particles and to thoroughly mix the sample. Thereafter, the equilibration time had to be sufficient to settle any turbulence but to also avoid the settling of the sample in the cup. This meant that lower solids concentrations, below 20 vol.%, required a pre-shear rate of around 120/s for a duration of 20s. Thereafter, the sample was equilibrated for 20s. However, samples above 20 vol.% were pre-sheared between 200/s and 350/s for 30s and then allowed to equilibrate for 10s.

Once the samples were equilibrated, the shear stress was recorded at pre-defined shear rates, which was set up in the continuous ramp settings. The shear stress was recorded at 200 sample points between shear rates of 10/s to 500/s for a duration of 2 minutes. The temperature of the experiment was maintained at 22 °C to avoid the influence of temperature changes on the rheology readings. The Bingham model was then applied to the rheology data which was then copied and pasted into an excel spreadsheet.

A good visual analysis of the data was to observe a linear relationship between the shear stress and shear rates, as previous work indicated what should be expected. Cases where this linear relationship did not show, such as instances where rheograms were curved, were interpreted as problematic and the conditioning settings were, therefore, adjusted.

3.5.2. Particle settling

Particle settling experiments were conducted to investigate the influence of SS on the settling rate, as a longer settling time is indicative of a more dispersed ore. An image of the particle settling experimental set-up and all particle settling raw data is provided in Appendix B.

The experiments were conducted using a 500 ml graduated cylindrical flask with an overhead impeller. To conduct the experiment at 35 wt.% solids, 227.6 g of representatively split milled and dried feed sample was added to the flask and topped with synthetic plant water to the 500 ml mark. The impeller was inserted into the flask and the slurry was allowed to mix at an impeller speed of approximately 800 rpm for a duration of 10 minutes. The slurry was then dosed and conditioned with the collector, frother and SS according to that displayed in Table 3.2. A baseline experiment was conducted without SS addition. After the conditioning of the reagents, the impeller was switched off and the timer started simultaneously. The impeller was then carefully and quickly removed from the flask. Thereafter, the height of the suspension-liquid interface was recorded every minute for a duration of 2 hours. The experiment was repeated after thoroughly allowing the sample to re-mix for 10 minutes.

3.6. Zeta potential

Zeta potential tests were carried out on a Malvern Zetasizer Nano ZS in the Analytical Laboratory at UCT. An image of the instrument and all zeta potential raw data is shown in Appendix B. This technique aims to understand the colloidal stability of chalcopyrite and serpentine (lizardite), and thus the electrostatic interaction between these minerals both with and without SS. The -38 μm chalcopyrite sample and -10 μm serpentine sample were used for the analysis. A characterisation of these samples is provided in Section 3.2.3.

A 0.15 g of serpentine was weighed and mixed in a 120 ml of 10^{-3} M KNO_3^- electrolyte solution containing 0 g/t, 215 g/t, 700 g/t, 1000 g/t, 1500 g/t, and 2000 g/t SS which was dosed based on sample weight. Chalcopyrite tests were conducted at 0 g/t and 2000 g/t SS only and underwent the same sample preparation procedure to that of serpentine. Each sample was mixed, ultrasonicated for 5 minutes and then representatively split into two 60 ml samples. Each sample was stirred, and the pH adjusted between pH 2 and 12 in increments of two for all dosages. Although SS is a natural pH buffer within the alkaline range and at pH 2, as observed during this work, other values including pH 4 and 6 required sodium tetraborate addition. The samples were then left to settle, and the supernatant drawn and injected into a folded capillary cell. The remaining 60 ml sample was used for the duplicate test.

The Zetasizer Nano ZS measures the zeta potential by firstly determining the electrophoretic mobility which is thereafter fit to the Smoluchowski model. This model is suitable for particles larger than 0.2 microns which is dispersed in an electrolyte containing more than 10^{-3} M salt aqueous solution. A standard operating procedure was created for both serpentine and chalcopyrite which required information of the sample material, the cell used and measurement settings. Importantly, the measurement duration was set to an automated minimum runs of 10 and a maximum of 100, and the number of measurements set to 3. All individual runs are accumulated and then averaged to give the final zeta-potential result.

Chapter 4: Results

The results for all experimental work necessary to answer the key questions outlined in Chapter 2 are presented in this chapter. A characterisation of the ores, with special emphasis on alteration minerals and PGMs, is given in Section 4.1. Section 4.2 presents the results for the SS and solids concentration batch flotation, froth stability, rheology, particle settling experiments, and the mineralogical characterisation of the flotation concentrates. All experimental work involving the handling of discrete mineral samples such as micro- and batch flotation, as well as zeta potential tests are presented in Section 4.3. The last section is focused on presenting the ultrasonication, CMC and Ore 2 SS batch flotation experiments in the context of evaluating SS's performance (Section 4.4).

4.1. Characterising the altered ores

4.1.1. Introduction

Process mineralogy can greatly contribute to the understanding of an ore and the associated challenges expected during processing (Bradshaw, 2014: 2). Process mineralogy studies have identified slime coatings through SEM-EDS, illustrated the occurrence of composite talc particles through QEMSCAN, and have identified minerals known to contribute to a rheologically complex pulp through XRD (Becker et al., 2009: 253; Peng & Bradshaw, 2012: 287; Ndlovu et al., 2014: 193). The attributes of process mineralogy, including the bulk modal mineralogy, grain size and mineral association data, will be integral for the evaluation of the SS effects observed during batch flotation, which will be presented within Sections 4.1.2 and 4.1.3. Consequently, this section aims to characterise i) the ore feeds used within this study with special emphasis on the alteration mineral characteristics, ii) selected coarse particles taken from the Ore 1 stockpile, and iii) the PGMs within the Ore 1 feed. This aim was made possible by combining QEMSCAN and Malvern PSD with other complementary chemical assay analytical techniques. Not all process mineralogy attributes are performed on both ores used in this study and this will be explicitly indicated. 'Ore 1' refers to the PPM ore used in most of the experiments in this study, whereas 'Ore 2' refers to an additional PPM ore sampled from a different bench that was used in selected experiments only. For a more detailed discussion of ores used for each experiment, please refer to the experimental section. Ore 2 is expected to differ from Ore 1 in that it is more altered and has a lower PGE grade, as mentioned in Chapter 3.

An overview of the ore characterisation section is provided in Figure 4.1. The topics covered in this section involve results performed on the feed samples (a to d) and coarse rock samples taken from the crushed rock stockpile (e). Topics 'a' to 'c' are applicable to both Ores 1 and 2, whereas topics 'd' and 'e' mainly covers Ore 1. Section 4.1.2 explores the characteristics of the gangue minerals with special emphasis on alteration minerals (boxes 'a' to 'c' and box 'e' in Figure 4.1), whereas section 4.1.3 explores

the PGM characteristics (box 'd' in Figure 4.1). The arrows indicate how each technique feeds into either the feed or coarse rock characterisation.

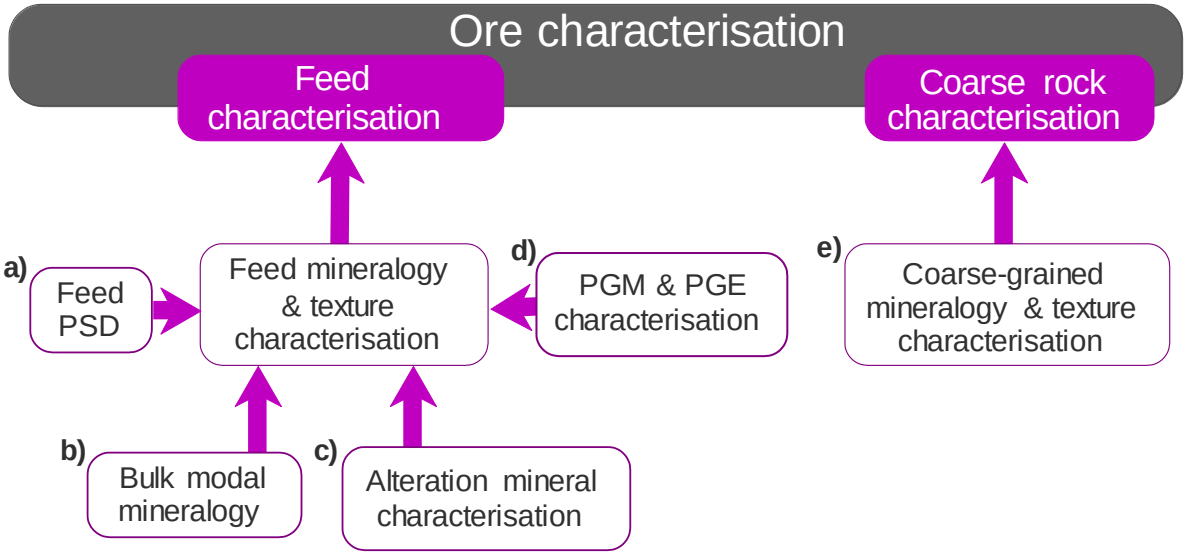

Figure 4.1: An overview of the topics which will be covered within Section 4.1.

4.1.2. Alteration mineral, PSD and BMS characterisation

The Malvern PSD of the two ores used in this study at the targeted 60% passing 75 µm grind is shown in Figure 4.2. The PSD of the plant primary grind data (plant PSD), which was taken from a recent report prepared for PPM based on work performed by the CMR, is also shown (van der Westhuizen, Pers. Comm. 2018). The choice of the target grind is crucial as it affects many of the sub-processes occurring during flotation, such as but not limited to, the degree of entrainment, and the liberation of the valuable PGMs (Liu & Peng, 2014: 218; Wang, Peng, Runge, et al., 2015: 82). The targeted grind of 60% passing 75 µm was chosen to be comparable to the primary grind of the PPM operation.

Milling the ores to achieve this target grind produced approximately 20 vol.% of fine minerals smaller than 10 µm in size. This size fraction may consist of fine alteration minerals and other gangue, but it is also likely to consist of a significant proportion of PGMs. Figure 4.2 further demonstrates that approximately 50 vol.% of particles are finer than 50 µm and therefore are more prone to entrainment. This observation holds for all the PSDs shown in Figure 4.2 and therefore entrainment and the management thereof will inevitably be very important. The PSD of the ores closely resembles that of the plant PSD, as illustrated in Figure 4.2, which demonstrates that the ores used within this study resemble a true PGM grind. The shape of the curves is slightly different between the plant Silicate reef ore and the ores within this work, but 60% passing 75 µm is the same. The differences in shape are due to milling type, as full-scale ball mills are used on site, whereas a laboratory rod mill was used on the ores in this laboratory study.

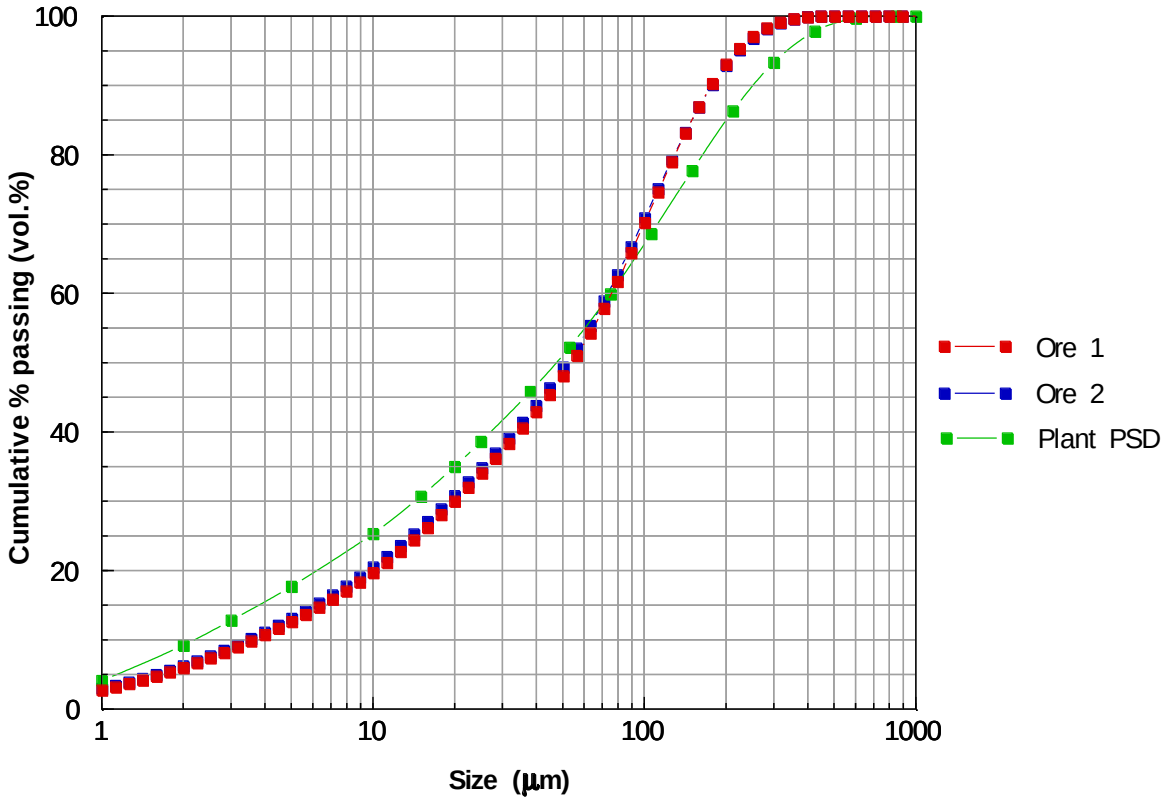

Figure 4.2: PSD of the milled ores used in this study (60% passing 75 µm). These grinds are compared to a PGM plant PSD (80% passing 144 µm) taken from a recent CMR report (van der Westhuizen, Pers. Comm. 2018). Laboratory and plant PSDs were analysed using a Malvern particle analyser.

To aid in the interpretation of the flotation performance of the ores, the bulk mineralogy of the feed was determined using QEMSCAN. A comparison of the ore bulk mineralogies is displayed in Table 4.1. Figure 4.3 illustrates the alteration mineral content of both ores for comparison of the proportions of individual alteration minerals within these ores. Both ores consist of large quantities of orthopyroxene, serpentine and talc. The alteration mineral content (comprising amphibole as well as the phyllosilicate minerals talc, serpentine, chlorite and micas) within Ore 1 is 33.6 wt.%. Within Ore 2, the alteration content is slightly higher and constitutes 36.5 wt.%, as shown within Table 4.1 and Figure 4.3. The alteration mineral proportions varied between the ores, as illustrated in Figure 4.3. Serpentine and talc are the dominant alteration minerals in both ores, as they constitute a large proportion of the alteration contents. Both ores contain similar proportions of serpentine, whereas Ore 2 has nearly twice the amount of talc compared to Ore 1. The ores also consist of other silicate minerals (orthopyroxene, olivine, and plagioclase feldspar), oxides (magnetite and lesser Fe-Ti oxides/ hydroxides) and some BMS.

Table 4.1: QEMSCAN bulk mineralogy of the PPM ore feeds in wt.%. The base-metal sulphide (BMS) group represents pyrrhotite, chalcopyrite and pentlandite.

Mineral group	Mineral	Ore 1	Ore 2
BMS	BMS	0.3	0.3
Pyroxenes	Orthopyroxene	35.7	32.7
	Clinopyroxene	7.7	7.6
Alteration minerals	*Amphibole	4.9	4.2
	Chlorite	3.0	3.0
	Serpentine	19.2	18.4
	Talc	5.0	9.5
	Mica	1.5	1.4
Fe-oxides	Chromite	4.1	0.8
	Magnetite	2.1	4.9
	Fe-Ti oxides/ hydroxides	0.9	1.4
Other silicates	Plagioclase	9.8	10.8
	Olivine	5.2	4.5
Other	Other minerals	0.5	0.5
	Total	100	100

*Not a phyllosilicate mineral

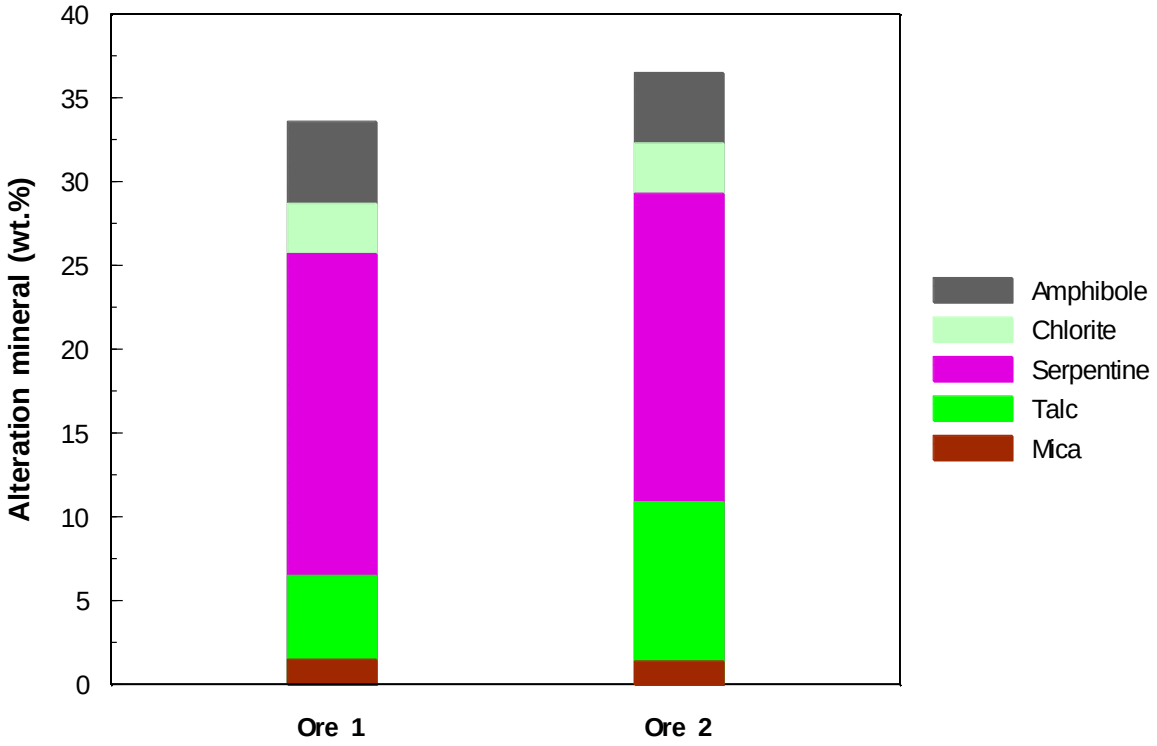

Figure 4.3: Proportions of alteration minerals within the ore feeds in wt.%.

The BMS contents within the ores are given in Figure 4.4. Relative to other minerals within the ores, the BMS contents are very low, as shown in Table 4.1 and Figure 4.4. Base-metal sulphide grades are slightly higher within Ore 1 which contains a variety of BMS compared to Ore 2. The main BMS are chalcopyrite, pentlandite and pyrrhotite within both ores, but the ratios between these minerals differ. The main BMS content in Ore 1 approximated to a 1:1:1 ratio (chalcopyrite, pentlandite and pyrrhotite respectively), whereas Ore 2 approximated to 4:1:1. Figure 4.4 also displays the BMS constituents within the 'others' category. Both ores contain minor quantities of secondary BMS such as millerite and violarite, with Ore 1 consisting of higher quantities of these secondary BMS than Ore 2. It is evident from the mineralogy that there are high quantities of altered minerals and low quantities of BMS within the feed, which indicates that the ore is likely altered (McCollom & Bach, 2009: 857; Becker, Wiese & Ramonotsi, 2014: 29).

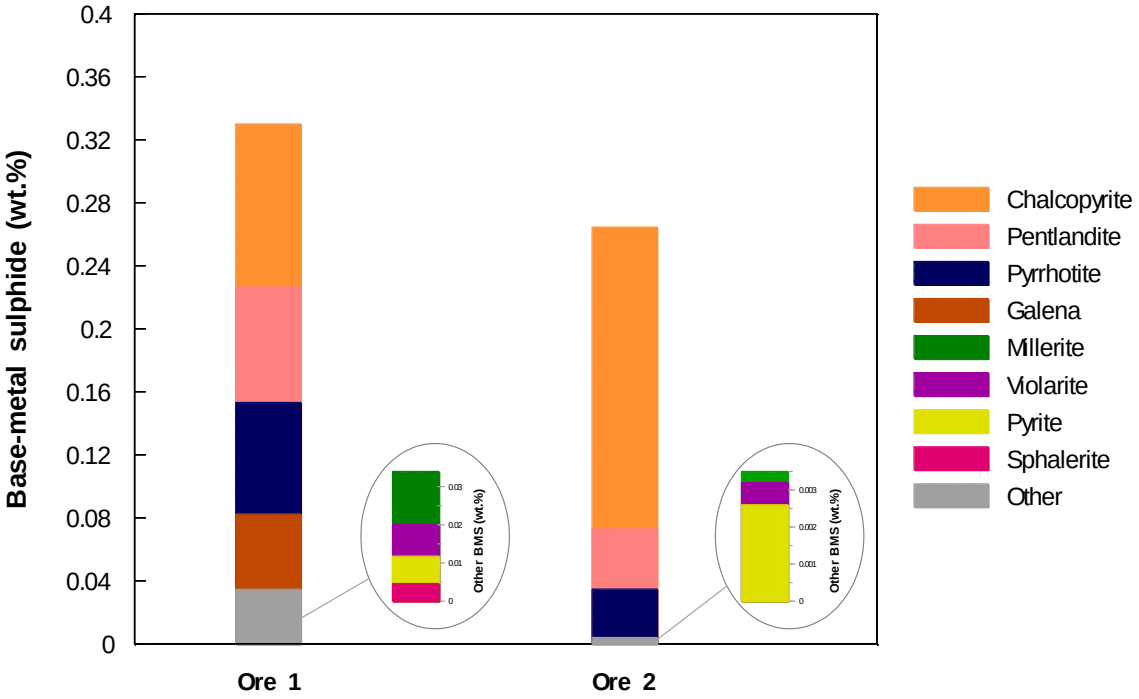

Figure 4.4: Proportions of BMS within the ore feeds in wt.%.

A QEMSCAN field analysis was performed on six selected coarse particles taken from the crushed rock stockpile before Ore 1 was further crushed at the CMR. The bulk mineralogy of the field images is presented in Figure 4.5, and the accompanying field images are illustrated in Figure 4.6. This information gives a sense of the variability in mineralogy and textures of the rock prior to milling, where many of the coarse rock textures would have been destroyed. Understanding the characteristics of the rocks may assist in interpreting the subsequent flotation response. The coarse rock particles were classified into three rock types: serpentinized olivine pyroxenites (A to C), a serpentinite (D), and orthopyroxenites (E to F). As the names suggest, samples A to C is dominated by orthopyroxene, serpentine and olivine (averaging 58.5 wt.%, 18.5 wt.% and 12.0 wt.% respectively), sample D by serpentine (60.9 wt.%) and samples E and F by

orthopyroxene (averaging 89.9 wt.%). Sample C and F also contain major quantities of talc (4.1 wt.% and 5.5 wt.% respectively), whereas minor quantities were observed in the other samples excluding sample D. Although the selected coarse particles are not representative of the ore, according to the theory of sampling, it gives a sense of the variability in mineralogy and provides useful information about the textural characteristics.

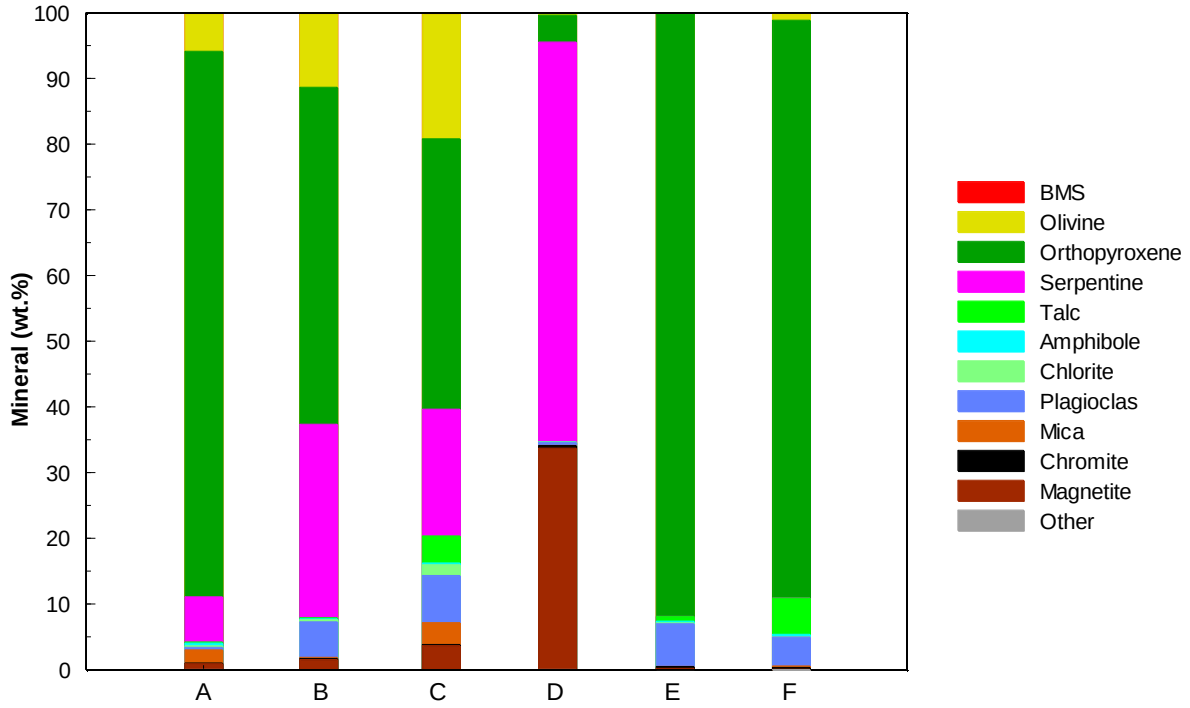

Figure 4.5: QEMSCAN bulk mineralogy of 6 selected coarse particles taken from the Ore 1 crushed rock stockpile.

Studying the coarse particles under reflected light microscopy and QEMSCAN field images revealed varying textures within the coarse particles. Serpentine and talc will be primarily addressed because these are the alteration minerals of interest in this study. Microscopy observations revealed that all olivine grains have been altered to mesh-textured serpentine, as shown in samples A to C in Figure 4.6. In these particles, serpentine veinlets extruding from altered olivine grains are joined to form a woven network. The serpentinization of orthopyroxene also occurred, which formed part of the serpentine network as shown within sample A, whereas the serpentinization shown in sample D is extensive. In the case of sample D, the original rock has been pervasively altered, where nearly all of the original rock forming minerals have been altered. This resulted in the total obliteration of the original mineral textures to new hydrothermal mineral textures. Raman analysis performed on sample D confirms that the type of serpentine is lizardite (Section 3.2.4). Talc particles are mainly associated with orthopyroxene as shown within samples C, E and F. The alteration of olivine and orthopyroxene to secondary serpentine and talc minerals is therefore strongly evident in these samples. A summary of the individual coarse particle characteristics is provided in Appendix B.

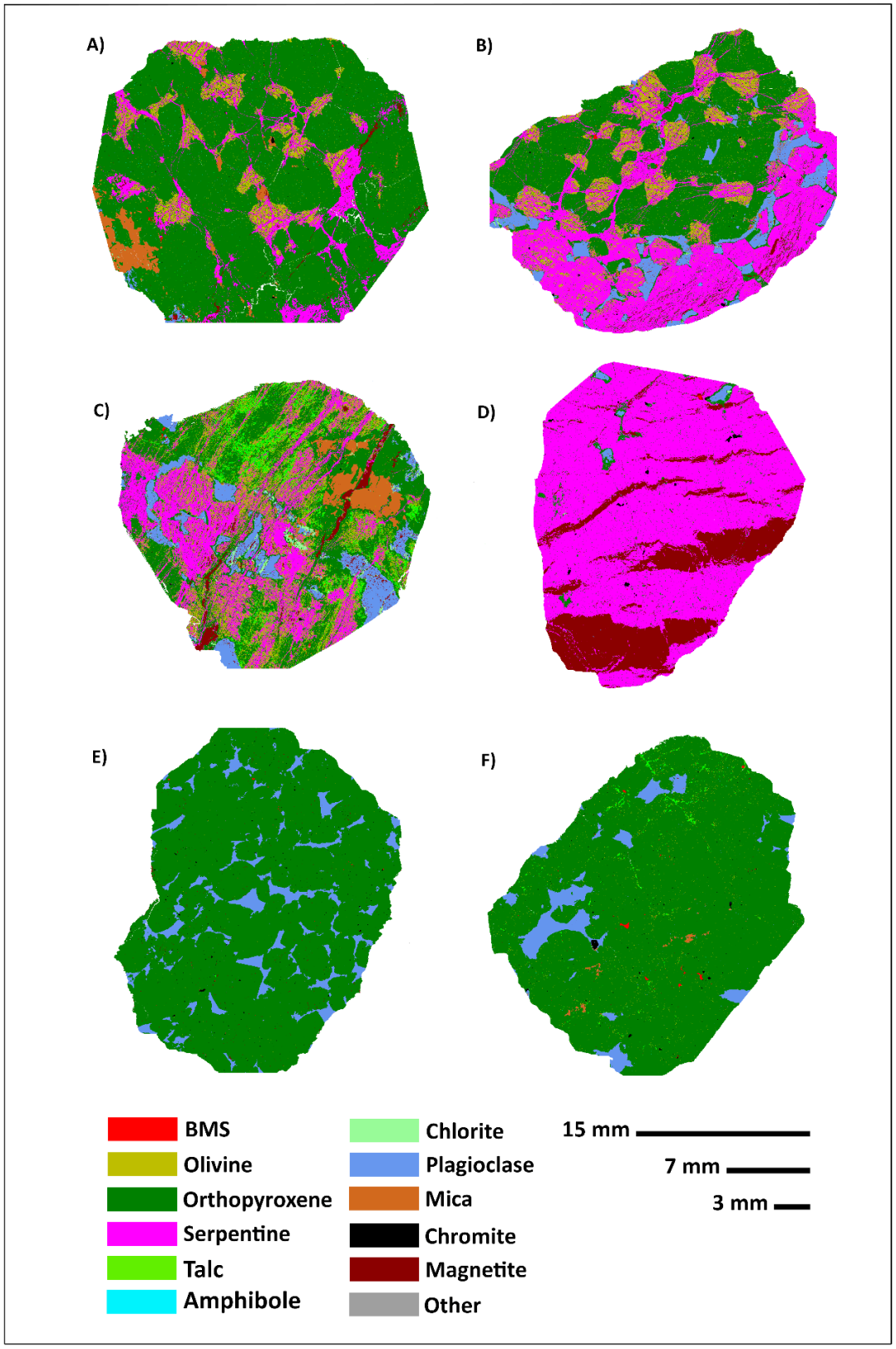

Figure 4.6: QEMSCAN false colour images of selected coarse rocks taken from the Ore 1 crushed rock stockpile. Samples 'A' to 'C' are serpentinized olivine pyroxenites, 'D' a serpentinite and samples 'E' and 'F' are orthopyroxenites.

Upon close visual observation of the mineral grain sizes in Figure 4.6, it is clear that serpentine and talc grains vary in size amongst the samples. For example, serpentine is coarser grained in the rocks shown in Figure 4.6b to Figure 4.6d, and is finer grained in Figure 4.6a, whereas talc is coarser grained in Figure 4.6c compared to Figure 4.6f. It is of importance to understand the grain sizes of these alteration minerals after they have been milled, because this can greatly impact the flotation performance. The cumulative size distribution of talc and serpentine grains within the Ore 1 feed after milling is shown in Figure 4.7. Most of the talc grains are very fine, where nearly 100% of talc is below 10 µm in size. In terms of serpentine, a significant amount of serpentine is coarse-grained, having a d50 of around 100 µm. The grain sizes of serpentine below 10 µm are of particular interest because this can contribute to the understanding of serpentine slimes. Figure 4.7 indicates that approximately 15% of serpentine grains are below 10 µm in size which indicates that the amount of serpentine occurring as slimes are small compared to the amount of serpentine overall in the feed. However, the size distribution of the serpentine does not account for whether the grains are liberated or not.

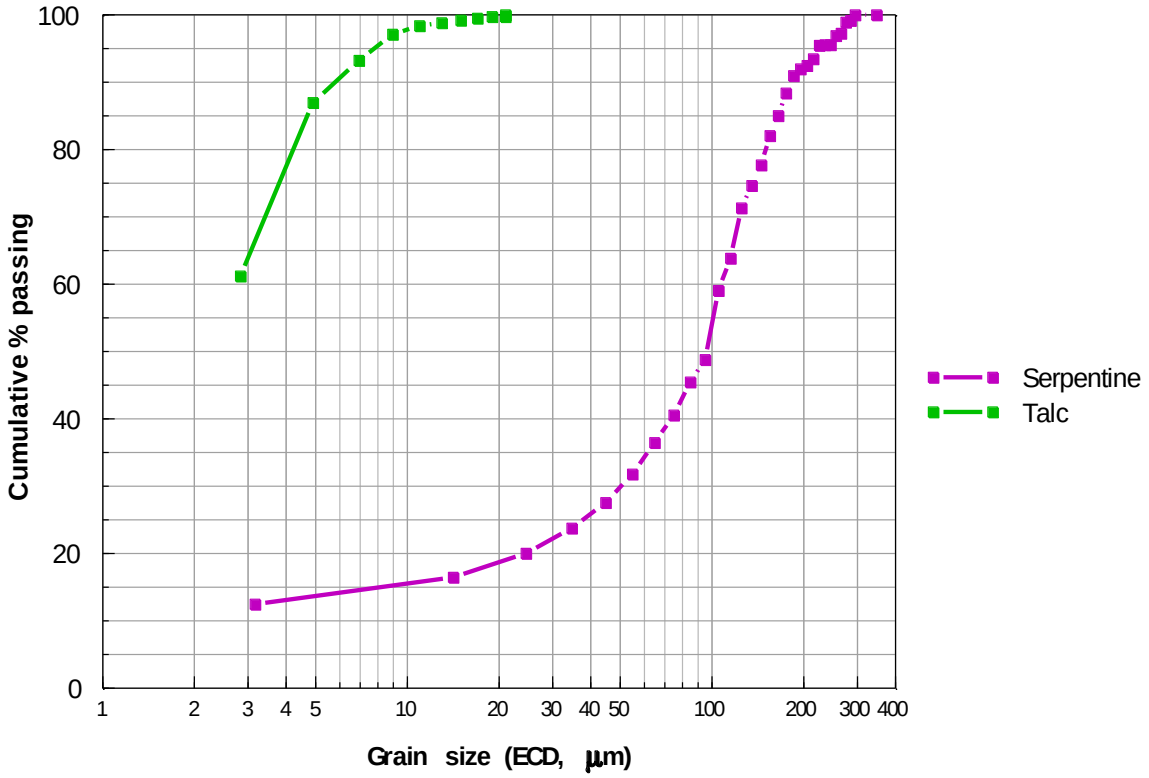

Figure 4.7: Grain size distribution of talc and serpentine in the Ore 1 feed. The total number of talc and serpentine grains are 28521 and 19760 respectively.

To determine the proportion of serpentine which is most likely to behave as serpentine slimes, the liberation characteristics of serpentine below 10 µm in size were measured using QEMSCAN and presented in Figure 4.8. Only measurements of serpentine below 10 µm in size are included, as those particles are likely to be characteristic of serpentine slimes. Figure 4.8 illustrates that a significant

proportion of serpentine below 10 µm in size occur as liberated and high grade middling particles, which collectively constitute 6.7% of the total amount of serpentine. Locked and low grade middling particles are thought to be less likely characteristic of serpentine slimes. This is dependent on the association between serpentine and other minerals within the locked and low grade middling particles. The overriding electrostatic force of the particles containing serpentine may either be repelling or attracting to the valuable mineral which could either prevent or induce slime coating, respectively. In the case of liberated or high grade middling particles, most of the surface area of the particles are comprised of serpentine and it is, therefore, more likely for the particles to be characteristic of true serpentine slimes. Since there is 19.2 wt.% of serpentine in the feed, as shown in Table 4.1, and 6.7% of this serpentine is liberated and high grade middling particles smaller than 10 µm, this equates to nearly 1.3 wt.% of serpentine slimes in the overall feed material. This indicates that the BMS to serpentine slime ratio in the feed is approximately 1:7. Obviously, the PGM to serpentine ratio would be orders of magnitude smaller due to the much lower PGM content in the ore. A significant quantity of serpentine is likely to be characteristic of true slimes in the feed, which can problematically lead to slime coating of valuable minerals.

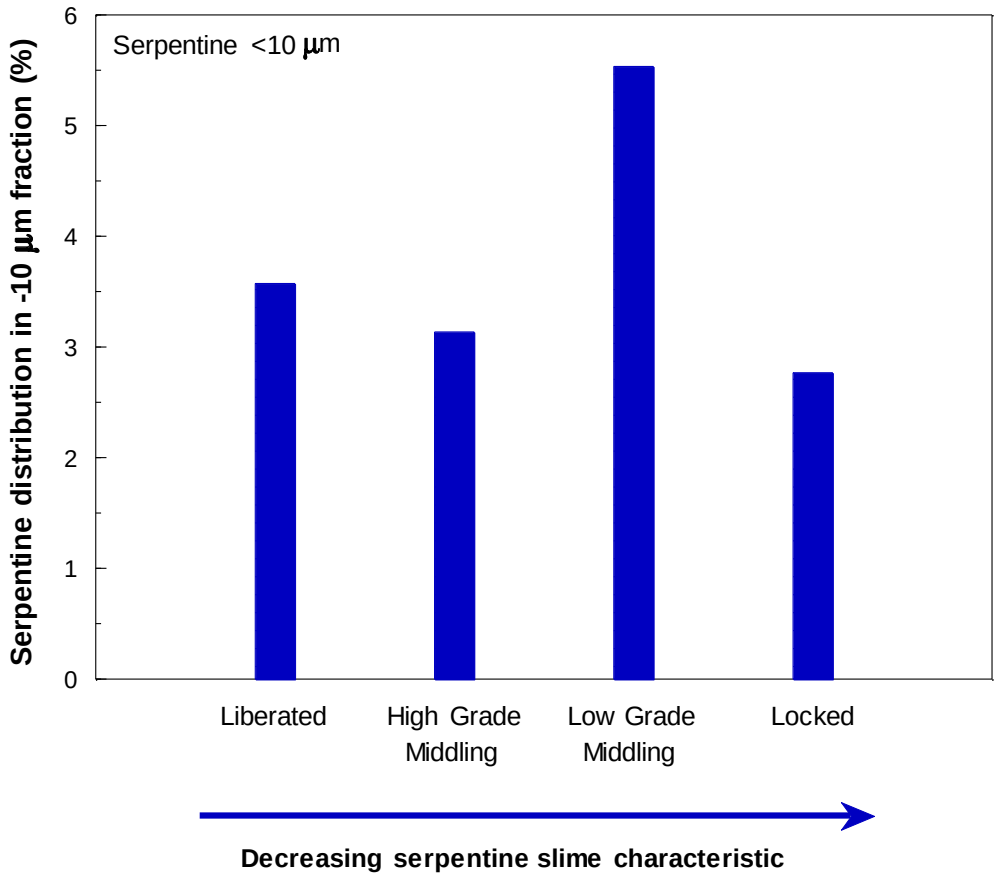

Figure 4.8: Serpentine liberation characteristics of serpentine below 10 µm in size within the Ore 1 feed. Liberated: Area % Serpentine > 90, High Grade Middlings: 90 ≥ Area % Serpentine > 60, Low Grade Middling: 60 ≥ Area % Serpentine > 30 and Locked: Area % Serpentine < 30.

In order to determine whether the talc contents within the feed may considerably dilute concentrate grade, the percent of liberated and unliberated talc within the feed was determined by QEMSCAN, and the results are presented in Table 4.2. Within the feed, a large mass of talc relative to the total talc mass is unliberated, whereas a small mass of talc is liberated, as shown in Table 4.2. The large proportion of unliberated talc could have serious consequences during flotation because of its association to gangue minerals, as mentioned in Chapter 2.

Table 4.2: Liberated and unliberated talc masses within the Ore 1 feed. Liberated: Area % Talc > 90 and Unliberated: 90 ≥ Area % Talc > 0.

	Talc mass (%)
Liberated talc	10.8
Unliberated talc	89.2
Total	100

The association of unliberated talc with other minerals within the feed is presented in Figure 4.9. Talc is mainly associated with orthopyroxene within the feed, which constitutes 59.1% of talc. This association between talc and orthopyroxene were also observed within the coarse particles. Other talc associations include serpentine and BMS. It is therefore expected that without a suitable depressant, dilution of the

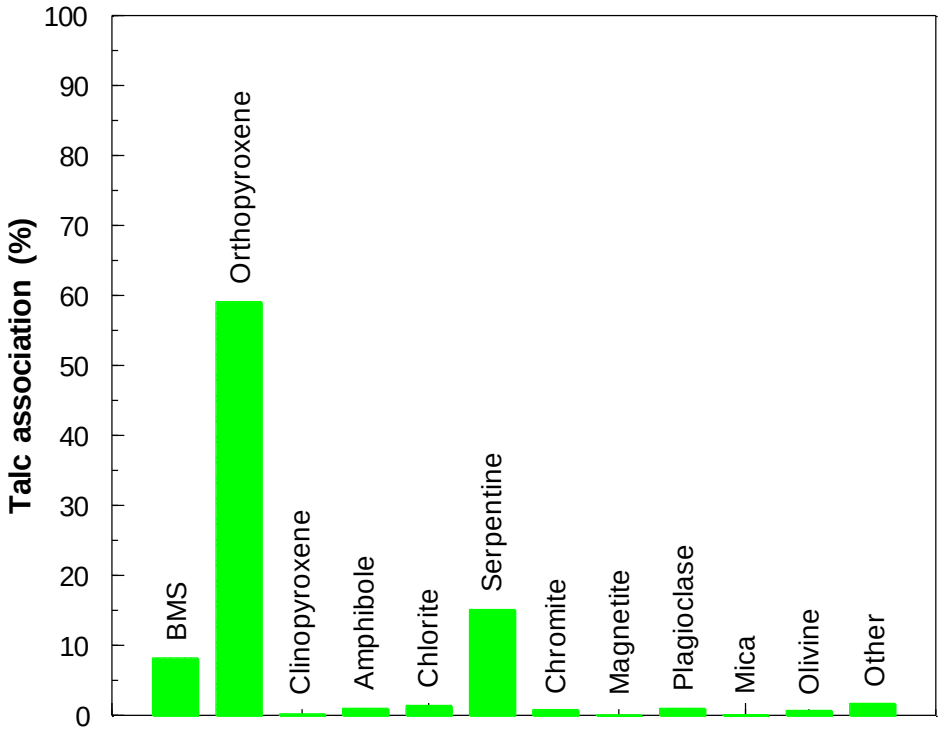

Figure 4.9: Association of unliberated talc in the Ore 1 feed. An unliberated particle has less than 90% of talc by area.

concentrate grade would in-part be due to the recovery of liberated talc grains and unliberated talc particles. Selected false colour particle images showing fine talc grains in association with orthopyroxene are illustrated in Figure 4.10. Here, fine talc was observed to be associated with a wide size range of orthopyroxene particles, where talc mainly occurs along the boundaries and fissures of the orthopyroxene particles. The presence of composite particles of orthopyroxene with finely disseminated talc emphasizes the need for a depressant.

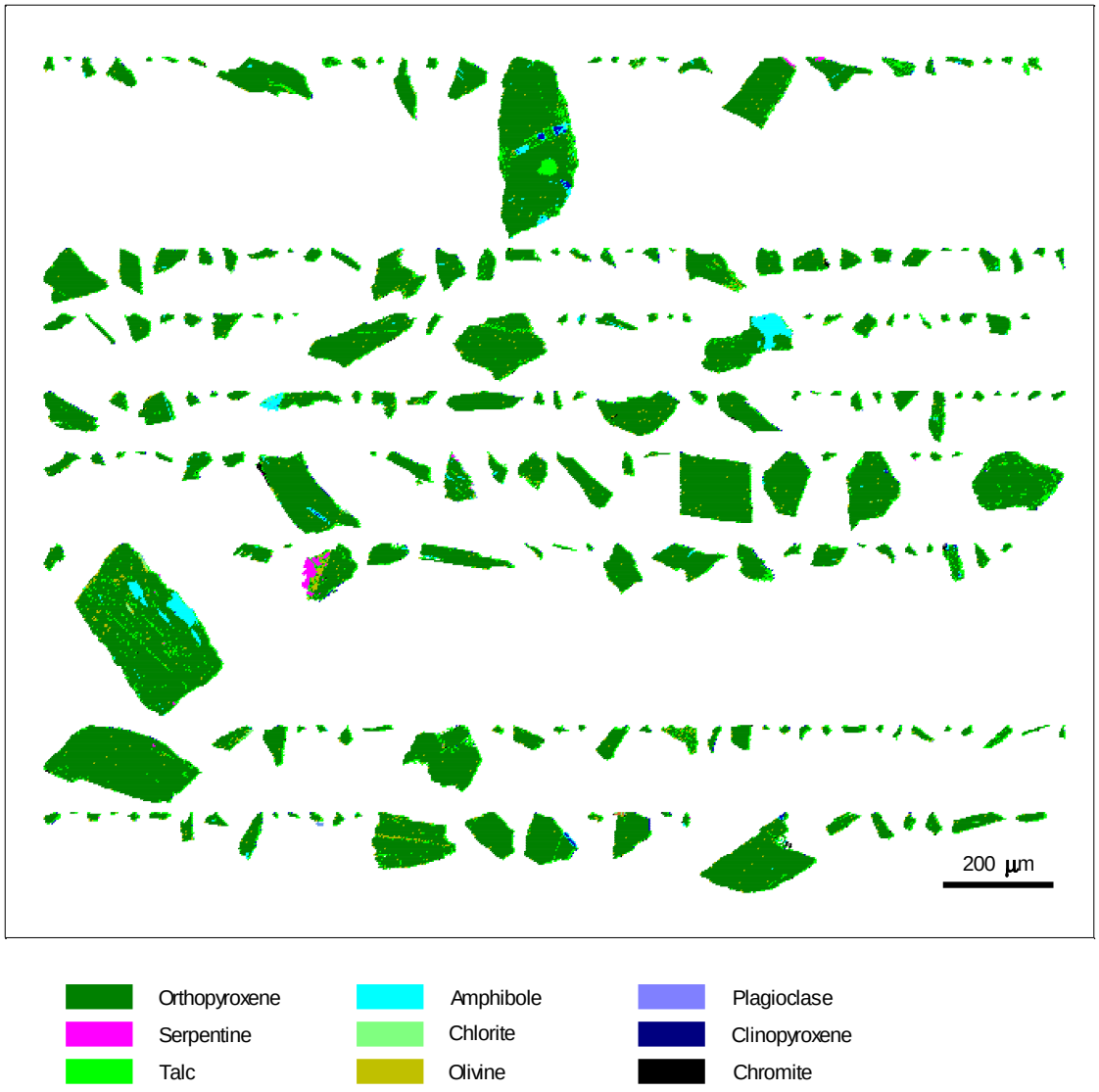

Figure 4.10: Selected QEMSCAN false colour particle images of fine-grained talc associated with orthopyroxene within the Ore 1 feed.

Key observations of Section 4.1.2 are summarized below:

1. Milling the ores produced gangue minerals smaller than 50 μm in size which makes minerals in this size fraction vulnerable to entrainment (Figure 4.2)
2. Both ores consist of large quantities of alteration minerals including serpentine and talc (Table 4.1 and Figure 4.3)
3. A significant proportion of serpentine occur as serpentine slimes in the feed, resulting in a BMS to serpentine slime ratio of approximately 1:7 (Figure 4.8), and
4. A small portion of talc is liberated, whereas the unliberated talc is mainly associated with orthopyroxene (Table 4.2 and Figure 4.9). Liberated and unliberated talc-orthopyroxene composites will likely constitute the floating gangue during flotation.

4.1.3. PGM characterisation

This section provides a PGM mineralogical and textural investigation of the Ore 1 feed. This includes a PGM species distribution, a PGE distribution, a PGM grain size analysis, and the liberation characteristics of the PGM species.

The quantitative PGM speciation data for the feed is provided in Figure 4.11. Gold is commonly included in the PGM analysis although it is often excluded in the PGE assay. In some cases, a fine-grained PGM locked within a silicate gangue particle will lead the QEMSCAN to analyze the whole particle. The EDS spectra picks up concentrations of PGEs in the silicate phase and the whole particle is classified as a PGM, which are known as 'PGE silicates'. Such PGMs are some of the liberated grains less than 10 μm in size. Most of the PGMs within the ore occurs as PGE arsenides, PGE sulphides, and PGE tellurides. Sperrylite, cooperite, and moncheite are the most common minerals within these groups, respectively. These mineral groups constitute 25.4, 25.3, and 12.5 of the PGM area %, respectively. Selected BSE images and corresponding false colour images are illustrated in Figure 4.12. This shows irregularly shaped and liberated characteristics of sperrylite and ferroplatinum grains (Figure 4.12a to c), where sperrylite is coarser in Figure 4.12c compared to sperrylite in Figure 4.12a. Due to the coarse grain size of the sperrylite grain illustrated in Figure 4.12c, which has a long axis of 35 μm and a short axis of 33 μm, the decision was made to exclude this particle nugget from all PGM statistics as it would bias the data. Unliberated PGMs have also been observed, as noted for ferroplatinum associate with chalcopyrite

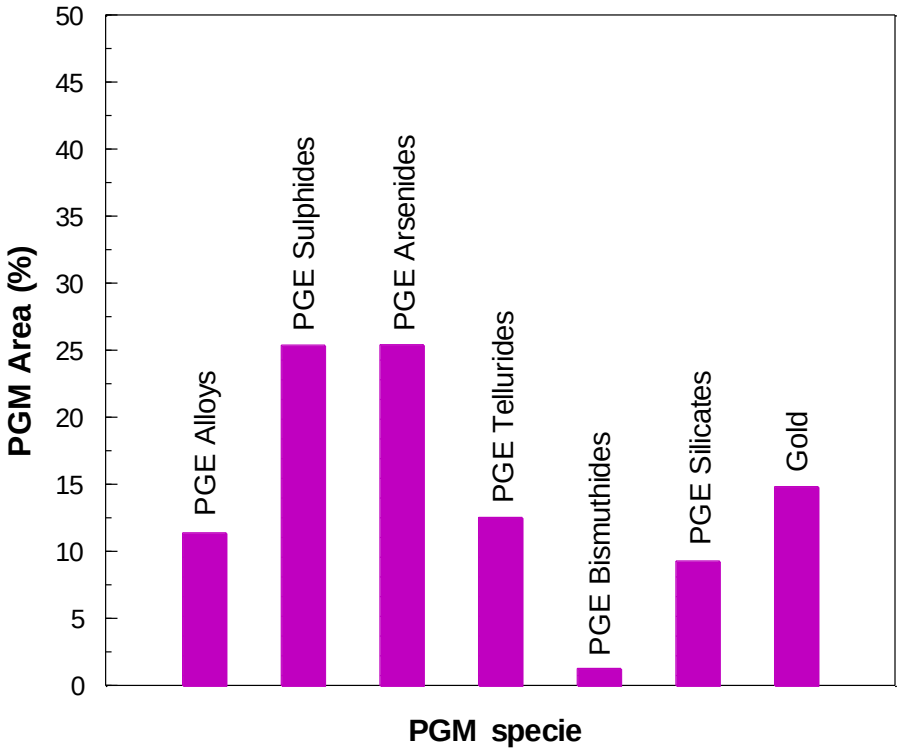

Figure 4.11: PGM distribution in the Ore 1 feed as determined using QEMSCAN. The total number of PGM-bearing particles was 112.

(Figure 4.12d), and PGMs such as sperrylite and kotulskite associated with the alteration minerals amphibole and serpentine in Figure 4.12e and Figure 4.12f, respectively.

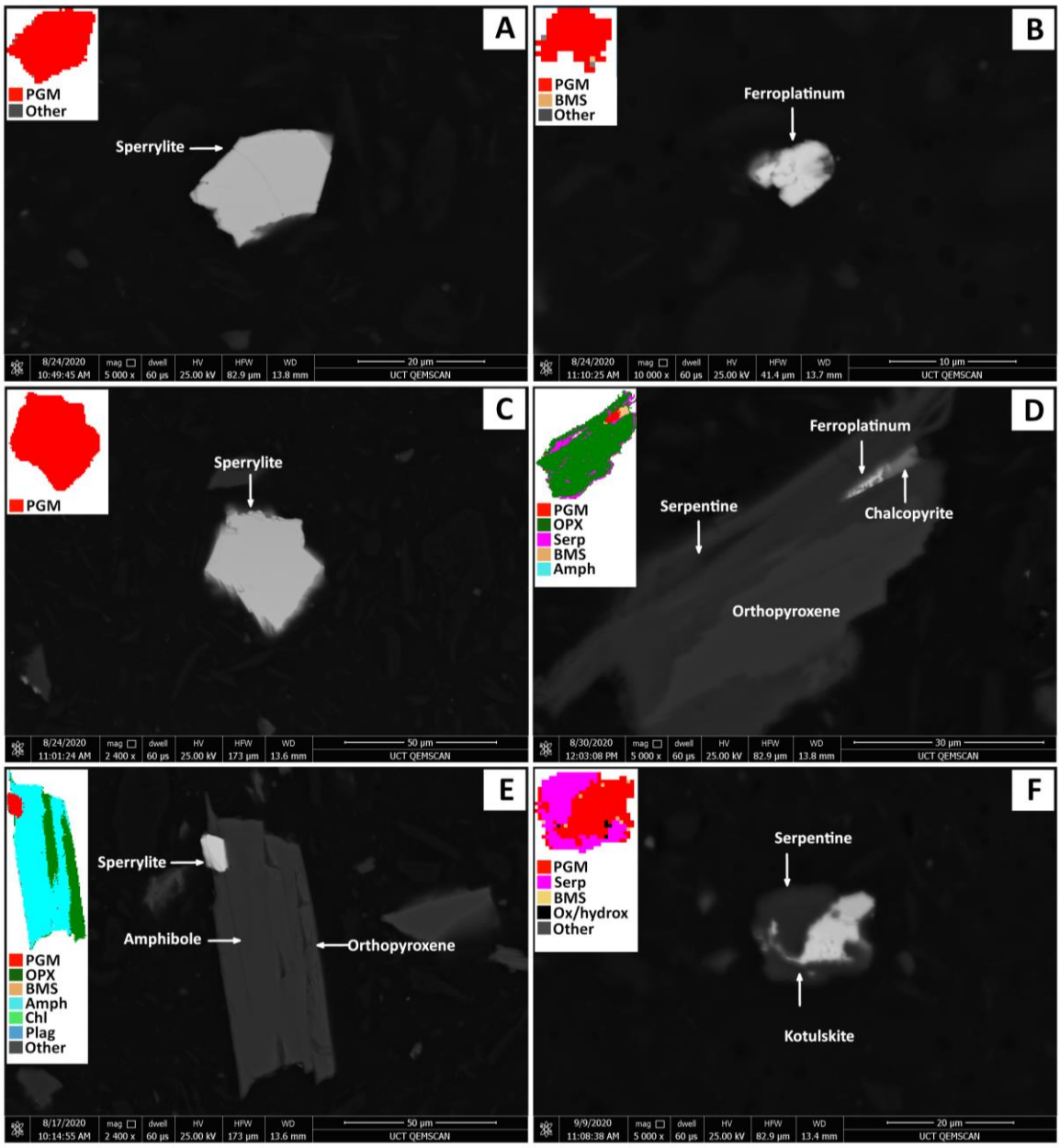

Figure 4.12: BSE and false colour images of a) liberated sperrylite (a PGE arsenide), b) liberated ferroplatinum, c) liberated sperrylite nugget, d) ferroplatinum associated with chalcopyrite which are in turn associated with orthopyroxene, e) sperrylite associated with amphibole, and f) kotulskite (a PGE telluride) associated with sperrylite.

The 6E PGE distribution within the -10 µm, +10/-53 µm, and +53 µm sized fractions are illustrated in Figure 4.13. The 6E PGE is the total grade of all PGEs including Au. Step-by-step calculations showing how the PGE distribution was determined are shown in Appendix A. The most dominant PGEs within

the ore are Pt and Pd, although a minor proportion of the other PGEs are found within each size fraction. The PGEs are mainly distributed within the +10/-53 µm sized fraction but are also found to occur within the coarse +53 µm sized fraction. Most Pt is present within the +53 µm sized fraction, whereas most Pd is present within the +10/-53 µm sized fraction. A significant proportion of the Pt and Pd are present within the +10 µm sized fraction, and the least within the -10 µm sized fraction.

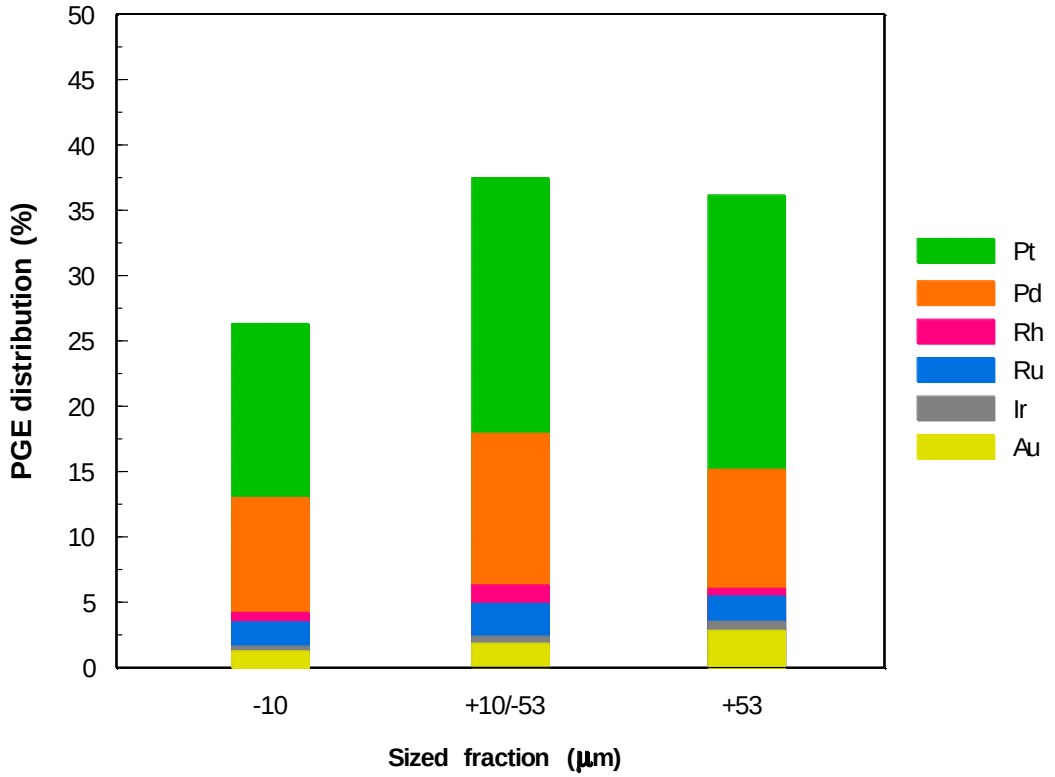

Figure 4.13: PGE distribution within the -10 µm, +10/-53 µm and +53 µm sized fractions of the Ore 1 feed.

Platinum-group element grades and the Pt/Pd ratios for both ores used in this study are shown in Table 4.3. Individual PGE feed grades are provided in Appendix A (Table A.4). The PGE grades for both ores are observed to be low. The Ore 1 6E PGE grade is 2.9 times higher than that of Ore 2, which contributed to higher individual PGE grades within Ore 1 relative to Ore 2. The majority of the 6E PGE grades are due to higher Pt and Pd grades relative to the other PGEs and Au, for both ores. However, it was observed that the Pt grades were higher than the Pd grades for both ores (Appendix A). The Pt/Pd ratio is much higher at 2.8 for Ore 1 compared to 2.0 for Ore 2. Ore 1 has a lower alteration content, and a higher 6E grade as observed in Figure 4.3 and Table 4.3, respectively. This is the reason for primarily investigating Ore 1 compared to Ore 2. It should be noted that both ores have Pt/Pd ratios between 2 and 5, which is the expected range for altered ores. This indicates that alteration greatly mobilized/removed Pd which was greatest in the location of Ore 1.

Table 4.3: PGE grades (g/t), and the Pt/Pd ratios for the ores used in this study.

PGE statistic	Ore 1	Ore 2
6E PGE + Au (g/t)	1.9	0.6
Pt/Pd ratio	2.8	2.0

The PGM grain size distribution within the feed is presented in Figure 4.14. The total amount of PGM particles analyzed was 112. Grains are discrete areas of a specific mineral hosted within a particle, whereas a particle consists of multiple mineral grains. Figure 4.14 clearly illustrates that the majority of PGMs are smaller than 10 µm in grain size, which accounts for approximately 65% of all PGM grains analyzed. The coarsest PGM grain size included in these statistics is 19.3 µm, which is the same grain that is illustrated in Figure 4.12a.

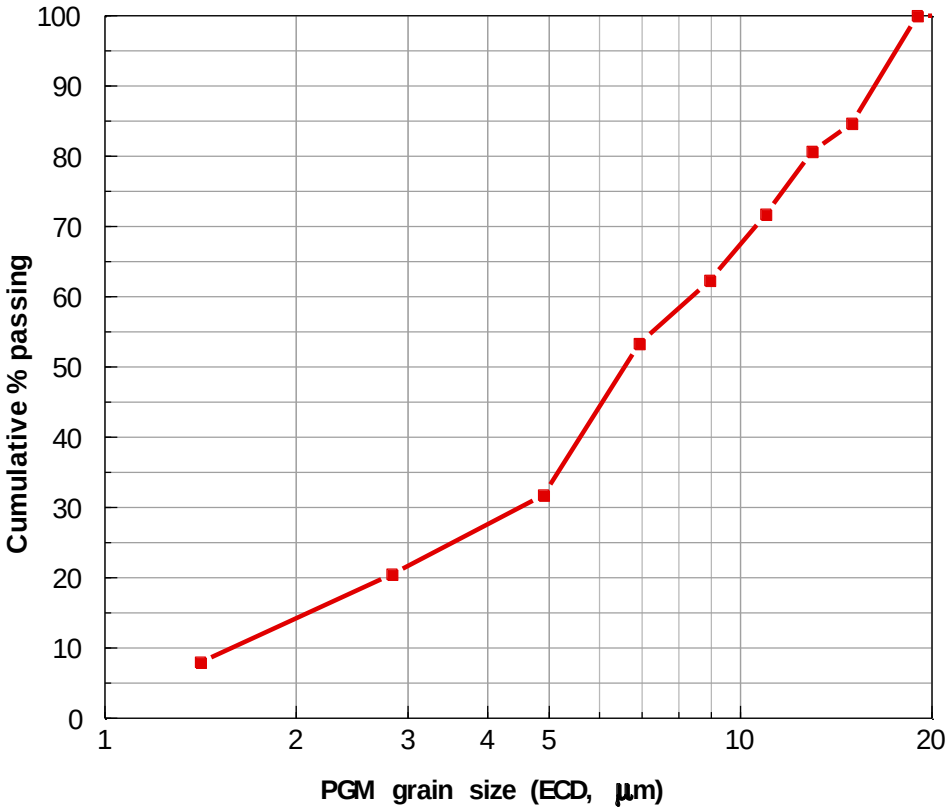

Figure 4.14: PGM grain size distribution within the Ore 1 feed. The total amount of PGM particles analysed was 112.

False colour images of liberated PGM grains, PGM/BMS particles, and these particles associated with alteration silicates, other silicates and oxides, by PGM grain size, are presented in Figure 4.15. Association statistics are commonly performed on a PGM and BMS as a combined unit, as this resembles the flotation response more closely than using PGMs alone. This is because PGMs are commonly associated with BMS which can contribute to the floatability of the PGM. Associations of PGM/BMS are therefore included. The mode of occurrence includes an "other silicate" mineral category, which refers to all non-alteration silicate minerals including orthopyroxene and plagioclase feldspar. The false colour image of the coarse liberated particles in the +15/-20 µm size fraction is the same as the high BSE grain illustrated in Figure 4.12a. Platinum-group minerals and PGM/BMS are associated with gangue below 15 µm in PGM size. It should be recognized that PGM/BMS occur in alteration silicates and PGMs are also attached to alteration silicates within Ore 1, which shows the association between PGMs as illustrated in Figure 4.15.

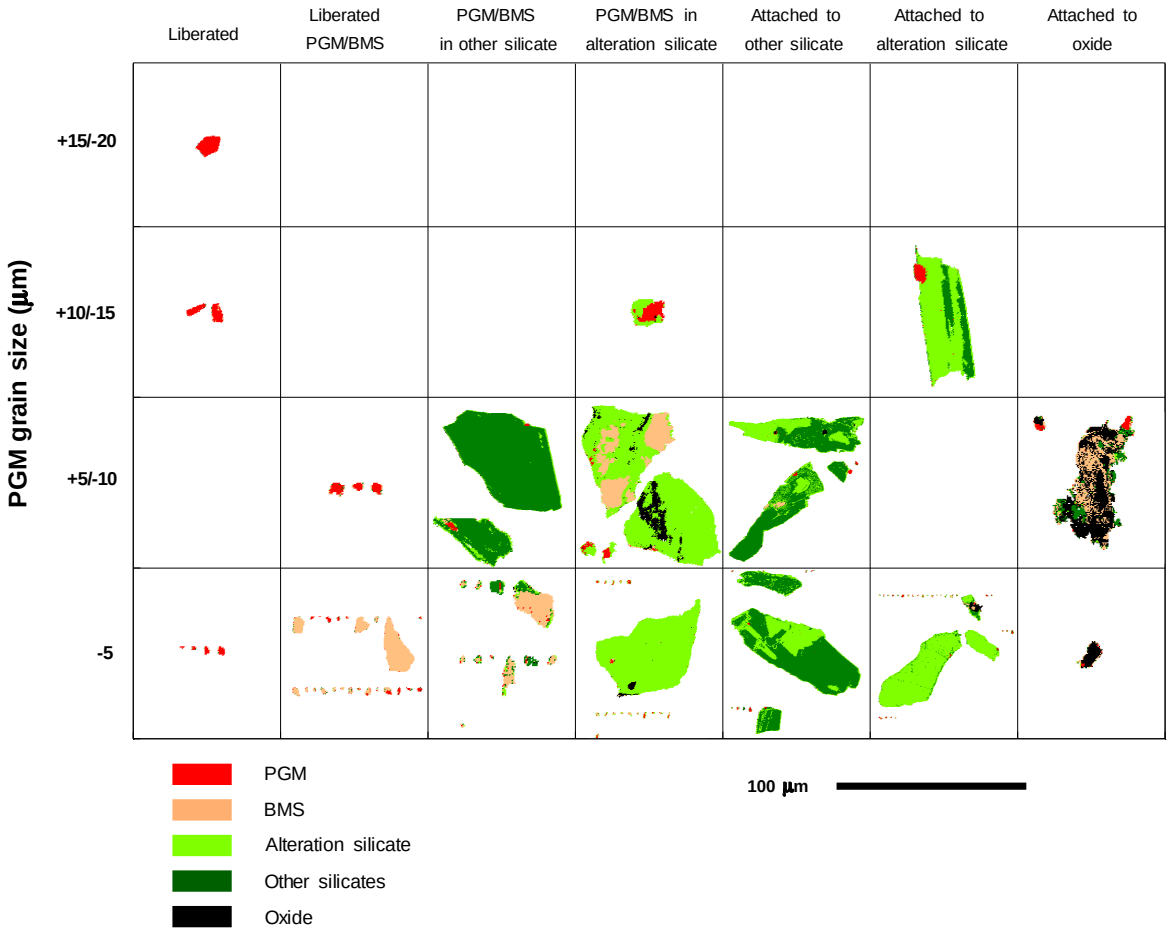

Figure 4.15: QEMSCAN false colour images of PGM and PGM/BMS liberation and association (Ore 1).

Liberation and association characterisation of the PGM species can indicate whether the recoveries may be limited by poor liberation. The PGM mode of occurrence are presented in Figure 4.16. Most PGMs are liberated which accounts for 33.0 area % of PGMs. This constitutes only seven of the 112 particles across fine to coarse-grained PGMs, as illustrated in Figure 4.15. There is also a significant proportion of PGMs associated with BMS which constitutes 12.6 area % PGMs. A significant portion of this is liberated PGM/BMS particles which, by observing the image grid in Figure 4.15, are below 10 μm in size. Collectively, liberated PGMs and liberated PGM/BMS accounts for 45.6 area %, which is nearly half of the PGM area distribution. This indicates that the other half of PGMs grains or PGM/BMS particles are associated with gangue which are expected to be more difficult to recover compared to liberated PGM grains or PGM/BMS particles. Figure 4.16 illustrates that unliberated PGMs and PGM/BMS are mainly associated with alteration silicates, which is also visually displayed in Figure 4.15. There are lesser associations of PGM/BMS particles associated with other silicates, and nearly equal amounts of PGMs associated with other silicates compared to alteration silicates. The smallest area % of PGMs are associated with oxides.

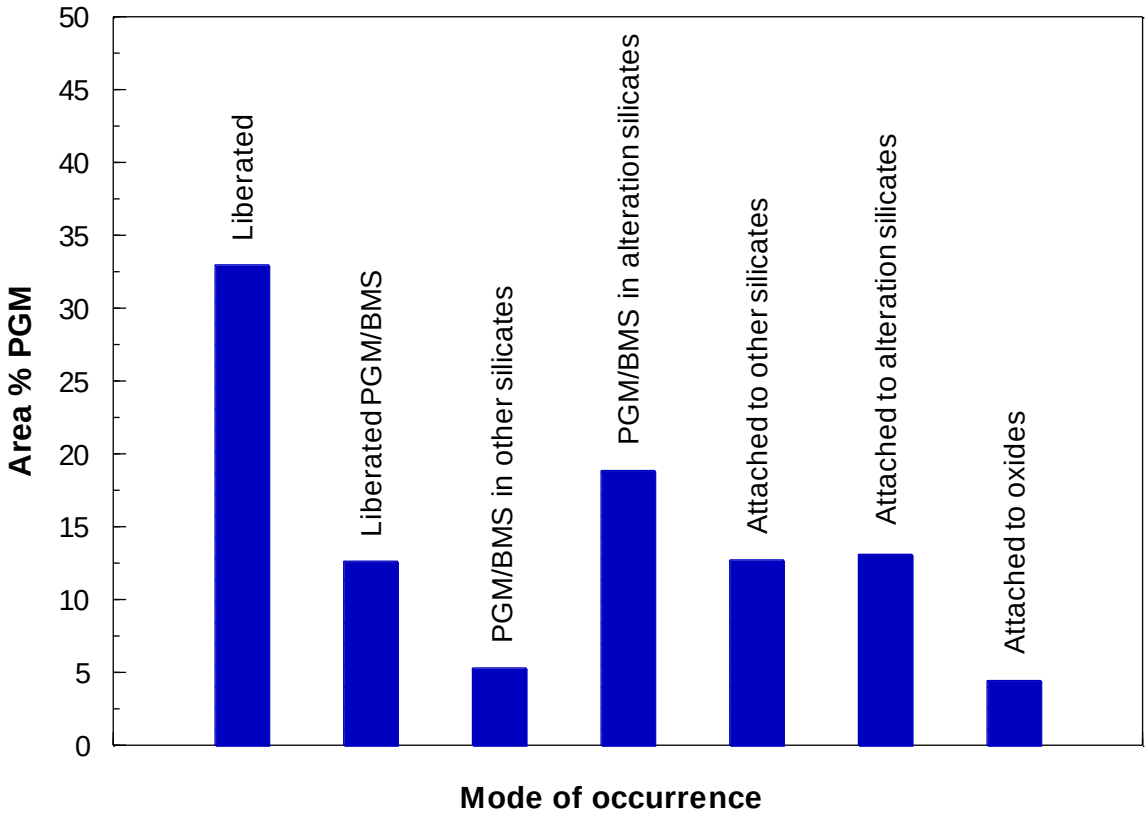

Figure 4.16: PGM mode of occurrence in the Ore 1 feed. Liberated: >80 area %. The 'PGM/BMS in' category indicates PGMs associated with BMS which are in turn associated with other minerals. The 'attached to' category refers to the association of discrete PGMs with other minerals: 30 ≥ Area % PGM > 0. The total number of PGM grains was 112.

Key observations in the PGM characterisation section are summarized below:

1. The dominant PGM species in the feed are the PGE arsenides, PGE sulphides and PGE tellurides, in decreasing order of abundance (Figure 4.11)
2. The most abundant minerals within these species are sperrylite, cooperite, and moncheite
3. Most PGEs occur in the +10 μm size fraction of the feed (Figure 4.13)
4. Both ores studied have very low PGE grades, however, Ore 1 has a higher PGE grade and Pt/Pd ratio than Ore 2 (Table 4.3)
5. The majority of PGMs are below 10 μm in grain size (Figure 4.14), and
6. Nearly half of the area proportion of PGMs constitutes of liberated PGM and PGM/BMS particles, whereas the rest of PGM grains and PGM/BMS particles are associated with gangue (Figure 4.16).

4.2. Bulk measurements

4.2.1. Introduction

Numerous studies in literature observed that SS was able to eliminate slime coatings, lower the pulp viscosity or yield stress, and depress silicate minerals (Amorós et al., 2010: 38; Feng et al., 2012: 12091; Silva et al., 2012: 209). However, most studies focused on idealized single mineral systems and therefore the addition of SS in a real system, containing many problematic mineral types, remains largely unstudied. This section aims to evaluate the flotation performance of a real ore as a function of SS dosage.

The first group of tests can be thought of as bulk response tests, i.e. the overall response of the ore is evaluated. This included both batch flotation and froth stability tests. Various batch flotation tests were performed where each aimed to address a specific objective. Firstly, to evaluate the flotation response of a real ore to SS addition, batch flotation tests at varying SS dosages were performed and the results are displayed in Section 4.2.2. Secondly, seeing as the addition of SS raised the solution pH, the isolated effect of this pH change was evaluated in a system absent of SS. These results are also displayed in Section 4.2.2. Lastly, seeing as most SS research was centered around the influence of SS on pulp viscosity, batch flotation tests at varying solids concentrations were performed to evaluate the pulp viscosity effect in the absence of SS. These results are also displayed in Section 4.2.2. It is well-known that batch flotation tests struggle to capture froth phase effects due to measurement scale. Therefore, dynamic froth stability measurements were made to aid the interpretation of the batch flotation results as well as to provide crucial information regarding isolated froth behaviour. The results from these froth stability tests at varying SS dosages are displayed in Section 4.2.3.

The second group of tests using a real ore is more specialized, focusing on a single aspect at a time. The batch flotation tests mentioned previously qualitatively evaluated the relationship between SS dosage and pulp rheology. However, direct measurements of slurry rheology at varying SS dosages were performed and these are displayed in Section 4.2.4. In addition to rheology measurements, particle settling tests were also performed. These experiments were mainly used to validate the results from the rheology experiments as particle settling will be directly related to pulp viscosity. The particle settling results for Ore 1 at varying SS dosages are displayed in Section 4.2.5. Lastly, mineralogical analyses of certain batch flotation concentrates were performed, and the results are displayed in Section 4.2.6. This was done to evaluate the effect of SS dosage on floatable gangue depression. Of particular interest during these mineralogical analyses were the behaviour of talc in Ore 1 as it represents the major floatable gangue component targeted by depressants.

A flow diagram outlining the results which will be presented in this section is provided in Figure 4.17. The white boxes show the information needed to understand each of the major topics addressed in this section (purple boxes). Boxes 'a' to 'd' serves to determine the effect of SS on the flotation performance, 'e' the froth stability in support of the recovered solids and water batch flotation results, 'f' to 'h' on the rheological modification effect of SS, 'i' the depressant effect of SS.

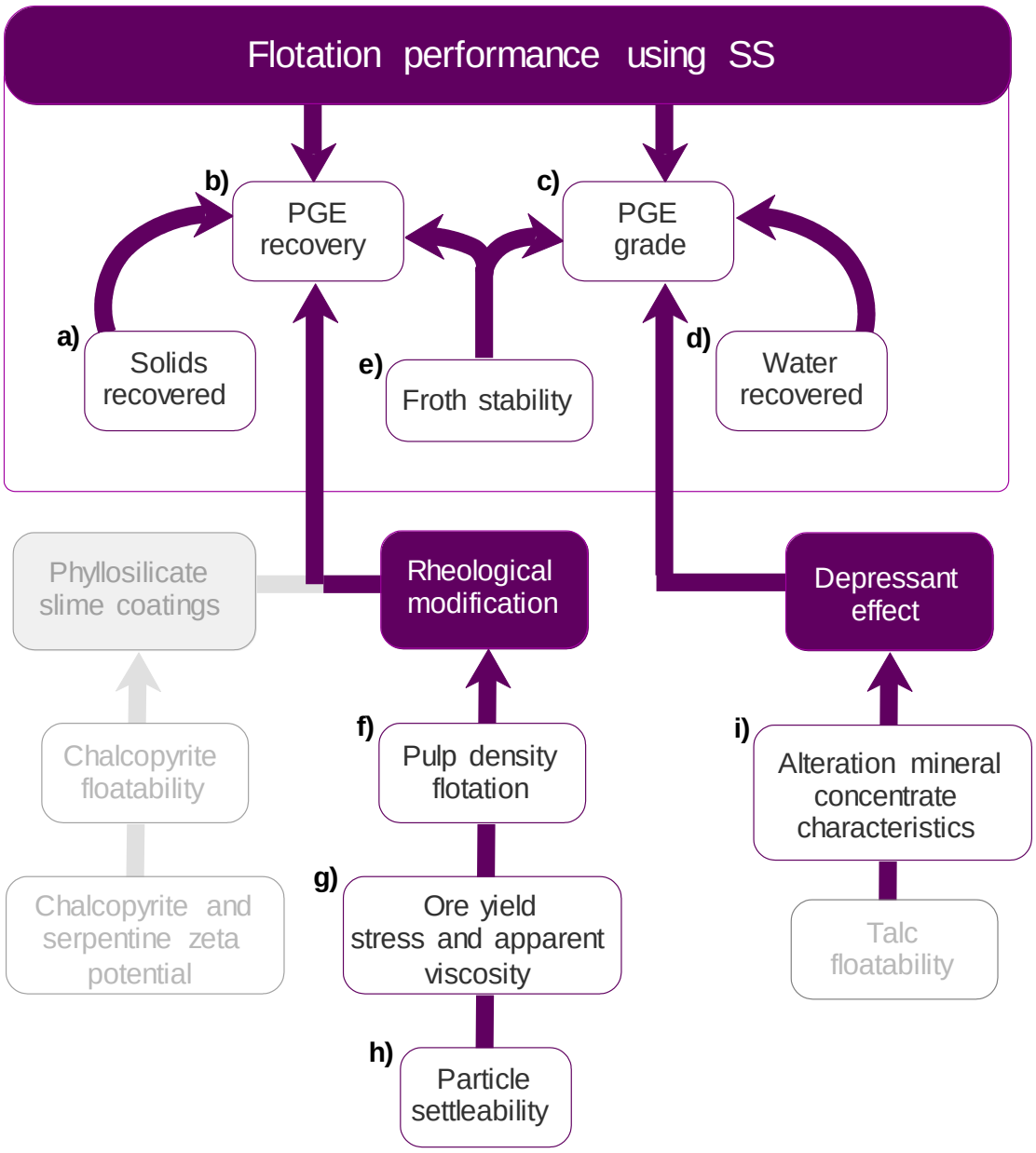

Figure 4.17: An outline of the bulk measurements section of the results showing the primary focus of the section (purple boxes), and presented information required to understand the main topics as indicated in white boxes. Greyed-out boxes represents a group of results which will be covered in another section.

4.2.2. Batch flotation

Effect of SS dosage on the flotation performance of Ore 1

The intention of this section is to present the SS batch flotation findings at 0 g/t, 215 g/t, 700 g/t, 1000 g/t, 1500 g/t and 2000 g/t performed on Ore 1. The results for selected SS dosages performed on Ore 2 will also be presented. The raw and calculated values for the Pt and Pd recovery and grade as well as the recovered mass of solids and water is displayed in Appendix B.

The recovered solids and water masses for each test is demonstrated in Figure 4.18 in terms of a) cumulative recovered solids and water and, b) total recovered solids and water as a function of SS dosage. Figure 4.18a highlights that the relationship between solids and water changes when SS dosages exceed 215 g/t and the data naturally separates into two distinct regimes. At higher SS dosages, less solids are recovered for the same water recovery. Figure 4.18b shows that the recovered solids decrease with increasing SS addition for dosages above 215 g/t. The 1500 g/t dosage resulted in the largest reduction in mass recovered with a 28.0% decrease over the baseline condition.

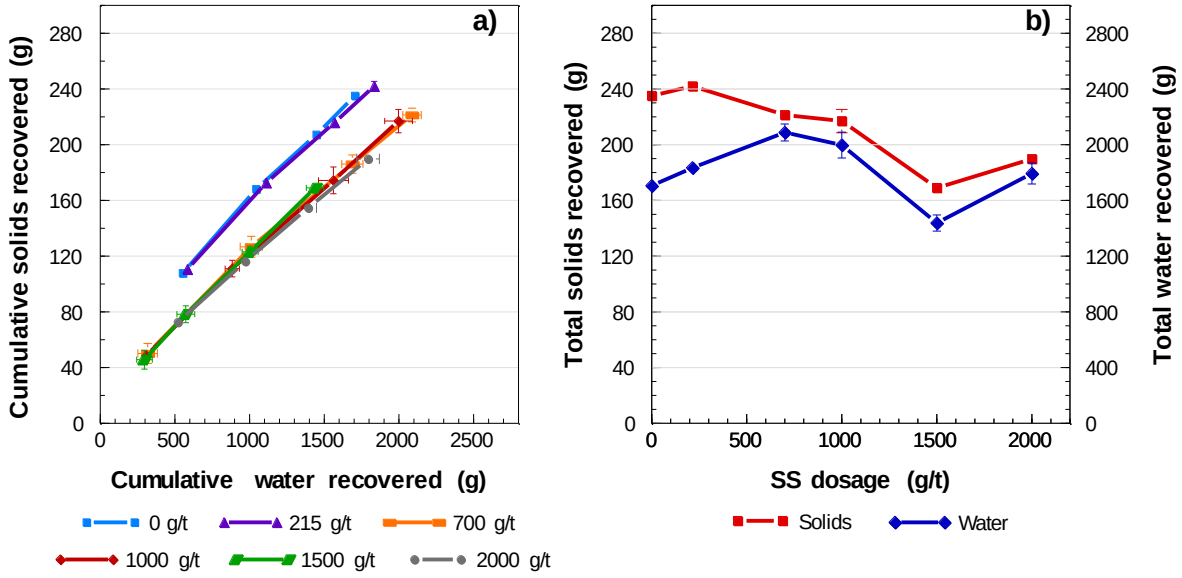

Figure 4.18: a) Cumulative recovered solids and water at various SS dosages and b) total solids and water recovered at various SS dosages. Error bars represent the standard error between duplicate tests.

Figure 4.19 plots the flotation performance of Pt and Pd at increasing SS dosages with respect to a) Pt recovery, b) Pd recovery, c) Pt grade/recovery, and d) Pd grade/recovery. Numerous interesting observations can be captured from this data. The baseline Pt and Pd recoveries are low compared to other PGM ores which is expected for an altered ore. The final Pt recovery achieved in the laboratory batch flotation cell was around 60%. Compared against a recent metallurgical survey (performed at the start of

2016) where a Pt recovery of nearly 70% was measured for the primary rougher, it is significantly lower. It should be noted that for a batch flotation cell with much higher mixing intensity coupled with little to no recovery loss due to froth effects, one would expect a higher recovery than the industrial device. Therefore, the significantly lower measured batch recovery points towards either a more altered test ore or a more defined response irrespective of scale in the absence of normal process variation accompanying industrial measurements. Regardless of the source of the difference, this further emphasizes the need of a dispersing agent to combat the effects brought about by an altered ore.

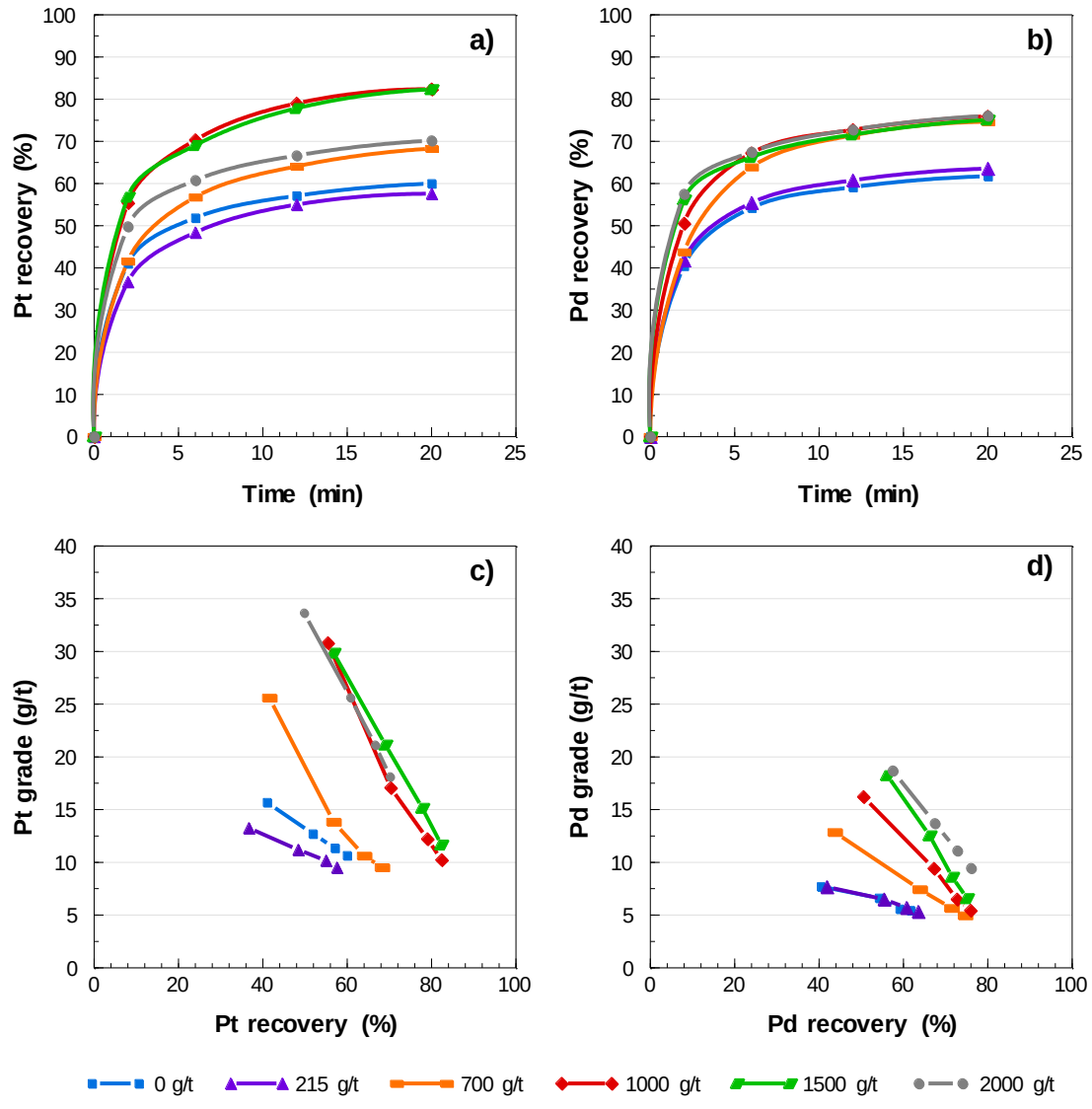

Figure 4.19: a) Pt recovery as a function of time, b) Pd recovery as a function of time, c) Pt grade as a function of Pt recovery and d) Pd grade as a function of Pd recovery at the various SS dosages.

Figure 4.20 shows the final recovery and grade for Pt and Pd presented in Figure 4.19, as a function of SS dosage. It is evident that the Pt and Pd recovery increased with an increase in SS dosage from 0 g/t to 2000 g/t, with some small deviations. Adding 1000 g/t and 2000 g/t SS resulted in the highest overall Pt and Pd recoveries respectively, which improved by 22.4% and 14.3% compared to the baseline. It should be noted from now onwards, a 'high dosage' refers to an experiment using more than 1000 g/t SS. It is thought that the significant improvement in Pt and Pd recoveries is mainly a function of slime dispersion and reduced pulp rheological complexity caused by SS addition.

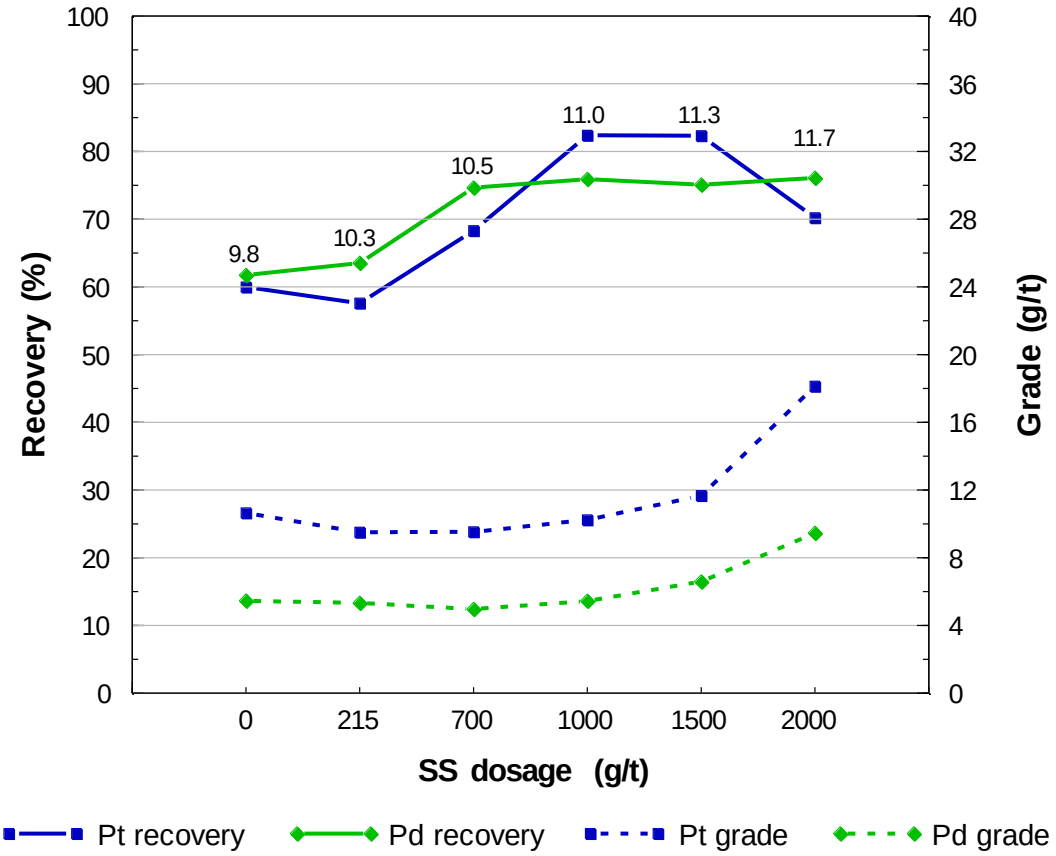

Figure 4.20: The final Pt and Pd recoveries and grades at the various SS experiments. The pulp pH at each dosage is presented above the recovery results.

In addition to poor flotation recoveries observed at the baseline and 215 g/t SS experiments, poor Pt and Pd grades were measured to be 10.6 g/t for Pt and 5.5 g/t for Pd, as shown in Figure 4.19 and Figure 4.20. This highlights the need for an effective depressant to control NFG recovery which is expected for an ore containing 5.0 wt.% talc. Grades typically increased with an increase in SS except for a few outliers. Using a SS dosage of 2000 g/t resulted in the highest Pt and Pd grade which increased by 7.5 g/t and 4.0 g/t, respectively. It should be noted that grade is a dependent variable, i.e. the outcome of a series of interrelated sub-processes. Therefore, the improvement in grade can be a function of floatable gangue

depression, decreasing slurry apparent viscosity, changing froth characteristics or a combination of all. The grade enhancements with high SS dosages might be a function of talc depression and/or an improvement in rheology which led to less entrainment. It is important to note that depressants not only influence the recovery of NFG, but also impact the froth stability based on the reduction of solids reporting to the froth. Special attention will be placed on these parameters to decouple the grade effect of SS so that the contributions towards improved concentrate grade is clear.

Figure 4.21 plots the flotation performance of Pt and Pd at increasing SS dosages with respect to a) Pt recovery/cumulative concentrate solids mass, b) Pd recovery/cumulative concentrate solids mass, c) Pt grade/cumulative concentrate water mass, and d) Pd grade/cumulative concentrate water mass. As expected, the Pt and Pd recoveries increased with an increase in concentrate solids recovered for each individual SS dosage. It is well-known that an increase in valuable mineral recovery correlates with an increase in solids recovery. In terms of a particular SS dosage, the recovery increased with increasing solids recovery, as expected. However, when different SS dosages are compared, this is not the case - a decrease in recovered solids correlated with an increase in Pt and Pd recovery, with the exception of some outliers. The recovery improvement is therefore not a by-product of solids recovery changes, but due to a fundamental change in separation efficiency. For example, the solids recovered between the baseline and 1000 g/t SS recorded similar values, however, their Pt recoveries are very different: 60.0% and 82.4% respectively.

The Pt and Pd grades decreased with an increase in the quantity of concentrate water recovered for each individual SS dosage, as expected. No trend relating final grades to water recoveries can be noted and points to a fundamental change in separation efficiency. For example, similar final water recovered masses were recorded for the 215 g/t and 2000 g/t SS experiments, however, very different Pt grades were noted between these dosages; 9.5 g/t as opposed to 18.1 g/t respectively.

Key observations of the SS flotation performance investigation are summarized below:

1. The Pt and Pd recoveries and grades were significantly improved at high SS dosages (Figure 4.19 and Figure 4.20) and
2. Observing the recovery/solids and grade/water curves highlights a fundamental change in separation efficiency (Figure 4.21).

The Cu and Ni recoveries and grades were also determined. The Cu and Ni results follow very similar trends to that of Pt and Pd and, therefore, there is no need to present the results in the main text. The batch flotation Cu and Ni recoveries and grades are provided in Appendix B.

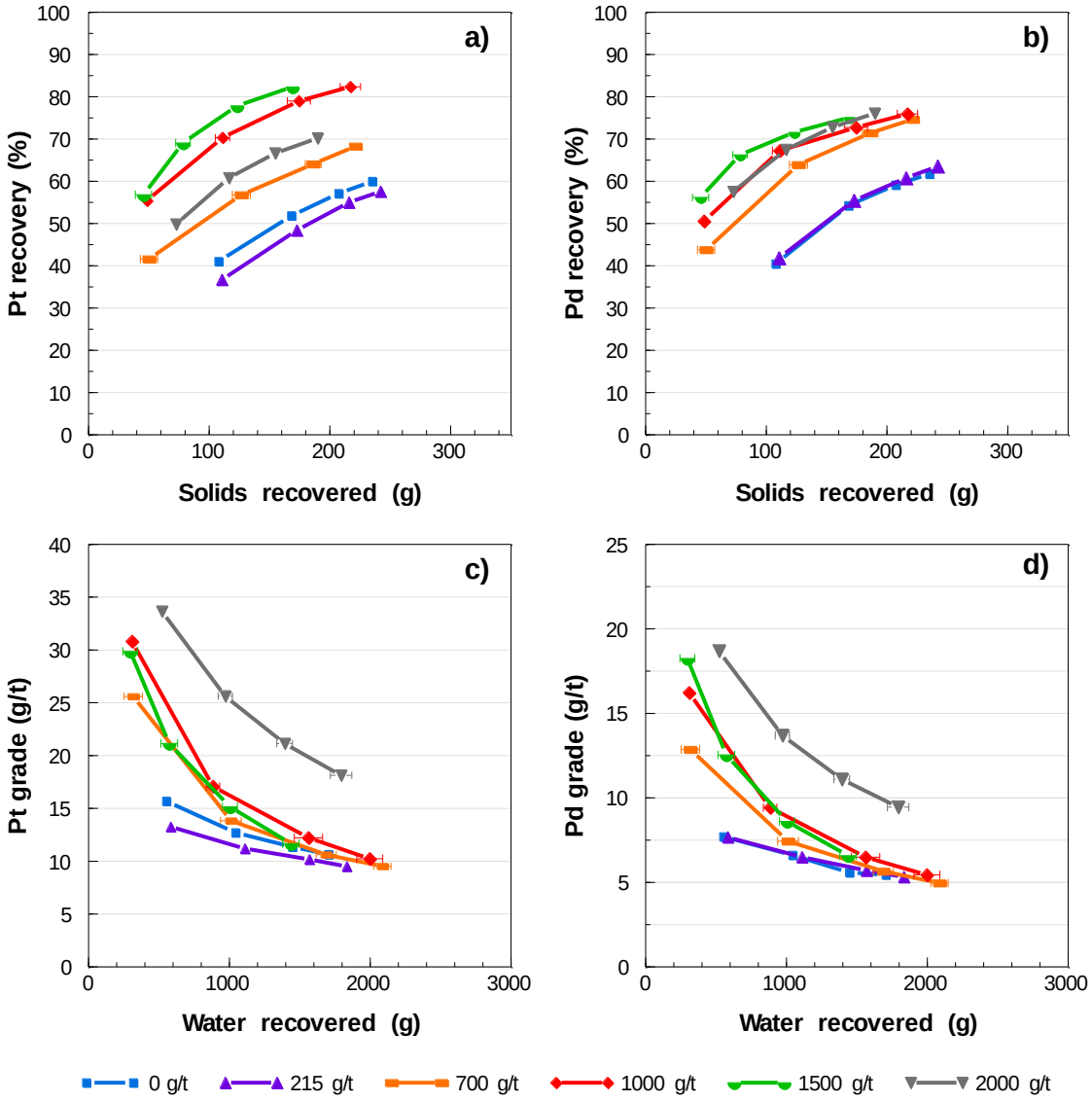

Figure 4.21: a) Pt recovery as a function of solids recovered, b) Pd recovery as a function of solids recovered, c) Pt grade as a function of water recovered and d) Pd grade as a function of water recovered at the various SS dosages. Error bars represent the standard error between duplicate tests.

Effect of pH on the flotation performance of Ore 1

The natural pH of the slurry at the various dosages is shown above the recovery results in Figure 4.20. With an increase in SS dosage, from 0 g/t to 2000 g/t, the pulp pH was observed to increase from pH 9.8 to 11.7, as shown in Figure 4.20. In earlier work, the effect of pH was identified as a key variable in the flotation response during sulphide and PGE froth flotation (Goktepe, 2002: 313; Miller et al., 2005: 857; Muzenda et al., 2011: 3). It was therefore critical to determine whether the pH effect was partially responsible for the improved flotation response observed in the SS dosage batch flotation tests. The 2000

g/t SS dosage, which had a pH of 11.7, was therefore compared to an experiment performed at pH 11.7 without SS addition, which is referred to as the 'pH modified test'.

The Pt and Pd recovery and grade for the 0 g/t, 2000 g/t SS and pH modified tests are compared in Figure 4.22. The Pt recovery at the pH modified test exceeded that of the 2000 g/t test, whereas the Pd recovery highlighted no real difference between the pH modified and 2000 g/t SS tests. It is important to note, however, that both these conditions still provide a significant improvement over the baseline. As opposed to the significant recovery improvements at the pH modified test, the Pt and Pd grades were much lower than both the 2000 g/t and the baseline tests. The results presented in Figure 4.22 clearly illustrate that pH has a large influence on flotation response; however, pH modification to improve recovery will inevitably lead to grade penalties.

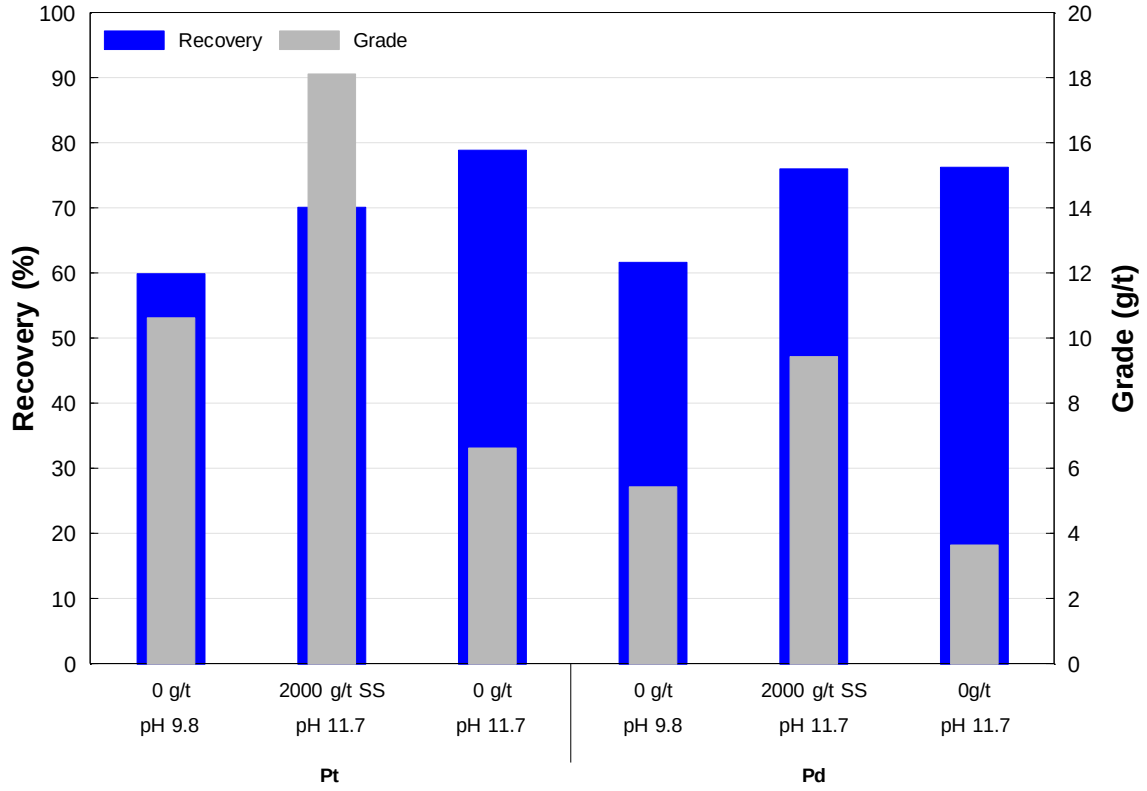

Figure 4.22: Comparison of the final Pt and Pd recovery (primary axis) and grades (secondary axis) between the baseline, 2000 g/ SS and pH 11.7 modification tests.

Similarly to what was presented in Figure 4.21, the flotation performance for the baseline, 2000 g/t SS and the pH modified tests are presented in Figure 4.23. The high solids recovery observed for the pH adjusted experiment correlates with higher Pt and Pd recoveries, compared to the baseline test. This clearly illustrates the common relationship between solids recovered with valuable mineral recovery. However, a selective increase in recovery can be noted, particularly for Pt, since the recovery-mass curves are not

overlaid on one another. It is clear from these curves that the addition of SS still results in a higher Pt and Pd recovery at a much lower solids recovery compared to the pH modified test. Poorer Pt and Pd grades at the pH adjusted experiment correlated with high water recoveries which is also the expected relationship found in various studies. The Pt/Pd grade-water relationship was very much the same for the pH adjusted and baseline (0 g/t) experiments. This showed that higher grades were achieved at the same water recovery for the 2000 g/t SS experiment than when no SS was added.

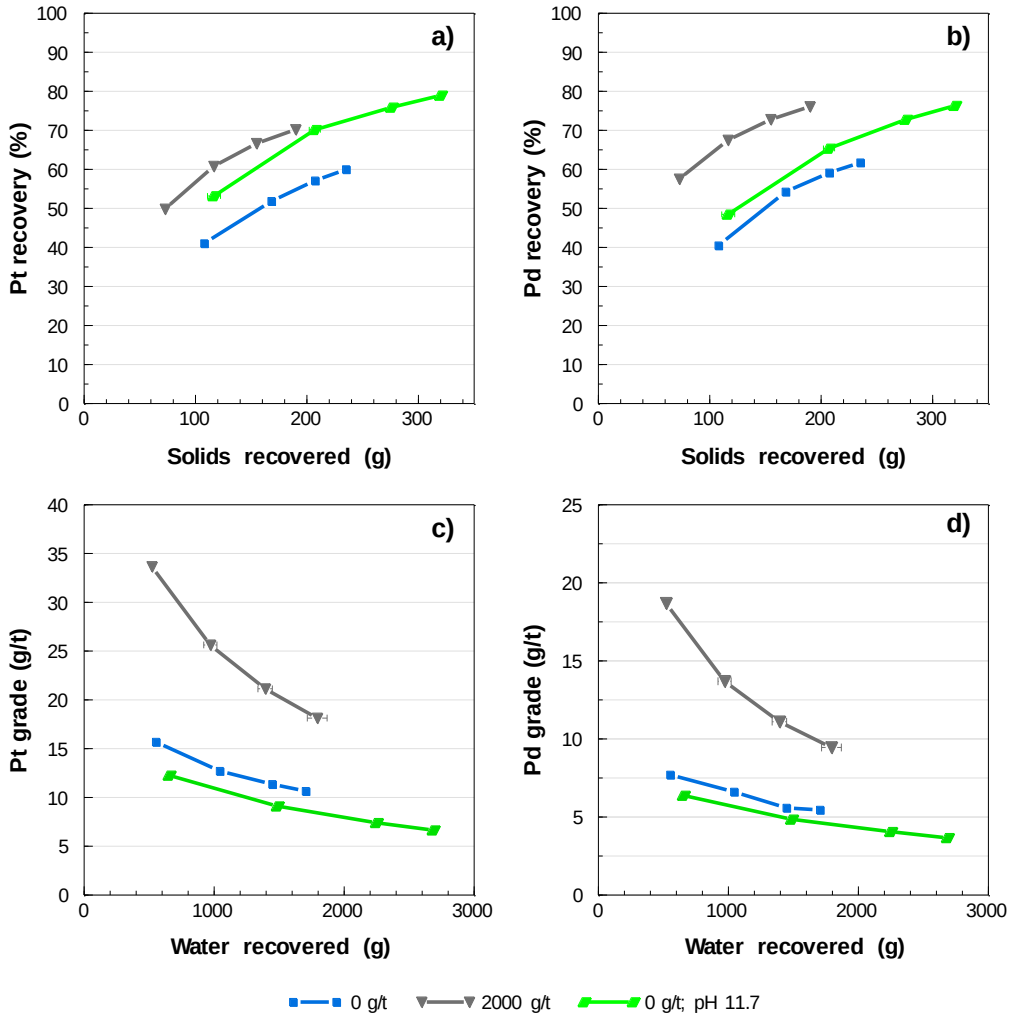

Figure 4.23: a) Pt recovery as a function of solids recovered, b) Pd recovery as a function of solids recovered, c) Pt grade as a function of water recovered and d) Pd grade as a function of water recovered at the baseline (0 g/t), 2000 g/t SS and the pH modified test. Error bars represent the standard error between duplicate tests.

Key findings of the effect of pH on the flotation response are summarized below:

1. The flotation response is sensitive to the solution pH as high Pt and Pd recoveries were noted, however, this comes at a substantial grade penalty (Figure 4.22), and

2. A pH 11.7 adjustment, without SS addition, resulted in higher solids and water recoveries (Figure 4.23). The higher solids mass recovered was not the only factor contributing to higher Pt and Pd recoveries, since these showed to have a higher recovery at a similar mass pull. The lower grade was a result of higher water recoveries and had a similar trend to that when no SS was added.

Effect of solids concentration on the flotation performance of Ore 1

It is well established in the literature that water addition has a beneficial effect on flotation performances. It is argued that the main reason behind this phenomenon is the reduction in rheological challenges in both the pulp and froth, as mentioned in Chapter 2. Earlier in this section, it was highlighted that SS addition has a significant influence on the flotation performance, which has been hypothesized to be due to the contribution of a reduced pulp rheological complexity. This section aims to evaluate how a decrease in solids concentration influenced the flotation response of Ore 1, and how the most successful solids concentration response compares to the most successful SS response. This serves to determine whether a reduced pulp viscosity benefited the recoveries observed during SS flotation. Batch flotation tests were performed at 15 wt.%, 25 wt.%, 30 wt.% and 35 wt.% solids concentrations by mass. A 35% concentration was chosen to be the baseline test because the PPM operation used this concentration within their primary roughers feed. This concentration at 35% solids is the same as the '0 g/t' condition displayed earlier in this section.

The cumulative solids and water recovered at various solids concentrations are illustrated in Figure 4.24. It

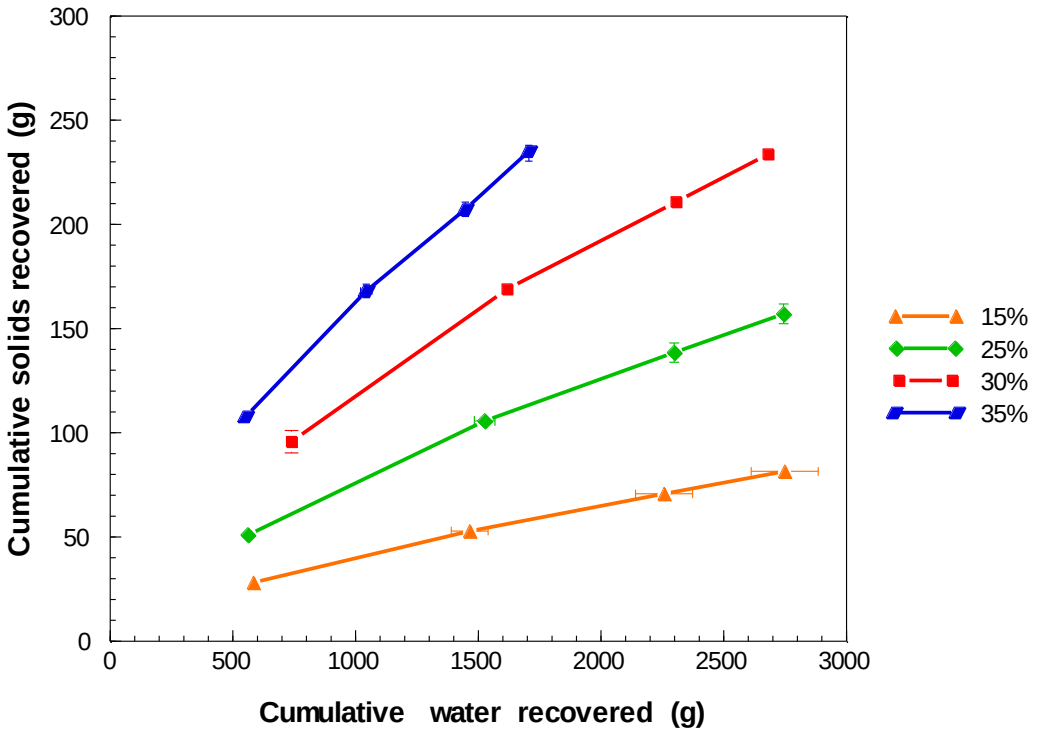

Figure 4.24: Cumulative solids and water recovery at various solids concentrations (wt.%). The 35 wt.% experiment is the baseline test and is the same result reported as '0 g/t' earlier in this section. Error bars represent the standard error between duplicate tests.

can be seen from Figure 4.24 that an increase in solids concentration has a significant relationship to recovered solids and water: an increase in solids concentration resulted in an increase in solids recovered per unit of water. The 35 wt.% run recovered the lowest amount of water but had the largest solids recovery. A 15 wt.% solids concentration obtained the lowest solids concentration, although the water recovery for this experiment is similar to that recovered at 25 wt.% and 30 wt.%.

Figure 4.25 illustrates the flotation performance at different solids concentrations with respect to a) Pt recovery, b) Pd recovery, c) Pt grade/recovery, and d) Pd grade/recovery. To summarize and highlight the trends of the data presented in Figure 4.25, Figure 4.26 plots the final recovery and grade for both Pt and Pd, as a function of solids concentration. The data highlighted that a decrease in solids concentration significantly improved the Pt and Pd recoveries. A recovery improvement of 14.5% and 21.2% were found relative to the baseline experiment for both Pt and Pd, respectively. The results clearly indicate that the flotation performance of Ore 1 is significantly improved at lower solids concentrations with regard to

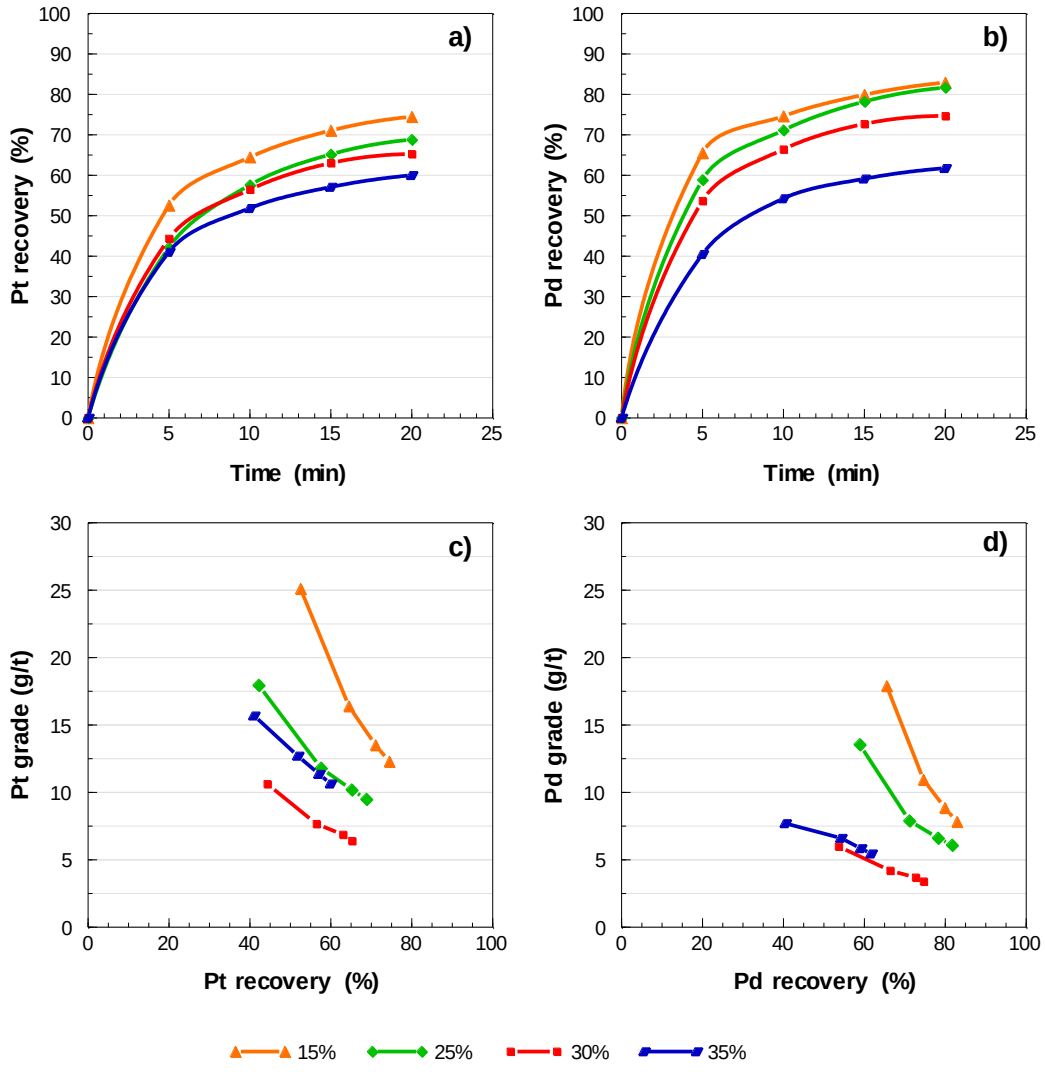

Figure 4.25: Pt recovery as a function of time, b) Pd recovery as a function of time, c) Pt grade as a function of Pt recovery and d) Pd grade as a function of Pd recovery at the various solids concentrations.

valuable recovery. Moreover, the magnitude of the improvement highlights the problematic rheological nature of the ore and how it impacts flotation performance.

Below 30 wt.%, a decrease in the solids concentration was found to increase the Pt and Pd grade, as indicated in Figure 4.25 and Figure 4.26. This comes with the exception at 35% solids, which was otherwise observed to deviate from this trend. Grades were enhanced by 1.6 g/t and 2.4 g/t relative to the baseline test for Pt and Pd, respectively, at 15 wt.%. Reducing the solids concentration was therefore not only found to enhance Pt and Pd recovery, but also their grades. Improvements in grade are correlated to less entrainment since entrainment is directly proportional to the amount of solids present in the pulp. In addition, froth characteristics are expected to change with decreasing solids concentration.

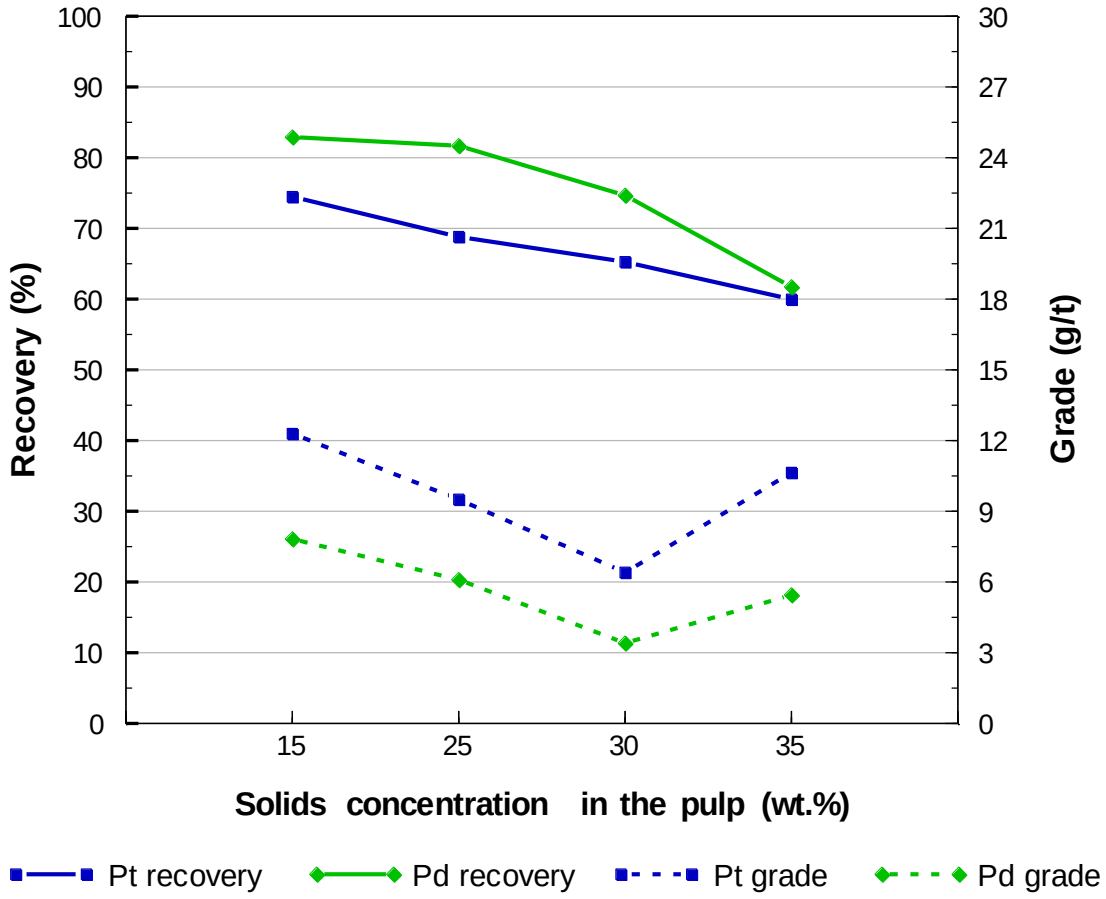

Figure 4.26: The final Pt and Pd recoveries and grades at the various solids concentrations.

A direct comparison between the behaviour of solids concentration and SS is provided in Figure 4.27. The 2000 g/t SS run was chosen because it performed overall best during the SS dosage investigation, as observed earlier in this section. Substantial Pt and Pd recovery improvements were observed for the solids concentration experiments over SS addition. However, the SS run performed substantially better when comparing the product grade. This highlights that the action of SS is somewhat different to a reduction in solids concentration and is not only a function of slurry rheology. Grade enhancements with SS addition is an indication that SS acted as a depressant and not only contributed towards a reduction in entrainment. A summary of the key findings in the ore dilution and SS investigations is provided in Table 4.4.

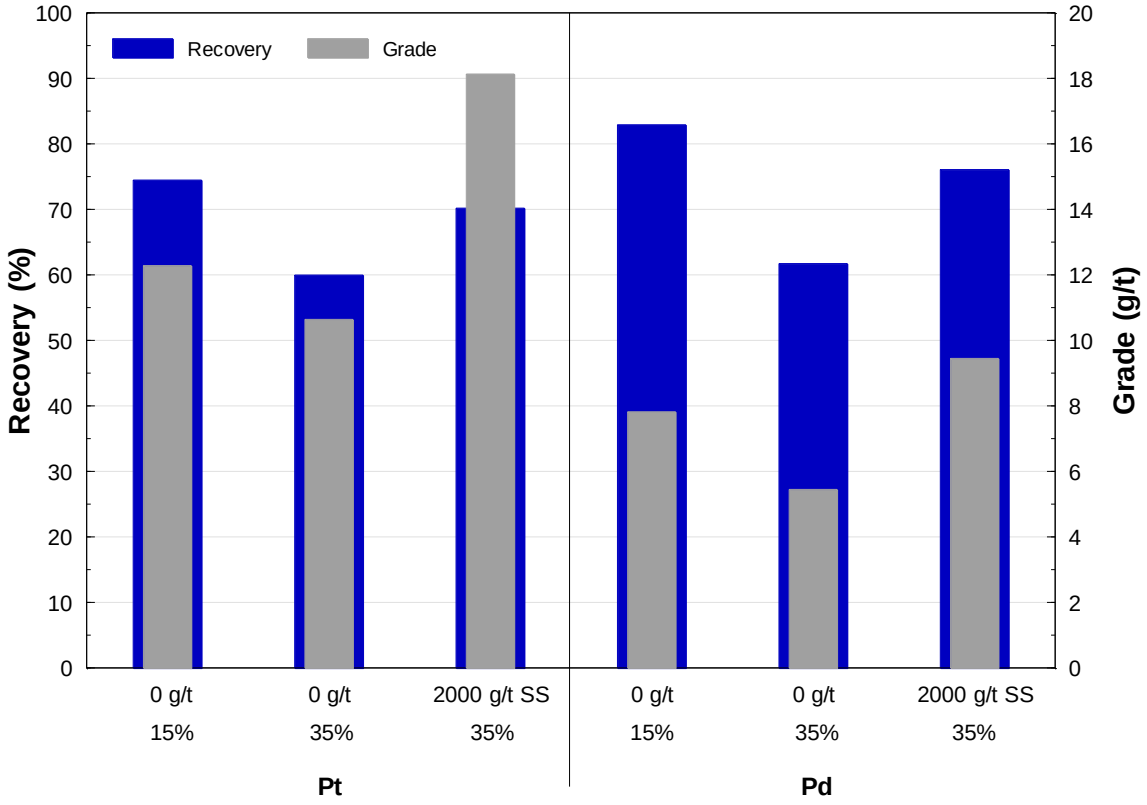

Figure 4.27: Comparing the Pt and Pd recovery and grade between the baseline, 15 wt.% solids concentration and the 2000 g/t SS experiments.

Table 4.4: Key findings of ore dilution and SS on the Pt and Pd recoveries, Pt and Pd grades, solids recovered, and water recovered.

Pulp factor change	Final Pt recovery (%)	Final Pd recovery (%)	Final solids recovered (g)	Final Pt grade (g/t)	Final Pd grade (g/t)	Water recovered (g)
↑ Dilution	Increase	Increase	Decrease	Increase	Increase	Increase
↑ SS	Increase	Increase	Decrease	Increase	Increase	Decrease

The following points highlight the key findings obtained from the solids concentration investigation:

1. A 15 wt.% solids concentration significantly benefited the Pt and Pd recoveries and slightly benefitted their grades (Figure 4.25 and Figure 4.26)
2. A 15 wt.% solids concentration resulted in higher Pt and Pd recoveries compared to SS, however, SS addition produced superior grades (Figure 4.27), and
3. Differences in solids concentration and SS responses indicate that the success of SS is not only due to a change in rheological properties of the pulp, but also a change in direct or indirect functions affecting grade (Figure 4.27).

4.2.3. Froth stability

Froth stability is known to greatly influence flotation behaviour, as mentioned in Chapter 2. This section will evaluate the change in froth stability at varying SS dosages. Previously, it has been shown that pH had a large influence on flotation behaviour and therefore this condition was also included in the froth stability investigation. This was done to decouple the influence of pH modification from the effect of SS species on froth stability. All tests were performed in both 2-phase and 3-phase systems. Two-phase tests were performed to determine whether the observed behaviour is due to interactions at the air/liquid interface as well as the interactions with solids.

Dynamic foam and froth stabilities for 2-phase and 3-phase experiments at the varying SS dosages are represented in Figure 4.28. Two-phase foam stability experiments revealed that there is an initial increase in stability up to a SS dosage of 215 g/t, which thereafter decreased with an increase in dosage. A change in foam stability with dosage in the 2-phase system is therefore an indication that SS impacted the properties at the air-water interface.

Introducing solids into the froth column, as indicated during 3-phase experiments, decreased the froth stability with an increase in SS dosage, as displayed in Figure 4.28. When no SS is present, relatively higher froth stability during 3-phase experiments compared to 2-phase experiments indicates that the presence of solids resulted in a more stable froth. This is expected because the presence of solids was observed to stabilize the froth by various other investigators (Johansson & Pugh, 1992: 20; Farrokhpay, 2011: 3). Using SS had a significant effect on the froth stability, with froth stability decreasing from 15.0 seconds at the baseline experiment, to 3.3 seconds at a dosage of 2000 g/t. With the addition of SS, the 3-phase experiments have a lower dynamic stability compared to the 2-phase experiments. As mentioned previously, the stabilizing effect of solids addition on a froth is well-known and therefore this is an unexpected result. This may be a direct result of two distinct influences of SS. Firstly, this may indicate that SS significantly depressed the NFG which decreased the froth stability. Secondly, it may be a result of the increased drainage characteristics of a less rheologically complex slurry. Three-phase froth stability results with added SS is lower than the 2-phase foam stability results with added SS.

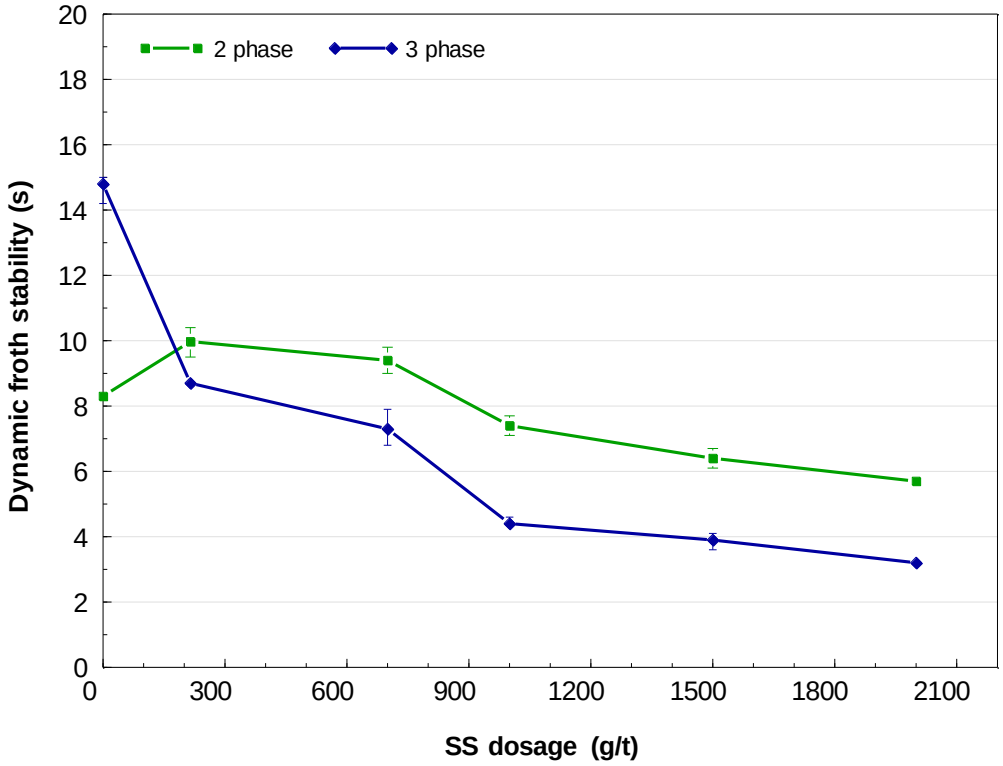

Figure 4.28: Two- and three-phase dynamic froth stability as a function of SS dosage (Ore 1).

It is well established that lower froth stabilities usually correlate with lower solids recoveries and lower valuable mineral recoveries. Lower froth stabilities also correlate with lower water recoveries which in turn correlates with higher grade. This trend is not strictly observed when SS is used, as lower froth stabilities correlates with lower water recoveries, higher concentrate grades, lower solids recoveries and higher valuable mineral recoveries. This indicates that the improvement in pulp phase Pt and Pd recoveries overrides the decrease in the froth stability at higher SS dosages.

Figure 4.29 compares the foam and froth stabilities between the baseline, 2000 g/t SS and pH modified tests for both 2-phase and 3-phase systems. It is clear that the large reduction in froth stability in the 3-phase system was not due to pH effects alone. There was a slight reduction in froth stability when moving from pH 9.8 to pH 11.7 in 3-phase. However, there is a dramatic decrease in froth stability when SS is added at the same pH of 11.7. For the 3-phase system, the froth stability at the pH adjusted experiment was higher than the equivalent pH within a 2-phase system. Here it is evident that the addition of solids stabilized the froth.

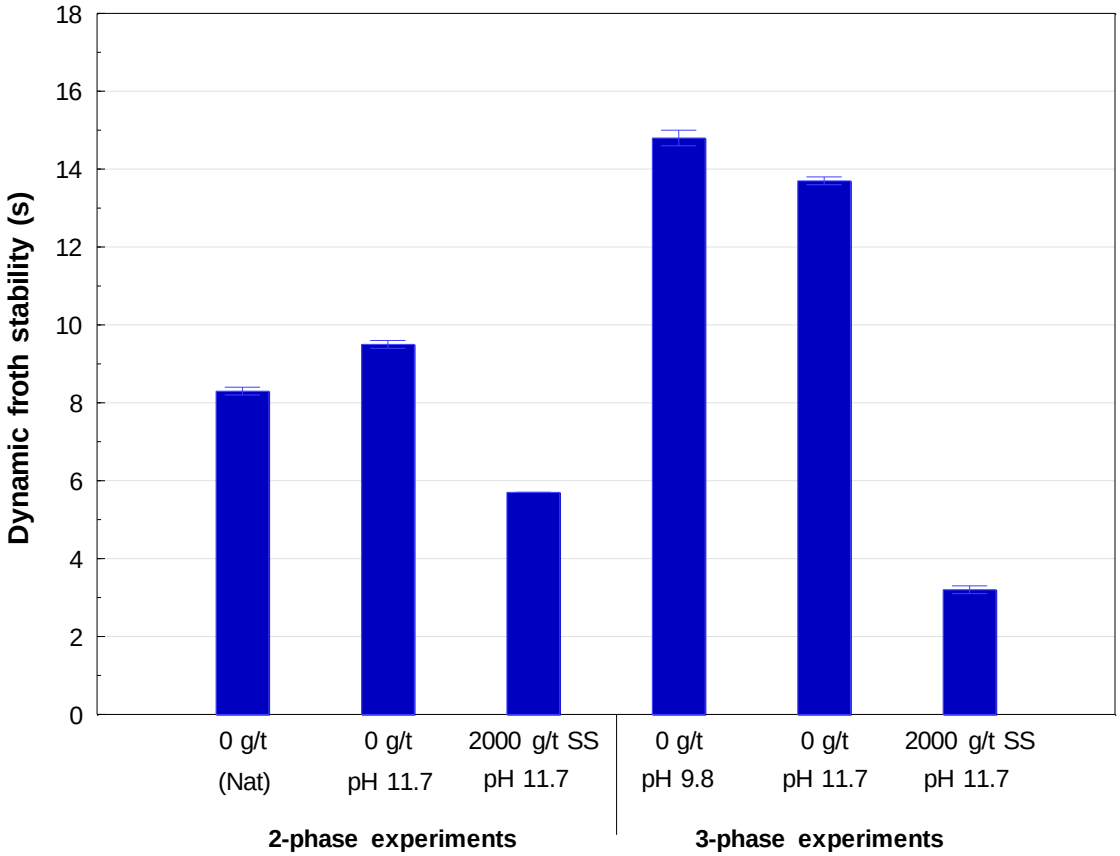

Figure 4.29: Comparing the froth stabilities between 0 g/t, the pH 11.7 modified and 2000 g/t SS experiments (Ore 1). Error bars represent the standard error between triplicate test runs.

The following points summarize the froth stability results:

1. Two-phase froth stability experiments show an initial increase in stability from 0 g/t to 215 g.t, and thereafter a decrease in stability with an increase in SS dosage (Figure 4.28)
2. The 3-phase froth stability decreases with an increase in SS dosage (Figure 4.28)
3. Considering 0 g/t, the 3-phase froth stability is higher than the 2-phase experiment, which is expected in a system containing solids, however, this further indicates that the introduction of SS in the system not only impacts froth structure, but determines the type of particles entering the froth which in turn has significant impacts on froth stability (Figure 4.28), and
4. The reduction in froth stability is not due to a pH effect (Figure 4.29).

4.2.4. Slurry rheology

Fluid flow properties of a slurry are often characterised by a plot of shear stress as a function of shear rate, as mentioned in Chapter 2. From such plots, rheology parameters such as yield stresses and apparent viscosities were calculated to better understand the rheology modifying effect of SS. These results will be presented in this section. In addition to the rheological behaviour at varying SS dosages, and selected data for a finer grind (100% passing 75 µm) will also be presented. It is well-known that slurry viscosity or yield stress will increase with decreasing particle size and therefore these results will be included (Kawatra & Eisele, 1988: 254; Zhou, Scales & Boger, 2001: 2913; Tangsathitkulchai, 2003: 42; Olhero & Ferreira, 2004: 73). Special emphasis will be placed on the behaviour of the 20 vol.% run seeing as this is close to the standard solids concentration used for batch flotation (35 wt.% is equivalent to 15.5 vol.% as shown in Appendix A).

Figure 4.30 illustrates the rheograms for the 20 vol.% run of the 0 g/t, 1000 g/t and 2000 g/t SS dosage at the standard grind as well as the 0 g/t and 2000 g/t SS dosage at the finer grind. The rheograms for other solids concentrations tested within this study are illustrated in Appendix B. It can be observed from the rheograms that shear stresses at all shear rates are lower at high SS dosages compared to the standard and finer grind baseline conditions. In the case of the standard grind, 2000 g/t SS obtained even lower shear stresses close to zero. This also indicates that SS reduced the shear stress of the suspension at 160/s, which is within the range of shear rates that are applicable to mechanical flotation cells and which has been used in previous rheological studies (Shabalala et al., 2011: 1449; Becker et al., 2013: 94). Grinding

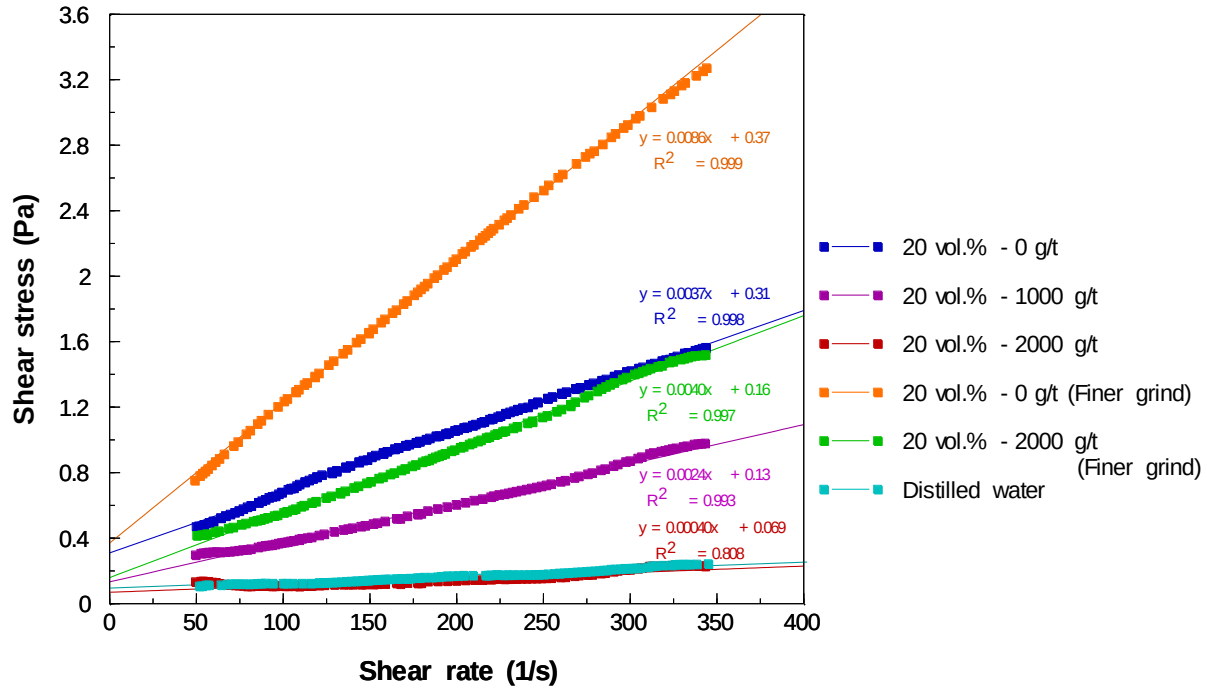

Figure 4.30: Bingham modelled rheograms for the 0 g/t (60% <75 µm grind or "standard grind"), 0 g/t (100 % <75 µm grind or "finer grind"), 1000 g/t SS and 2000 g/t SS (standard and finer grinds) tests at 20 vol.% (Ore 1). Error bars, which are too small to be seen, represents the standard error between triplicate tests.

fine significantly increased the shear stresses but this was found to be reduced to values close to the standard grind baseline using 2000 g/t SS. The shear stress during batch flotation using 2000 g/t SS is therefore expected to have been low. A reduction in shear stress at the finer grind at 160/s indicates that SS lowered the rheological complexity which was increased by the presence of fines in the cell. It is clear that the suspensions are specifically experiencing Bingham plastic behaviour (a characteristic of non-Newtonian fluids) which is identified by linear rheograms having a yield stress.

Calculated Bingham yield stresses as a function of solids concentration for the various experimental conditions tested are illustrated in Figure 4.31. Yield stresses for all conditions were observed to increase exponentially with an increase in solids concentration which indicates that flow properties changed. When comparing the yield stresses at the same solids concentrations in the absence and presence of SS, the yield stress with SS was significantly lowered, although these yield stresses also increased with increasing solids concentration. For example, the yield stress of 20 vol.% at the standard and finer grinds were 0.31 Pa and 0.37 Pa, respectively, and with 2000 g/t SS in the system these values were reduced to 0.069 Pa and 0.16 Pa respectively. Reduced yield stresses with SS indicates that SS improved the fluid flow during froth flotation.

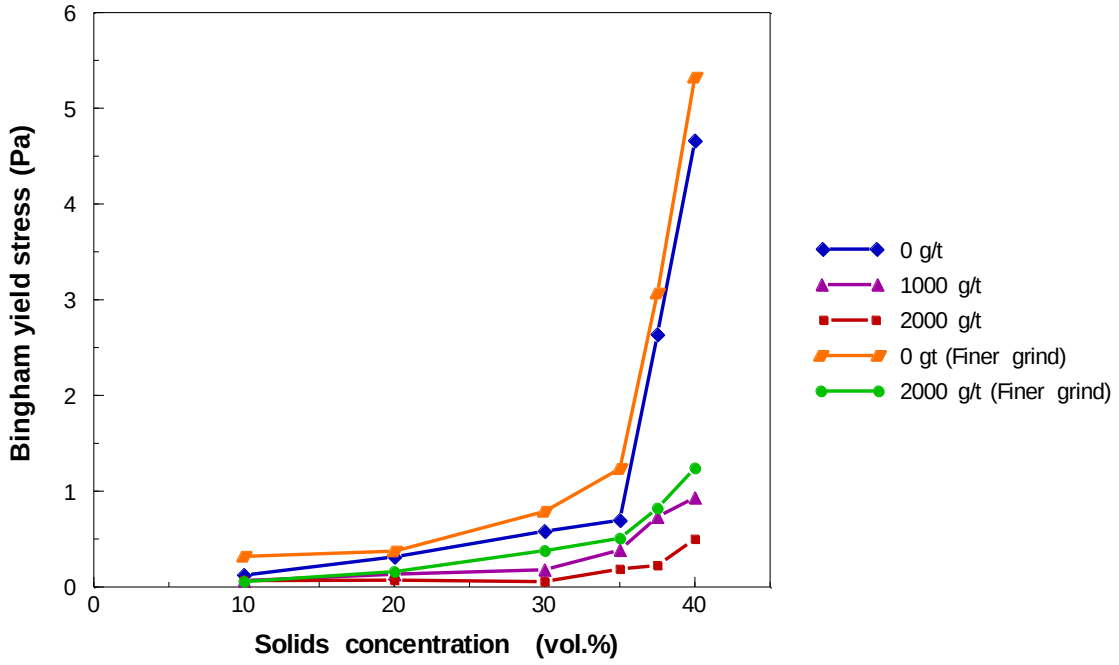

Figure 4.31: The Bingham yield stress for the 0 g/t (60% <75 μm grind or "standard grind"), 0 g/t (100 % <75 μm grind or "finer grind"), 1000 g/t SS and 2000 g/t SS (standard and finer grinds) tests at the various solids concentrations (Ore 1). Error bars, which are too small to be seen, represents the standard error between triplicate tests.

The Bingham apparent viscosity as a function of solids concentration at the various experimental conditions is displayed in Figure 4.32. The apparent viscosity of distilled water is 9.4×10^{-4} Pa.s, as shown in Appendix B and Figure 4.32. Very similar trends were observed between the apparent viscosity and

yield stress with and without SS addition at both grinds. With added SS in the suspension, the apparent viscosity was significantly reduced for both grinds. This reduction with SS, considering 20 vol.%, compared to the baseline indicates that the pulp was less viscous during batch flotation. Reductions in the shear stresses at 160/s, yield stresses and apparent viscosities at high SS dosages for both grinds indicate that SS effectively lowered the rheological complexity of the slurry. This infers that during batch flotation, using 2000 g/t SS lowered the apparent viscosity of the pulp which was similar to that of distilled water.

High yield stress and apparent viscosities were observed at higher solids concentrations for both ore grinds, which indicates that slurry properties were rheological much more complex. This could be combated using SS which showed to effectively reduce yield stresses and apparent viscosities even at higher solids concentrations.

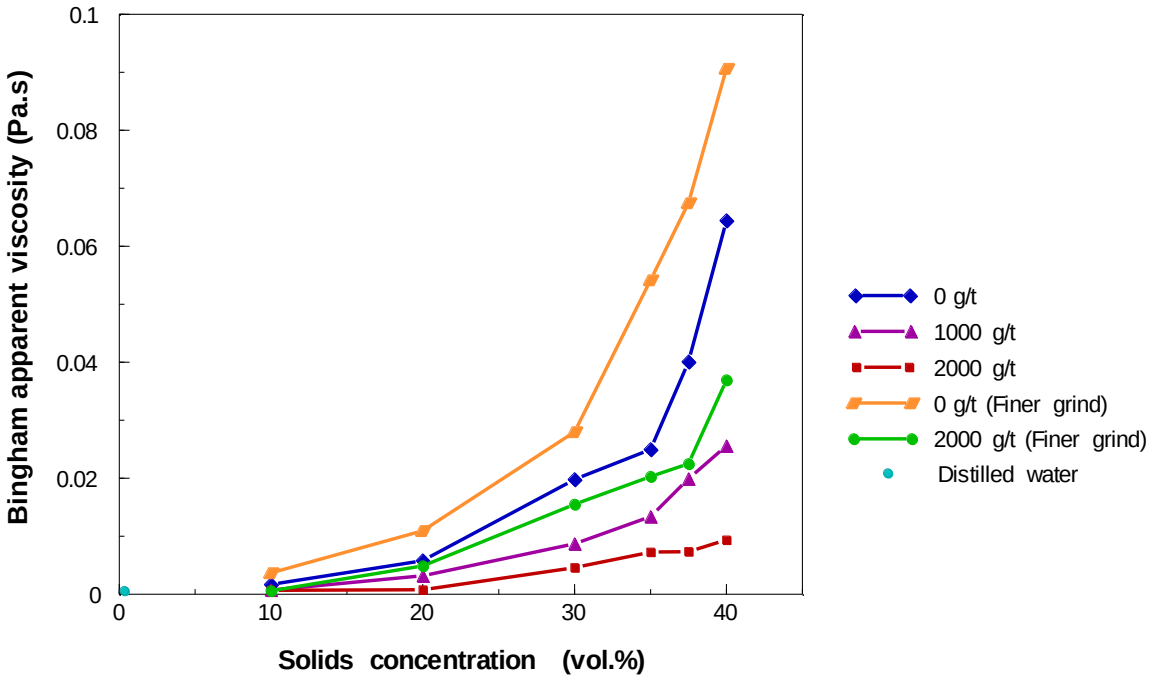

Figure 4.32: The Bingham apparent viscosity for the 0 g/t (60% <75 µm grind or "standard grind"), 0 g/t (100 % <75 µm grind or "finer grind"), 1000 g/t SS and 2000 g/t SS (standard and finer grinds) tests at the various solids concentrations (Ore 1). Also presented is the viscosity of distilled water. Error bars, which are too small to be seen, represents the standard error between triplicate tests.

The following points summarize key findings of the rheology results:

1. Reductions in shear stress, yield stress and apparent viscosities with added SS were noted for the 20 vol.% experiments which indicates that the rheological complexity of the ore during batch flotation at high SS dosages was effectively lowered (Figure 4.30 to Figure 4.32)
2. The presence of fines can dramatically increase the rheological complexity of the ore, but this can be lowered using high SS dosages (Figure 4.30 to Figure 4.32), and
3. Higher solids concentrations experience a reduction in rheological complexity in the presence of

high SS dosages (Figure 4.31 and Figure 4.32).

4.2.5. Particle settling

This section intends to determine the influence of SS on the settling rate of the particles within the feed. It is agreed that faster settling rates infer a higher degree of particle aggregation than slower settling rates (Van Leussen & Cornelisse, 1993: 239; Lee, Hyeong & Cho, 2020: 6). The change in suspension-liquid interface height was recorded for a duration of two hours, and the results are displayed in this section. From this determination, the interface height at 20 minutes of settling time and the particle settling velocity from the beginning of the experiment to 20 minutes of settling time are presented for the various SS dosages. Settling experiments were performed at 0 g/t, 215 g/t SS, 700 g/t SS, 1000 g/t SS and 2000 g/t SS dosages in duplicate. Because similar results were recorded between the duplicate runs, no error bars are visible in the figures presented.

Batch settling curves showing the change in the suspension-liquid interface with time, at the various test conditions, are presented in Figure 4.33. The data in Figure 4.33 begins after 3 minutes of settling time because the suspension interface under 3 minutes could not be measured due to the turbulence at the start of the experiment. Increasing SS dosages corresponded with longer particle settling times. This is indicated by an increase in the interface height with an increase in SS dosage, as observed at all settling time durations. Two hours of experimental time for the 2000 g/t SS experiment did not visibly show a change in the interface height, which marked a much slower settling rate relative to other tests.

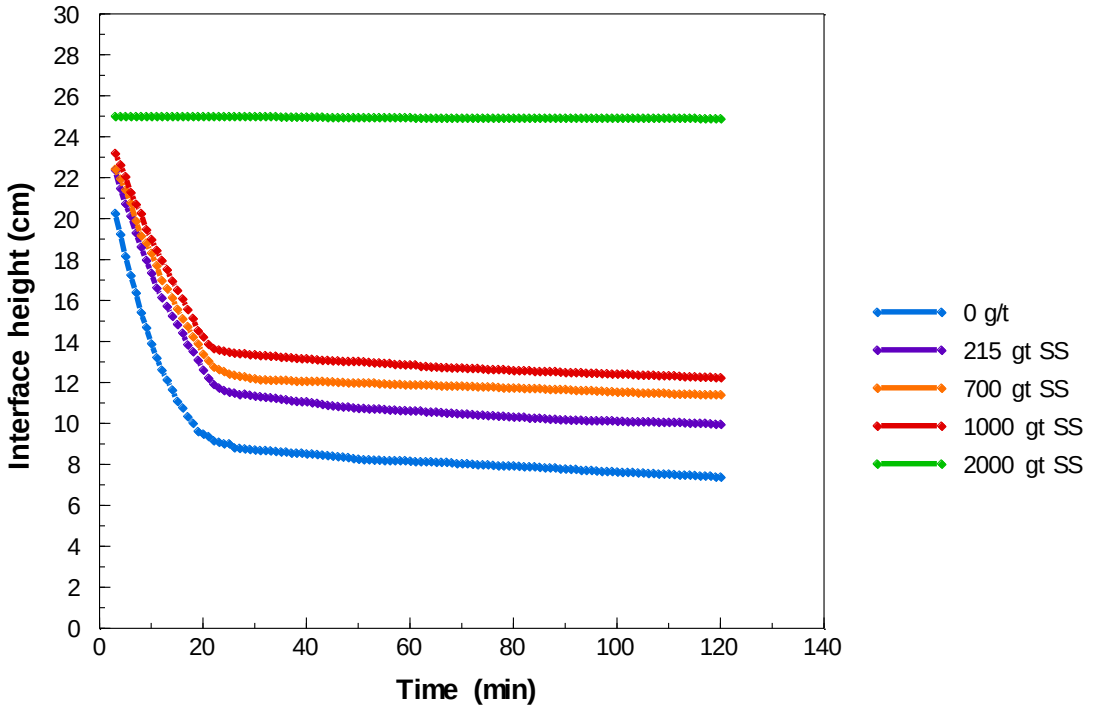

Figure 4.33: Evolution of the suspension-liquid interface height over time at the baseline and various SS dosages (Ore 1). The data begins at 3 minutes due to turbulence at the start of the experiment.

Particle settling for a duration of 20 minutes commonly marked the transition from a faster decline in the interface height to a slower decline in the interface height, apart from the 2000 g/t SS test, which did not display this transition within the first two hours. The interface height at 20 minutes are displayed in Figure 4.34, and the corresponding settling column images for the first repeat of each experiment is illustrated in Appendix B. As illustrated in Figure 4.34, the interface height at 20 minutes increased as the SS dosage was increased. The column test images in Appendix B shows the presence of fine particles within the suspension from 215 g/t to 2000 g/t SS which appear to be more with increasing dosage (Figures B to E) in comparison to the the absence of fines in the suspension at the 0 g/t test (Figure A). No suspension-liquid interface developed within the first two hours of experimental time for the 2000 g/t SS dosage. However, after 2.5 hours an interface of 24.8 cm was measured and after 24 hours the interface height was about 8 cm.

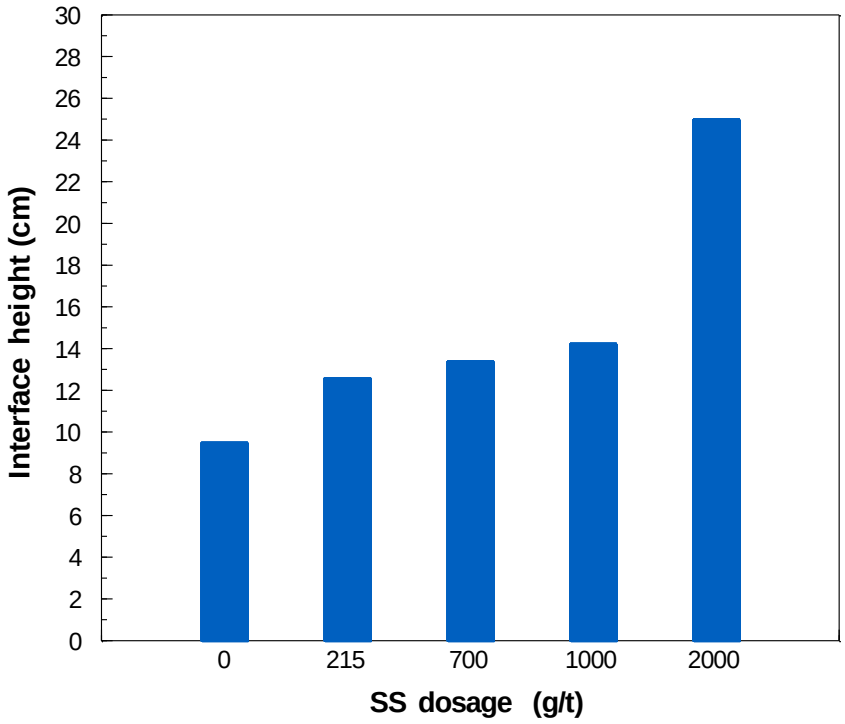

Figure 4.34: Suspension-liquid interface at approximately 20 minutes of particle settling at the various SS dosages (Ore 1).

The particle settling velocity is the rate of change of the interface height over time. The particle settling velocities for the various experiments are presented in Figure 4.35. Calculations for the determination of the particle settling velocities are displayed in Appendix A. As expected, faster settling velocities are obtained in the absence of SS. With increasing SS dosage, the settling velocity gradually decreases, while at 2000 g/t there was no reduction in interface height within the first two hours. This point was therefore excluded from the graph because particle settling is thought to have occurred but the method of particle

settling used in this work could not measure this. This confirms that particles are increasingly dispersed with increasing dosage, as aggregates would result in faster settling velocities.

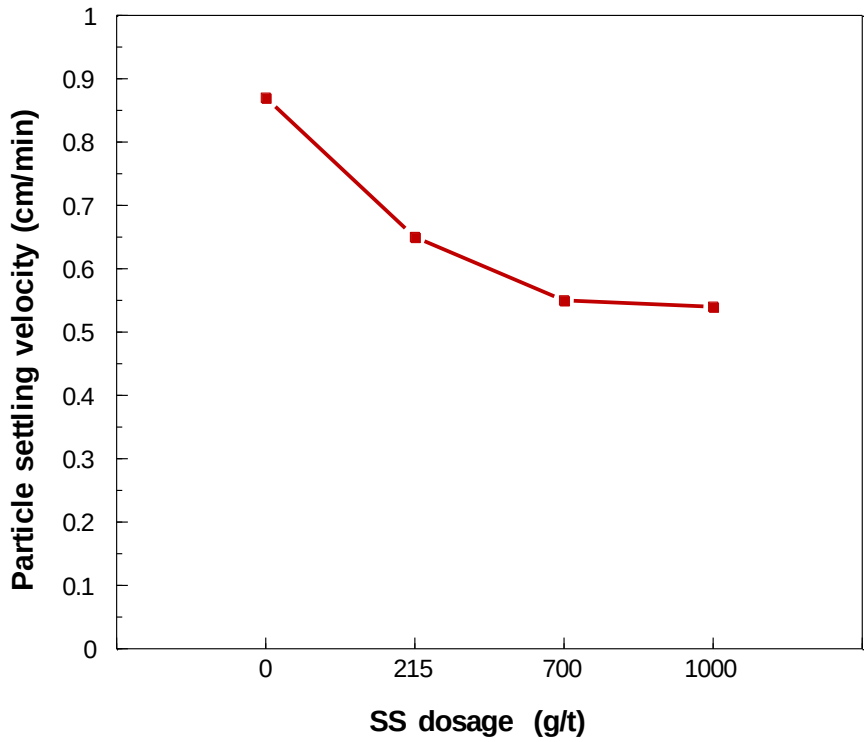

Figure 4.35: Particle settling velocity at the baseline and SS dosages (Ore 1).

The following points summarize key particle settling findings:

1. Increasing SS dosages corresponded with longer particle settling times (Figure 4.33 and Figure 4.34)
2. Particles are very dispersed at high SS dosages, which is visually indicated by fine particles in the suspension (Appendix B), and
3. Particle settling velocities at high SS dosages are much slower than in the absence of SS, which confirms that particles are dispersed (Figure 4.35).

4.2.6. QEMSCAN concentrate analysis

The primary aim of this section is to determine how SS's depressant effect enhanced concentrate grades. This was accomplished by firstly comparing the talc characteristics in the concentrates of two flotation conditions: experiments conducted at 215 g/t and 2000 g/t SS. The second part determines whether a reduction in talc recovery correlated with a reduction in entrained minerals. The entrained behaviour was not directly measured but will be inferred from the recovery of liberated orthopyroxene and serpentine seeing as these minerals have no natural floatability.

The 215 g/t and 2000 g/t SS mineral masses of the first concentrates are illustrated in Figure 4.36. At 215 g/t SS, a larger mass of talc reported to the concentrate compared to using 2000 g/t SS, where the mass of talc was lower (11.2 g of talc in the 215 g/t SS first concentrate compared to 6.1 g in the 2000 g/t SS first concentrate). This indicates that talc was depressed at 2000 g/t SS. The depression of talc will have contributed towards higher Pt and Pd grades at 2000 g/t SS compared to the grades at 215 g/t SS. Orthopyroxene and serpentine, which constitutes a large quantity of the feed material, as shown in Table 4.1, is considerably lower within the 2000 g/t SS concentrate compared to the 215 g/t SS concentrate, as illustrated in Figure 4.36. Talc was found to be largely associated with orthopyroxene and serpentine within the feed, as illustrated in Figure 4.9. Therefore, understanding the talc associations can help to explain the depression of various minerals seen at higher SS dosages.

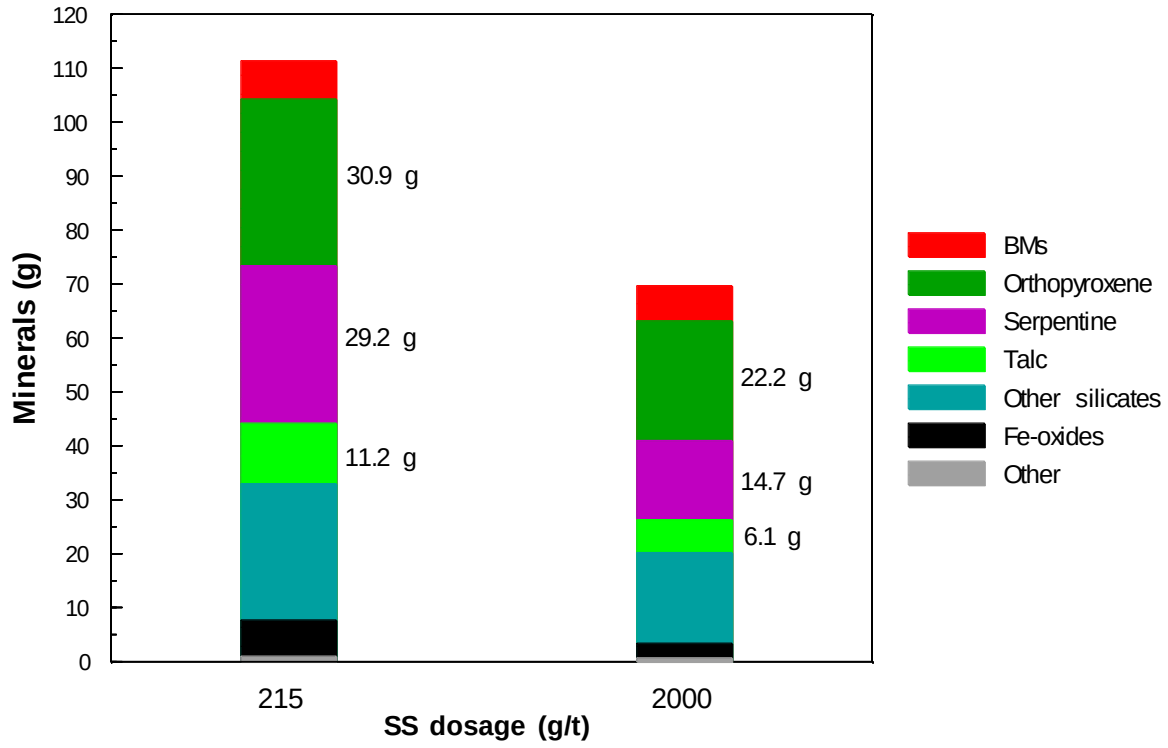

Figure 4.36: Masses of minerals in the Ore 1 batch flotation first concentrate samples at 215 g/t and 2000 g/t SS.

The masses of liberated and unliberated talc are illustrated in Figure 4.37. Lower liberated and unliberated talc masses were observed at 2000 g/t SS compared to 215 g/t. This indicates that using high SS dosages can depress talc significantly and that this would have greatly contributed to the enhanced Pt and Pd grades observed during batch flotation results at 2000 g/t SS (Figure 4.19 and Figure 4.20). A lower quantity of unliberated talc at 2000 g/t SS is also an indication that composite particles, possibly talc-orthopyroxene composites, which are known to have problematic impacts on concentrate grade in various studies (Lotter et al., 2008: 906; Becker et al., 2009: 248), have been reduced.

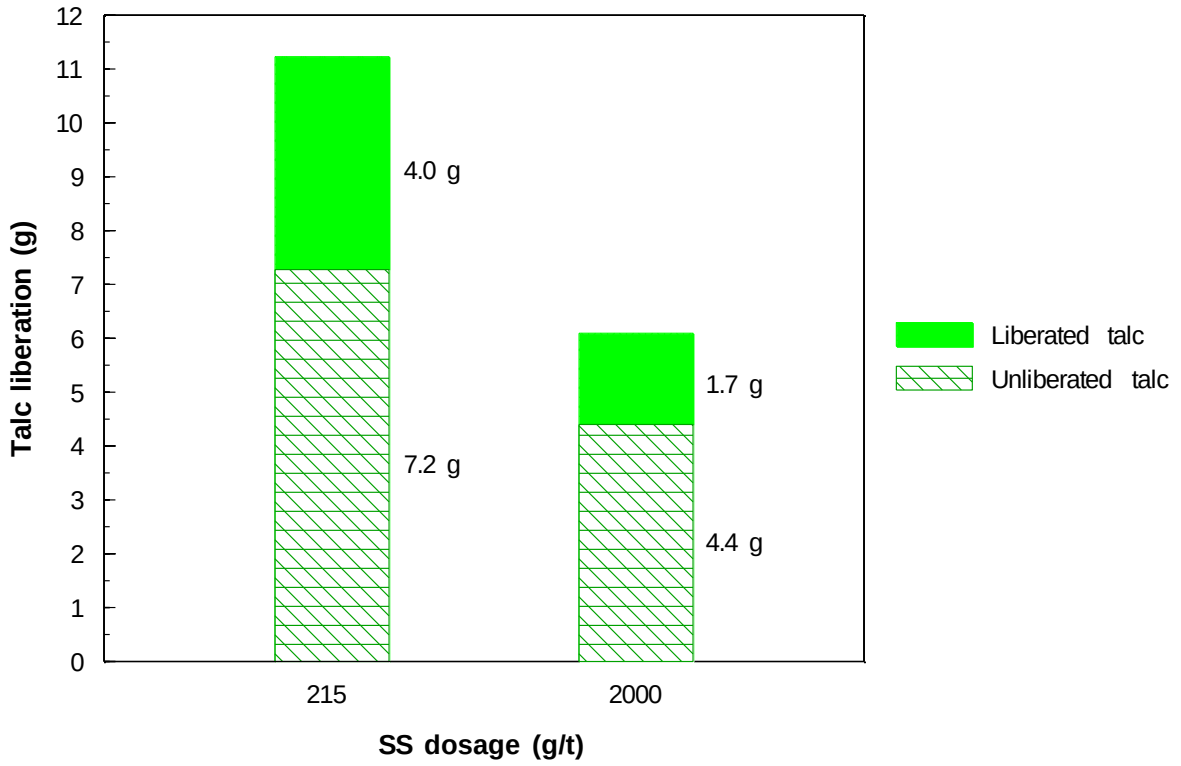

Figure 4.37: Liberated and unliberated talc within unsized Ore 1 first concentrate samples at 215 g/t SS and 2000 g/t SS flotation. Liberated: Area % Talc > 90, Unliberated: 90 ≥ Area % Talc > 0.

The mass of talc associated with gangue minerals in the 215 g/t and 2000 g/t SS first concentrate samples are illustrated in Figure 4.38. At 2000 g/t SS, lower masses of talc are associated with orthopyroxene and serpentine compared to the 215 g/t SS condition (e.g. 4.9 g of talc in the 215 g/t SS first concentrate as opposed to 2.6 g at 2000 g/t SS in terms of orthopyroxene). This indicates that composite talc associated with orthopyroxene and serpentine were depressed at 2000 g/t, which in turn led to reduced recoveries of orthopyroxene and serpentine. Figure 4.38 also shows similar masses of talc associated with BMS at the 215 g/t and 2000 g/t SS experiments. This further indicates that SS's depressant effect had only slightly depressed talc associated with BMS and therefore the recovery of BMS, and BMS associated PGMs, were not negatively affected by the depressant effect of SS.

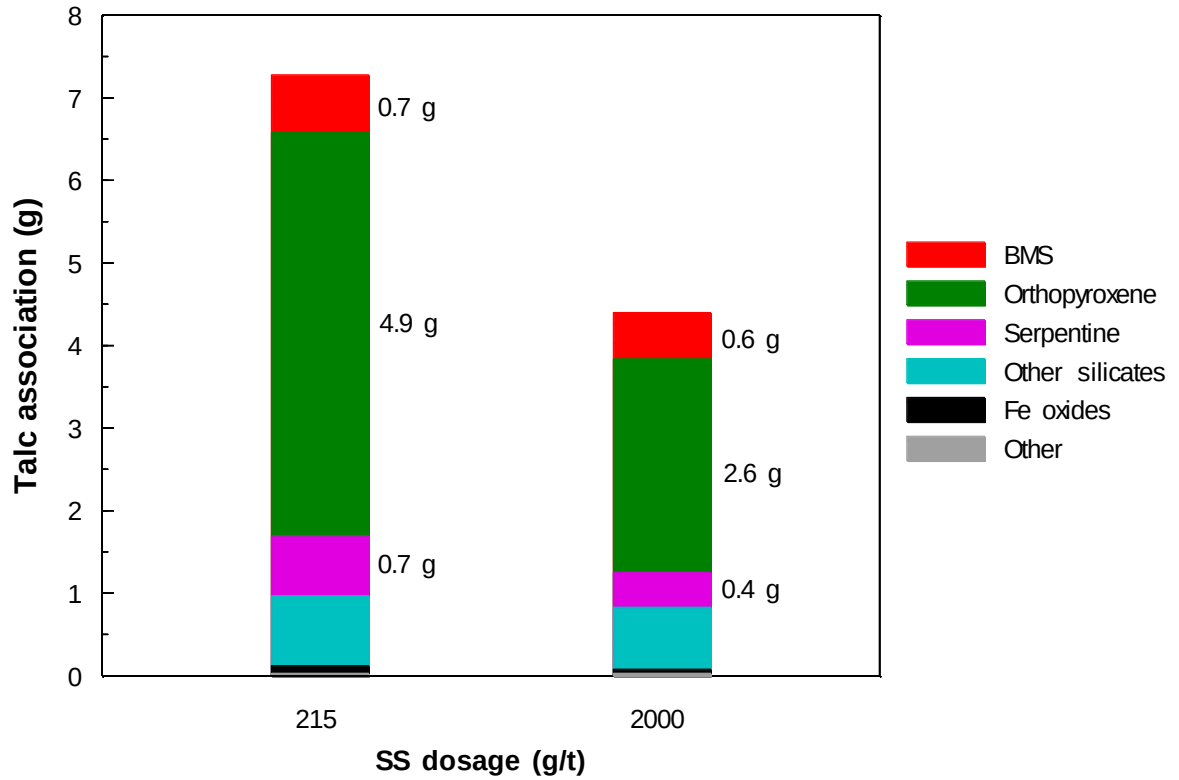

Figure 4.38: Unliberated talc associated with minerals within the unsized Ore 1 first concentrates at 215 g/t SS and 2000 g/t SS flotation. Unliberated: 90 ≥ Area % Talc > 0.

Masses of serpentine and orthopyroxene associated with minerals/mineral groups in the 215 g/t and 2000 g/t SS first concentrates are presented in Figure 4.39. The unliberated orthopyroxene and serpentine particles were effectively reduced at 2000 g/t SS compared to 215 g/t SS, as illustrated in Figure 4.38 and Figure 4.39. The orthopyroxene and serpentine in the concentrates are predominantly associated with talc and BMS. This suggests that the association between orthopyroxene and serpentine with floatable minerals resulted in their recovery. When 2000 g/t SS was added, less of the orthopyroxene and serpentine that was associated with talc reported to the concentrate. This confirms that the depression of talc using 2000 g/t SS minimized the recovery of composite talc-serpentine and talc-orthopyroxene particles. No orthopyroxene associated with BMS was depressed at 2000 g/t SS, whereas there was some depression of BMS that were associated with serpentine. This is very informative since it confirms that the addition of SS selectively depressed serpentine associated with BMS but not orthopyroxene associated with BMS.

Due to higher quantities of orthopyroxene and serpentine in the concentrate compared to other gangue, a consideration of how these large feed constituents may have reported to the concentrate, and ultimately influence the concentrate grade, were considered. The mass portion of liberated orthopyroxene and serpentine within the concentrates are shown at the position of the arrows in Figure 4.40.

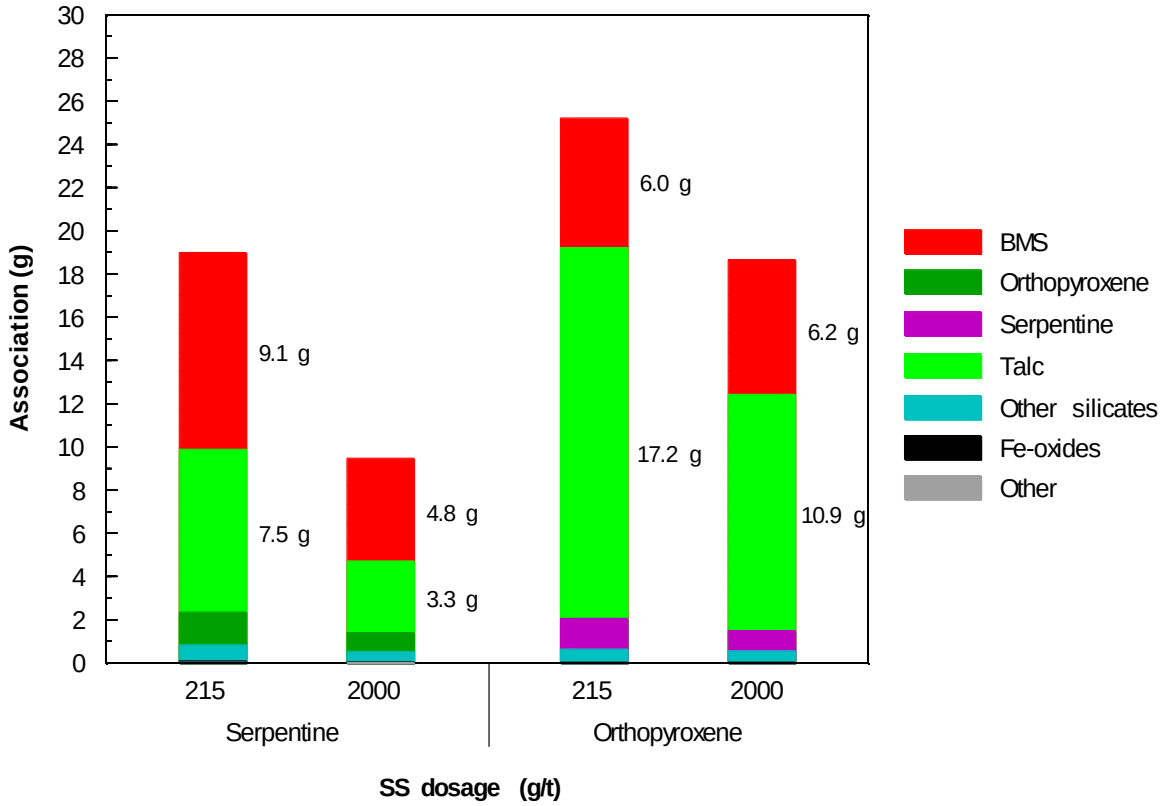

Figure 4.39: Associations of unliberated orthopyroxene and serpentine with minerals within the unsized Ore 1 215 g/t and 2000 g/t SS first concentrate samples.

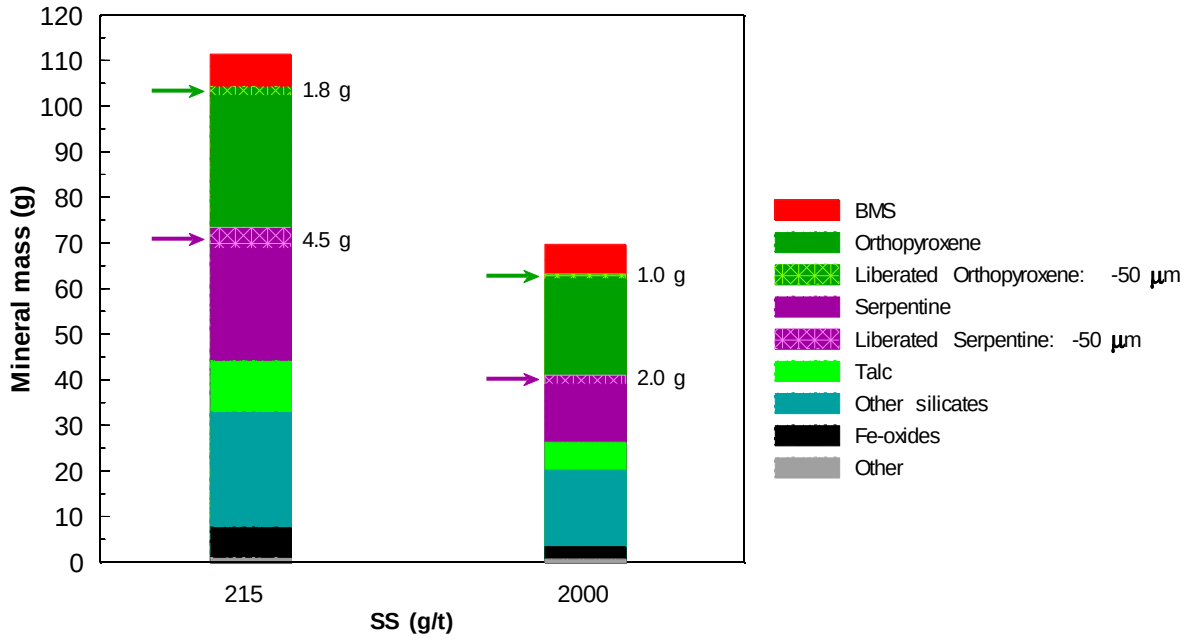

Figure 4.40: Masses of liberated and unliberated orthopyroxene and serpentine within the unsized Ore 1 215 g/t and 2000 g/t SS first concentrate samples. Liberated grains have been split into -50 µm and +50 µm grain sizes.

The liberated masses were split into <50 μm and >50 μm size classes to compare the mass fractions which are susceptible to entrainment (those which are <50 μm in size). There was less liberated orthopyroxene and serpentine at 2000 g/t SS compared to 215 g/t, as illustrated in Figure 4.40. There is only half as much liberated orthopyroxene and serpentine below 50 μm in size reporting to the concentrate at the 2000 g/t SS condition compared to 215 g/t SS. This indicates that at 2000 g/t SS, the recovery of entrained orthopyroxene and serpentine particles have been reduced.

Key findings of the QEMSCAN concentrate investigation are summarized below:

1. Lower talc masses in the 2000 g/t concentrate compared to the 215 g/t SS concentrate indicate that a significant quantity of liberated and unliberated talc was depressed (Figure 4.36 and Figure 4.37)
2. The recovery of composite talc-serpentine and talc-orthopyroxene particles were reduced at 2000 g/t, which indicates that the depression of talc using 2000 g/t SS lowered the recovery of serpentine and orthopyroxene (Figure 4.38 and Figure 4.39)
3. Using 2000 g/t SS did not depress orthopyroxene associated with BMS but had depressed serpentine associated with BMS. This confirms that SS selectively depressed serpentine but not BMS (Figure 4.39), and
4. Using 2000 g/t SS effectively reduced the quantity of entrained orthopyroxene and serpentine particles (Figure 4.40).

4.3. Single mineral measurements

4.3.1. Introduction

Experiments using single minerals are commonly employed to decouple the flotation response of individual mineral species from the more complex interactions occurring within a natural ore. Some researchers have studied the floatability of BMS with added serpentine slimes and determined how SS mitigated slime coatings to enhance the BMS floatability (Feng et al., 2012: 12091; Liu et al., 2018: 4; Yang et al., 2020: 2). These investigations commonly paired the BMS flotation with serpentine and BMS zeta potential measurements to better understand the floatability of the BMS. However, there is a lack of understanding whether PGMs are prone to slime coating and how this compromises the recovery of PGMs. In direct context to this study, it is necessary to determine whether slime coatings contributed to the poor Pt and Pd recoveries observed in Section 4.2.2. at the 0 g/t and 215 g/t SS flotation conditions, and whether improved Pt and Pd recoveries at higher SS dosages occurred as a result of slime cleaning of the PGMs. To acquire pure PGMs is challenging due to their scarcity in nature and cost. Therefore, chalcopyrite was selected as a proxy representing PGMs, as stated in Chapter 1. Understanding the floatability of talc in the presence of SS by microflotation experiments can help to understand the depressant effect of SS during the SS batch flotation experiments. Following from this, this section aims to address three key points. Firstly, whether the addition of SS led to talc depression in a microflotation cell, as displayed in Section 4.3.2. Secondly, whether the addition of SS improved the floatability of chalcopyrite in the presence of serpentine, as displayed in Section 4.3.3. Lastly, how the addition of SS effected the zeta potential of chalcopyrite and serpentine surfaces, as presented in Section 4.3.4.

A flow diagram outlining the results which will be presented in this section is provided in Figure 4.41, which is a modification of Figure 4.17. The highlighted boxes indicate the experiments which are addressed in this section. Boxes 'j' and 'k' serves to determine the impact of SS on the PGM floatability, which is linked to the dispersant effect of SS, whereas box 'l' determined the talc floatability which links to the depressant effect of SS.

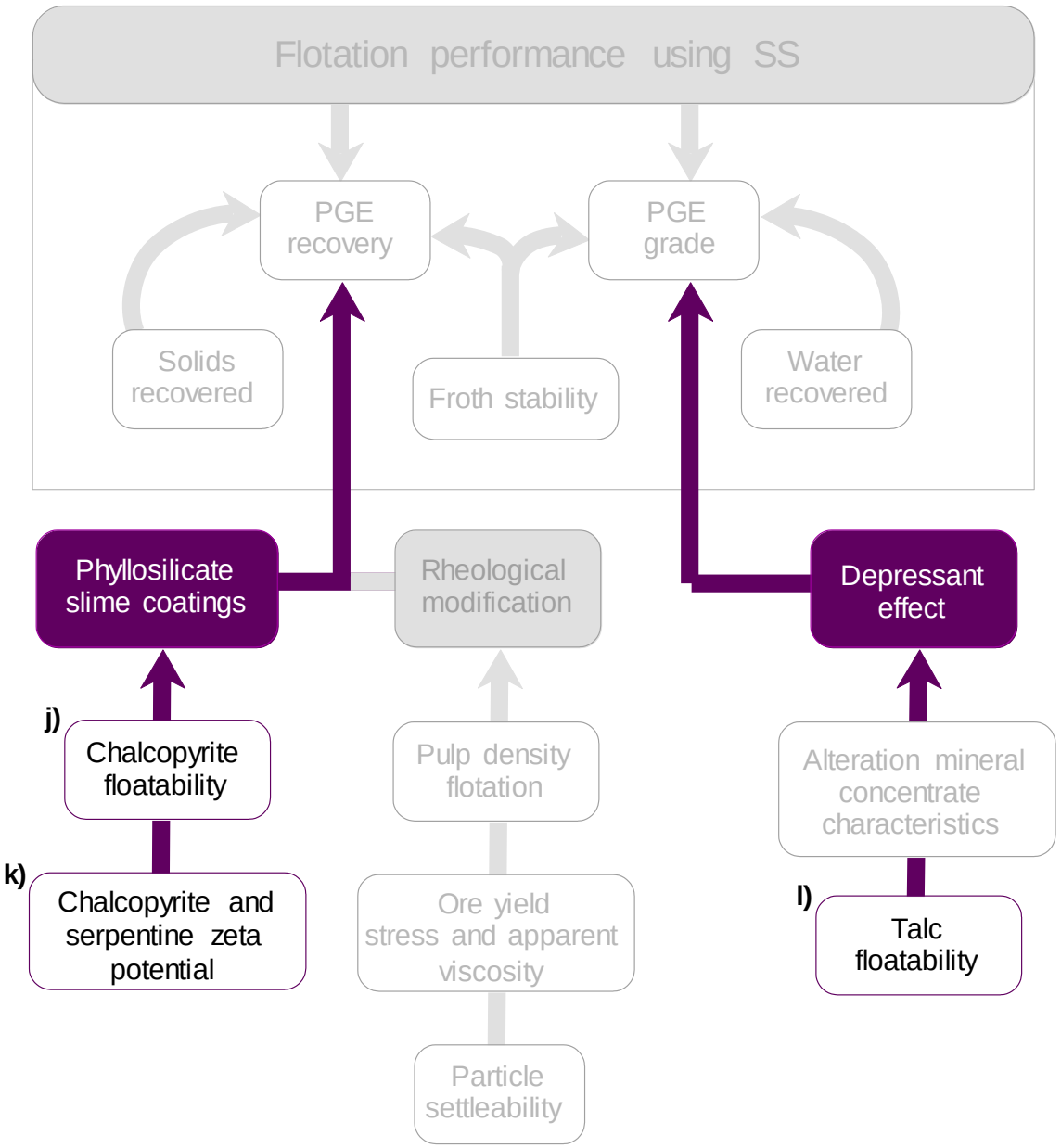

Figure 4.41: An outline of the single mineral measurements section of the results showing the primary focus of the section (purple boxes), and presented information required to understand the main topics as indicated in white boxes. Greyed-out boxes represents a group of results which will be covered in another section.

4.3.2. Talc microflotation

Numerous studies have tested the effect of depressants at varying dosages on the floatability of talc to determine the optimal conditions to minimize talc recovery and enhance grade (Beattie et al., 2006b: 601; Feng et al., 2012: 70). The effect of SS solutions on the talc floatability had not been studied, until the QEMSCAN concentrate analysis presented in Section 4.2.6. The concentrate analysis revealed that SS had reduced the recovery of composite talc particles. This section intends to further investigate the effect of

SS on the recovery of talc, where a relatively lower talc recovery indicates a stronger SS depressant effect. Dosage comparisons between the talc microflotation and batch flotation tests can be found in Chapter 3. It is well-known that talc floats readily at all pH ranges without a depressant.

Talc microflotation recoveries at the various SS dosages and a single CMC dosage, given in mg/L, are presented in Figure 4.42. The pH that corresponds to each dosage is presented at the top of each bar. The CMC experiment was performed at the natural pH (pH 8.6). The results indicate a general decrease in talc recovery with an increase in SS dosage, at dosages higher than 270 mg/L. The 1064 mg/L dosage had a significantly lower talc recovery of 52.6% compared to a recovery of 69.6% in the absence of SS. These results confirm that SS can depress talc, and that this effect is stronger at higher SS dosage (530 to 1064 mg/L). It is important to note that this does not lead to complete depression of talc and 50% of the talc is still recovered at the highest SS dosage. Talc microflotation results for the 0 g/t pH 11.7 experiment which are presented in Appendix B show that the talc floatability is much higher at pH 11.7 without SS (91.1 %) than the 1064 mg/L recovery. This confirms that talc depression is not due to a pH effect. The depressant effect of SS does not appear to be stronger than the depressant effect of CMC, because less talc was recovered using CMC at 100 mg/L (64.2%) compared to SS at a similar dosage of 120 mg/L (71.7%).

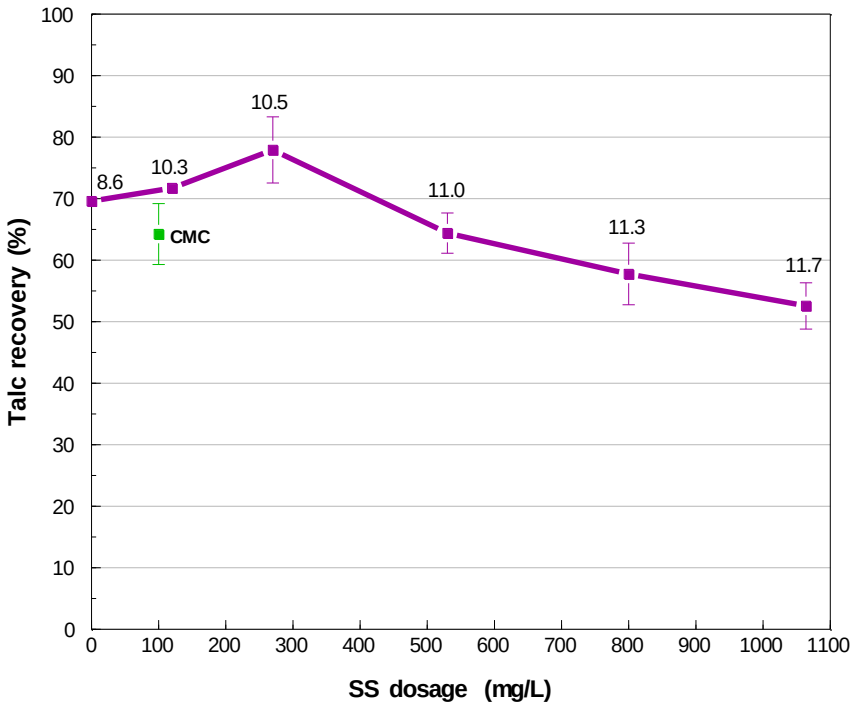

Figure 4.42: The recovery of pure talc (in mg/L) at selected SS dosages and pH conditions determined during microflotation tests. Error bars represents the standard error between duplicate tests.

4.3.3. Chalcopyrite micro- and batch flotation

This section intends to investigate the effects of serpentine slimes on the recovery of valuable minerals. This is done by presenting the results of the chalcopyrite floatability in the presence of serpentine. Two ratios of chalcopyrite to serpentine were used: 1:2 and 2:1. A single dosage of 2000 g/t SS was chosen to represent the effects of SS addition. A final test on the serpentine: chalcopyrite 1:2 mixture was conducted at pH 11.7 in the absence of SS to decouple the effects of pH and SS dosage.

The chalcopyrite floatability as a function of time for the various experimental conditions is presented in Figure 4.43. Pure chalcopyrite was fast-floating and achieved a 100% recovery within the first 5 minutes of flotation. When serpentine was added to the chalcopyrite, recoveries dropped to 2.8% and 5.2% for the 1:2 and 2:1 chalcopyrite to serpentine ratios, respectively. Upon the addition of 2000 g/t SS, chalcopyrite recoveries were restored to 99%, although the kinetics were slightly slower. To determine whether this was a function of the SS species in solution or the increase in pH upon the addition of SS, a test was performed without SS at pH 11.7. This indicates that a high pH run has virtually the same effect to SS addition, implying that slime coatings can be dispersed by pH manipulation, as well as SS addition.

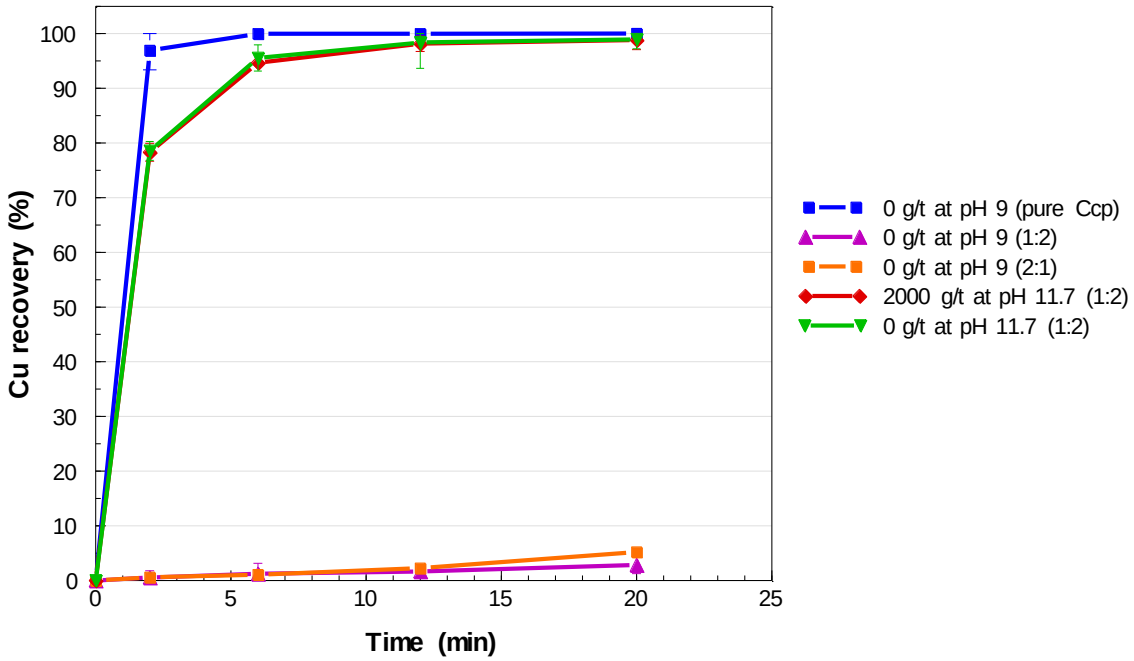

Figure 4.43: Cu recovery as a function of time for tests conducted using the microflotation cell.

Similar tests were performed in a 500 ml batch flotation cell, as illustrated in Figure 4.44, which illustrates the chalcopyrite recovery as a function of time. In this case, the chalcopyrite achieved almost 100% recovery both in the absence and the presence of serpentine. This difference signifies that solution chemistry is not the only factor governing slime dispersion or aggregation, but physical pulp parameters also play a role. This may be because of the increased energy input in the 500 ml batch flotation cell as

opposed to the energy input during microflotation, which enables slimes to be detached from the chalcopyrite surface. However, this effect was not evident when the PGE ore was floated since Pt and Pd were still depressed when using the 8L batch flotation cell.

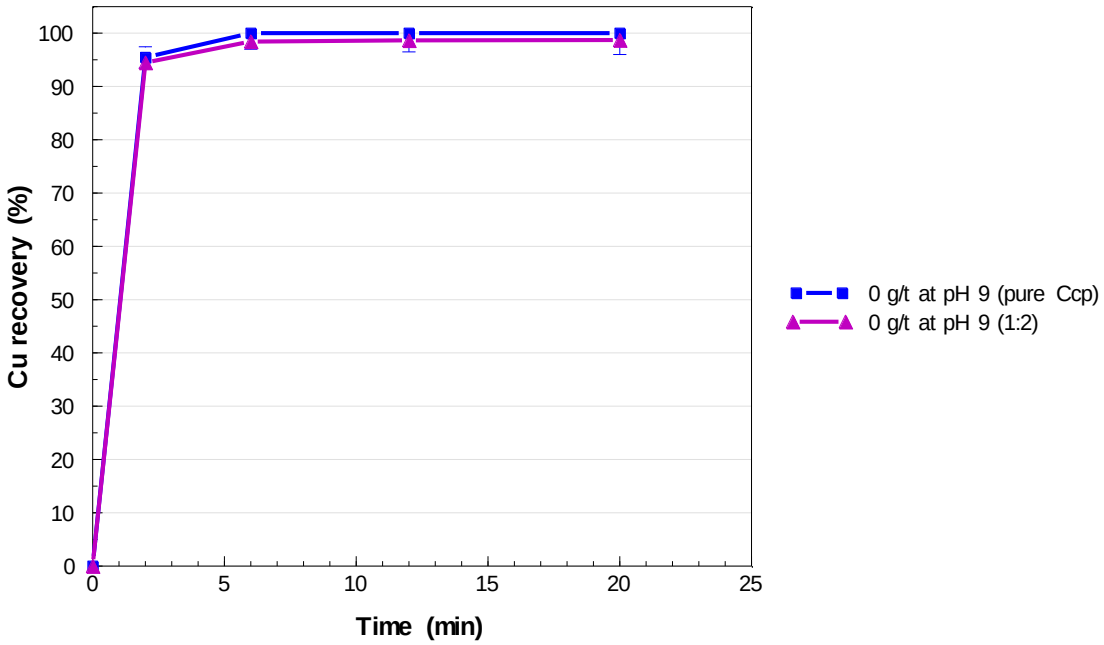

Figure 4.44: Cu recovery as a function of time for tests conducted using the 500 ml batch flotation cell.

The following points highlight the key findings obtained from the chalcopyrite floatability investigation:

1. The chalcopyrite floatability was significantly lower when serpentine was introduced into the system at both 1:2 and 2:1 chalcopyrite to serpentine ratios (Figure 4.43)
2. The chalcopyrite floatability was restored using 2000 g/t SS when serpentine was added in a 1:2 ratio (Figure 4.43)
3. A pH 11.7 adjustment to a system containing serpentine in a 1:2 ratio restored the floatability of chalcopyrite similarly to that of the 2000 g/t condition (Figure 4.43), and
4. The chalcopyrite floatability was high at the 1:2 ratio experiment using the 500 ml batch flotation cell, which highlights that physical parameters can also significantly remove serpentine slime coatings from valuable minerals (Figure 4.44).

4.3.4. Zeta potential

The colloidal interaction of serpentine slimes and PGMs in SS solutions have not been studied. This section determines the zeta potential of serpentine and a chalcopyrite proxy in the presence of SS solutions. This allows an understanding of the colloidal interaction between these minerals in solutions.

Zeta potentials of chalcopyrite and serpentine in the absence and presence of various SS solutions are presented in Figure 4.45. The serpentine zeta potentials in the absence of SS decreased with an increase in pH, with an i.e.p at pH 10.3. The chalcopyrite zeta potential in the absence of SS was found to be negative at all pH conditions, with a steady decrease from pH 2 to 12. At pH 9 without SS, the zeta potential of chalcopyrite is negative (-35.9 mV), whereas the zeta potential of serpentine is positive (17.2 mV). The attractive force between oppositely charged serpentine and chalcopyrite at these conditions will therefore result in slime coating of serpentine particles onto chalcopyrite. As shown in Appendix B, the addition of 2000 g/t SS further reduced the zeta potential of chalcopyrite.

The addition of SS at increasing dosages reduced the zeta potentials of serpentine with an increase in pH relative to the zeta potential at 0 g/t SS. The i.e.p values were observed to decrease with an increase in SS dosage with the exception of 1500 and 2000 g/t dosages, where the i.e.p was slightly higher at 2000 g/t compared to 1500 g/t. The pH 10.3 to 11.7 range is of interest because the SS dosages used during froth flotation experiments altered the pH of the pulp to values within this range, as displayed in Figure 4.20. The zeta potentials of serpentine and chalcopyrite within this range were both negative (-43.3 mV and -46.7 mV, respectively). At these conditions, the repulsive force between serpentine and chalcopyrite will, therefore, result in the dispersion of serpentine slimes from chalcopyrite. In addition, the zeta potentials of 0 g/t serpentine at pH 11.7 and 2000 g/t SS experiments are different (-22.4 mV and -43.3 mV), with the

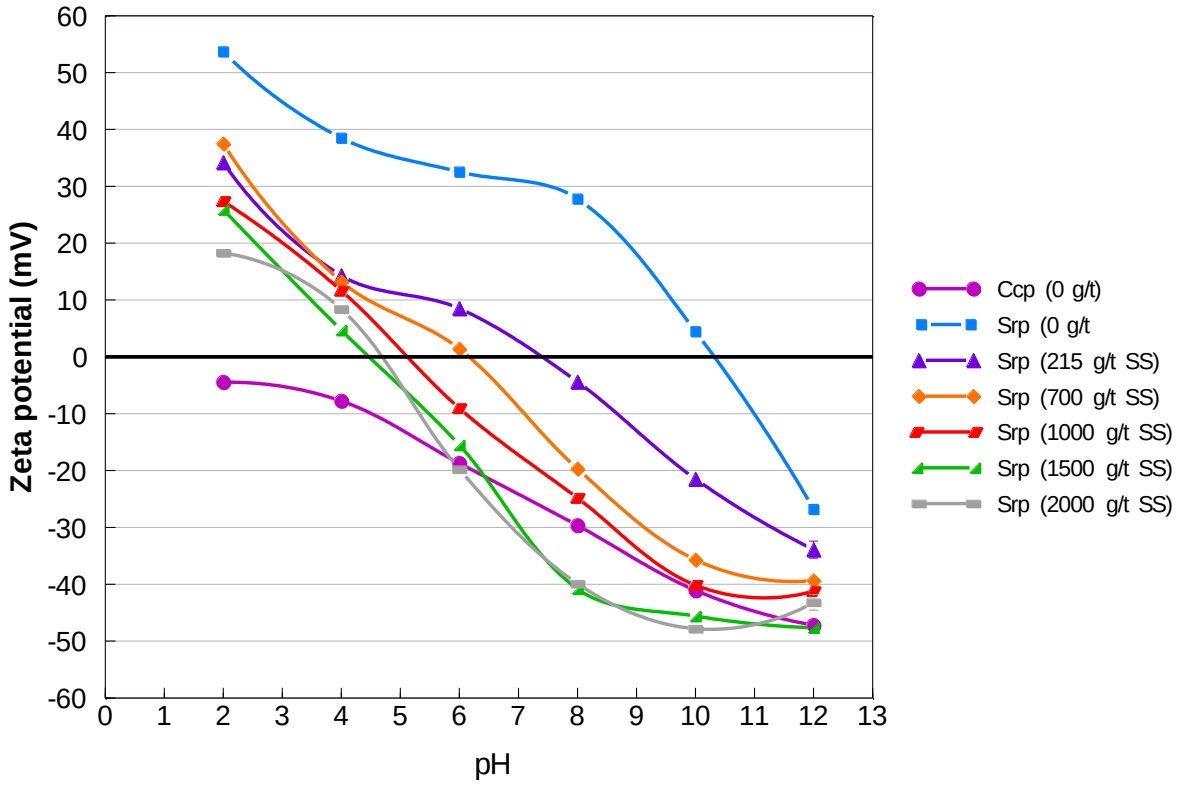

Figure 4.45: Zeta potential test for chalcopyrite (Ccp) and serpentine (Srp) with and without SS. Error bars represent the standard error between duplicate tests (averaged between three runs each), which are too small to be seen.

latter condition having a more negative zeta potential. This confirms that SS species adsorbed onto serpentine which in turn changed the zeta potential of serpentine from positive to negative. Above the i.e.p, the zeta potential of serpentine, without SS, are negative, which indicates that at these highly alkaline pH's, an electrostatic repulsion could also occur between chalcopyrite and serpentine. The 1:2 pH 11.7 microflotation experiment had obtained successful chalcopyrite recoveries, which indicates that slime cleaning had occurred.

The following points highlight the key findings obtained from the zeta potential investigation (Figure 4.45):

1. At pH 9, the zeta potentials of chalcopyrite and serpentine are oppositely charged, indicating that they will have an electrostatic attraction which will result in slime coatings
2. High SS dosages changed the zeta potential of serpentine from positive to negative, which induced an electrostatic repulsion between chalcopyrite and serpentine, and
3. Without SS, serpentine above the i.e.p has negative zeta potentials, which indicates that the successful chalcopyrite recovery during the 1:2 pH 11.7 microflotation experiment was due to slime dispersion.

4.4. Evaluating the performance of SS

4.4.1. Introduction

A flow diagram of the results which will be presented in this section is provided in Figure 4.46. Results 'a' to 'c' will be compared to the flotation response of Ore 1 using SS.

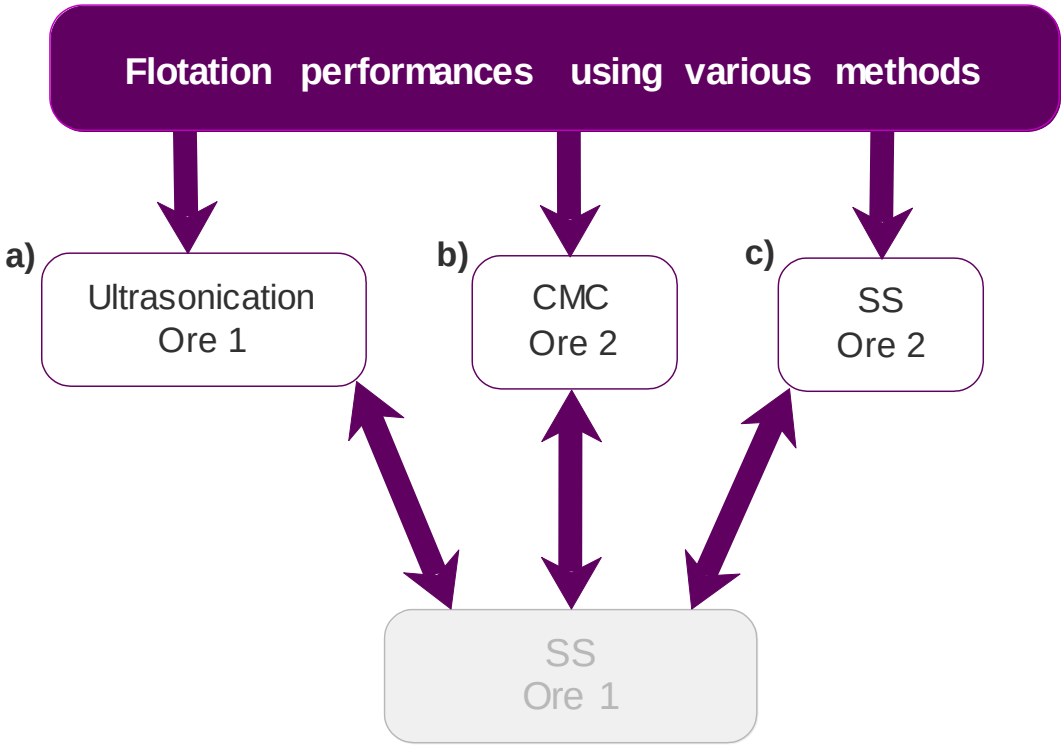

Figure 4.46: Flow diagram of the results presented in this section and the ores the tests were performed on. All tests will be compared to the flotation performance of SS using Ore 1, which was presented in Section 4.2.2.

As outlined in Chapter 2, there is a general understanding of how mitigation methods such as ultrasonication and CMC can combat the challenges associated with altered ores. Ultrasonication has proved effective at removing slime coatings from valuable minerals to benefit recovery in previous studies, and is therefore comparable in terms of the dispersant effect of SS. Carboxymethyl cellulose is widely used in industry and has extensively been researched in relation to complex ores as it can provide depressant and dispersant effects (Pietrobon et al., 1997: 779; Bremmell, Fornasiero & Ralston, 2005: 209; Laskowski, Liu & Connor, 2007: 60; McFadzean et al., 2011: 465). It is therefore comparable to SS in terms of both the depressant and dispersant effects, although CMC is mainly known for its good depressant effect. The concentrate grades using ultrasonication were also compared to SS grades for a complete performance comparison. In addition, it is critical to understand whether the same SS effects can occur using other altered PGE ores. To explore this, the effects of high SS dosages will be presented using Ore 2. The aim

of this section is to explore i) the flotation performances of ultrasonication and a comparison between the best ultrasonication and SS responses, ii) the flotation performances of CMC and a comparison between the best CMC and SS responses iii) the flotation performances of SS using Ore 2 and a comparison between the best SS responses between the two ores. It was intended for the CMC tests to be performed on Ore 1, however, Ore 1 was depleted by the time the CMC tests needed to be carried out, and it was therefore decided that CMC experiments will be performed on Ore 2. This decision was made based on the similarity in the bulk mineralogies between the ores, as shown in Table 4.1.

4.4.2. Batch flotation

Effect of ultrasonication preconditioning on the flotation response of Ore 1

Ultrasonication preconditioning before froth flotation was performed in an ultrasonication bath for 5, 10, 15 and 20 minutes. An additional test was performed using an overhead ultrasonication probe for 20 minutes before the commencement of the flotation procedure, as described in Chapter 3. The flotation performance between the 20 minute ultrasonication bath and probe experiments were compared to determine the ultrasonication method which improved the flotation performance best. Emphasis is placed on the recoveries between the two methods as ultrasonication is expected to mainly influence the recovery, however, grade will also be impacted and will also be presented. This section will firstly present the flotation performance of the ultrasonication experiments and will thereafter illustrate a performance comparison to the best SS response.

The recovered solids and water results will not be included because it was observed that there is no trend relating the recovered solids and water to ultrasonication times. Figure 4.47 plots the flotation performance at different ultrasonication times with respect to a) Pt recovery, b) Pd recovery, c) Pt grade/recovery, and d) Pd grade/recovery. High ultrasonication times improved the Pt and Pd recovery significantly. Preconditioning the ore in the bath for 20 minutes improved the Pt recovery by 9.6%, whereas 15 minutes improved the Pd recovery by 7.8%. No trend relating the Pt and Pd recovery to ultrasonication times was noted, however, ultrasonicating the ore for the different time durations improved the Pt and Pd recovery relative to the baseline. The ultrasonication probe also improved the recoveries by 7.2% and 6.6% for Pt and Pd, respectively, but not as much using the ultrasonication bath at the equivalent time. This shows that ultrasonication can be used to improve recovery, presumably through its dispersing effect. Using the ultrasonication bath also slightly improved grades. The Pt grade was enhanced by 2.0 g/t at 20 minutes of ultrasonication bath time, whereas there was a minimal increase in Pd grade of 0.02 g/t.

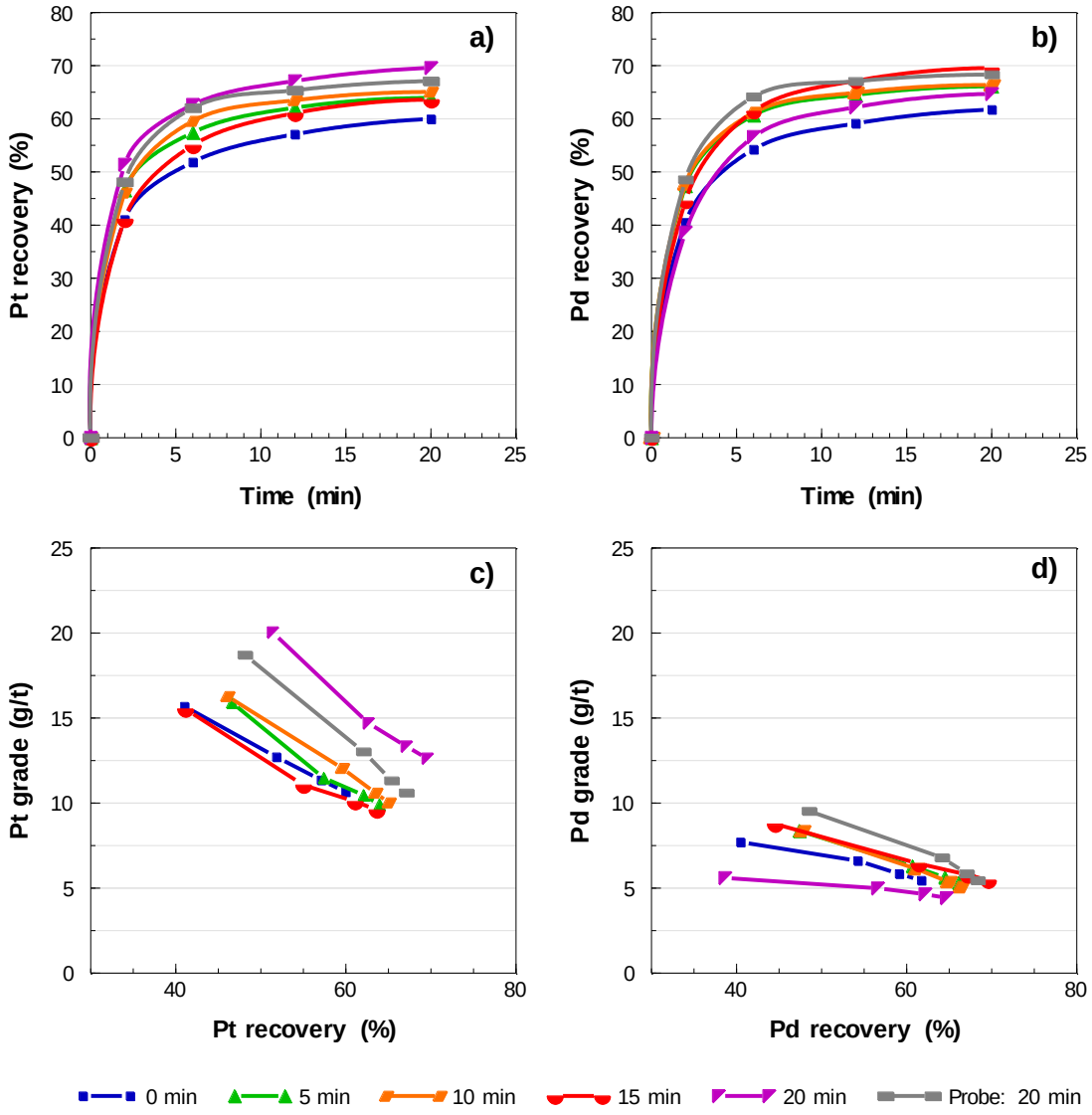

Figure 4.47: a) Pt recovery as a function of time, b) Pd recovery as a function of time, c) Pt grade as a function of recovery and d) Pd grade as a function of recovery at the various ultrasonication times. Note that the x-axis range for 'c' and 'd' starts at 30% and ends at 80%.

The best Pt and Pd recoveries and grades obtained through ultrasonication and SS are compared in Figure 4.48. The addition of 2000 g/t SS resulted in a similar Pt recovery, and a higher Pd recovery, relative to the best ultrasonication bath outcome. The use of SS resulted in an improved grade compared to using ultrasonication. Ultrasonication has a similar effect on slimes, as indicated by comparable recovery increases, but SS outperformed ultrasonication. In addition, ultrasonication cannot enhance grade to any significance. This demonstrates that SS was more effective than using ultrasonication, due to its ability to significantly improve the Pt and Pd recoveries and grades.

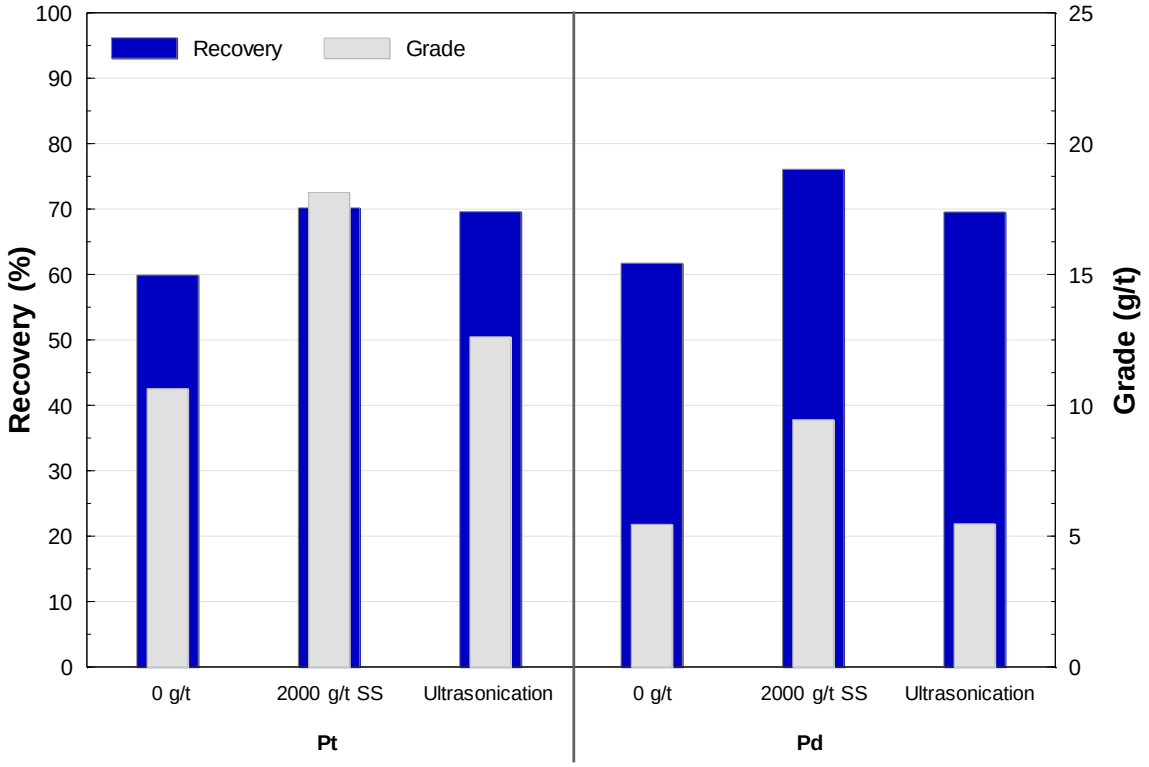

Figure 4.48: Comparing PGE recoveries and grades between ultrasonication and SS experiments.

Key findings of the ultrasonication investigation are summarized below:

1. Ultrasonication preconditioning for 15- to 20 minutes before batch flotation significantly benefited Pt and Pd recoveries (Figure 4.47)
2. The Pt grade was also enhanced at the high ultrasonication time, but Pd grade improvement was negligible (Figure 4.47), and
3. Ultrasonication and SS obtained similar Pt recoveries, however, using SS obtained a better Pd recovery, as well as Pt and Pd grades (Figure 4.48).

Effect of CMC dosage on the flotation response of Ore 2

This section illustrates the effect of 0 g/t, 100 g/t, 200 g/t and 300 g/t CMC on the flotation performance of Ore 2 in order to compare the best overall CMC and SS flotation responses. A dosage of 0 g/t is considered the baseline condition for CMC experiments, and this baseline between both ores used in this study are also compared in this section.

The averaged cumulative solids and water recovered at the various CMC dosages were determined, and these results are presented in Figure 4.49. The results clearly demonstrate that with increasing CMC dosage, the final solids and water recovered decreased. This relation between solids and water recovered with increasing CMC dosage was as expected, as similar trends were observed in previous work (Wiese, 2009: 48).

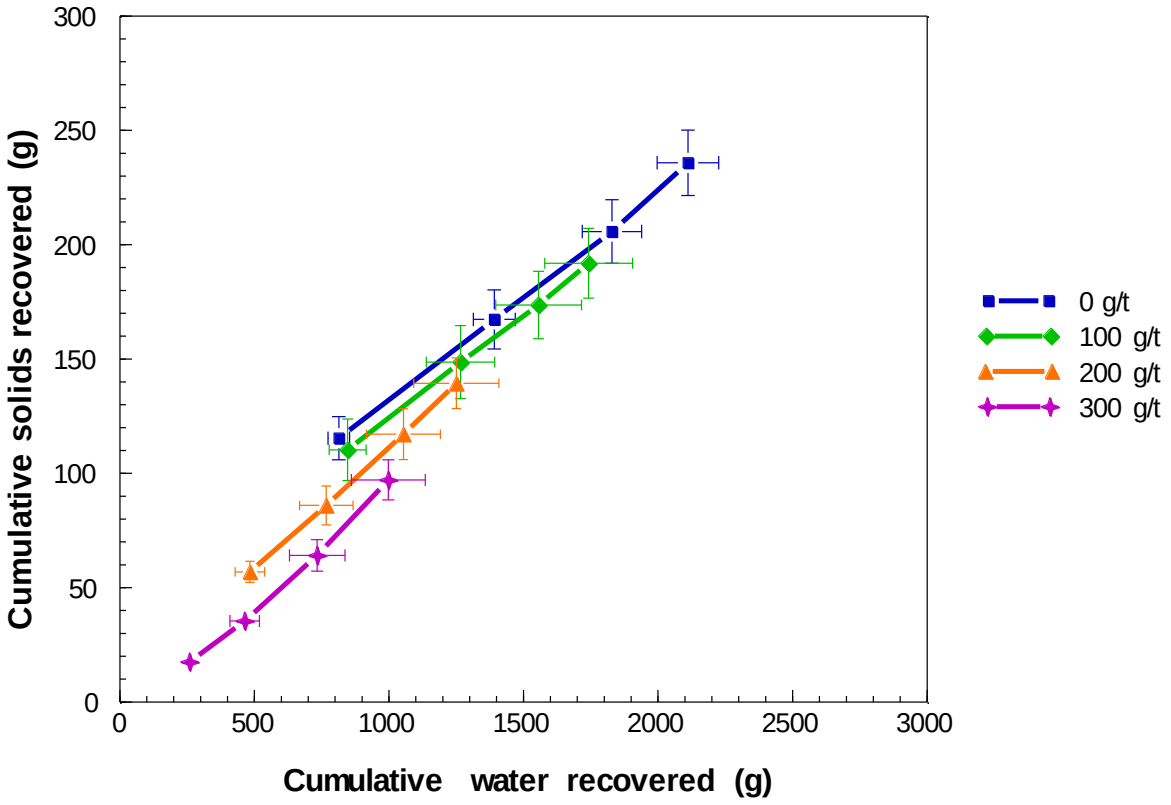

Figure 4.49: Cumulative solids and water recovered at the various CMC dosages. Error bars represent the standard error between duplicate tests.

Figure 4.50 plots the flotation performance at different CMC dosages with respect to a) Pt recovery, b) Pd recovery, c) Pt grade/recovery, and d) Pd grade/recovery. Using CMC did not enhance either Pt or Pd recoveries beyond the baseline recoveries, as increasing CMC dosage generally decreased the recoveries. A slight decrease in the Pt and Pd recoveries was the expected outcome because froth stability generally decreases with an increase in depressant dosage, and recoveries generally decreases with a decrease in

froth stability. Also, at high depressant dosages, it is known that depressant adsorption can become non-selective, therefore, it can actively depress valuable minerals. However, the CMC dosages used here are aligned with common CMC dosages in industrial processes and are, therefore, fairly conservative. For these reasons, a Pt recovery drop of nearly 20% at the highest CMC dosage is quite unexpected

This is likely due to the association between valuable minerals and gangue. With increasing dosage, grades were expected to increase as both recovered solids and water were reduced, but this was found not to be the case, as there is no trend relating grade with dosage for both Pt and Pd. Overall, the Pt and Pd grades were not significantly enhanced using CMC with only 200 g/t CMC showing a grade increase, being a 1.6 g/t Pt enhancement.

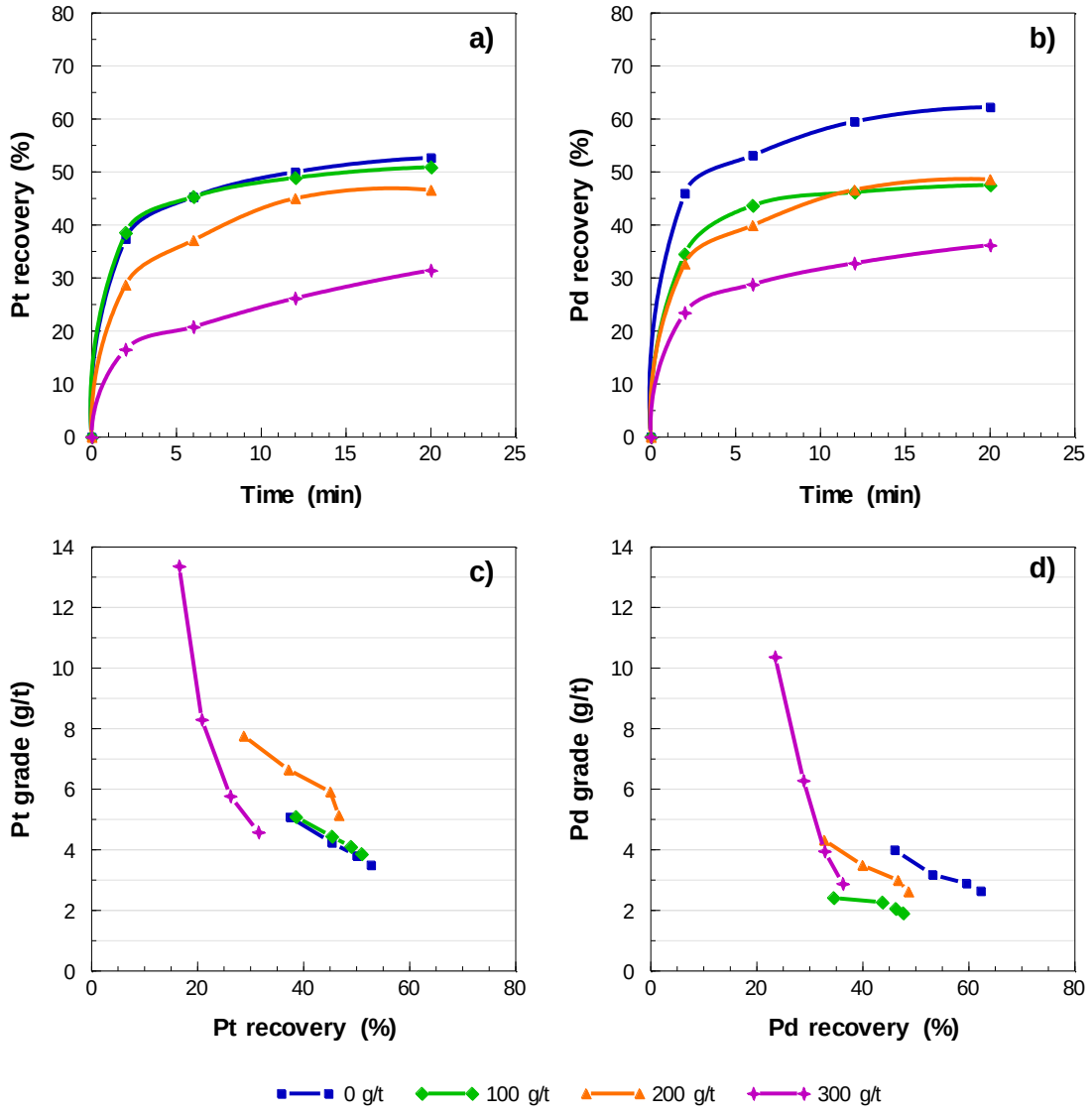

Figure 4.50: a) Pt recovery as a function of time, b) Pd recovery as a function of time, c) Pt grade as a function of recovery and d) Pd grade as a function of recovery at the various CMC dosages.

The best overall CMC flotation response is compared to the best SS response in Figure 4.51. A 100 g/t CMC dosage was chosen for comparison as it obtained the highest overall recovery amongst the CMC dosages used, although it did not improve recovery. Grades were also not significantly enhanced using CMC, but 100 g/t CMC was chosen for grade comparisons as well. The baseline for SS was the 0 g/t response using Ore 1, and that for CMC was 0 g/t using Ore 2. The results indicate that Ore 2 obtained a lower final Pt recovery and a similar Pd recovery compared to Ore 1. Using SS is clearly a superior reagent on the PGE ores investigated because it enhanced the flotation response whereas CMC did not: both the Pt and Pd recoveries and grades were enhanced using SS, whereas CMC performed poorly compared to the Ore 2 baseline. This indicates that while SS could be used to sufficiently remove slime coatings from PGMs and depress talc during batch flotation, CMC should not be used for these purposes on the ore investigated.

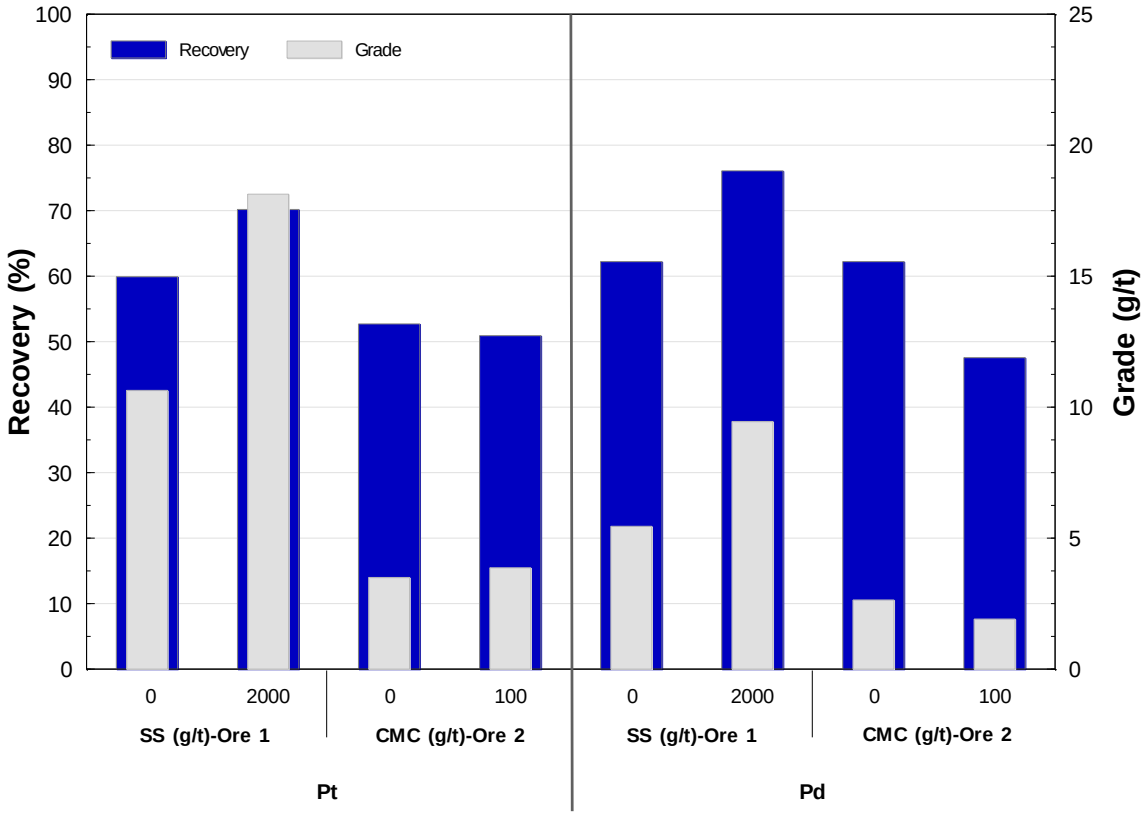

Figure 4.51: Comparing the Pt and Pd recoveries and grades between the Ore 1 and Ore 2 baselines and the 2000 g/t SS and CMC dosages. The CMC baseline is the flotation experiment performed on Ore 2.

Key findings of the CMC investigation are summarized below:

1. Increasing the CMC dosage decreased the recovered solids and water, as expected (Figure 4.49)
2. Using CMC did not improve the Pt and Pd recoveries, however, 200 g/t CMC only slightly enhanced the Pt grade (Figure 4.50)
3. The Ore 1 baseline Pt recovery was slightly higher than Ore 2, but the ores obtained similar Pd

recoveries, whereas the Ore 1 baseline grades were much higher compared to that of Ore 2 (Figure 4.51), and

4. Using 2000 g/t SS enhanced the Pt and Pd recoveries and grades better than using CMC (Figure 4.51).

Effect of SS dosage on the flotation performance of Ore 2

Thus far, it is clear that serpentine and talc had serious consequences on the flotation response of Ore 1, but these challenges were mitigated using SS. This section aims to firstly determine whether the same responses can be observed on Ore 2 and then to compare the best SS responses between the ores. Batch flotation experiments were conducted at 1000 g/t and 2000 g/t SS on Ore 2 because these dosages enhanced the flotation response of Ore 1 best, as observed in Section 4.2.2. Table 4.1 and Figure 4.3 shows that the talc content between the ores differed, where Ore 2 had a substantially higher talc quantity compared to Ore 1.

The average cumulative recovered solids and water for the 0 g/t, 1000 g/t SS and 2000 g/t SS tests are illustrated in Figure 4.52. Increasing the SS dosage from 0 g/t to 2000 g/t SS led to a reduction in the final cumulative recovered solids and water. This trend has not been observed for Ore 1 using SS addition which was otherwise found to have similar water recoveries between the baseline and high SS dosages, although the baseline conditions recovered higher quantities of solids in the case of both ores.

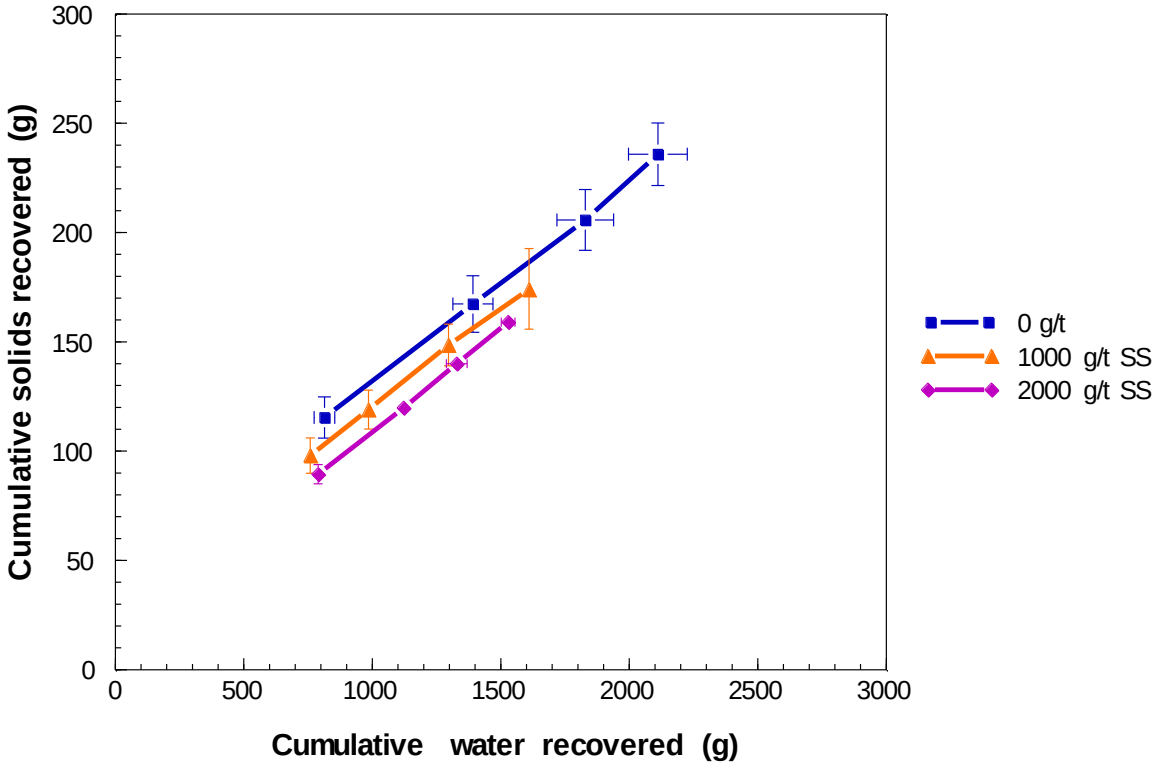

Figure 4.52: Cumulative solids and water recovered at various SS dosages (Ore 2). Error bars represent the standard error between duplicate tests.

The flotation performance at different SS dosages in terms of a) Pt recovery, b) Pd recovery, c) Pt grade/recovery, and d) Pd grade/recovery for Ore 2 is highlighted in Figure 4.53. Using high SS dosages also benefitted the flotation performance of Ore 2 in terms of both recovery and grade. The highest Pt and Pd recoveries were obtained using 1000 g/t and 2000 g/t SS, respectively, which improved by 16.2% and 19.6%. At the same dosages, their grades were enhanced by 3.0 g/t and 2.6 g/t for Pt and Pd, respectively. Benefits to recoveries are attributed to slime cleaning and a reduction in the pulp rheology, whereas grade improvements are due to the depression of NFG.

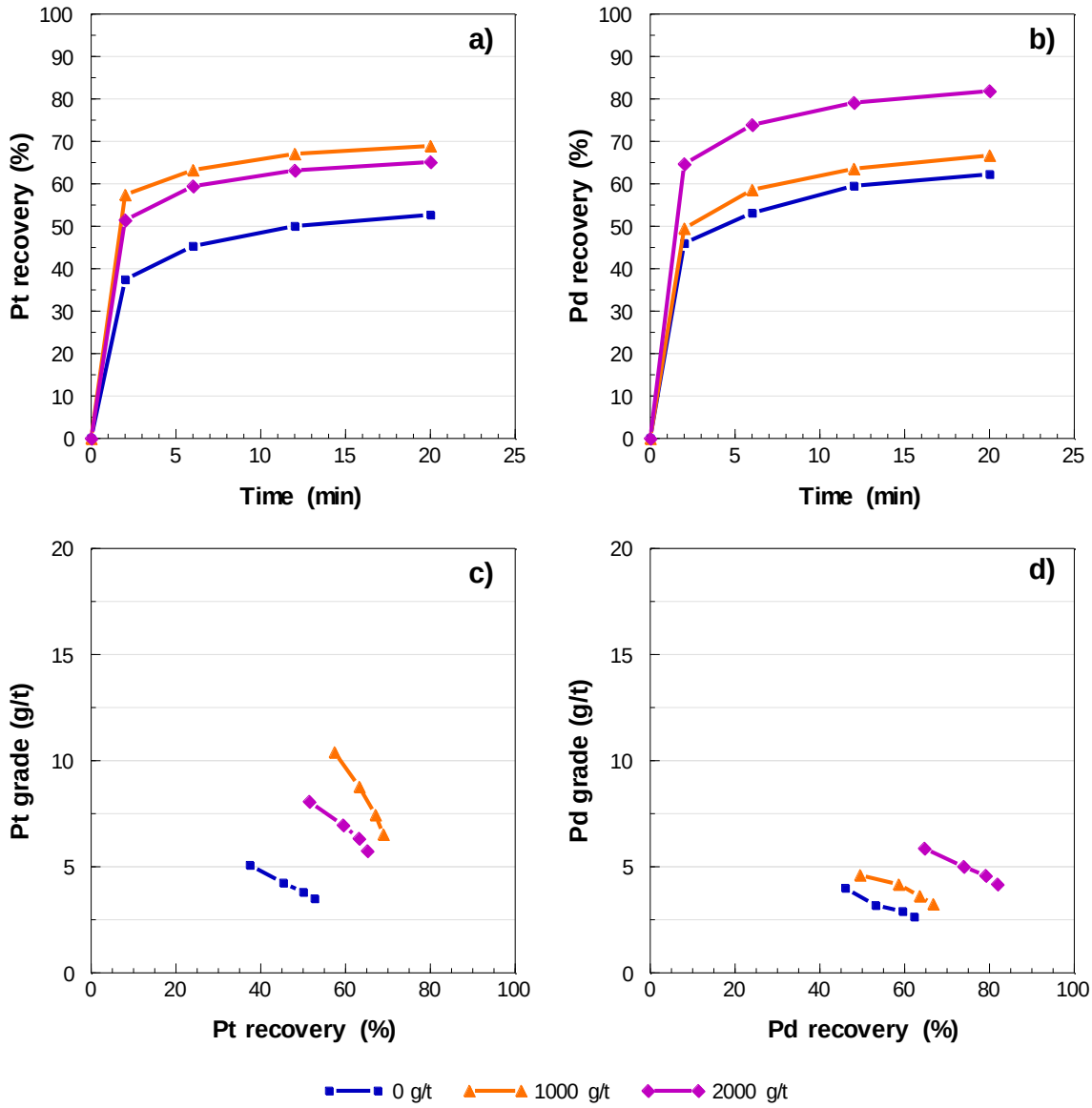

Figure 4.53: Pt recovery as a function of time, b) Pd recovery as a function of time, c) Pt grade as a function of Pt recovery and d) Pd grade as a function of Pd recovery at the various SS dosages (Ore 2).

Figure 4.54 compares the Pt and Pd recoveries and grades between the baseline and 2000 g/t conditions for both ores. Overall, it should be noted that 2000 g/t SS improved the Pt and Pd recoveries significantly

in both ores, however, using 2000 g/t SS obtained a higher Pt recovery using Ore 1, but Ore 2 obtained a higher Pd recovery. This suggests that SS was also effective in handling slime coating and rheological problems within Ore 2. Grades were enhanced in the case of both ores, however, Pt and Pd grades were higher in Ore 1 compared to Ore 2. This was expected considering a higher talc content and lower PGE feed grade in Ore 2 compared to Ore 1, as observed in Table 4.1 and Table 4.3. It is expected that the feed grade would be the main effect leading to poorer concentrate grades in Ore 2. Table 4.3 shows that Ore 1 has a ± 3.2 higher 6E grade than Ore 2, and Figure 4.54 indicates that the sum of the Pt and Pd concentrate grades at 2000 g/t SS for Ore 1 is approximately 27.6 g/t (18.1 g/t Pt + 9.5 g/t for Pd). For Ore 2 this is approximately 10.0 g/t (5.8 g/t Pt + 4.2 g/t Pd). The ratio of the concentrate grades is 2.8 (27.6:10.0), which is slightly lower than the difference in head grade.

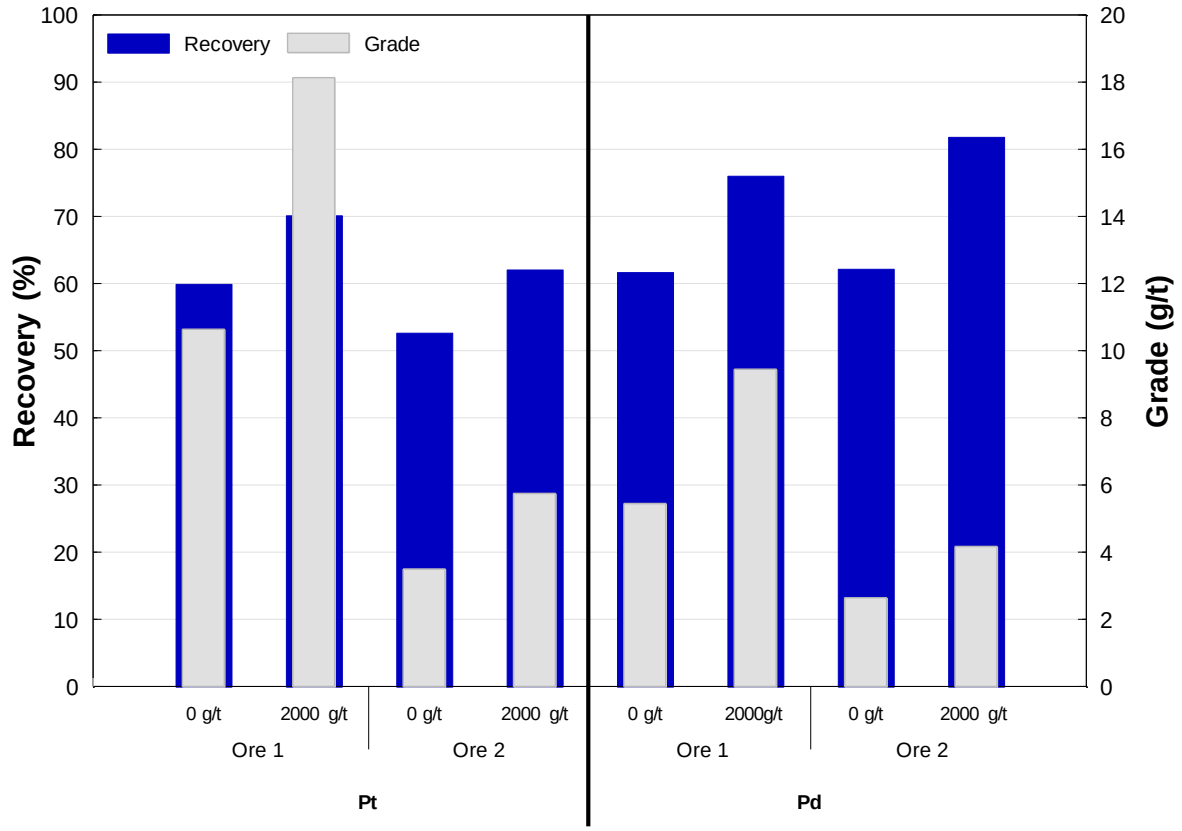

Figure 4.54: Comparing the Pt and Pd recoveries and grades between the baseline (0 g/t) and 2000 g/t SS dosages for both ores.

Key findings of the effect of SS on Ore 2 investigation are summarized below:

1. Increasing the SS dosage decreased the quantity of recovered solids and water using Ore 2, which was not a defined trend using Ore 1 (Figure 4.18 and Figure 4.52)
2. Using high SS dosages significantly enhanced Pt and Pd recoveries and grades using Ore 2, which

suggests that slime coatings, pulp rheology issues, and NFG were also mitigated in Ore 2 using SS (Figure 4.53), and

3. Batch flotation tests using 2000 g/t SS resulted in higher Pt and Pd grades using Ore 1 compared to using Ore 2. This was as expected considering a high talc content and lower feed grade in Ore 2 compared to Ore 1 (Figure 4.54, Table 4.1 and Table 4.3).

Chapter 5: Discussion

This chapter serves to interpret and describe the importance of the results presented in this work. The discussion includes implications for recovery and grade based on mineralogy findings (Section 5.1), the mitigation of slime coatings using SS (Section 5.2), the effect of SS on pulp rheology (Section 5.3), enhancing concentrate grade using SS (Section 5.4), and evaluating the performance of SS against other methods (Section 5.5).

5.1. Mineralogy - Implications for recovery and grade

5.1.1. Geology

The presence of alteration minerals within the crushed rock illustrated in Figure 4.6 indicates that the Pseudo reef was in contact with hydrothermal fluids and that chemico-physical parameters, such as low temperatures or the ratio of fluid to rock, favoured the alteration of rock forming minerals. What was possibly previously harzburgite rock, as indicated by large quantities of olivine and orthopyroxene in Figure 4.6a to Figure 4.6c, underwent alteration of the olivine to mesh-textured serpentine, and orthopyroxene to serpentine and talc. These rock forming minerals in ultrabasic rocks are known to be vulnerable to hydration reactions (McCollom & Bach, 2009: 857; Rouméjon et al., 2014: 726). The units are not completely altered as some of the relict grains, such as olivine mesh cores, are still visible which indicates that the rock underwent stage 2 alteration (Ningthoujam et al., 2012: 131). The same cannot be said for the serpentinite unit in Figure 4.6d, which underwent extensive stage 3 serpentinization and the development of well-defined secondary magnetite veins. Alteration of the pyroxenite units also occurred, which is more prone for the olivine pyroxenite in Figure 4.6a than the orthopyroxenites in Figure 4.6e and f. This is possibly due to a higher rate of olivine alteration compared to orthopyroxene (Bach et al., 2004: 15). The orthopyroxenites are mostly unaltered, except for talc rimming and talc along fissures of orthopyroxene which indicates that they have undergone stage 1 alteration, as commonly observed in other parts of the BIC (Zingg, 1996: 25; Penberthy & Merkle, 1999: 242; Li, Ripley & Merino, 2004: 176; Lotter et al., 2008: 907). Interstitial plagioclase remained mostly unaltered except for some alteration to chlorite and mica. As determined from the feed XRF data presented in Appendix B, the molar olivine to orthopyroxene ratio, which is indicated by MgO/SiO_2, was less than 1. This indicates that Merensky reef-Pseudo reef unit alteration would result in serpentine-talc assemblages and not serpentine-brucite assemblages (Li, Rahn & Bucher, 2004). Overall, this indicates that near-surface olivine-bearing peridotites and pyroxenites in the location of these PGE deposits were thermodynamically unstable which made the units susceptible to alteration.

5.1.2. Bulk mineralogy and implications for flotation performance

Ore 1 is mainly composed of orthopyroxene and serpentine with lesser amounts of olivine, magnetite, plagioclase, and talc, as indicated in Table 4.1. There is a very large concentration of alteration minerals in this ore, which could have serious implications for the flotation performance. It has been shown that even small quantities of serpentine can have detrimental effects on valuable mineral recoveries due to slime coating (Edwards, Kipkie & Agar, 1980: 36; Bremmell & Addai-Mensah, 2005: 209). The results revealed that 1.3 wt.% of the ore feed constitutes serpentine slimes, and that the BMS to serpentine ratio is approximately 1:7. However, the occurrence of slime coating is not the only problem which may impact PGE recoveries. The abundance of orthopyroxene and serpentine in both ores may lead to rheological problems during froth flotation. Firstly, the likelihood of hetero- aggregation between orthopyroxene and serpentine remains high due to their opposite charges in solutions. Secondly, large amounts of serpentine, which have been identified as lizardite by Raman and XRD analyses, may pose their own rheological challenges due to homo- aggregation (Johnson, Russell & Scales, 1998: 12; Burdukova et al., 2008: 2176; Behnsen & Faulkner, 2012: 54; Ndlovu et al., 2014: 195). All of these factors may have serious consequences on PGE recovery due to the linkage between increased pulp rheology to poor gas dispersion and bubble-particle collisions (Bakker, Meyer & Deglon, 2009: 949, 2010: 972; Shabalala et al., 2011: 1452). This all points to the fact that the ore could respond favourably to a method that will disperse slime coatings from valuable minerals as well as lower the pulp viscosity by reducing the rheological complexity of the slurry.

Although serpentine is the major alteration mineral present in the ores, there are also relatively large quantities of talc present (5.0% in Ore 1 and 9.5% in Ore 2), as indicated in Table 4.1. It is well-known that talc is a NFG mineral that can detrimentally affect the grade of the concentrate and needs to be managed with depressants. However, it has been shown that the disproportionate effects of talc on grade and froth characteristics come mostly from talc that is associated with other gangue minerals, such as pyroxene (Becker et al., 2009: 253). According to QEMSCAN talc association data, 89.2% of the talc in the Ore 1 feed is unliberated and is mainly associated with orthopyroxene as composite talc-orthopyroxene particles as shown Table 4.2 and Figure 4.9. Talc mainly occurs along the boundaries (talc rimming) and fissures of orthopyroxene, as illustrated in Figure 4.10, which indicates that orthopyroxene easily breaks along cleavage planes during milling. If talc is not depressed, the association of talc to orthopyroxene will induce natural floatability of the composite orthopyroxene particles and subsequently decrease PGE concentrate grade and increase bubble loading. This can hinder PGM attachment and also lead to downstream smelter penalties. The recovery of talc-serpentine composites will also have the same consequences as the recovery of talc-orthopyroxene composites, although its significance is smaller due to their lower association compared to talc-orthopyroxene composites. In addition, both liberated and unliberated talc will increase froth stability and consequently will increase the recovery of water and

entrained gangue, which will further reduce PGE grades (Wiese, Harris & Bradshaw, 2010: 1012; Farrokhpay, Ndlovu & Bradshaw, 2018: 273). A higher quantity of talc in Ore 2 is expected to result in lower PGE concentrate grades compared to Ore 1 due to the recovery of higher quantities of composite talc particles and a higher froth stability which will recover higher quantities of water and entrained minerals. This indicates that a method of depressing talc will be necessary to improve concentrate grade. A summary of the observations using various analytical techniques and implications for PGE recovery and/or grade are provided in Table 5.1.

Table 5.1: Observations using various analytical techniques and implications for PGE recovery/grade.

Analytical techniques	Observations	Possible implications for PGE recovery and/or concentrate grade
QEMSCAN – quantification of mineral content, liberation, and association	Significant quantity of serpentine in the feed (19.2 wt.%), of which 1.4 wt.% are characteristic of serpentine slimes The BMS to serpentine slime ratio is approximately 1:7	Serpentine slime coatings of valuables which will reduce recoveries
QEMSCAN – quantification of mineral content	Large quantities of orthopyroxene (35.7 wt.%), serpentine (19.2 wt.%) and talc (5.0 wt.%) in the feed	Rheology issues due to orthopyroxene-serpentine hetero-aggregates as well as serpentine and talc homo aggregates which may lower recoveries
QEMSCAN – quantification of mineral, liberation, and association	Dominant talc-orthopyroxene association (59.1% of talc) in the feed	Poor PGE concentrate grades, increased bubble loading, downstream smelter penalties and increased froth stability

5.1.3. PGE characteristics

Using QEMSCAN paired with chemical assays made studying the low grade PGE Ore 1 possible. The PGMs in this work were named and grouped PGE species instead of exact PGM names because using this nomenclature is more meaningful given the diversity of PGM species typically encountered in these ores (Chetty et al., 2009: 590). Of the 112 PGMs particles analyzed in the feed, PGE arsenides, PGE sulphides and PGE tellurides dominate in terms of PGM area % (occurring at 25.4%, 25.3% and 12.5%, respectively), as illustrated in Figure 4.11. Sperrylite, cooperite and moncheite are the most common minerals in these groups, respectively. These PGMs are typically negatively charged at pH 9, as determined by zeta potential measurements of sperrylite, cooperite and moncheite in previous work (Shackleton, 2007: 86; Shackleton, Malysiak & O'Connor, 2007b: 1237, a: 30). This observation played an important role in understanding the vulnerability of PGMs to slime coatings later in the study, especially considering that serpentine is known to be positively charged. The major PGM assemblage is similar to that reported

for the Silicate reef in Becker, Ramonotsi and Petersen (2012: 3), which may indicate that the ores had similar Merensky reef-Pseudo reef unit blends.

Common to ores in the Merensky reef and Pseudo reef unit, Pt and Pd are the dominant PGEs and are primary economic elements mined at PPM and other mines within the Bushveld Complex. The grades of PGEs are, however, much lower for Ore 2 compared to Ore 1, as observed in Table 4.3. Seeing as Pt and Pd are the major PGEs within the ores, the study focused mainly on improvements to Pt and Pd recovery and grade. It was observed that the PGEs are not only confined to discrete PGMs considering that Ore 1 has a Pt/Pd ratio of 2.8 which indicates that Pd had been mobilized. It is expected that PGEs can occur in solid solution of BMS due to sulphide liquid fractionation as previously noted within the Merensky reef and Pseudo reef unit (Godel, Barnes & Maier, 2007: 1579; Osbahr et al., 2013: 230; Molifie, 2016: 29). The occurrence of secondary BMS such as millerite and violarite gives evidence that BMS were in fact prone to alteration. However, much of the Pd may have been re-mobilized as indicated by the high Pt/Pd ratio, which is similar to that of pervasively altered Great Dyke ores in Zimbabwe (Oberthür et al., 2013: 200). The re-mobilization could have occurred via hydrothermal fluids when unstable BMS PGE-carriers (or even PGMs) were altered (Li, Ripley & Merino, 2004: 183; Polovina, Hudson & Jones, 2004: 274; Locmelis, Melcher & Oberthür, 2010: 101; Oberthür et al., 2013: 196). It is possible that the Pd could occur in solid solution with alteration minerals such as talc and amphibole because this has been detected in Pseudo reef unit drill cores in previous work (Molifie, 2016: 43). This suggests that PGEs are incorporated into the hydration hydrothermal alteration products when it is mobilized in hydrothermal fluids. The BMS host to PGEs must also be recovered to improve recoverable PGEs. The association between PGMs and BMS would, therefore, not only benefit PGM recovery, but also recoverable PGEs overall. However, important PGE losses will occur due to alteration, as PGEs possibly occur in silicates (refractory PGEs) and the Pt/Pd ratio indicated that Pd had been mobilized. This does come as a great consequence during the processing of altered PGE ores. In addition, low feed grades, and high NFG contents can have detrimental impacts on concentrate grades (as mentioned in Section 5.1.2). Ore 2 has a lower feed grade and higher talc content compared to Ore 1 and is, therefore, expected to have a lower concentrate grade compared to Ore 1.

The majority of PGMs are smaller than 10 μm in grain size (65% PGMs), as demonstrated in Figure 4.14 which, together with a consideration of the mode of occurrence of PGMs, can be used to infer some characteristics or challenges on the floatability of PGMs. Approximately 45.6% of PGM grains and PGM/BMS particles are liberated, as illustrated in Figure 4.16 which, considering a system absent of alteration mineral challenges, approximately half of the PGMs are expected to recover fairly well. However, some species will be difficult to recover due to the following slow-floating PGM characteristics, as inferred from the observations in previous work. Firstly, liberated PGMs above 10 μm in size have been identified as sperrylite, which is known to be slower-floating compared to other PGMs and have

been observed to report to the tailings (Shamaila & Connor, 2008: 903; Becker, Ramonotsi & Petersen, 2012: 3; Becker, Wiese & Ramonotsi, 2014: 28). Secondly, a large quantity of liberated PGMs are below 5 μm in size which are slower-floating PGMs (Penberthy, Oosthuyzen & Merkle, 2000: 220). Lastly, poorly liberated PGMs have been observed to mostly report to the tailings (Bushell, 2012: 4; Becker, Wiese & Ramonotsi, 2014: 28). Due to low PGM particle counts and the limitations of electron beam analytical instruments, obtaining high quality x-ray data on particles around 1 μm in size is challenging. Therefore, quantitative PGM data could not be accurately gathered. In previous work on the Silicate reef, occurrences of PGMs and PGM/BMS particles attached to gangue had difficulty being recovered as significant proportions of these PGM associated particles have shown to report to the tailings (Becker, Ramonotsi & Petersen, 2012: 3). Therefore, since another Silicate reef in the same location showed gangue associated losses, it is likely to also be the case for the ores used in this work. A summary of the observations using various analytical techniques and implications for PGE recovery and/or grade is provided in Table 5.2.

Table 5.2: Observations using various analytical techniques and implications for PGE recovery/grade.

Analytical techniques	Observations	Possible implications for PGE recovery and/or concentrate grade
QEMSCAN - measurement of trace PGMs and quantification of mineral content	Abundance of negatively charged PGMs and positively charged serpentine slimes in the feed	PGM slime coating
PGE fire assay and ICP-OES – measurement of PGE content	High Pt/Pd ratio in the feed	Remobilization of PGEs
QEMSCAN - measurement of trace PGMs	The presence of sperrylite, PGMs below 5 μm in size and poorly liberated PGMs in the feed	Slow-floating PGMs may report to the tailings
QEMSCAN – measurement of mineral content	Larger quantities of talc in the Ore 2 feed (9.5 wt.%) compared to the Ore 1 feed (5.0 wt.%) and a lower Ore 2 feed grade (0.6 6E g/t) compared to Ore 1 (1.9 6E g/t)	Poorer concentrate grades in Ore 2 compared to Ore 1

5.2. Mitigation of slime coatings using SS

The hypothesis relating to this section is stated below:

> Sodium metasilicate will act as a dispersant and remove surface phyllosilicate slime coatings from PGMs and BMS by adsorbing onto the phyllosilicate slime particles, thus creating an electrostatic repulsion between PGMs/BMS and slimes.

Batch flotation of the ore without SS addition produced poor Pt and Pd recoveries in the region of 60%, as illustrated in Figure 4.19 and Figure 4.20. Previous studies with other PGE ores have achieved rougher

batch flotation recoveries as high as 78%, which illustrates the poor flotation performance of this ore (Solomon et al., 2011b: 1376; Ramlall & Loveday, 2015: 222). Various studies, which focused on BMS recovery, have concluded that the presence of excessive slimes results in low flotation recoveries, on account of a hydrophilic layer of slimes on valuable mineral surfaces (Arnold & Aplan, 1986a: 240, b: 258; Bandini, Prestidge & Ralston, 2001: 490; Forbes, Davey & Smith, 2014: 138). It was noted that the ore feed contained 19.2 wt.% serpentine and milling of the ore to the primary grind target of the operation produced 1.3 wt.% of serpentine that could exhibit slime behaviour (Table 4.1 and Figure 4.8). This makes the ore particularly vulnerable to the negative impacts of slimes and the need for a suitable dispersant reagent was emphasized. This work has therefore chosen to investigate the dispersant effect of SS in the mitigation of serpentine slimes to enhance recovery. This section is aimed at discussing the hypothesis as stated above. The hypothesis correlates with the key question; "*How does the dispersant effect of SS improve PGE recovery, and how can this knowledge be utilized to provide an optimum PGE recovery?*" To answer this, the findings of the chalcopyrite microflotation, zeta potential and pH modification experiments, which served to decouple SS's dispersant effect, will be discussed before it is placed into the context of SS batch flotation experiments.

The high chalcopyrite recoveries obtained during the microflotation experiments (100%), as illustrated in Figure 4.43, reflect what is commonly observed in literature when pure chalcopyrite is floated in the presence of xanthates (Goktepe, 2002: 313; Peng, Wu & Abdelmonem, 2017: 3569; Bai et al., 2018: 4; Ramirez et al., 2018: 11; Mhonde et al., 2020: 10). However, when serpentine particles in the -10 μm size class were added, the recovery of chalcopyrite was severely compromised at both 1:2 and 2:1 chalcopyrite to serpentine ratios (Figure 4.43). This indicates that the presence of serpentine slimes was responsible for the poor floatability of chalcopyrite. This is in agreement with many studies which observed that BMS, such as pentlandite, galena, and pyrite, were depressed with the introduction of serpentine slimes (Edwards, Kipkie & Agar, 1980: 36; Bremmell, Fornasiero & Ralston, 2005: 209; Peng & Bradshaw, 2012: 286; Cao et al., 2017: 624; Feng et al., 2019: 488).

Changing the chalcopyrite to serpentine ratio from 2:1 to 1:2 further reduced the floatability of chalcopyrite by 2.4% on average, which indicates that chalcopyrite became further depressed with increasing serpentine concentration (Figure 4.43). The reduction in BMS floatability with increasing serpentine concentration was also observed by various investigators (Edwards, Kipkie & Agar, 1980: 36; Bremmell, Fornasiero & Ralston, 2005: 209; Peng & Bradshaw, 2012: 286; Zhou & Feng, 2015: 430). Of particular interest is the significant depression of BMS in the presence of trace amounts of serpentine slimes such as 100:1 and 20:1 BMS to serpentine ratios (Bremmell, Fornasiero & Ralston, 2005: 36; Zhou & Feng, 2015: 431). This may indicate that low concentrations of serpentine covered the surface of the BMS to the point where the adsorption of the collector was inhibited. The ore used for this investigation had a very low BMS to serpentine ratio of 1:64 and even lower PGM to serpentine ratios. It is, therefore,

expected to be highly detrimental to PGE recoveries. High serpentine concentrations in this and various other South African PGE orebodies listed in Table 5.3 are therefore expected to affect PGM and BMS recoveries due to slime coating. Platinum-group mineral recoveries will possibly be even more affected with an abundance of serpentine, i.e. a low BMS to serpentine ratio.

Table 5.3: Serpentine and BMS content in various South African PGE ores.

Ore type	Serpentine content (wt.%)	BMS content (wt.%)	Approximate BMS to serpentine ratio	Reference
Chromium-rich PGE ore (BIC)	8.0	0.2	1:40	(Bulatovic, 2003: 932)
Sulphide PGE ore (Merensky)	15.2	1.7	1:9	(Bulatovic, 2003: 932)
Platreef	6.9	2.1	1:3	(Corin, Bezuidenhout & O'Connor, 2012: 101)
"Silicate reef"	10.6	0.2	1:53	(Becker, Wiese & Ramonotsi, 2014: 28)
Merensky reef	2.1	1.1	1:2	(Becker et al., 2009: 248)

Zeta potential measurements have commonly been used to support microflotation findings on the effects of slimes in literature and are also used in this work. At pH 9.0, it was found that lizardite and chalcopyrite are oppositely charged which indicates that a strong electrostatic attraction occurs between them, as illustrated in Figure 4.45. It is therefore anticipated that the poor chalcopyrite recoveries observed during microflotation at the same pH (Figure 4.43) were due to hetero-aggregation between serpentine slimes and chalcopyrite particles The surface charge of serpentine was positive due to the preferential dissolution of OH^- ions, leaving Mg^{2+} ions exposed on the surface of serpentine, as suggested by Feng et al. (2013: 1126). It can be expected that the total interaction energy between serpentine and chalcopyrite was negative, which allowed the electrostatic attraction between the minerals and led to coatings of serpentine slimes onto chalcopyrite. This is inferred by various DLVO interaction energy investigations which commonly found this occurrence between serpentine and BMS such as pyrite and pentlandite (Bremmell & Addai-Mensah, 2005: 211; Feng et al., 2012: 12093; Feng, Lu & Luo, 2015: 5; Long, Huang & Xiao, 2019: 9). The interaction between serpentine and chalcopyrite is further supported by studies which found that $Mg(OH)_2$, which represents the chemistry of serpentine, precipitated onto negatively charged BMS (Li et al., 2017: 8, 2018: 10, 2019; Suyantara et al., 2018: 126).

It was previously explained that, due to the inability to obtain pure PGMs for this work, chalcopyrite was used as a PGM proxy. This was based on the similarities in the zeta potential sign (both negative) and also the close association between the PGMs and BMS such as chalcopyrite in PGE ores (Shackleton, 2007:

86; Shackleton, Malysiak & O'Connor, 2007b: 1237, a: 30; Petrus et al., 2012: 120; Zeng et al., 2020: 5). Therefore, opposite charges between serpentine and PGMs indicate that PGMs would also be prone to slime coating, although the degree of slime coating might differ for PGMs and BMS. The PGM feed characterisation depicted the common PGM species in the ore currently under investigation to be sperrylite, cooperite, and moncheite. Sperrylite, cooperite and moncheite surfaces are negatively charged at pH 9 and are reported to be -13 mV, -5 mV and -18 mV, respectively (Shackleton, 2007: 86; Shackleton, Malysiak & O'Connor, 2007a: 34, b: 1237). This means that the chalcopyrite value of -35.9 mV at pH 9 found in this study is slightly lower, but still in the negative region (Figure 4.45). It follows, therefore, that there would be an electrostatic attraction between positively charged serpentine and negatively charged PGMs, which would hinder collector adsorption and reduce recovery.

The occurrence of slime coated BMS in the feed can also impact the floatability of PGMs due to the association between BMS and PGMs. Common BMS in the feed are chalcopyrite and pentlandite (Figure 4.4), which are BMS known to be vulnerable to serpentine slime coating (Edwards, Kipkie & Agar, 1980: 36; Bremmell, Fornasiero & Ralston, 2005: 209; Chen et al., 2021: 7). It was shown that significant amounts of PGMs within the -10 μm size fraction are associated with BMS and therefore PGM recovery will benefit from recovery of these PGM/BMS composites (Figure 4.15 and Figure 4.16). In addition, it is speculated that PGEs could occur, through solid solution substitution, in BMS, such as the occurrence of Pd in pentlandite. Slime coating of BMS within the slurry at the standard flotation operating conditions without added dispersant could therefore minimize PGE recovery due to the loss of the PGM-BMS association advantage and loss of PGEs hosted in non-recoverable BMS. The addition of a suitable dispersant is, therefore, also needed to remove serpentine slime coatings from BMS to improve PGE recovery, especially since pentlandite is slower-floating compared to chalcopyrite and is expected to be host to Pd (Heiskanen, Kirjavainen & Laapas, 1991: 268).

Solution chemistry is not the only factor which governs slime dispersion or aggregation. This was illustrated by the fact that the chalcopyrite recovery was close to 100% when using a 1:2 chalcopyrite to serpentine ratio in a batch flotation cell (Figure 4.44). This was compared to the almost zero recovery obtained in the microflotation cell under the same conditions. This observation appeared to point to the fact that energy input was a significant factor in mitigating the effects of slime coatings since the energy input in mechanically agitated flotation cells is typically between 1 to 2 kW/m^3, and since microflotation cells are not stirred by an impeller, the energy input is expected to be lower (Deglon, 2005: 839; Yu et al., 2017: 128; Ross, Singh & Pillay, 2019: 134). However, this effect was not evident when running the batch flotation test on the actual ore since the floatability of Pt and Pd remained low. This may simply be due to the combination of experimental parameters which made the recovery of the chalcopyrite in the synthetic mixture better than the PGM and BMS recovery in the natural ore. These included: a lower solids concentration used for the synthetic ore (0.8 wt.% in the synthetic ore versus 35 wt.% for the natural ore);

different impeller and cell dimensions resulting in a higher energy turbulent zone surrounding the impeller in the cell used for the synthetic ore than the cell used for the natural ore, which removed slimes from chalcopyrite; at BMS to serpentine ratios of 1:2 for the synthetic ore and 1:64 for the natural ore. However, it is still likely that energy input has a marked positive effect on valuable mineral recovery in the presence of slimes due to the vast improvement between the microflotation cell performance compared to the batch flotation cell performance. It is important to note that differences in valuable mineral recoveries between synthetic ore flotation (either micro- or batch flotation) and natural ore batch flotation can also be due to a viscosity effect, as there is a vast difference in the solids concentrations between the systems, as previously mentioned.

During microflotation experiments, adding 2000 g/t SS restored the chalcopyrite floatability at a 1:2 chalcopyrite to serpentine ratio which is assumed to be due to the induced electrostatic repulsion between serpentine and chalcopyrite (Figure 4.43). This is supported by the zeta potential data which demonstrated that adding 2000 g/t SS changed the zeta potential of serpentine from +17.2 mV at pH 9 to -43.3 mV at pH 11.7 (Figure 4.45). The serpentine zeta potentials at the high dosages had a similar zeta potential to that of chalcopyrite. Due to the similarity in charge and magnitude of the zeta potentials of serpentine and chalcopyrite at these dosages, the repulsive force between serpentine and chalcopyrite is strong. Interaction energies have also demonstrated the repulsive forces between serpentine (or $Mg(OH)_2$ which is representative of serpentine) and BMS in the presence of SS (Feng et al., 2012: 12093; Li et al., 2019: 5). Therefore, a high chalcopyrite floatability is attributed to the dispersion of serpentine slimes from chalcopyrite surfaces.

The chalcopyrite behaviour in the presence of serpentine and SS can, therefore, be placed into the context of PGE recoveries during SS batch flotation experiments. It was found that using SS at 1000 g/t and 2000 g/t gave the highest Pt and Pd recoveries, which improved by 22.4% and 14.3%, respectively, relative to the baseline, as illustrated in Figure 4.19 and Figure 4.20. Similarly, chalcopyrite in the presence of serpentine (1:2 ratio) showed significant improvement in recovery upon addition of 2000 g/t SS, as demonstrated in Figure 4.43. From zeta potential measurements, it was observed that 1000 g/t SS also reversed the zeta potential of serpentine to be negative in value, similarly to that at 2000 g/t SS (Figure 4.45). Similar surface charges between serpentine and PGMs/BMS at high SS dosages resulted in the removal of serpentine slime coatings from PGM and BMS surfaces. This allowed better interaction of the collector on PGM and BMS surfaces due to the absence of surface slime coatings. The zeta potential of chalcopyrite decreased slightly using SS, as similarly observed by Li et al. (2019: 4). This indicates that SS species had adsorbed onto chalcopyrite which further reduced the net surface charge of chalcopyrite. There is no concern whether SS adsorbed onto chalcopyrite, or other BMS and PGMs, because this will further reduce their zeta potentials which will continue to maintain the negative surface charge (Xia et al., 2018: 2908; Li et al., 2019: 5). In addition, the adsorption of SS onto chalcopyrite does not appear to

negatively impact the collector behaviour, as high chalcopyrite recoveries were observed at the 1:2 2000 g/t SS microflotation experiment (Figure 4.43). Furthermore, it was confirmed through microflotation experiments that a high SS dosage can remove serpentine slime coatings from chalcopyrite which gives chalcopyrite associated PGMs the added advantage of a faster floatability and also for PGEs hosted in BMS to be recovered. In PGE ores, Pd commonly occurs, by solid solution substitution, in BMS. The recovery profile of Pd may, therefore, not follow the same recovery profile as Pt which are otherwise primarily host in PGMs.

Similar to other studies, high SS dosages were more effective at dispersing slimes than lower dosages (Al-Thyabat, 2009: 290; Ma, 2011: 234; Feng et al., 2012: 12091; Li et al., 2019: 4). The $SiO(OH)_3^-$ SS species are dominant between pH 9.4 and 12.6 in an aqueous solution and are, therefore, expected to be the species adsorbing onto serpentine slimes during froth flotation at high SS dosages, where the pulp pH ranged between 10.3 and 11.5 (Furlong, Sing & Parfitt, 1979: 415; Phair, Van Deventer & Smith, 2001: 151; Feng et al., 2012: 12092; Bo et al., 2015: 47). Sodium metasilicate dosages above 1000 g/t appear to be far more effective than lower dosages. This implies that many more Mg^{2+} serpentine sites have been occupied by $SiO(OH)_3^-$, lowering the serpentine surface charge more than at lower SS dosages. There will, however, be a limit to the effectiveness of SS's dispersant effect when the positive sites on serpentine are saturated by SS species. Using higher SS dosages than the maximum dosage investigated may therefore not have a stronger dispersant effect, and there will also be economic and downstream implications to higher dosages.

Batch flotation experiments using SS revealed that, as the SS dosage increased, the cumulative solids recovered decreased, which correlated with an increase in Pt and Pd recovery, as demonstrated in Figure 4.21. This occurrence is contrary to the norm where an increase in recovered solids commonly correlated with an increase in recovery (Hadler, Smith & Cilliers, 2010: 998). The solids recovered between the baseline and 1000 g/t SS recorded similar values, however, their Pt recoveries were very different. This indicates that the increased recoveries were not as a by-product of increased solids recovery, but that there was a fundamental change in separation efficiency. The combination of microflotation and zeta potential findings infer that at high SS dosages, the PGMs and BMS were recovered mainly by true flotation after serpentine slimes were removed, and that this was not due to a change in operational parameters.

High SS dosages were also found to be successful using another altered PGE ore, as observed using Ore 2 (Figure 4.53). A 1000 g/t SS dosage obtained the highest Pt recoveries for both ores, which had similar recovery improvements (22.4% using Ore 1 and 16.2% using Ore 2). In terms of their Pd recoveries, 2000 g/t obtained the highest recoveries for both ores, which obtained similar recovery improvements (14.3% using Ore and 19.6% using Ore 2). The total 2E recovery improvements between the two ores are similar (36.7% 2E using Ore 1 and 35.8% 2E using Ore 2), which was expected considering the very similar ore mineralogies. Most notably are the similarities in the BMS to serpentine ratios between the ores (1:64 for

Ore 1 and 1:62 for Ore 2), which infers that the ores faced similar slime coating issues. However, the slightly lower recoveries in Ore 2 are likely related to the higher talc content which contributed to more rheological issues compared to Ore 1. This will be addressed in Section 5.3. Key outcomes comparing froth flotation, chalcopyrite microflotation and zeta potential findings which are applicable to the discussion in this section are presented in Table 5.4.

Table 5.4: Key outcomes for selected conditions which inferred (froth flotation) and elucidated (Ccp microflotation and zeta potential) serpentine slime coatings and its dispersion from PGMs and BMS (Ccp as a PGM proxy).

Analytical technique	0 g/t (pH 9)	2000 g/t SS (pH 11.7)	0 g/t (pH 11.7)
Froth flotation	Low PGE recovery Low Cu recovery	High PGE recovery High Cu recovery	High PGE recovery High Cu recovery
Ccp microflotation (Ccp=PGM proxy)	Low Ccp recovery	High Ccp recovery	High Ccp recovery
Zeta potential	Electrostatic attraction between Ccp and Srp	Electrostatic repulsion between Ccp and Srp	Electrostatic repulsion between Ccp and Srp

5.2.1. Effect of pH on recovery

The addition of SS has a relatively large effect on pH of the flotation pulp. This is due to the release of OH^- ions at high SS dosages (Amorós et al., 2010: 34; Park & Jeon, 2010: 1369). During batch flotation experiments, the pH changed from 9.8 in the absence of SS to 11.7 at 2000 g/t SS, as illustrated in Figure 4.20. It was therefore necessary to decouple the effects of pH to see whether the positive effects were due to the presence of SS species, or to the effects of a higher pH. It was found that increasing pH did, indeed, have a positive effect on Pt and Pd recovery, as demonstrated in Figure 4.22. These were found to be higher (Pt) or similar (Pd) at the modified pH of 11.7, without SS addition, compared to using 2000 g/t SS at the same pulp pH. The microflotation experiments with chalcopyrite and serpentine slimes at an adjusted pulp pH of 11.7, without SS addition, demonstrated that the chalcopyrite flotation can be restored by adjusting the pulp pH to 11.7 (Figure 4.43). In support of this, the serpentine zeta potential measurement at pH 11.7 is indeed negative (-22.4 mV), which shows that an electrostatic repulsion between chalcopyrite and serpentine was responsible for the improved chalcopyrite recoveries (Figure 4.45). This indicates that floating at a high pH, beyond the i.e.p value of the slime (which is pH 10.3 for serpentine in this work), can create an electrostatic repulsion between valuable minerals and slimes, thus leading to improved recoveries.

Therefore, whether operating at a high pH beyond serpentine's i.e.p or using a high SS dosage would give a similar PGE recovery outcome. However, a much more negative zeta potential at 2000 g/t (pH 11.7)

indicates that the adsorption of SS species was also responsible for lowering the zeta potential of serpentine, as observed in Figure 4.45. This indicates that the high PGE recoveries between the pH modified condition and the use of SS occurred via the same mechanisms but through different surface species adsorption: the adsorption of $SiO(OH)_3^-$ in the case of using SS and the adsorption of OH^- in the case of the pH modified condition. The use of high pH in the absence of SS resulted in a much higher quantity of recovered solids compared to when no SS was used, as illustrated in Figure 4.23. This increase in recovered solids may be partially responsible for the higher PGE recoveries and also resulted in a much lower grade than for the experiments performed at higher SS dosages. Therefore, although modifying the pulp pH may improve PGE recoveries, this adjustment is an unlikely practice at plant scale due to the increase in recovered solids, reduction in grade and because pH modifiers are costly and large amounts of alkaline pH modifiers will be necessary. Using SS is more practical because it is relatively inexpensive compared to other depressants/dispersants (SS costs approximately R9.50/kg and CMC approximately R55.00/kg at commercial suppliers) (Ramonotsi, Pers. Comm. 2021), improves recovery, grade, decreases recovered solids and modifies the pH. It should be acknowledged that pH governs the type of SS species available for adsorption and that in this regard, it is an important parameter to consider when using SS during flotation.

In answer to the key question; *"How does the dispersant effect of SS improve PGE recovery, and how can this knowledge be utilized to provide an optimum PGE recovery?",* it can be concluded that SS species at high dosages adsorbed onto serpentine which reversed the surface charge of serpentine, thus created an electrostatic repulsion between serpentine and PGMs/BMS. This allowed better adsorption of the collector onto PGMs and BMS which improved PGE recoveries. High SS dosages could therefore be used to mitigate the negative impacts of slimes to improve PGE recovery.

5.3. Effect of SS on pulp rheology

The hypothesis relating to this section is stated below:

> Sodium metasilicate will reduce the viscosity and yield stress of the pulp because its rheology modifying effect will disperse aggregated phyllosilicate alteration minerals in the pulp which will result in better gas dispersion and bubble-particle collisions and therefore improve flotation recoveries.

Having discussed one of the main impacts on recovery (slime coating), it is now necessary to decouple the rheological behaviour of phyllosilicate bearing minerals of the pulp and determine how SS impacted this behaviour. This section intends to discuss the hypothesis stated above by answering the correlating key question: *"How does the rheology modifying effect of SS improve PGE recovery, and how can this knowledge be utilized to provide an optimum PGE recovery?"*. A discussion of the solids concentration, rheology and particle settling results will answer this question.

At the baseline condition, increasing the solids concentration increased the shear stresses, yield stresses, and apparent viscosities, as displayed in Figure 4.30 to Figure 4.32. This observation aligns with the findings of other studies which concluded that increasing solids concentrations increased the rheological complexity (Bakker, Meyer & Deglon, 2009: 946; Becker et al., 2009: 95; Mueller, Llewellin & Mader, 2010: 1216; Genovese, 2012: 5; Ndlovu et al., 2014: 197). It is thought that the measured behaviour is mainly a function of the presence of serpentine, talc and orthopyroxene, which are major mineral constituents in the ore and are thought to significantly contribute to the pulp rheology. The presence of lizardite and talc increases the suspension viscosity due to its platy morphology, whereas orthopyroxene itself is not expected to contribute to the complexity due to its stubby habit morphology. However, its involvement in hetero- aggregation can significantly contribute to the suspension rheology which will be discussed later in this section (Ndlovu et al., 2014: 198). At the flotation operating conditions, which is represented by a solids concentration of 20 vol.%, the apparent viscosity was 5.8×10^{-3} Pa.s and that of distilled water was 9.4×10^{-4} Pa.s (Appendix B and Figure 4.32). This indicates that the apparent viscosity of the pulp at the baseline flotation experiment was approximately 6 times higher than that of water and would have a greater rheological complexity, which is, obviously, expected. Past research found that the flow within a flotation cell is considerably widespread in the case of water, however the flow is considerably restricted to an impeller region in the presence of 60 wt.% solids (Bakker, Meyer & Deglon, 2009: 949). The presence of 35 wt.% solids during the 8L batch flotation experiments and a higher apparent viscosity compared to that of water indicate that the flow was most likely stagnated during batch flotation experiments due to the formation of a cavern around the impeller. This turbulent zone was therefore confined closer to the cavern which minimized gas dispersion, bubble-particle interaction and bubble particle mobility, hence reduced recoveries (Bakker, Meyer & Deglon, 2009: 949; Shabalala et al., 2011: 1452).

Increased pulp viscosity is thought to be aggravated by the presence of homo- and hetero-aggregates as well as fines in the pulp. At pH 9, the p.z.c value for lizardite is expected to be slightly higher than 9, and below the value of the i.e.p, which is 10.3, as determined in this work, because the basal plane of lizardite is known to be positively charged (Gillery, 1959: 147). Moreover, there will also be a close balance between positive and negative charges on the face and edges of lizardite due to the similarities in the pH of interest (pH 9) and the expected p.z.c. The i.e.p and p.z.c of lizardite are also expected to be similar, which infers that it is likely that lizardite faces are weakly positive, which may also be nearly neutral. It is, therefore, likely that lizardite homo- aggregation would be a combination of EE and EF aggregation. It is expected that EE aggregation would be dominant for lizardite due to similar p.z.c and i.e.p values which indicates that the face would carry a weakly positive charge, and that the edge would be weakly negative or even neutral. It is known that EE configurations can raise yield stress, but this is not as significant as EF configurations (Rand & Melton, 1977: 310; Ndlovu et al., 2011: 1319) For talc, pH 9 is close to the estimated p.z.c values (7.7 to 8.4) reported in the literature (Burdukova et al., 2007: 341; Ndlovu et al.,

2014: 195). This indicates that there is likely to be a close balance between positive and negative charges of faces and edges on the surfaces of talc, which is likely to result in a combination of both EF and EE aggregation (Burdukova et al., 2007: 341; Ndlovu et al., 2014: 196). It is expected that EF aggregation would be dominant for talc due to a clear difference between the p.z.c and i.e.p of talc which indicates that the faces would carry a strong negative charge. Talc aggregation is therefore expected to contribute significantly to the rheological complexity of the ore, as EF configurations are known to be associated with high yield stresses (Rand & Melton, 1977: 310; Ndlovu et al., 2011: 1319).

The abundance of lizardite and orthopyroxene in the pulp indicates that there is likely a dominance of serpentine-orthopyroxene aggregates on the basis of their opposite surface charges and expected electrostatic attraction at pH 9.8 (Yang et al., 2018: 4). Other aggregates consisting of serpentine-plagioclase and serpentine-talc are also likely to have occurred as plagioclase and talc are known to have highly negative zeta potentials around this pH (Fuerstenau, Lopez-Valdivieso & Fuerstenau, 1988: 164; Kursun, 2010: 137). The baseline particle settling tests confirmed the presence of aggregates by a rapid decrease in interfacial height, fast settling velocities and a clear supernatant compared to SS experiments after 20 minutes (Figure 4.33 to Figure 4.35 and Appendix B). The clear supernatant suggests that dispersed lizardite would have aggregated with other silicates.

By comparing the rheological parameters between the standard and finer grinds, the rheological effects contributed by fines in the pulp can be acknowledged, especially since it is known that there is a significant number of fines in the ore (Figure 4.2). During rheology measurements, the total particle masses were kept constant, but the particle size of the solids was reduced at the finer grind. The finer grind therefore contained a higher surface area of minerals which binds water molecules, thus, the effective solids concentration was increased (Kawatra & Eisele, 1988: 254). The viscosity is higher at the finer grind which indicates that smaller particles increased the number of particle-particle interactions (which may enhance aggregation) and flow resistance in the fluid suspension. The electroviscous effects are more prominent for the fine particles which may be due to the larger double layer for smaller particles or that there is a larger extension of the double layer interaction as the mean distance between particles is shorter (Zhou, Scales & Boger, 2001: 2913). An even higher Bingham yield stress indicates that a higher initial energy input is required before fluid begins to flow compared to that of the standard grind. This indicates that the presence of fines can increase the rheological complexity and illustrates that a standard plant secondary grind would have even greater detrimental viscosity problems compared to the primary grind tested during this project. For example, the apparent viscosity at the finer grind is double that of the standard grind at the baseline experiments.

Now understanding the influences of increased pulp viscosity at the baseline experiment, it is important to assess how a reduction in the rheological complexity improved recoveries. It is known from literature that reducing the solids concentration corresponds with a reduction in the apparent viscosity (Gao et al., 2018:

5). This work showed that a low solids concentration significantly improved both Pt and Pd recoveries, as illustrated in Figure 4.25 and Figure 4.26. This low density corresponds to a relatively lower volume fraction in the rheology measurements of the baseline and, therefore, a lower pulp viscosity which correlates to better mixing (expansion of the turbulent zone around the impeller) and improved particle/bubble collision efficiency (Schubert, 1999: 263; Bakker, Meyer & Deglon, 2009: 949; Shabalala et al., 2011: 1452; Bhunia, Kundu & Mukherjee, 2017: 1302). Interactions between particles and reduced friction between possible aggregates are thought to also be reduced. The increase in recovery at low solids concentrations can, therefore, be attributed to the reduction in viscosity of the system compared to the higher solids concentration systems. This is another indication that the batch flotation pulp at the baseline conditions was more rheologically complex, which had a major impact on recoveries, and that a reduction in the rheological complexity for this ore will improve recoveries. Grade also improved at the lowest solids concentrations due to less entrainment (Figure 4.25 and Figure 4.26). Entrainment is the non-selective recovery of fine particles during water recovery and is, therefore, directly proportional to the concentration of those particles in the pulp. At lower solids concentrations, there were fewer solids available to be entrained and better drainage in the froth. It should be noted that using SS enhanced grade much better than operating at a lower solids concentration. This is left for further discussion in Section 5.4.

A reduction in the pulp viscosity at high SS dosages is thought to be mainly due to the ability of SS to adsorb onto serpentine and talc. This work showed that SS can change the magnitude and sign of serpentine's zeta potential from highly positive to low negative values (Figure 4.45). This occurred by the adsorption of anionic SS species onto serpentine, as discussed in Section 5.2. The adsorption of SS species onto face (and edge planes) resulted in the dispersion of lizardite homo-aggregates, as similarly observed for kaolinite in the presence of a higher SS dosage (Amorós et al., 2010: 38). It is postulated that SS adsorption on the face and edge planes induced the same surface charge which dispersed lizardite configurations on account of an electrostatic repulsive force. The talc microflotation investigation revealed that SS can adsorb onto talc through various pH-dependent mechanisms, which will be discussed in Section 5.4. It is postulated that the adsorption of SS onto talc edge and face planes at high SS dosages resulted in the dispersion of talc homo-aggregates which contributed to a lower yield stress, as similarly observed for CMC in a past study (Burdukova, Bradshaw & Laskowski, 2007: 276). At alkaline pH's, a strong repulsion is expected because serpentine and orthopyroxene (also other silicates such as olivine and plagioclase) both have very low negative zeta potentials (Yang et al., 2018: 4). Therefore, hetero-aggregates are expected to disperse. The dispersion of homo- and hetero-aggregates are mimicked by slower declination of interfacial heights, slower settling velocities and the large number of suspended fines present in the supernatant due to particle dispersion (Figure 4.33 to Figure 4.35 and Appendix B). This reduction in apparent viscosity at high SS dosages, especially at 2000 g/t SS, is observed to be similar to that of distilled water (for 20 vol.% this is 7.6×10^{-4} Pa.s at 2000 g/t SS and 9.4×10^{-4} Pa.s for distilled

water), as illustrated in Figure 4.32. Past research indicated that fluid flow in a flotation cell containing water is sufficient and that there is no stagnation of the fluid around the impeller (Bakker, Meyer & Deglon, 2009: 949). Due to the fact that the introduction of SS reduced apparent viscosities closer to that of water, the fluid flow during batch flotation is therefore also expected to improve and the presence of a cavern region to be diminished.

In addition, SS was also found to significantly lower the rheological complexity of a system containing fines (Figure 4.30 to Figure 4.32). Although particle-particle interactions are expected to remain similar, this does not lead to the formation of aggregates due to repulsive forces, thus, the flow resistance is expected to be lowered. The dispersion of both homo- and hetero-aggregates lowered the yield stress and apparent viscosity, which indicates that a lower force is needed to initiate flow and overcome the initial molecular friction in the pulp. The reduction in rheological complexity allowed the turbulent zone during flotation to expand, as yield stresses are closer to that of water which is similar to that expected for a lower solids concentration. This enhanced gas dispersion, bubble-particle collision and attachment, particle and bubble mobility, and improved gas hold-up which improved recoveries.

In answer to the key question, *"How does the rheology modifying effect of SS improve PGE recovery, and how can this knowledge be utilized to provide optimum PGE recovery?"*. There are three effects that negatively impact rheology: i) homo- aggregation of serpentine and talc particles due to their irregular surface charges and platy morphologies, ii) hetero- aggregation due to the electrostatic attraction between serpentine and mainly orthopyroxene due to their opposite surface charges and iii) fine particles which increases particle-particle interactions. Sodium metasilicate can adsorb onto serpentine and talc resulting in the dispersal of the homo-aggregates due to the ability of SS to induce the same charge on the edge and face planes of the phyllosilicates. Sodium metasilicate can also disperse serpentine-orthopyroxene hetero-aggregates due to the ability of SS to change the zeta potential of serpentine from positive to negative values. The ability of SS to disperse phyllosilicate minerals in the pulp can also reduce the rheological complexity of a system containing fines. High SS dosages could therefore lower the apparent viscosity of the pulp to similar values to that of water which improved fluid flow in the cell. Gas dispersion and bubble-particle interactions and mobility were also improved as a result, which enhanced PGE recoveries. A summary of the problem, causes, solutions and knowledge contribution of the solids concentration, pulp rheology and particle settling findings are summarized in Table 5.5.

Table 5.5: Summary of the solids concentration, pulp rheology and particle settling problem, causes, solution and knowledge contribution. Note the commonality in the cause.

	Flotation: solids concentration	**Pulp rheology**	**Particle settling**
Problem	▪ Low PGE recoveries at a 35% solids concentration	▪ High pulp viscosity at the standard grind which is indicated by a high shear stress, yield stress, and apparent viscosity	▪ Faster particle settling rates at the baseline test compared to SS dosage tests as indicated by a lower interfacial settling height with time and a faster settling velocity
Cause	▪ Inter-particle interaction between serpentine and predominantly orthopyroxene giving rise hetero-aggregates ▪ Inter-particle interactions between serpentine edge planes (mainly EE configurations) and talc edge and face planes (mainly EF configurations) giving rise to homo-aggregates ▪ Fine particles increase particle-particle interactions		
Solution	▪ A reduction in solids concentration to 15% improved PGE recoveries (and grades)	▪ High SS dosages lowers the pulp viscosity at both standard and finer grinds ▪ Aggregates are dispersed due to SS' ability to adsorb onto and reverse the surface charge of serpentine	▪ High SS dosages lowers the particle settleability which is indicated by higher interfacial height with time and slower settling velocities
Knowledge contribution	▪ Improved PGE recoveries at the lower solids concentration indicates that this ore could benefit from a reduction in viscosity ▪ High SS dosages during froth flotation reduced the pulp viscosity	▪ This confirms that the viscosity was effectively reduced using high SS dosages during froth flotation	▪ This confirms that aggregates were effectively dispersed using high SS dosages during froth flotation

5.4. Enhancing concentrate grade using SS

The hypothesis relating to this section is stated below:

> Sodium metasilicate will depress talc because anionic SS species will adsorb onto talc. The depression of talc, especially when occurring in composite particles, will improve PGE concentrate grade.

Rougher batch flotation at the baseline condition resulted in a Pt grade of 10.6 g/t and a Pd grade of 5.5 g/t, which mimics the low grades expected without the intervention of a depressant (Figure 4.19 and Figure 4.20). Using 2000 g/t SS was found to improve the Pt and Pd grade by 7.5 g/t and 4.0 g/t, respectively, as illustrated in Figure 4.19 and Figure 4.20. The results of the feed bulk mineralogy and talc association characteristics revealed that there is a significant quantity of NFG which largely constitutes talc in association with orthopyroxene and serpentine, as shown in Table 4.1 and illustrated in Figure 4.9. This is likely to have largely contributed to the poor concentrate grades during froth flotation. Various investigators have linked high quantities of NFG to poor concentrate grades (Witney & Yan, 1997: 153; Wiese, Harris & Bradshaw, 2008: 480; Becker, Wiese & Ramonotsi, 2014: 27). In addition to the contribution of NFG to the dilution of concentrate grade, recovery of gangue by entrainment and their association to floatable valuable minerals can also dilute grade. This section aims to discuss the contributors to the dilution of concentrate grade and the effect of SS on grade. The hypothesis corresponds with the key question; "*How does the depressant effect of SS improve PGE grade, and how can this knowledge be utilized to provide an optimum PGE grade?*". To answer this, the findings of the QEMSCAN concentrate analysis, talc microflotation and froth stability experiments, which served to decouple SS's depressant effect, will be discussed and placed into the context of SS batch flotation experiments.

The concentrate QEMSCAN analysis demonstrated that using 2000 g/t SS resulted in less talc being recovered compared to 215 g/t SS which infers that SS adsorbed onto and depressed talc at high SS dosages, as demonstrated in Figure 4.36 and Figure 4.37. Talc is both liberated and unliberated in the feed, although, given the greater abundance of unliberated talc constituting 89.2%, the contribution of composite talc particles which diluted concentrate grade will be focused on for now (Table 4.2). The concentrate analysis indicated that using a high SS dosage could effectively lower the quantity of composite talc particles that reported to the concentrate, as a result of SS's depressant effect, as illustrated in Figure 4.38. The depression of talc did not affect the recovery of BMS, because the mass of orthopyroxene (which has a large association to talc) associated with BMS is the same in the 215 g/t and 2000 g/t SS first concentrates (Figure 4.39). This does, however, indicate that the recovery of BMS will result in the recovery of some orthopyroxene and other gangue, but this contribution to the dilution of concentrate grade is expected to be very minor compared to the recovery of talc-orthopyroxene composites. Lower talc floatability at high SS dosages during microflotation experiments confirms that SS

was increasingly able to adsorb onto and depress talc with increasing SS dosages, as demonstrated in Figure 4.42. Without SS, 69.6% of talc was recovered which was effectively reduced to 52.6% at the equivalent 2000 g/t SS dosage. The depressant effect of SS is not due to a pH effect as both this work, and many other researchers, have demonstrated that talc recoveries are high in the absence of depressants at all pH (Shortridge et al., 2000: 223; Beattie et al., 2006a: 245, b: 601; Feng et al., 2012: 70). This indicates that anionic SS species were responsible for the depression of talc.

It is expected that $Si(OH)_4$ species adsorbed directly onto the basal planes of talc below pH 10, through ligand exchange where electron pairs are shared between SS and the talc surface, as this specie is known to prevail in this pH range (Yang, Roonasi & Holmgren, 2008: 43; Silva et al., 2012: 210). This was similarly suggested for quartz which has a similar structure to the silicate tetrahedral sheet of talc, and similar zeta potentials (Martinovic, Bradshaw & Harris, 2005: 152). However, this adsorption mechanism is expected to be significantly reduced or absent above pH 10 due to the strong electrostatic repulsion between talc and the $SiO_2(OH)_2^{2-}$ and $SiO(OH)_3^-$ species which are known to prevail in this pH region (Yang, Roonasi & Holmgren, 2008: 43). This agrees with studies which observed the adsorption of $Si(OH)_4$ species below pH 10, and no SS adsorption directly onto the mineral surface above pH 10 (Furlong, Sing & Parfitt, 1979: 415; Phair, Van Deventer & Smith, 2001: 151). The adsorption of SS onto talc at high pH's is therefore expected to occur through another mechanism, and not the adsorption of SS directly onto talc's surface.

It is suggested that the adsorption of bridging cations will play a significant role in the adsorption of SS onto talc at high pH's, on the basis that it hydrates the surface of talc. Bridging cations are known to improve the adsorption of CMC and guar gum onto talc and have previously been found to enhance the adsorption of SS onto minerals such as zirconia (Phair, Van Deventer & Smith, 2001: 154). Bridging divalent and trivalent cations, including Zn^{2+}, Al^{3+}, $Mg^{2+,}$ and Ca^{2+}, have also enhanced quartz depression at high pH's due to the activation of the cations (Tohry & Dehghani, 2016: 31).

During talc microflotation experiments, divalent cations were sourced from the dissolution of Mg^{2+} from the edge planes of talc. This mechanism is supported by Bremmell and Addai-Mensah (2005: 388) and Liu et al. (2019: 26) who demonstrated that Mg^{2+} ions dissolved from talc edge planes with reducing pH. The authors Bremmell and Addai-Mensah (2005: 388) and Liu et al. (2015: 43, 2019:26) further demonstrated that the dissolution of Mg^{2+} ions below pH 10 adsorbed onto the basal planes of talc as hydrolyzed $Mg(OH)_2$ species above pH 10. This indicates that during talc microflotation, Mg^{2+} ions at the natural talc solution pH of 8.6 dissolved Mg^{2+} ions into solution from the edge places of talc, and when the pH was increased with SS addition, the bridging $Mg(OH)_2$ species facilitated the adsorption of colloidal SS species onto the basal and edge planes of talc. A shift of talc's zeta potential to more positive values allowed better adsorption of $SiO(OH)_3^-$ onto talc. Approximately 50% of the talc was still recovered and it is hypothesized that better depression could be achieved during experiments containing synthetic plant

water where there is an abundance of divalent cationic species present to act as bridging ligands. The microflotation experiments were not performed in synthetic plant water, but distilled water to better understand the SS adsorption mechanism. Better talc depression could also be achieved by firstly adjusting the pH to an acidic pH, which would allow greater dissolution of Mg^{2+} species, before raising the pH to alkaline pH's, which would allow greater adsorption of $Mg(OH)_2$ onto the basal plane of talc. This indicates that during microflotation experiments, small amounts of SS species were able to adsorb onto talc which was possibly due to a low surface coverage of $Mg(OH)_2$.

The dissolution of Na^+ into solution when SS is added is not expected to play a major role in talc's depression at high pH's. This is because previous studies associated monovalent cations such as Na^+ and K^+ with inducing less positive zeta potentials, lower concentration of depressant adsorption and higher talc recoveries compared to divalent cations (Parolis, Groenmeyer & Harris, 2005: 13; Parolis et al., 2008: 111; Manono, Corin & Wiese, 2019: 220, 2020: 5). Moreover, because the depressant effect of SS is poor at high pH's only further supports that Na^+ ions dissolved into solution do not play a significant role in enhancing the adsorption of SS. The Na^+ ion is also expected not to have a sufficient charge suppression to overcome the repulsion between SS and the negative charge of talc, as similarly observed with quartz at a high pH (Silva et al., 2012: 209). The Na^+ ions can also not form hydrolyzed species as observed for $CaOH^+$ and $Mg(OH)^+$ and, therefore, are not expected to adsorb onto and hydrate the surface of talc at high pH's.

In terms of investigating SS on another PGE ore, batch flotation experiments using high SS dosages were also investigated using Ore 2, as illustrated in Figure 4.53. Lower Pt and Pd concentrate grades compared to Ore 1 during baseline experiments (10.64 g/t and 5.45 g/t for Pt and Pd in Ore 1, respectively, and 3.50 g/t and 2.65 g/t for Pt and Pd in Ore 2, respectively) are as a result of a lower feed grade and larger quantity of talc in Ore 2 compared to Ore 1. However, considering the upgrade ratios between the ores at 2000 g/t SS, Ore 2 obtained higher Pt and Pd upgrade ratios compared to Ore 1 (14.98 and 21.97 for Pt and Pd in Ore 1, respectively, vs. 19.17 and 27.80 for Pt and Pd in Ore 2, respectively). This indicates that SS can depress talc in Ore 2 as well, and that this upgrade is better compared to Ore 1, although higher final grades were obtained using Ore 1 compared to Ore 2.

5.4.1. Gangue recovery by entrainment

Sodium metasilicate has been observed to depress NFG by adsorbing onto talc though a bridging cation mechanism at high dosages. However, it is well-known that gangue recovered by entrainment can also decrease concentrate grades. The PSD of the feed indicates that nearly 50% of particles are below 50 μm in size, and therefore vulnerable to be recovered by entrainment (Figure 4.2). To understand the influence of SS on entrainment, the quantities of liberated serpentine and orthopyroxene below 50 μm in size within the 215 g/t and 2000 g/t SS first concentrate samples were analyzed and the results presented in Figure 4.40. Using a high SS dosage was observed to lower the recovery of entrained minerals, as indicated by a

reduction in liberated serpentine and orthopyroxene masses by 0.8 g and 2.5 g, respectively, at 2000 g/t SS. This indicates that lower quantities of entrained minerals were recovered into the 2000 g/t SS concentrate compared to the 215 g/t SS concentrate. Three-phase froth stability results revealed that high SS dosages significantly lowered the froth stability, as illustrated in Figure 4.28. This suggests that aggregated particles in the froth would have hindered drainage and the dispersion of these aggregates with added SS in the system would have improved the froth drainage. This agrees with a lower quantity of recovered solids observed at 2000 g/t SS compared to 215 g/t SS, as observed by the results presented in Figure 4.18.

The recovery of lower amounts of talc due to the depressant effect of SS is postulated to have also contributed to the destabilization of the froth, although this influence was minor compared to the dispersion of aggregates in the froth. Other researchers have also found NFG able to stabilize the froth which was destabilized with the addition of depressants such as CMC and guar gum (Wiese, Harris & Bradshaw, 2010: 1013). It is inferred that at 2000 g/t SS, lower bubble loading of NFG had ruptured and thinned liquid films which resulted in the coalescence of bubbles. This agrees with studies which demonstrated that lower mineral concentrations in the froth destabilized the froth (Tao, Luttrell & Yoon, 2000: 35). Table 5.6 summarizes relative observations between the talc recovery during microflotation, froth stability, mass of recovered solids during batch flotation as well as the PGE concentrate grades during batch flotation experiments for the 215 g/t and 2000 g/t SS conditions.

Table 5.6: Mechanisms leading to relatively low and high concentrate grades between 215 g/t and 2000 g/t SS experiments.

SS dosage (g/t)	Talc recovery	Froth stability	Recovered solids	Grade
215	High	High	High	Low
2000	Low	Low	Low	High

5.4.2. Effect of pH on grade

The Pt and Pd grades were lowest at the modified pH 11.7 flotation experiment without SS addition, as demonstrated in Figure 4.22. This is due to high quantities of solids and water recovered at the pH modified test, which agrees with the observed high froth stability at the pH 11.7 froth stability experiment (Figure 4.23 and Figure 4.29). A similar observation was recorded by Sheni, Corin and Wiese (2018: 17) who summarized that an increasing pH corresponded with increasing solids recovered, water recovered, and froth stability. A high froth stability at the pH modified experiment shows that the observed lower froth stabilities at 2000 g/t SS discussed earlier was not due to a pH effect. The high froth stability is presumed to be primarily due to the froth stabilizing effect of talc because the recovery of talc at pH 11.7 was found to be exceptionally high (91.1%) as determined by microflotation experiments in this and other

work (Appendix B; Feng et al., 2012: 70). High talc recoveries during froth flotation greatly stabilized the froth with the resulting recovery of high quantities of solids and water. Modifying the pulp pH to 11.7 was found to be very beneficial for PGE recoveries (Section 4.2.2) due to both slime cleaning of PGMs and due to high quantities of recovered solids, however, this is detrimental to grade. A modification in pH to obtain high recoveries at the expense of grade seems an unlikely practice at plant scale, as costly amounts of alkaline pH modifiers will be necessary to adjust the pH.

In summary, the main concentrate diluting minerals are orthopyroxene, serpentine, and talc. These minerals are mainly recovered by i) the association of orthopyroxene and serpentine to talc (NFG), and ii) entrainment. In answer to the key question; *"How does the depressant effect of SS improve PGE grade, and how can this knowledge be utilized to provide an optimum PGE grade?",* it can be concluded that using SS at relatively high dosages depressed talc by the adsorption of the $SiO(OH)_3^-$ SS species onto bridging $Mg(OH)_2$ species on the basal planes of talc. The depression of talc reduced the floatability of both liberated and unliberated talc. Entrained gangue is also reduced through improved drainage of the froth due to the dispersing nature of the SS. In addition, less talc recovered to the froth results in a less stable froth, which also minimized the recovery of entrained minerals. Therefore, an improved PGE grade can be achieved by dosing the ore with relatively high concentrations of SS due to the combined effects of depression of NFG and reduced entrainment.

5.5. Evaluating the performance of SS against other methods

Brief comparisons were done to evaluate other methods capable of mitigating some of the problems known to be associated with altered ores, and importantly to assess SS against these methods. Ultrasonication for 15 and 20 minutes of preconditioning bath time was found to successfully enhance Pt and Pd recoveries using Ore 1, as illustrated in Figure 4.47. This is due to the dislodging of serpentine slimes from PGM and BMS surfaces, resulting from the force of microjets of fluid at slime coated surfaces. The removal of slimes using ultrasonication also improved BMS recovery in other work (Celik, 1989: 1163; Aldrich & Feng, 1999: 703; Misra, Raichur & Lan, 2003: 95; Videla et al., 2016: 91). This is because cleaner surfaces allowed better adsorption of the collector. The adsorption of the collector immediately after the slime was dislodged is thought to prevent the re-attachment of the slime on the mineral surface. In addition, the presence of microbubbles on hydrophobic surfaces due to ultrasonication could also have benefitted recoveries when the ore was batch floated after preconditioning. A slight grade enhancement at the high ultrasonication bath time might be due to the dislodgement of slimes from floatable minerals, which improved grade. Using the ultrasonication probe also resulted in high recoveries which suggest that the combination of a high intensity ultrasonication at a small surface area of sound streamlines, together with sufficient circulation of the slurry, can improve recoveries even at higher slurry volumes.

Ultrasonication is nearly as effective as using SS in terms of recovery enhancement, as demonstrated by the similar Pt recoveries, however, the Pd recovery, as well as the Pt and Pd grades using SS far exceeded that of using ultrasonication (Figure 4.48). This suggests that pentlandite may be more susceptible to slimes than discrete Pt-bearing PGMs, and that the improvement of Pd recovery was a function of the increased performance of pentlandite seeing as Pd often occurs in solid solution with pentlandite. This indicates that SS is likely better at slime removal than ultrasonication. However, it is important to note that SS addition far outperforms ultrasonication in improving the grade. Nonetheless, the ability of slime coating removal by a mechanical approach was seen in the experimental results and therefore it could be considered commercially to improve recovery. Hydrodynamic cavitation devices such as the Mach HCD reactor have already found application in the PGM mining industry (Ross, Singh & Pillay, 2019). This investigation found that the formation of nano- and microbubbles and the cleaning of particle surfaces led to the activation of valuable mineral surfaces and depressed gangue. At plant scale, this method can potentially remove slime coatings from PGMs and BMS by circulating the feed slurry through the device which imparts high shear and energy dissipation in the feed. The Mach reactor has impacted the rougher, cleaner and recleaner applications and is currently in operation at two UG2 chromitite Tailings Scavenger Plants in the BIC (Ross, Singh & Pillay, 2019: 138).

Using CMC was found to be ineffective at improving the flotation response of Ore 2, where only a 1.6 g/t Pt grade enhancement was observed, whereas no Pt and Pd recoveries, nor the Pd grade, was enhanced (Figure 4.50). This was unexpected since CMC is a well-known depressant, as observed in various investigations and since it carries a negative charge, was also expected to act as a dispersant (Parolis, Groenmeyer & Harris, 2005: 13; Wiese, Harris & Bradshaw, 2010: 1017; Manono, Corin & Wiese, 2019: 220). At the least, it was expected that grades would be enhanced with the addition of CMC, since it was found to be a stronger depressant than SS during microflotation experiments (Figure 4.42). It is possible that even higher CMC dosages than the highest dosage investigated could improve grade. However, this could occur at the expense of recovery, as increasing CMC dosages from 100 g/t to 300 g/t lowered the Pt and Pd recoveries. The chosen CMC dosages for this study closely follow accepted practice on many industrial operations. It is therefore clear that using SS was much better at enhancing the flotation performance compared to CMC (Figure 4.51), especially since using SS on Ore 2 significantly improved the flotation performance (Figure 4.53).

This work found that using SS can improve the flotation performance at high SS dosages by dispersing slimes, lowering the pulp rheological complexity and depressing NFG simultaneously. Therefore, both recovery and grade can be simultaneously enhanced. Sodium metasilicate is commercially available, is a relatively cheap reagent (CMC is approximately 6 times more expensive than SS) and can also be used as an affordable pH modifier, all with the added benefits of reducing water consumption to mitigate altered ore challenges. In addition, SS was found to significantly reduce MgO-bearing minerals including talc,

orthopyroxene and serpentine which will minimize the negative impacts of MgO content in downstream processes, most notably the impacts on the smelter capacity. On the point of smelter capacity, higher concentrate grades and the lower concentrate mass coupled with this will reduce transporting costs and energy consumption of smelter operations, which will inevitably lower the net carbon emissions of the process.

Sodium silicate is also a known deflocculant, which raises concern regarding how problematic this would be to downstream processes, such as the concentrate handling in the thickeners. The ability of flocculants to settle slurries containing high SS dosages (1000 g/t to 1500 g/t SS) were investigated by Magudu and Wali (2019) on the Ore 2 feed, where the proportions of serpentine are similar to that of Ore 1, as shown in Table 4.1. The study showed that the settling rate increased significantly when both anionic and non-ionic flocculants were used together with SS compared to experiments with SS alone, as illustrates in Figure 5.1. This confirmed that flocculants were able to aggregate dispersed slurries containing high SS dosages and suggest that downstream effects of SS on thickeners and filtering can be managed.

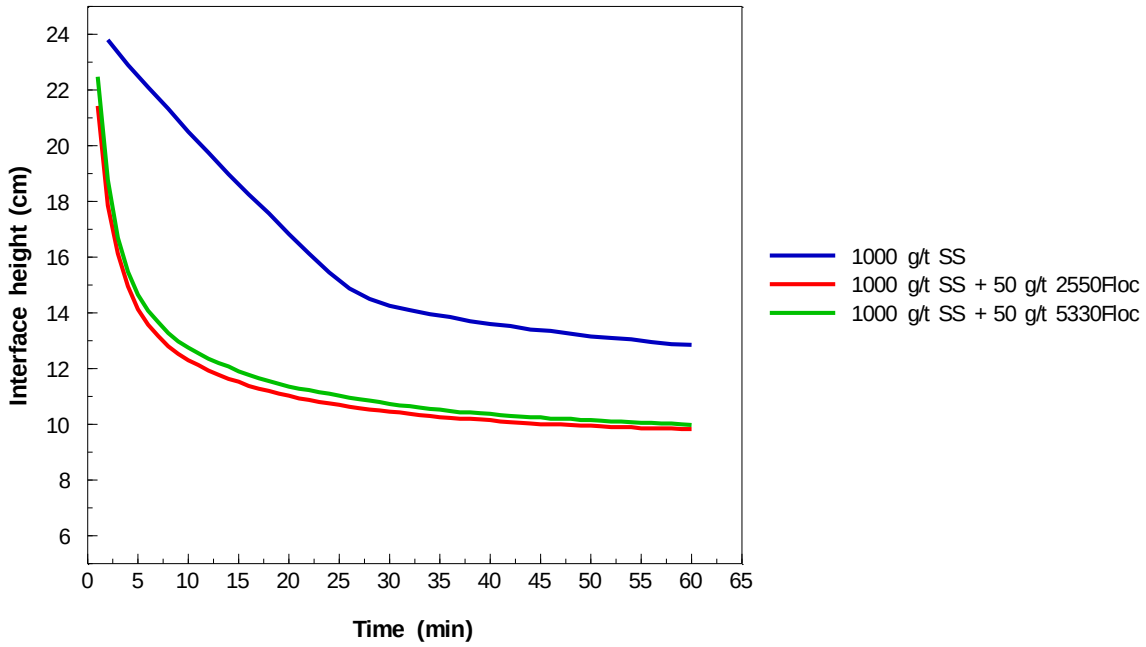

Figure 5.1: Effect of anionic (2550Floc) and non-ionic (5330Floc) flocculants on particle settling in pulps containing 1000 g/t SS compared to an experiment without flocculant (1000 g/t SS only), gathered from Magudu and Wali (2019).

Chapter 6: Conclusions

The primary objective of this work was to investigate SS in the context of enhancing both recovery and grade of an altered PGE ore. This was accomplished by studying SS's dispersant, rheology modifying and depressant effects individually to understand the conditions which will simultaneously enhance recovery and grade. This work showed that a single reagent, SS, can simultaneously overcome the three major problems of hydrothermal alteration: a) serpentine slimes on PGM and BMS surfaces can be removed by SS's dispersant effect, b) increased pulp viscosity caused by aggregation can be reduced by SS's rheology modifying effect, and c) talc can be depressed by SS's depressant effect, all at a recommended high SS dosage.

This chapter summarises the key findings of this work which includes conclusions on the mineralogy component of this work (Section 6.1), the effects of SS which summarize using SS to remove slime coatings from PGMs and BMS, reduce pulp viscosity, and to depress talc (Section 6.2), evaluating SS's performance (Section 6.3), implications of this work (Section 6.4), and recommendations for future work (Section 6.5).

6.1. Mineralogy

The major alteration minerals, serpentine and talc, which are the alteration minerals of interest in this work, were derived from the hydrothermal alteration of olivine and orthopyroxene. This is evident by mesh-textured serpentine, extensive serpentinization of orthopyroxene and by the alteration of orthopyroxene boundaries to talc. Although there is no scale to measure the degree of alteration, previous studies have subdivided the extensiveness of alteration of these types of rocks into three stages. Amongst coarse particles taken from the crushed rock stockpile before further jaw crushing, all three stages of alteration have been identified. Stage 1 alteration was recognized by the presence of mostly unaltered orthopyroxene which contained talc rimming and talc along fissures (mainly unaltered minerals), stage 2 alteration by olivine mesh cores and the presence of orthopyroxene (some relict minerals are still visible) and stage 3 by extensive alteration of olivine and orthopyroxene (relict minerals of the alteration products are not visible). A molar MgO/SiO_2 ratio of less than 1 indicates that the alteration mineral assemblage in the Silicate reef will contain serpentine and talc. The presence of these minerals and the absence of brucite in the feed confirms this.

Characterisation of the milled feed indicates that both ores consist largely of orthopyroxene and serpentine, and lesser quantities of olivine, magnetite, plagioclase, and talc. The abundance of alteration minerals can have serious consequences on PGE recovery and concentrate grade. Firstly, the presence of serpentine slimes can lead to slime coating of valuable minerals, which can reduce PGE recoveries because of the inability of the collector to adsorb onto the PGM and BMS surfaces. Secondly, serpentine-

orthopyroxene hetero-aggregates, as well as serpentine and talc homo-aggregates, can increase the pulp viscosity which can hinder fluid flow and gas dispersion and reduce recoveries. Lastly, the presence of talc can have serious PGE concentrate grade consequences. This is because talc is naturally floatable and any minerals, such as pyroxenes, associated with talc can also be rendered floatable through association. Talc can also increase bubble loading which can hinder PGM attachment, and its occurrence in the froth can increase froth stability which can increase the recovery of entrained gangue. This emphasized the need for a method to disperse slimes, reduce the pulp viscosity and depress talc to improve the PGE flotation performance.

The PGE analysis performed on Ore 1 revealed that PGE arsenides, PGE sulphides and PGE tellurides dominate in the feed. The main PGMs in these groups are sperrylite, cooperite and moncheite, respectively. It is known from literature that these PGMs are negatively charged at pH 9 and may be prone to slime coating by positively charged serpentine at this pH. A high Pt/Pd ratio in the ore feed is a strong indication that Pd has been remobilized. The PGE mobilization may have occurred via hydrothermal fluids and been distributed in solid solution of minerals such as BMS (mainly Pd), talc and amphibole, as observed in the Silicate reef in past studies. Considering the PGM characteristics in the feed, nearly half of PGM grains and PGM/BMS particles are liberated which are expected to recover well. However, there are PGMs which may be problematic to recover such as slow-floating sperrylite, very small grain size PGMs (<5 μm), and poorly liberated PGMs. This shows that in the scenario free of alteration mineral challenges, half of PGMs in the feed are expected to recover well, but it is anticipated that the presence of alteration minerals can significantly impact the recovery of these PGMs.

6.2. Sodium metasilicate effects

6.2.1. Using SS as a method of removing PGM and BMS slime coatings

Without SS addition, poor Pt and Pd recoveries were obtained for both ores investigated, due to the presence of serpentine slime coatings. High SS dosages, namely 1000 g/t and 2000 g/t, significantly improved the Pt and Pd recoveries. To decouple whether poor recoveries were due to slime coatings and mitigated by SS addition, this study conducted microflotation and zeta potential measurements using chalcopyrite as a PGM proxy. Microflotation experiments revealed that chalcopyrite's floatability was significantly compromised at pH 9 in the presence of serpentine slimes due to a strong electrostatic attraction which led to slime coating. This indicates that during baseline batch flotation, serpentine would have slime coated PGMs and BMS, which consequently significantly compromised the floatability of these minerals. Using 2000 g/t SS effectively restored the chalcopyrite floatability due to a strong electrostatic repulsion between serpentine and chalcopyrite which enhanced collector adsorption. This indicates that at high SS dosages during batch flotation, the prevailing $SiO(OH)_3^-$ species adsorbed onto serpentine and changed the surface charge of serpentine from positive to negative, which removed slime coatings from PGMs and BMS which enhanced recoveries.

It is well-known that pH plays an important role during froth flotation, and since SS is a pH modifier, it was important to decouple whether the pH effect improved PGE recoveries or whether this was due to the adsorption of SS species onto serpentine slimes. Batch flotation at a modified pH 11.7 experiment, without SS addition, resulted in high Pt and Pd recoveries. A high chalcopyrite recovery was also observed during the 1:2 chalcopyrite to serpentine microflotation experiments at pH 11.7. This is thought to be due to the removal of serpentine slimes from PGMs and BMS, as the zeta potential of serpentine at pH 11.7 without SS was in fact negative. This suggests that flotation at a critical pH above the i.e.p can remove slime coatings from PGMs and BMS and improve PGE recoveries due to an electrostatic repulsion between PGMs/BMS and serpentine slimes. Although operating at a high pH alone can improve recoveries, a more negative serpentine zeta potential at 2000 g/t SS (pH 11.7), indicates that the adsorption of SS species onto serpentine played a critical role in lowering the zeta potential of serpentine which led to improved recoveries.

The statement of hypothesis one was proved to be correct, as high SS dosages behaved as a dispersant and removed serpentine slimes from PGMs and BMS. This occurred by the adsorption of SS species onto serpentine slimes, which changed the surface charge of serpentine from positive to negative. Sodium metasilicate induced an electrostatic repulsion between serpentine slimes and PGMs/BMS, which allowed better collector adsorption onto the PGMs and BMS. This significantly improved PGE recoveries.

6.2.2. Using SS to combat pulp rheological challenges

Poor Pt and Pd recoveries are also due to rheological challenges because of particle aggregation and fines in the pulp. Aggregates in the pulp arose by inter-particle interactions between lizardite and predominantly orthopyroxene (hetero-aggregates) due to electrostatic attractive forces, and inter-particle interactions between lizardite particles, and also between talc particles (homo-aggregates). In terms of lizardite homo-aggregation, it is likely that lizardite faces are weakly positive due to the similarities in the expected p.z.c and the i.e.p value of lizardite determined in this work, which may also be near neutral. Therefore, EE configuration is expected to dominate above EF configurations. In terms of talc, there is a clear discrepancy between the p.z.c and i.e.p values, as determined in previous work, which indicates that the faces would be strongly negative, and the edges would be oppositely charged due to the similarities in the p.z.c and the pH of interest (pH 9). Therefore, EF configurations are expected to dominate above EE configurations for talc. The presence of aggregates was confirmed by a faster declination of interfacial height and settling velocities during particle settling measurements. The presence of 35 wt.% solids and a higher apparent viscosity compared to that of water conditions indicates that the pulp at the baseline condition was rheologically complex. Past studies indicate that this would lead to the formation of a

cavern around the impeller which is known to be associated with poor gas dispersion, bubble-particle collisions, and recoveries.

The study decoupled the rheology modifying effect of SS by solids concentration, particle settling and rheology experiments. A low solids concentration performed on Ore 1 greatly benefitted recoveries due to the expansion of the turbulent zone which improved gas dispersion and bubble-particle collisions. Particle interaction and friction between aggregates were also lower. This indicated that lowering the apparent viscosity of the ore will improve PGE recoveries. Therefore, during batch flotation experiments in the presence of high SS dosages, a reduction in the rheological complexity due to SS's rheology modifying effect improved recoveries. The solids concentration measurements further demonstrated that batch flotation at the baseline conditions corresponded with rheological challenges which reduced recoveries. A low solids concentration also improved grade due to a lower degree of entrainment and better froth drainage. Overall, using a high SS dosage improved the flotation performance better compared to a low solids concentration. The use of SS over operating at low solids concentrations would benefit flotation operations aiming to maximize tonnages and throughput.

The reduced rheological complexity of the pulp at high SS dosages is thought to be due to the following SS abilities: i) to adsorb onto the surfaces of serpentine and talc which induced the same charge on edge and face planes of the phyllosilicates thereby dispersing the homo-aggregates, ii) to change the zeta potential of serpentine from positive to negative which dispersed serpentine-orthopyroxene hetero-aggregates, and iii) to lower the rheological contribution of fines. The dispersal of aggregates is confirmed by a slower declination of interfacial height, slower settling velocities and many fine particles present in the supernatant at high SS dosages. Rheology measurements at high SS dosages indicate that the shear stress, yield stress and apparent viscosity at the solids concentration used during batch flotation were much lower than those in the absence of SS. In addition, a high SS dosage also lowered the rheological complexity of the same ore containing a higher number of fine particles, which indicates that SS combated the negative rheological impacts of fine particles. This suggests that during secondary grinds at the plant, the ore will experience much more viscous effects and that SS will have an even greater benefit. This also indicates that during batch flotation at high SS dosages, the turbulent zone expanded, as the yield stress decreased. This improved gas dispersion, bubble-particle collision and attachment, particle bubble mobility and improved gas hold-up.

The statement of hypothesis two was proved to be correct. Firstly, SS adsorbed onto serpentine and talc which induced the same charges on edge and face planes of the phyllosilicates and dispersed the homo-aggregates. Secondly, SS reversed the surface charge of serpentine which dispersed serpentine-orthopyroxene aggregates. Thirdly, SS also created a strong electrostatic repulsion in the pulp, due to the interactions mentioned in the first two points, which minimized particle-particle interactions and rheological challenges brought about by fines in the pulp. All three factors contributed to a lower rheological complexity of the pulp as noted by a low shear stress, yield stress and apparent viscosity. Fluid flow and gas dispersion was improved due to the expansion of the turbulent zone, and all accompanied benefits contributed to improved Pt and Pd recoveries.

6.2.3. Effect of SS on concentrate grade

Without a suitable depressant, the Pt and Pd concentrate grades were 10.6 g/t and 5.5 g/t., respectively. The low Pt and Pd concentrate grades emphasized the need for a suitable depressant especially considering that the feed contained a significant quantity of talc. Using a high SS dosage improved the Pt and Pd concentrate grades by 7.5 g/t and 4.0 g/t, respectively. Concentrate mineralogy and microflotation experiments were undertaken to understand the poor recoveries without depressant, and the increased recoveries using a high SS dosage. The presence of composite talc-orthopyroxene particles is thought to have significantly contributed to low PGE concentrate grades during froth flotation. This was mitigated by using a high SS dosage which depressed both liberated and unliberated talc compared to using a low SS dosage. Microflotation experiments confirmed that SS adsorbed onto and depressed talc although the adsorption mechanism is postulated to differ depending on the solution pH. Below pH 10, $Si(OH)_4$ species adsorbed onto the basal plane of talc, which is suggested to be through ligand exchange, as this species is known to prevail in this pH range. Above pH 10, the mechanism of talc adsorption is postulated to be different due to the strong electrostatic repulsion between talc and the $SiO(OH)_3^-$ at alkaline pH's.

Bridging divalent cations are thought to play a major role in the adsorption of SS species onto talc at high pH's. During microflotation, divalent cations were sourced from the dissolution of Mg^{2+} from the edge planes of talc when the pH was raised from natural to moderately alkaline once SS was added into solution and adsorbed onto talc as $Mg(OH)_2$ species. This allowed the adsorption of SS onto talc by a bridging cation mechanism as the zeta potential of talc was lowered to less negative values. It is suggested that the abundance of divalent cations species present in the pulp during froth flotation can act as bridging ligands and improve talc depression. A pH adjustment by firstly lowering the pH to acidic values, to facilitate the dissolution of Mg^{2+}, before raising the pH to alkaline can also improve the adsorption of SS.

Adding SS also introduced Na^+ ions into solution which is thought to have a minor role in the depressant ability of talc. This is because monovalent cations were observed to have little effect on the zeta potential

of talc, allow only minor adsorption of depressants and have been correlated with higher talc recoveries, compared to divalent cations in previous work. Using a high SS dosage therefore induced the most favourable pH and concentration for the dissolution and adsorption of cations which allowed talc to become depressed which in turn improved concentrate grade.

The impact of SS on gangue recovery by entrainment was also considered because approximately 50% of particles in the feed were in the size range vulnerable to entrainment. A high SS dosage could effectively lower the recovery of serpentine and orthopyroxene, the major gangue constituents. This was indicated by lower amounts of serpentine and orthopyroxene in the first concentrate sample from batch flotation tests at 215 g/t and 2000 g/t SS. Three-phase froth stability tests highlighted a decrease in froth stability with increasing SS dosage. This suggests that the dispersal of aggregates in the froth improved froth drainage. This also corresponds with lower quantities of recovered solids and higher Pt and Pd grades. Another contribution to a reduced froth stability is due to the destabilization of the froth as lower amounts of talc reported to the concentrate at a high SS dosage.

The statement of hypothesis three was proved to be correct. Using 2000 g/t SS depressed talc by the adsorption of $SiO(OH)_3^-$ species onto bridging $Mg(OH)_2$ species on the basal planes of talc. This significantly lowered the quantities of both liberated and unliberated talc. In addition, the dispersant effect of SS is postulated to have dispersed aggregates in the froth which improved drainage, and lower recoveries of talc would also have destabilized the froth. Therefore, PGE grades could be improved using SS.

6.3. Evaluating SS's performance

This study evaluated SS's performance against other well-known methods of mitigating ore alteration issues: ultrasonication and CMC. Ultrasonicating the pulp in an ultrasonication bath, or using an overhead probe, as a preconditioning step for a duration of 20 and 15 minutes, respectively, significantly improved the Pt and Pd recoveries. Ultrasonication was found to enhance recoveries to similar values compared to using SS which indicates that using Mach HCD reactor devices in industry can greatly benefit PGE recoveries. However, SS was better at improving concentrate grades compared to ultrasonication which demonstrates that SS is a superior option.

The CMC depressant did not improve the recoveries, and only resulted in a minor improvement in Pt grade at the dosages investigated. Poor grade improvements using CMC were unexpected because talc microflotation experiments indicated that CMC was a superior talc depressant compared to SS. It is possible that higher CMC dosages would have improved concentrate grades, but recoveries are not expected to be enhanced at higher dosages. The dosages investigated were similar to what is generally used

on a rougher bank at plant scale. Overall, using SS revealed to be better at enhancing the flotation performance of the ores investigated compared to using CMC. Using 2000 g/t SS was found to enhance grade better than using either ultrasonication or CMC.

6.4. Implications of this work

Processing low grade altered PGE ores in Southern Africa is a problem that is causing mines to leave ores *in situ*, to process them at the expense of significant PGE losses, to blend altered ores with less altered ores for processing, or to stockpile them until a new metallurgical process is in place to improve beneficiation. Therefore, alternative methods of processing such ores are continuously being investigated. Many near-surface PGE ores have undergone alteration, which produced large quantities of alteration minerals, making the processing of these ores complicated. Three major alteration mineral challenges can simultaneously occur during flotation. Firstly, the presence of serpentine can slime coat PGMs and BMS which makes PGE recoveries difficult to obtain. Secondly, serpentine, talc and orthopyroxene can cause rheological challenges due to aggregation, which can also greatly compromise PGE recoveries. Lastly, the natural floatability of talc can reduce concentrate grade.

This study showed that a single reagent, SS, can be used to mitigate all three of these major challenges simultaneously. Sodium metasilicate improved PGE recoveries by removing slime coatings from the surfaces of PGMs and BMS, reduced the rheological complexity by altering the surface charges of serpentine and talc, and by depressing talc. This is due to SS's dispersant, rheology modifying and depressant effects which can be effective simultaneously, given that the pH and SS concentration are favourable. High SS dosages, >1000 g/t, simultaneously enhanced recoveries and grades due to the three above mentioned effects. It also shifted the recovery-grade curve into a zone of significantly improved performance. It is expected that the processing of these altered ores and the subsequent process challenges can be mitigated by the use of SS as it improved both recovery and grade. Low SS dosages were found to be ineffective mainly due to the lack of certain SS species and a relatively lower slurry pH.

Sodium metasilicate is a relatively cheap reagent (CMC is approximately 6 times more expensive than SS), can be used as a dispersant, rheology modifier, depressant (or simultaneously), and pH modifier. The dispersed slurry containing high SS dosages can be aggregated using flocculants.

6.5. Recommendations for future work

Although this study makes a significant contribution to the body of knowledge, it also raises further questions for future research. The following are recommendations for future work:

1) ***Exploring SS on other PGE ores***

   Sodium metasilicate's dispersant, rheology modifying, and depressant effects should be explored on other altered UG2 chromitite, Platreef, Merensky reef and Great Dyke ores to determine

whether high SS dosages can also benefit other PGE ore types. This is not limited to PGE ores only, but other ores consisting of alteration minerals.

2) ***Adding divalent and monovalent cations to understand the bridging adsorption mechanism of SS onto talc***

Past literature highlighted that using divalent cations can greatly improve the depressant effect of CMC compared to monovalent cations (Parolis, Groenmeyer & Harris, 2005: 13; Manono, Corin & Wiese, 2019: 220, 2020: 5). Firstly, adsorption studies can be conducted to determine the extent of SS adsorption on talc in the presence of divalent and monovalent cations. Secondly, talc microflotation experiments in the presence of SS can be explored with the addition of various divalent and monovalent cations. Thirdly, particle settling experiments of talc in the presence of SS and various divalent and monovalent cations can be explored. Lastly, bridging cations using SS can also be explored in the context of changing water quality. This will provide a better understanding of the adsorption of SS onto talc.

3) ***Various SS moduli***

Previous studies demonstrated that the SS modulus can govern the type of SS species in solution and the effect this will have on the response variables (Rao et al., 2011: 522; Zhang, Chen & Liu, 2017: 6). For example, increasing SS moduli decreased the shear yield stress of a fluorite-quartz mixture (Zhang, Chen & Liu, 2017: 9). Increasing SS moduli also had a negative effect on fluorite recovery. This suggests that different SS moduli can be explored to determine how this might impact the dispersant, rheology modifying and depressant effects of SS and also to compare costs, as different moduli would have cost implications.

4) ***Exploring pH's above the i.e.p to understand the critical pH needed to remove slime coatings from valuable minerals***

This work suggested that an electrostatic repulsion could occur between serpentine and PGMs/BMS above serpentine's i.e.p. It should be decoupled whether this includes all pH's above the i.e.p, or whether there is a critical pH at which dispersion will occur. Zeta potential experiments can also be explored using other PGM species to better understand the possibility of slime coatings on various other PGM species and the role of SS in mitigating these slimes.

5) ***The interaction between SS and other reagents (e.g. SS-CMC interactions)***

Using SS together with another reagent, such as CMC, might improve the flotation response. It would be interesting to determine how the reagents can complement the effects of the other.

Chapter 7: References

Adeyinka, O.B., Samiei, S., Xu, Z. & Masliyah, J.H. 2009. Effect of particle size on the rheology of Athabasca clay suspensions. *Canadian Journal of Chemical Engineering*. 87:422–434. DOI: 10.1002/cjce.20168.

Aktas, Z., Cilliers, J.J. & Banford, A.W. 2008. Dynamic froth stability: Particle size, airflow rate and conditioning time effects. *International Journal of Mineral Processing*. 87:65–71. DOI: 10.1016/j.minpro.2008.02.001.

Al-Thyabat, S. 2009. Empirical evaluation of the role of sodium silicate on the separation of silica from Jordanian siliceous phosphate. *Separation and Purification Technology*. 67:289–294. DOI: 10.1016/j.seppur.2009.03.034.

Aldrich, C. & Feng, D. 1999. Effect of ultrasonic preconditioning of pulp on the flotation of sulphide ores. *Minerals Engineering*. 12:701–707. DOI: 10.1016/S0892-6875(99)00053-9.

Alvarez-Silva, M., Mirnezami, M., Uribe-Salas, A. & Finch, J.A. 2010. Point of Zero Charge , Isoelectric Point and Aggregation of Phyllosilicate Minerals. *Canadian Metallurgical Quarterly*. 49:405–410. DOI: 10.1179/cmq.2010.49.4.405.

Alvarez-Silva, M., Uribe-salas, A., Mirnezami, M. & Finch, J.A. 2010. The point of zero charge of phyllosilicate minerals using the Mular – Roberts titration technique. *Minerals Engineering*. 23:383–389. DOI: 10.1016/j.mineng.2009.11.013.

Alvarez-Silva, M., Uribe-Salas, A., Waters, K.E. & Finch, J.A. 2016. Zeta potential study of pentlandite in the presence of serpentine and dissolved mineral species. *Minerals Engineering*. 85:66–71. DOI: 10.1016/j.mineng.2015.10.018.

Amorós, J.L., Beltrán, V., Sanz, V. & Jarque, J.C. 2010. Electrokinetic and rheological properties of highly concentrated kaolin dispersions: Influence of particle volume fraction and dispersant concentration. *Applied Clay Science*. 49:33–43. DOI: 10.1016/j.clay.2010.03.020.

Andreola, F., Romagnoli, M., Castellini, E., Lusvardi, G. & Menabue, L. 2006. Role of the surface treatment in the deflocculation of kaolinite. *Journal of the American Ceramic Society*. 89:1107–1109. DOI: 10.1111/j.1551-2916.2005.00814.x.

Arantes, R.S. & Lima, R.M.F. 2013. Influence of sodium silicate modulus on iron ore flotation with sodium oleate. *International Journal of Mineral Processing*. 125:157–160. DOI: 10.1016/j.minpro.2013.09.002.

Arnold, B.J. & Aplan, F.F. 1986a. The effect of clay slimes on coal flotation, part I: The nature of the clay. *International Journal of Mineral Processing*. 17:225–242. DOI: 10.1016/0301-7516(86)90058-X.

Arnold, B.J. & Aplan, F.F. 1986b. The effect of clay slimes on coal flotation, part II: The role of water

quality. *International Journal of Mineral Processing*. 17:243–260. DOI: 10.1016/0301-7516(86)90059-1.

Ata, S., Ahmed, N. & Jameson, G.J. 2003. A study of bubble coalescence in flotation froths. *International Journal of Mineral Processing*. 72:255–266. DOI: 10.1016/S0301-7516(03)00103-0.

Ata, S., Ahmed, N. & Jameson, G.J. 2004. The effect of hydrophobicity on the drainage of gangue minerals in flotation froths. *Minerals Engineering*. 17:897–901. DOI: 10.1016/j.mineng.2004.04.005.

Auzende, A.L., Pellenq, R.J.M., Devouard, B., Baronnet, A. & Grauby, O. 2006. Atomistic calculations of structural and elastic properties of serpentine minerals: the case of lizardite. *Physics and Chemistry of Minerals*. 33:266–275. DOI: 10.1007/s00269-006-0078-x.

Bach, W., Garrido, C.J., Paulick, H., Harvey, J. & Rosner, M. 2004. Seawater-peridotite interactions: First insights from ODP Leg 209, MAR 15°N. *Geochemistry, Geophysics, Geosystems*. 5:1–22. DOI: 10.1029/2004GC000744.

Bahrami, A., Ghorbani, Y., Hosseini, M.R., Kazemi, F., Abdollahi, M. & Danesh, A. 2019. Combined effect of operating parameters on separation efficiency and kinetics of copper flotation. *Mining Engineering*. 71:43–45. DOI: 10.1007/s42461-018-0005-y.

Bai, L., Liu, J., Han, Y., Jiang, K. & Zhao, W. 2018. Effects of xanthate on flotation kinetics of chalcopyrite and talc. *Minerals*. 8:1–14. DOI: 10.3390/min8090369.

Bakker, C.W., Meyer, C.J. & Deglon, D.A. 2009. Numerical modelling of non-Newtonian slurry in a mechanical flotation cell. *Minerals Engineering*. 22:944–950. DOI: 10.1016/j.mineng.2009.03.016.

Bakker, C.W., Meyer, C.J. & Deglon, D.A. 2010. The development of a cavern model for mechanical flotation cells. *Minerals Engineering*. 23:968–972. DOI: 10.1016/j.mineng.2010.03.016.

Bandini, P., Prestidge, C.A. & Ralston, J. 2001. Colloidal iron oxide slime coatings and galena particle flotation. *Minerals Engineering*. 14:487–497. DOI: 10.1016/S0892-6875(01)00036-X.

Barbian, N., Ventura-Medina, E. & Cilliers, J.J. 2003. Dynamic froth stability in froth flotation. *Minerals Engineering*. 16:1111–1116. DOI: 10.1016/j.mineng.2003.06.010.

Beattie, D.A., Huynh, L., Kaggwa, G.B. & Ralston, J. 2006a. Influence of adsorbed polysaccharides and polyacrylamides on talc flotation. *International Journal of Mineral Processing*. 78:238–249. DOI: 10.1016/j.minpro.2005.11.001.

Beattie, D.A., Huynh, L., Kaggwa, G.B.N. & Ralston, J. 2006b. The effect of polysaccharides and polyacrylamides on the depression of talc and the flotation of sulphide minerals. *Minerals Engineering*. 19:598–608. DOI: 10.1016/j.mineng.2005.09.011.

Becker, M., Harris, P.J., Wiese, J.G. & Bradshaw, D.J. 2009. Mineralogical characterisation of naturally floatable gangue in Merensky Reef ore flotation. *International Journal of Mineral Processing*. 93:246–255. DOI:

10.1016/j.minpro.2009.10.004.

Becker, M., Ramonotsi, M. & Petersen, J. 2012. Effect of alteration on the mineralogy and flotation performance of PPM platinum ore. In *Proceedings of the 10th International Congress for Applied Mineralogy (ICAM)*. 1–8. DOI: 10.1007/978-3-642-27682-8.

Becker, M., Yorath, G., Ndlovu, B., Harris, M., Deglon, D. & Franzidis, J.P. 2013. A rheological investigation of the behaviour of two Southern African platinum ores. *Minerals Engineering*. 49:92–97. DOI: 10.1016/j.mineng.2013.05.007.

Becker, M., Wiese, J. & Ramonotsi, M. 2014. Investigation into the mineralogy and flotation performance of oxidised PGM ore. *Minerals Engineering*. 65:24–32. DOI: 10.1016/j.mineng.2014.04.009.

Behnsen, J. & Faulkner, D.R. 2012. The effect of mineralogy and effective normal stress on frictional strength of sheet silicates. *Journal of Structural Geology*. 42:49–61. DOI: 10.1016/j.jsg.2012.06.015.

Benco, L. & Smrcok, L. 1998. Hartree-Fock study of pressure-induced strengthening of hydrogen bonding in lizardite-lT. *Europena Journal of Mineralogy*. 10:483–490.

Bhunia, K., Kundu, G. & Mukherjee, D. 2017. Gas holdup characteristics in a flotation column with different solids. *Separation Science and Technology (Philadelphia)*. 52:1298–1309. DOI: 10.1080/01496395.2017.1287196.

Bikerman, J.J. 1965. Foams and emulsions. *Industrial and Engineering Chemistry Research*. 57:56–62.

Bo, F., Xianping, L., Jinqing, W. & Pengcheng, W. 2015. The flotation separation of scheelite from calcite using acidified sodium silicate as depressant. *Minerals Engineering*. 80:45–49. DOI: 10.1016/j.mineng.2015.06.017.

Bogusz, E., Brienne, S.R., Butler, I., Rao, S.R. & Finch, J.A. 1997. Technical note metal ions and dextrin adsorption on pyrite. *Minerals Engineering*. 10:441–445.

Boudreau, A.E. & Meurer, W.P. 1999. Chromatographic separation of the platinum-group elements, gold, base metals and sulfur during degassing of a compacting and solidifying igneous crystal pile. *Contributions to Mineralogy and Petrology*. 134:174–185. DOI: 10.1007/s004100050477.

Bradshaw, D. 2014. The role of "process mineralogy" in improving the process performance of complex sulphide ores. In *IMPC 2014 - 27th International Mineral Processing Congress*. 1–24.

Bradshaw, D.J. & O'Connor, C.T. 1996. Measurement of the sub-process of bubble loading in flotation. *Minerals Engineering*. 9:443–448. DOI: 10.1016/0892-6875(96)00029-5.

Bremmell, K.E. & Addai-Mensah, J. 2005. Interfacial-chemistry mediated behavior of colloidal talc dispersions. *Journal of Colloid and Interface Science*. 283:385–391. DOI: 10.1016/j.jcis.2004.09.048.

Bremmell, K.E., Fornasiero, D. & Ralston, J. 2005. Pentlandite-lizardite interactions and implications for

their separation by flotation. *Colloids and Surfaces A: Physicochemical and Engineering Aspects*. 252:207–212. DOI: 10.1016/j.colsurfa.2004.10.100.

Bulatovic, S. 2003. Evaluation of alternative reagent schemes for the flotation of platinum group minerals from various ores. *Minerals Engineering*. 16:931–939. DOI: 10.1016/S0892-6875(03)00240-1.

Burdukova, E., Becker, M., Bradshaw, D.J. & Laskowski, J.S. 2007. Presence of negative charge on the basal planes of New York talc. *Journal of Colloid and Interface Science*. 315:337–342. DOI: 10.1016/j.jcis.2007.06.067.

Burdukova, E., Bradshaw, D.J. & Laskowski, J.S. 2007. Effect of CMC and pH on the Rheology of Suspensions of Isotropic and Anisotropic Minerals. *Canadian Metallurgical Quarterly*. 46:273–278. DOI: 10.1179/cmq.2007.46.3.273.

Burdukova, E., Becker, M., Ndlovu, B., Mokgethi, B. & Deglon, D. 2008. Relationship between slurry rheology and its mineralogical content. In *XXIV International Mineral Processing Congress*. 2169–2178.

Bushell, C. 2012. The PGM flotation predictor: Predicting PGM ore flotation performance using results from automated mineralogy systems. *Minerals Engineering*. 36:75–80. DOI: 10.1016/j.mineng.2012.02.016.

Campbell, I.H., Naldrett, A.J. & Barnes, S.J. 1983. A model for the origin of the Pt-rich sulfide horizons of the Bushveld and Stillwater Complexes. *J. Petrol.* 24:133–165.

Cao, J., Tian, X.D., Luo, Y.C., Hu, X.Q. & Xu, P.F. 2017. The effect of graphene oxide on the slime coatings of serpentine in the flotation of pentlandite. *Colloids and Surfaces A: Physicochemical and Engineering Aspects*. 522:621–627. DOI: 10.1016/j.colsurfa.2017.03.043.

Cawthorn, R.G. 1999. The platinum and palladium resources of the Bushveld Complex. *South African Journal of Science*. 95:481–489.

Cawthorn, R.G., Lee, C.A., Schouwstra, R.P. & Mellowship, P. 2002. Relationship between PGE and PGM in the bushveld complex. *Canadian Mineralogist*. 40:311–328. DOI: 10.2113/gscanmin.40.2.311.

Celik, M.S. 1989. Effect of Ultrasonic Treatment on the Floatability of Coal and Galena. *Separation Science and Technology*. 24:1159–1166. DOI: 10.1080/01496398908049894.

Chen, T., Zhao, Y. & Song, S. 2017. Electrophoretic mobility study for heterocoagulation of montmorillonite with fluorite in aqueous solutions. *Powder Technology*. 309:61–67. DOI: 10.1016/j.powtec.2016.12.086.

Chen, X., Hadde, E., Liu, S. & Peng, Y. 2017. The effect of amorphous silica on pulp rheology and copper flotation. *Minerals Engineering*. 113:41–46. DOI: 10.1016/j.mineng.2017.08.001.

Chen, X., Gu, G., Liu, D. & Zhu, R. 2019. The flotation separation of barite-calcite using sodium silicate as depressant in the presence of sodium dodecyl sulfate. *Physicochemical Problems of Mineral Processing*. 55:346–

355. DOI: 10.5277/ppmp18136.

Chen, Y., Truong, V.N.T., Bu, X. & Xie, G. 2020. A review of effects and applications of ultrasound in mineral flotation. *Ultrasonics Sonochemistry*. 60:1–12. DOI: 10.1016/j.ultsonch.2019.104739.

Chen, Z., Wang, Y., Luo, L., Peng, T. & Guo, F. 2021. Enhancing flotation separation of chalcopyrite and magnesium silicate minerals by surface synergism between PAAS and GA. *Scientific Reports*. 11:1–16. DOI: 10.1038/s41598-021-85984-y.

Chetty, D., Gryffenberg, L., Lekgetho, T.B. & Molebale, I.J. 2009. Automated SEM study of PGM distribution across a UG2 flotation concentrate bank: Implications for understanding PGM floatability. *Journal of the Southern African Institute of Mining and Metallurgy*. 109:587–593.

Choi, J., Seo, J., Kim, S.B. & Kim, W. 2020. Flotation behavior of malachite using hydrophobic talc nanoparticles as collectors. *Minerals*. 10:1–9. DOI: 10.3390/min10090756.

Collins, B., Napier-Munn, T.J. & Sciarone, M. 1974. Production, Properties, and Selection of Ferrosilicon Powders for Heavy-Medium Separation. *Journal of The South African Institute of Mining and Metallurgy*. 75:103–119.

Comley, B.A., Harris, P.J., Bradshaw, D.J. & Harris, M.C. 2002. Frother characterisation using dynamic surface tension measurements. *International Journal of Mineral Processing*. 64:81–100. DOI: 10.1016/S0301-7516(01)00065-5.

Corin, K.C. & Wiese, J.G. 2014. Investigating froth stability : A comparative study of ionic strength and frother dosage. *Minerals Engineering*. 66:130–134. DOI: 10.1016/j.mineng.2014.03.001.

Dare, S.A.S., Barnes, S.J. & Prichard, H.M. 2010. The distribution of platinum group elements (PGE) and other chalcophile elements among sulfides from the Creighton Ni-Cu-PGE sulfide deposit, Sudbury, Canada, and the origin of palladium in pentlandite. *Mineralium Deposita*. 45:765–793. DOI: 10.1007/s00126-010-0295-6.

Deglon, D.A. 2005. The effect of agitation on the flotation of platinum ores. *Minerals Engineering*. 18:839–844. DOI: 10.1016/j.mineng.2005.01.024.

Derjaguin, B. V. & Churaev, N. V. 1992. The current state of the theory of long-range surface forces. *Progress in Surface Science*. 40:272–285. DOI: 10.1016/0079-6816(92)90054-L.

Djendova, S. & Mehandjiski, V. 1992. Study of the effects of acoustic vibration conditioning of collector and frother on flotation of sulphide ores. *International Journal of Mineral Processing*. 34:205–217. DOI: 10.1016/0301-7516(92)90074-7.

Douillard, J.M., Zajac, J., Malandrini, H. & Clauss, F. 2002. Contact angle and film pressure: Study of a talc surface. *Journal of Colloid and Interface Science*. 255:341–351. DOI: 10.1006/jcis.2002.8611.

Dzingai, T.C. 2017. A Process Mineralogical Study on the effect of Alteration on the Flotation of Great Dyke Platinum Group Element (PGE) Ores. MSc Thesis. University of Cape Town.

Dzvinamurungu, T., Viljoen, K.S., Knoper, M.W. & Mulaba-Bafubiandi, A. 2013. Geometallurgical characterisation of Merensky Reef and UG2 at the Marikana Mine, Bushveld Complex, South Africa. *Minerals Engineering*. DOI: 10.1016/j.mineng.2013.04.010.

Edwards, C.R., Kipkie, W.B. & Agar, G.E. 1980. The effect of slime coatings of the serpentine minerals, chrysotile and lizardite, on pentlandite flotation. *International Journal of Mineral Processing*. 7:33–42. DOI: 10.1088/1751-8113/44/8/085201.

Eggleton, R.A. & Boland, J.N. 1982. Weathering of enstatite to talc through a sequence of transitional phases. *Clays and Clay Minerals*. 30:11–20.

Farrokhpay, S. 2011. The significance of froth stability in mineral flotation - A review. *Advances in Colloid and Interface Science*. 166:1–7. DOI: 10.1016/j.cis.2011.03.001.

Farrokhpay, S. 2012. The importance of rheology in mineral flotation: A review. *Minerals Engineering*. 36–38:272–278. DOI: 10.1016/j.mineng.2012.05.009.

Farrokhpay, S. & Bradshaw, D. 2012. Effect of clay minerals on froth stability in mineral flotation: a review. In *XXVI International Mineral Processing Congress*. 04601–04611. DOI: 10.13140/2.1.2025.0567.

Farrokhpay, S. & Zanin, M. 2012. An investigation into the effect of water quality on froth stability. *Advanced Powder Technology*. 23(4):493–497. DOI: 10.1016/j.apt.2012.04.012.

Farrokhpay, S., Ndlovu, B. & Bradshaw, D. 2018. Behavior of talc and mica in copper ore flotation. *Applied Clay Science*. 160:270–275. DOI: 10.1016/j.clay.2018.02.011.

Fedorockova, A., Raschman, P., Sucik, G., Plesingerova, B., Popovic, L. & Briancin, J. 2015. Processing of serpentinite tailings to pure amorphous silica. *Ceramics - Silikaty*. 59:275–282.

Feng, D. & Aldrich, C. 2004. Effect of ultrasonication on the flotation of talc. *Industrial and Engineering Chemistry Research*. 43:4422–4427. DOI: 10.1021/ie034057g.

Feng, B., Lu, Y., Feng, Q. & Li, H. 2012. Solution Chemistry of Sodium Silicate and Implications for Pyrite Flotation. *Industrial and Engineering Chemistry Research*. 51:12089–12094. DOI: 10.1021/ie301307a.

Feng, B., Lu, Y., Feng, Q., Zhang, M. & Gu, Y. 2012. Talc-serpentine interactions and implications for talc depression. *Minerals Engineering*. 32:68–73. DOI: 10.1016/j.mineng.2012.03.004.

Feng, B., Feng, Q. & Lu, Y. 2012. A novel method to limit the detrimental effect of serpentine on the flotation of pentlandite. *International Journal of Mineral Processing*. 114:11–13. DOI: 10.1016/j.minpro.2012.08.001.

Feng, B., Lu, Y.P., Feng, Q.M., Ding, P. & Luo, N. 2013. Mechanisms of surface charge development of

serpentine mineral. *Transactions of Nonferrous Metals Society of China (English Edition)*. 23:1123–1128. DOI: 10.1016/S1003-6326(13)62574-1.

Feng, B., Lu, Y. & Luo, X. 2015. The effect of quartz on the flotation of pyrite depressed by serpentine. *jJournal of materials research and technology*. 138:1–6.

Feng, B., Zhang, W., Guo, Y., Wang, T., Luo, G., Wang, H. & He, G. 2019. The flotation separation of galena and pyrite using serpentine as depressant. *Powder Technology*. 342:486–490. DOI: 10.1016/j.powtec.2018.09.070.

Flynn, S.A. & Woodburn, E.T. 1987. A froth ultra-fine model for the selective separation of coal from mineral in a dispersed air flotation cell. *Powder Technology*. 49:127–142. DOI: 10.1016/0032-5910(87)80055-4.

Forbes, E., Davey, K.J. & Smith, L. 2014. Decoupling rehology and slime coatings effect on the natural flotability of chalcopyrite in a clay-rich flotation pulp. *Minerals Engineering*. 56:136–144. DOI: 10.1016/j.mineng.2013.11.012.

Fuerstenau, M.C., Gutierrez, G. & Elgillani, D.A. 1968. The Influence of Sodium Silicate in Nonmetallic Flotation Systems. *Society of Mining Engineers of AIME, Transactions*. 241:319–323.

Fuerstenau, M.C., Lopez-Valdivieso, A. & Fuerstenau, D.W. 1988. Role of Hydrolyzed Cations in the Natural Hydrophobicity of Talc. *International Journal of Mineral Processing*. 23:161–170.

Furlong, D.N., Sing, K.S.W. & Parfitt, G.D. 1979. The precipitation of silica on titanium dioxide surfaces. I. Preparation of coated surfaces and examination by electrophoresis. *Journal of Colloid And Interface Science*. 69:409–419. DOI: 10.1016/0021-9797(79)90130-9.

Gao, Y., Zhang, G., Wang, M. & Liu, D. 2018. The critical role of pulp density on flotation separation of nickel-copper sulfide from fine serpentine. *Minerals*. 8:1–10. DOI: 10.3390/min8080317.

Garrido, L., Gainza, J. & Pereira, E. 1988. Influence of sodium silicate on the rheological behaviour of clay suspensions-Application of the ternary Bingham model. *Applied Clay Science*. 3:323–335. DOI: 10.1016/0169-1317(88)90023-3.

Genovese, D.B. 2012. Shear rheology of hard-sphere, dispersed, and aggregated suspensions, and filler-matrix composites. *Advances in Colloid and Interface Science*. 171:1–16. DOI: 10.1016/j.cis.2011.12.005.

Gillery, F.H. 1959. The X-ray study of synthetic Mg-Al serpentines and chlorites. *American Mineralogist*. 44:143–152.

Godel, B., Barnes, S.J. & Maier, W.D. 2007. Platinum-group elements in sulphide minerals, platinum-group minerals, and whole-rocks of the Merensky Reef (Bushveld Complex, South Africa): Implications for the formation of the reef. *Journal of Petrology*. 48:1569–1604. DOI: 10.1093/petrology/egm030.

Goktepe, F. 2002. Effec of pH on pulp potential and sulphide mineral flotation. *Turkish J.Eng. Env. Sci.* 26:309–318.

Groppo, C., Rinaudo, C., Cairo, S., Gastaldi, D. & Compagnoni, R. 2006. Micro-Raman spectroscopy for a quick and reliable identification of serpentine minerals from ultramafics. *European Journal of Mineralogy*. 18:319–329. DOI: 10.1127/0935-1221/2006/0018-0319.

Hadler, K., Smith, C.D. & Cilliers, J.J. 2010. Recovery vs. mass pull: The link to air recovery. *Minerals Engineering*. 23:994–1002. DOI: 10.1016/j.mineng.2010.04.007.

Han, Y., Liu, W. & Chen, J. 2016. DFT simulation of the adsorption of sodium silicate species on kaolinite surfaces. *Applied Surface Science*. 370:403–409. DOI: 10.1016/j.apsusc.2016.02.179.

Hassanzadeh, A., Gholami, H., Özkan, S.G., Niedoba, T. & Surowiak, A. 2021. Effect of power ultrasound on wettability and collector-less floatability of chalcopyrite, pyrite and quartz. *Mineralogy and Petrology*. 11:1–16.

Hatton, C.J. & Schweitzer, J.K. 1995. Evidence for synchronous extrusive and intrusive Bushveld magmatism. *Journal of African Earth Sciences*. 21:579–594. DOI: 10.1016/0899-5362(95)00103-4.

Heiskanen, K., Kirjavainen, V. & Laapas, H. 1991. Possibilities of collectorless flotation in the treatment of pentlandite ores. *International Journal of Mineral Processing*. 33:263–274. DOI: 10.1016/0301-7516(91)90057-P.

Hirajima, T., Mori, M., Ichikawa, O., Sasaki, K., Miki, H., Farahat, M. & Sawada, M. 2014. Selective flotation of chalcopyrite and molybdenite with plasma pre-treatment. *Minerals Engineering*. 66:102–111. DOI: 10.1016/j.mineng.2014.07.011.

Hunter, R.J. 2001. Measuring zeta potential in concentrated industrial slurries. *Colloids and Surfaces A: Physicochemical and Engineering Aspects*. 195:205–214. DOI: 10.1016/S0927-7757(01)00844-5.

Irannajad, M., Ejtemaei, M. & Gharabaghi, M. 2009. The effect of reagents on selective flotation of smithsonite-calcite-quartz. *Minerals Engineering*. 22:766–771. DOI: 10.1016/j.mineng.2009.01.012.

Iyer, K., Austrheim, H., John, T. & Jamtveit, B. 2008. Serpentinization of the oceanic lithosphere and some geochemical consequences: Constraints from the Leka Ophiolite Complex, Norway. *Chemical Geology*. 249:66–90. DOI: 10.1016/j.chemgeo.2007.12.005.

Jasieniak, M. & Smart, R.S.C. 2009. Collectorless flotation of pyroxene in Merensky ore: Residual layer identification using statistical ToF-SIMS analysis. *International Journal of Mineral Processing*. 92:169–176. DOI: 10.1016/j.minpro.2009.04.002.

Johannes, W. 1968. Experimental investigation of the reaction forsterite + H2O ⇌ serpentine + brucite. *Contributions to Mineralogy and Petrology*. 19:309–315. DOI: 10.1007/BF00389413.

Johansson, G. & Pugh, R.J. 1992. The influence of particle size and hydrophobicity on the stability of mineralized froths. *International Journal of Mineral Processing*. 34:1–21. DOI: 10.1016/B978-0-444-88284-4.50011-1.

Johnson, S.B., Russell, A.S. & Scales, P.J. 1998. Volume fraction e ffects in shear rheology and electroacoustic studies of concentrated alumina and kaolin suspensions. *Colloids and Surfaces A: Physicochemical and Engineering Aspects*. 141:119–130.

Johnson, S.B., Franks, G. V., Scales, P.J. & Healy, T.W. 1999. The binding of monovalent electrolyte ions on α-alumina. II. The shear yield stress of concentrated suspensions. *Langmuir*. 15:2844–2853. DOI: 10.1021/la9808768.

Jorjani, E., Barkhordari, H.R., Tayebi Khorami, M. & Fazeli, A. 2011. Effects of aluminosilicate minerals on copper-molybdenum flotation from Sarcheshmeh porphyry ores. *Minerals Engineering*. 24:754–759. DOI: 10.1016/j.mineng.2011.01.005.

Jung, I.H., Decterov, S.A. & Pelton, A.D. 2006. Critical thermodynamic evaluation and optimization of the MnO-SiO2-"TiO2"-"Ti2O3" system. *Metallurgical and Materials Transactions*. 30:226–234. DOI: 10.1007/s11663-004-0082-9.

Kawatra, S.K. & Eisele, T.C. 1988. Rheological effects in grinding circuits. *International Journal of Mineral Processing*. 22:251–259. DOI: 10.1016/0301-7516(88)90067-1.

Khalili-Garakani, A.H., Mostoufi, N., Sadeghi, F., Hosseinzadeh, M., Fatourechi, H., Sarrafzadeh, M.H. & Mehrnia, M.R. 2011. Comparison between different models for rheological characterization of activated sludge. *Iranian Journal of Environmental Health Science and Engineering*. 8:255–264. DOI: 10.1515/jwld-2017-0053.

Khraisheh, M., Holland, C., Creany, C., Harris, P. & Parolis, L. 2005. Effect of molecular weight and concentration on the adsorption of CMC onto talc at different ionic strengths. 75:197–206. DOI: 10.1016/j.minpro.2004.08.012.

Kinloch, E.D. 1982. Regional trends in the platinum-group mineralogy of the critical zone of the Bushveld complex, South Africa. *Economic Geology*. 77:1328–1347. DOI: 10.2113/gsecongeo.77.6.1328.

Kinloch, E.D. & Peyerl, W. 1990. Platinum-group minerals in various rock types of the Merensky Reef: genetic implications. *Economic Geology*. 85:537–555. DOI: 10.2113/gsecongeo.85.3.537.

Kirjavainen, V.M. 1992. Mathematical model for the entrainment of hydrophilic particles in froth flotation. *International Journal of Mineral Processing*. 35:1–11. DOI: 10.1016/0301-7516(92)90002-E.

Kirjavainen, V. & Heiskanen, K. 2007. Some factors that affect beneficiation of sulphide nickel-copper ores. *Minerals Engineering*. 20:629–633. DOI: 10.1016/j.mineng.2007.01.001.

Kursun, I. 2010. Determination of flocculation and adsorption-desorption characteristics of Na-feldspar concentrate in the presence of different polymers. *Physicochemical Problems of Mineral Processing*. 44:127–142.

Laplante, A.R., Kaya, M. & Smith, H.W. 1989. The effect of froth on flotation kinetics a mass transfer approach. *Mineral Processing and Extractive Metallurgy Review*. 5:147–168. DOI: 10.1080/08827508908952648.

Laskowski, J.S., Liu, Q. & Connor, C.T.O. 2007. Current understanding of the mechanism of polysaccharide adsorption at the mineral / aqueous solution interface. 84:59–68. DOI: 10.1016/j.minpro.2007.03.006.

Lee, U.J., Hyeong, K.S. & Cho, H.Y. 2020. Estimation of Settling Velocity and Floc Distribution through Simple Particles Sedimentation Experiments. *Journal of Marine Science and Engineering*. 8:1–14. DOI: 10.3390/jmse8070500.

Van Leussen, W. & Cornelisse, J.M. 1993. The determination of the sizes and settling velocities of estuarine flocs by an underwater video system. *Netherlands Journal of Sea Research*. 31:231–241. DOI: 10.1016/0077-7579(93)90024-M.

Li, C., Ripley, E.M. & Merino, E. 2004. Replacement of Base Metal Sulphides by actinolite, epidote, calcite, and magnetite in the UG2 and Merensky Reef of the Bushveld Complex, South Africa. *Journal of the American College of Emergency Physicians*. 99:173–184. DOI: 10.1016/S0361-1124(78)80358-X.

Li, H., Zhou, Z.A., Xu, Z. & Masliyah, J.H. 2005. Role of acidified sodium silicate in low temperature bitumen extraction from poor-processing oil sand ores. *Industrial and Engineering Chemistry Research*. 44:4753–4761. DOI: 10.1021/ie048998k.

Li, W., Li, Y., Xiao, Q., Wei, Z. & Song, S. 2018. The influencing mechanisms of sodium hexametaphosphate on chalcopyrite flotation in the presence of MgCl2 and CaCl2. *Minerals*. 8:1–18. DOI: 10.3390/min8040150.

Li, X.P., Rahn, M. & Bucher, K. 2004. Serpentinites of the Zermatt-Saas ophiolite complex and their texture evolution. *Journal of Metamorphic Geology*. 22:159–177. DOI: 10.1111/j.1525-1314.2004.00503.x.

Li, Y., Li, W., Xiao, Q., He, N., Ren, Z., Lartey, C. & Gerson, A.R. 2017. The influence of common monovalent and divalent chlorides on chalcopyrite flotation. *Minerals*. 7:1–10. DOI: 10.3390/min7070111.

Li, Y., Zhu, H., Li, W. & Zhu, Y. 2019. A fundamental study of chalcopyrite flotation in sea water using sodium silicate. *Minerals Engineering*. 139:1–6. DOI: 10.1016/j.mineng.2019.105862.

Liang, L., Wang, L., Nguyen, A. V. & Xie, G. 2017. Heterocoagulation of alumina and quartz studied by zeta potential distribution and particle size distribution measurements. *Powder Technology*. 309:1–12. DOI: 10.1016/j.powtec.2016.12.054.

Lins, F.F. & Adamian, R. 1993. The influence of some physical variables on gold flotation. *Minerals*

Engineering. 6:267–277. DOI: 10.1016/0892-6875(93)90035-L.

Liu, D. & Peng, Y. 2014. Reducing the entrainment of clay minerals in flotation using tap and saline water. *Powder Technology*. 253:216–222. DOI: 10.1016/j.powtec.2013.11.019.

Liu, Q.I. & Laskowski, J.S. 1989. The interactions between Dextrin and metal hydroxides in aqueous solutions. *Journal of Colloid and Interface Science*. 130:101–111.

Liu, C., Zhang, W., Song, S. & Li, H. 2019. A novel method to improve carboxymethyl cellulose performance in the flotation of talc. *Minerals Engineering*. 131:23–27. DOI: 10.1016/j.mineng.2018.11.003.

Liu, D., Zhang, G., Chen, Y., Chen, W. & Gao, Y. 2018. A Novel Method to Limit the Adverse Effect of Fine Serpentine on the Flotation of Pyrite. *Minerals*. 8:1–11. DOI: 10.3390/min8120582.

Liu, R., Sun, W., Hu, Y. & Wang, D. 2010. Surface chemical study of the selective separation of chalcopyrite and marmatite. *Mining Science and Technology*. 20(4):542–545. DOI: 10.1016/S1674-5264(09)60240-4.

Liu, W., Zhang, S., Wang, W., Zhang, J., Yan, W., Deng, J. & Feng, Q. 2015. The effects of Ca (II) and Mg (II) ions on the flotation of spodumene using NaOL. *Minerals Engineering*. 79:40–46. DOI: 10.1016/j.mineng.2015.05.008.

Locmelis, M., Melcher, F. & Oberthür, T. 2010. Platinum-group element distribution in the oxidized Main Sulfide Zone, Great Dyke, Zimbabwe. *Mineralium Deposita*. 45:93–109. DOI: 10.1007/s00126-009-0258-y.

Long, T., Huang, X. & Xiao, W. 2019. The effect of surface charge on the separation of pyrite from serpentine by flotation. *Minerals*. 9:1–14. DOI: 10.3390/min9100629.

Lotter, N.O., Bradshaw, D.J., Becker, M., Parolis, L.A.S. & Kormos, L.J. 2008. A discussion of the occurrence and undesirable flotation behaviour of orthopyroxene and talc in the processing of mafic deposits. *Minerals Engineering*. 21:908–912. DOI: 10.1016/j.mineng.2008.02.023.

Lu, J., Sun, M., Yuan, Z., Qi, S., Tong, Z., Li, L. & Meng, Q. 2019. Innovative insight for sodium hexametaphosphate interaction with serpentine. *Colloids and Surfaces A: Physicochemical and Engineering Aspects*. 560:35–41. DOI: 10.1016/j.colsurfa.2018.09.076.

Luckham, P.F. & Rossi, S. 1999. The colloidal and rheological properties of bentonite suspensions. *Advances in Colloid and Interface Science*. 82:43–92.

Luo, X., Feng, B., Wong, C., Miao, J., Ma, B. & Zhou, H. 2016. The critical importance of pulp concentration on the flotation of galena from a low grade lead-zinc ore. *Journal of Materials Research and Technology*. 5:131–135. DOI: 10.1016/j.jmrt.2015.10.002.

Ma, M. 2011a. The dispersive effect of sodium silicate on kaolinite particles in process water: Implications for iron-ore processing. *Clays and Clay Minerals*. 59:233–239. DOI: 10.1346/CCMN.2011.0590302.

Ma, M. 2011b. The dispersive effect of sodium silicate on kaolinite particles in process water: Implications for iron-ore processing. *Clays and Clay Minerals*. 59(3):233–239. DOI: 10.1346/CCMN.2011.0590302.

Maachar, A. & Dobby, G.S. 1992. Measurement of feed water recovery and entrainment solids recovery in flotation columns. *Canadian Metallurgical Quarterly*. 31:167–172.

Magudu, A. & Wali, A. 2019. Effects of dispersants on downstream processing in a PGM Plant. Fourth year project. University of Cape Town.

Mälhammar, G. 1990. Determination of some surface properties of talc. *Colloids and Surfaces*. 44:61–69. DOI: 10.1016/0166-6622(90)80187-9.

Manono, M.S., Corin, K.C. & Wiese, J.G. 2012. An investigation into the effect of various ions and their ionic strength on the flotation performance of a platinum bearing ore from the Merensky reef. *Minerals Engineering*. 36–38:231–236. DOI: 10.1016/j.mineng.2012.03.035.

Manono, M.S., Corin, K.C. & Wiese, J.G. 2019. Inorganic Electrolytes on the Efficacy of a Carboxymethyl Cellulose as a Coagulant for Talc: Implications for Talc Depression in Flotation. In *International Mine Water Association*. 217–224. Available: http://www.mwen.info/docs/imwa_2019/IMWA2019_Manono_217.pdf.

Manono, M.S., Corin, K.C. & Wiese, J.G. 2020. The Behavior of Gangue During the Flotation of a Sulfidic PGM-Bearing Ore in Response to Various Monovalent and Divalent Ions in Process Water. *Frontiers in Chemistry*. 8:1–12. DOI: 10.3389/fchem.2020.00079.

Martinez, E. & Zucker, G.L. 1960. Asbestos ore body minerals studied by zeta potential measurements. *Journal of Physical Chemistry*. 64:924–926. DOI: 10.1021/j100836a028.

Martinovic, J., Bradshaw, D.J. & Harris, P.J. 2005. Investigation of surface properties of gangue minerals in platinum bearing ores. *Journal of The South African Institute of Mining and Metallurgy*. 105:349–356.

Mason, T.J. 2003. High powered ultrasound in physical and chemical processing. *Selected topics of the new acoustics*. 95–136.

McCollom, T.M. & Bach, W. 2009. Thermodynamic constraints on hydrogen generation during serpentinization of ultramafic rocks. *Geochimica et Cosmochimica Acta*. 73:856–875. DOI: 10.1016/j.gca.2008.10.032.

McFadzean, B., Dicks, P., Groenmeyer, G., Harris, P. & O'Connor, C. 2011. The effect of molecular weight on the adsorption and efficacy of polysaccharide depressants. *Minerals Engineering*. 24:463–469. DOI: 10.1016/j.mineng.2010.12.015.

Mehrotra, S.P. & Kapur, P.C. 1974. The effects of aeration rate, particle size and pulp density on the flotation rate distributions. 9:213–219.

Mellini, M. 1982. The crystal structure of lizardite 1T: hydrogen bonds and polytypism. *American*

Mineralogist. 67:587–598.

Mével, C. 2003. Serpentinization of abyssal peridotites at mid-ocean ridges. *Geoscience*. 335:825–852. DOI: 10.1016/j.crte.2003.08.006.

Mhonde, N., Smart, M., Corin, K. & Schreithofer, N. 2020. Investigating the electrochemical interaction of a thiol collector with chalcopyrite and galena in the presence of a mixed microbial community. *Minerals*. 10:1–16. DOI: 10.3390/min10060553.

Miller, J.D., Li, J., Davidtz, J.C. & Vos, F. 2005. A review of pyrrhotite flotation chemistry in the processing of PGM ores. *Minerals Engineering*. 18:855–865. DOI: 10.1016/j.mineng.2005.02.011.

Misra, M., Raichur, A.M. & Lan, A.P. 2003. Improved flotation of arsenopyrite by ultrasonic pretreatment. *Minerals and Metallurgical Processing*. 20:93–96. DOI: 10.1007/bf03403138.

Mitchell, A.A., Scoon, R.N. & Sharpe, M.R. 2019. The upper critical zone in the swartklip sector, north-western Bushveld complex, on the farm wilgerspruit 2JQ: II. origin by intrusion of ultramafic sills with concomitant partial melting of host norite-anorthosite cumulates. *South African Journal of Geology*. 122:143–162. DOI: 10.25131/sajg.122.0011.

Mitchell, A.A., Henckel, J. & Mason-Apps, A. 2019. The upper critical zone of the Rustenburg layered suite in the swartklip sector, North-Western Bushveld complex, on the farm wilgerspruit 2JQ: I. stratigraphy and PGE mineralization patterns. *South African Journal of Geology*. 122:117–142. DOI: 10.25131/sajg.122.0010.

Molifie, A. 2016. Mineralogical and textural characterization of UG2 chromitite and Pseudo reef ore with implications for mineral beneficiation. BSc(Hons) Thesis. Stellenbosch University.

Moore, I.P.T., Cossor, G. & Baker, M.R. 1995. Velocity distributions in a stirred tank containing a yield stress fluid. *Chemical Engineering Science*. 50:2467–2481. DOI: 10.1016/0009-2509(95)00086-K.

Morris, G.E., Skinner, W.A., Self, P.G. & Smart, R.S.C. 1999. Surface chemistry and rheological behaviour of titania pigment suspensions. *Colloids and Surfaces A: Physicochemical and Engineering Aspects*. 155:27–41. DOI: 10.1016/S0927-7757(98)00631-1.

Morris, G.E., Fornasiero, D. & Ralston, J. 2002. Polymer depressants at the talc – water interface : adsorption isotherm, microflotation and electrokinetic studies. *International Journal of Mineral Processing*. 67:211–227.

Mueller, S., Llewellin, E.W. & Mader, H.M. 2010. The rheology of suspensions of solid particles. *Proceedings of the Royal Society*. 466:1201–1228. DOI: 10.1007/BF01432034.

Mustafa, S., Hamid, A., Naeem, A. & Sultana, Q. 2004. Effect of pH, temperature and time on the stability of potassium ethyl xanthate. *Journal of the Chemical Society of Pakistan*. 26:363–366.

Muzenda, E., Afolabi, A.S., Abdulkareem, A.S. & Ntuli, F. 2011. Effect of pH on the recovery and grade of base metal sulphides (PGMs) by flotation. In *Proceedings of the World Congress on Engineering and Computer Science*. V. 2. 1–4. DOI: 10.1007/978-94-007-4786-9_19.

Ndlovu, B. 2013. The Effect of Phyllosilicate Mineralogy and Surface Charge on the Rheology of Mineral Slurries. PhD Thesis. University of Cape Town.

Ndlovu, B., Becker, M., Forbes, E., Deglon, D. & Franzidis, J.P. 2011. The influence of phyllosilicate mineralogy on the rheology of mineral slurries. *Minerals Engineering*. 24:1314–1322. DOI: 10.1016/j.mineng.2011.05.008.

Ndlovu, B., Forbes, E., Farrokhpay, S., Becker, M., Bradshaw, D. & Deglon, D. 2014. A preliminary rheological classification of phyllosilicate group minerals. *Minerals Engineering*. 55:383–389. DOI: 10.1016/j.mineng.2013.06.004.

Neethling, S.J. & Cilliers, J.J. 2002. The entrainment of gangue into a flotation froth. *International Journal of Mineral Processing*. 64:123–134. DOI: 10.1016/S0301-7516(01)00067-9.

Ningthoujam, P.S., Dubey, C.S., Guillot, S., Fagion, A.S. & Shukla, D.P. 2012. Origin and serpentinization of ultramafic rocks of Manipur Ophiolite Complex in the Indo-Myanmar subduction zone, Northeast India. *Journal of Asian Earth Sciences*. 50:128–140. DOI: 10.1016/j.jseaes.2012.01.004.

O'Connor, C.T., Wiese, J.G., Corin, K.C. & McFadzean, B. 2018. On the management of gangue minerals in the flotation of platinum group minerals. *Mining, Metallurgy and Exploration*. 36:1–8.

Oats, W.J., Ozdemir, O. & Nguyen, A. V. 2010. Effect of mechanical and chemical clay removals by hydrocyclone and dispersants on coal flotation. *Minerals Engineering*. 23:413–419. DOI: 10.1016/j.mineng.2009.12.002.

Oberthür, T., Melcher, F., Buchholz, P. & Locmelis, M. 2013. The oxidized ores of the Main Sulphide Zone, Great Dyke, Zimbabwe: turning resources into minable reserved - mineralogy is the key. *The Journal of the Southern African Institute of Mining and Metallurgy*. 113:191–201.

October, L.L., Corin, K.C., Manono, M.S., Schreithofer, N. & Wiese, J.G. 2019. Considering the Ionic Strength and pH of Process Water on Bubble-Particle Attachment of Sulfide Minerals : Implications for Froth Flotation in Saline Water. In *International Mine Water Association*. 437–444.

Olhero, S.M. & Ferreira, J.M.F. 2004. Influence of particle size distribution on rheology and particle packing of silica-based suspensions. *Powder Technology*. 139:69–75. DOI: 10.1016/j.powtec.2003.10.004.

Oliveira, H., Azevedo, A. & Rubio, J. 2018. Nanobubbles generation in a high-rate hydrodynamic cavitation tube. *Minerals Engineering*. 116:32–34. DOI: 10.1016/j.mineng.2017.10.020.

Osbahr, I., Klemd, R., Oberthür, T., Brätz, H. & Schouwstra, R. 2013. Platinum-group element

distribution in base-metal sulfides of the Merensky Reef from the eastern and western Bushveld Complex, South Africa. *Mineralium Deposita*. DOI: 10.1007/s00126-012-0413-8.

Osbahr, I., Oberthür, T., Klemd, R. & Josties, A. 2014. Platinum-group element distribution in base-metal sulfides of the UG2 chromitite, Bushveld Complex, South Africa—a reconnaissance study.

Park, C.. & Jeon, H.. 2010. The effect of sodium silicate as pH modifier and depressant in the froth flotation of molybdenite ores. *Materials Transactions*. 51:1367–1369. DOI: 10.2320/matertrans.M2009397.

Parolis, L., Groenmeyer, G. & Harris, P. 2005. Equilibrium adsorption studies of polysaccharides on talc: The effect of molecular weight, charge, and the influence of metal cations. *Minerals and Metallurgical Processing*. 22:12–16.

Parolis, L.A.S., van der Merwe, R., Groenmeyer, G. V. & Harris, P.J. 2008. The influence of metal cations on the behaviour of carboxymethyl celluloses as talc depressants. *Colloids and Surfaces A: Physicochemical and Engineering Aspects*. 317:109–115. DOI: 10.1016/j.colsurfa.2007.10.001.

Patra, P., Bhambhani, T., Nagaraj, D.R. & Somasundaran, P. 2012. Colloids and Surfaces A : Physicochemical and Engineering Aspects Impact of pulp rheological behavior on selective separation of Ni minerals from fibrous serpentine ores. *Colloids and Surfaces A: Physicochemical and Engineering Aspects*. 411:24–26. DOI: 10.1016/j.colsurfa.2012.06.037.

Penberthy, C.J. & Merkle, R.K.W. 1999. Lateral variations in the platinum-group element content and mineralogy of the UG2 Chromitite Layer, Bushveld Complex. *South African Journal of Geology*. 102:240–250.

Penberthy, C.J., Oosthuyzen, E.J. & Merkle, R.K.W. 2000. The recovery of platinum-group elements from the UG-2 chromitite, Bushveld Complex - a mineralogical perspective. *Mineralogy and Petrology*. 68:213–222. DOI: 10.1007/s007100050010.

Peng, Y. & Bradshaw, D. 2012. Mechanisms for the improved flotation of ultrafine pentlandite and its separation from lizardite in saline water. *Minerals Engineering*. 36:284–290. DOI: 10.1016/j.mineng.2012.05.015.

Peng, H., Wu, D. & Abdelmonem, M. 2017. Flotation performances and surface properties of chalcopyrite with xanthate collector added before and after grinding. *Results in Physics*. 7:3567–3573. DOI: 10.1016/j.rinp.2017.09.028.

Petriglieri, J.R., Salvioli-Mariani, E., Mantovani, L., Tribaudino, M., Lottici, P.P., Laporte-Magoni, C. & Bersani, D. 2015. Micro-Raman mapping of the polymorphs of serpentine. *Journal of Raman Spectroscopy*. 46:953–958. DOI: 10.1002/jrs.4695.

Petrus, H.T.B.M., Hirajima, T., Sasaki, K. & Okamoto, H. 2012. Effects of sodium thiosulphate on chalcopyrite and tennantite: An insight for alternative separation technique. *International Journal of Mineral*

Processing. 102:116–123. DOI: 10.1016/j.minpro.2011.11.002.

Phair, J.W., Van Deventer, J.S.J. & Smith, J.D. 2001. Interaction of sodium silicate with zirconia and its consequences for polysialation. *Colloids and Surfaces A: Physicochemical and Engineering Aspects*. 182:143–159. DOI: 10.1016/S0927-7757(00)00737-8.

Pietrobon, M.C., Grano, S.R., Sobieraj, S. & Ralston, J. 1997. Recovery mechanisms for pentlandite and MgO-bearing gangue minerals in nickel ores from Western Australia. *Minerals Engineering*. 10:775–786. DOI: 10.1016/s0892-6875(97)00056-3.

Polovina, J.S., Hudson, D.M. & Jones, R.E. 2004. Petrographic and geochemical characteristics of postmagmatic hydrothermal alteration and mineralization in the J-M reef, Stillwater Complex, Montana. *Canadian Mineralogist*. 42:261–277. DOI: 10.2113/gscanmin.42.2.261.

Ramirez, A., Rojas, A., Gutierrez, L. & Laskowski, J.S. 2018. Sodium hexametaphosphate and sodium silicate as dispersants to reduce the negative effect of kaolinite on the flotation of chalcopyrite in seawater. *Minerals Engineering*. 125:10–14. DOI: 10.1016/j.mineng.2018.05.008.

Ramlall, N. V. & Loveday, B.K. 2015. A comparison of models for the recovery of minerals in a UG2 platinum ore by batch flotation. *Journal of the Southern African Institute of Mining and Metallurgy*. 115:221–228. DOI: 10.17159/2411-9717/2015/v115n3a7.

Rand, B. & Melton, I.E. 1977. Particle Interactions in Aqueous Kaolinite Suspensions. *Journal of Colloid and Interface Science*. 60:308–320.

Rao, D.S., VijayaKumar, T.V., Rao, S.S., Prabhakar, S. & Raju, G.B. 2011. Effectiveness of sodium silicate as gangue depressants in iron ore slimes flotation. *International Journal of Minerals, Metallurgy and Materials*. 18:515–522. DOI: 10.1007/s12613-011-0471-4.

Reinen, L.A., Weeks, J.D. & Tullis, T.E. 1994. The frictional behavior of lizardite and antigorite serpentinites: Experiments, constitutive models, and implications for natural faults. *Pure and Applied Geophysics*. 143:317–358. DOI: 10.1007/BF00874334.

Rose, D., Viljoen, F., Knoper, M. & Rajesh, H. 2011. Detailed assessment of platinum-group minerals associated with chromitite stringers in the merensky reef of the eastern bushveld complex, South Africa. *Canadian Mineralogist*. 49:1385–1396. DOI: 10.3749/canmin.49.6.1385.

Ross, V., Singh, A. & Pillay, K. 2019. Improved flotation of PGM tailings with a high-shear hydrodynamic cavitation device. *Minerals Engineering*. 137:133–139. DOI: 10.1016/j.mineng.2019.04.005.

Rouméjon, S., Cannat, M., Agrinier, P., Godard, M. & Andreani, M. 2014. Serpentinization and fluid pathways in tectonically exhumed peridotites from the southwest Indian ridge (62-65°E). *Journal of Petrology*. 56:703–734. DOI: 10.1093/petrology/egv014.

Sarghini, D. 1966. Flotation kinetics and residence time studes on coal flotation. University of New South Wales. DOI: 10.5694/j.1326-5377.1966.tb73588.x.

Savassi, O.N., Alexander, D.J., Franzidis, J.P. & Manlapig, E. V. 1998. An empirical model for entrainment in industrial flotation plants. *Minerals Engineering*. 11:243–256. DOI: 10.1016/S0892-6875(98)00003-X.

Schouwstra, R.P., Kinloch, E.D. & Lee, C.A. 2000. A short geological review of the Bushveld Complex. *Platinum Metals Review*. 44:33–39.

Schreithofer, N., Wiese, J., McFadzean, B., Harris, P., Heiskanen, K. & OConnor, C. 2011. Frother-depressant interactions in two and three phase systems. *International Journal of Mineral Processing*. 100:33–40. DOI: 10.1016/j.minpro.2011.04.008.

Schubert, H. 1999. On the turbulence-controlled microprocesses in flotation machines. *International Journal of Mineral Processing*. 56:257–276. DOI: 10.1016/S0301-7516(98)00048-9.

Schwartz, S., Guillot, S., Reynard, B., Lafay, R., Debret, B., Nicollet, C., Lanari, P. & Auzende, A.L. 2013. Pressure-temperature estimates of the lizardite/antigorite transition in high pressure serpentinites. *Lithos*. 178:197–210. DOI: 10.1016/j.lithos.2012.11.023.

Schwarz, S. & Grano, S. 2005. Effect of particle hydrophobicity on particle and water transport across a flotation froth. *Colloids and Surfaces A: Physicochemical and Engineering Aspects*. 256:157–164. DOI: 10.1016/j.colsurfa.2005.01.010.

Schwellnus, J.S.I., Hiemstra, S.A. & Gasparrini, E. 1976. The Merensky Reef at the Atok platinum mine and its environs. *Economic Geology*. 71(1):249–260. DOI: 10.2113/gsecongeo.71.1.249.

Scoon, R.N. 1987. Metasomatism of cumulus magnesian olivine by iron-rich postcumulus liquids in the upper Critical Zone of the Bushveld Complex. *Mineralogical Magazine*. 51:389–396. DOI: 10.1180/minmag.1987.051.361.05.

Scoon, R.N. & De Klerk, W.J. 1987. The Relationship of Olivine Cumulates and Mineralization To Cyclic Units in Part of the Upper Critical Zone of the Western Bushveld Complex. *Conadion Mineralogist*. 25:51–77.

Scoon, R.N. & Teigler, B. 1994. Platinum-group element mineralization in the critical zone of the western Bushveld Complex: I. Sulfide poor-chromitites below the UG-2. *Economic Geology*. 89:1094–1121. DOI: 10.2113/gsecongeo.89.5.1094.

Sefako, R., Sekgarametso, K. & Sibanda, V. 2017. Potential Processing Routes for Recovery of Platinum Group Metals from Southern African Oxidized PGM Ores: A Review. *Journal of Sustainable Metallurgy*. 3:797–807. DOI: 10.1007/s40831-017-0146-0.

Shabalala, N.Z.P., Harris, M., Leal Filho, L.S. & Deglon, D.A. 2011. Effect of slurry rheology on gas dispersion in a pilot-scale mechanical flotation cell. *Minerals Engineering*. 24:1448–1453. DOI: 10.1016/j.mineng.2011.07.004.

Shackleton, N.J. 2007. Surface characterisation and flotation behaviour of the platinum and palladium arsenide, telluride and sulphide mineral species. University of Cape Town.

Shackleton, N.J., Malysiak, V. & O'Connor, C.T. 2007a. Surface characteristics and flotation behaviour of platinum and palladium arsenides. *International Journal of Mineral Processing*. 85:25–40. DOI: 10.1016/j.minpro.2007.08.002.

Shackleton, N.J., Malysiak, V. & O'Connor, C.T. 2007b. Surface characteristics and flotation behaviour of platinum and palladium tellurides. *Minerals Engineering*. 20:1232–1245. DOI: 10.1016/j.mineng.2007.05.004.

Shamaila, S. & Connor, C.T.O. 2008. The role of synthetic minerals in determining the relative flotation behaviour of Platreef PGE tellurides and arsenides. *Minerals Engineering*. 21:899–904. DOI: 10.1016/j.mineng.2008.07.006.

Sheni, N., Corin, K. & Wiese, J. 2018. Considering the effect of pulp chemistry during flotation on froth stability. *Minerals Engineering*. 116:15–23. DOI: 10.1016/j.mineng.2017.11.002.

Shortridge, P.G., Harris, P.J., Bradshaw, D.J. & Koopal, L.K. 2000. The effect of chemical composition and molecular weight of polysaccharide depressants on the flotation of talc. *International Journal of Mineral Processing*. 59:215–224. DOI: 10.1016/S0301-7516(99)00077-0.

Silva, J.P.P., Baltar, C.A.M., Gonzaga, R.S.G., Peres, A.E.C. & Leite, J.Y.P. 2012. Identification of sodium silicate species used as flotation depressants. *Minerals and Metallurgical Processing*. 29:207–210. DOI: 10.1007/bf03402458.

Smith, P.G. & Warren, L.J. 1989. Entrainment of Particles into Flotation Froths. *Mineral Processing and Extractive Metallurgy Review*. 5:123–145. DOI: 10.1080/08827508908952647.

Solomon, N., Becker, M., Mainza, A., Petersen, J. & Franzidis, J.P. 2011a. Understanding the influence of HPGR on PGM flotation behavior using mineralogy. In *Minerals Engineering*. DOI: 10.1016/j.mineng.2011.07.015.

Solomon, N., Becker, M., Mainza, A., Petersen, J. & Franzidis, J.P. 2011b. Understanding the influence of HPGR on PGM flotation behavior using mineralogy. *Minerals Engineering*. 24:1370–1377. DOI: 10.1016/j.mineng.2011.07.015.

Song, S., Lopez-Valdivieso, A., Martinez-Martinez, C. & Torres-Armenta, R. 2006. Improving fluorite flotation from ores by dispersion processing. *Minerals Engineering*. 19:912–917. DOI: 10.1016/j.mineng.2005.10.005.

Steenberg, E. & Harris, P.J. 1984. Adsorption of carboxymethylcellulose, guar gum, and starch onto talc, sulphides, oxides, and salt-type minerals. *South African Journal of Chemical Engineering*. 37:85–90.

Suyantara, G.P.W., Hirajima, T., Miki, H. & Sasaki, K. 2018. Floatability of molybdenite and chalcopyrite in artificial seawater. *Minerals Engineering*. 115:117–130. DOI: 10.1016/j.mineng.2017.10.004.

Tabatabaei, R.H., Nagaraj, D.R., Vianna, S.M.S.M., Napier-Munn, T.J. & Gorain, B. 2014. The effect of non-sulphide gangue minerals on the flotation of sulphide minerals from Carlin-type gold ores. *Minerals Engineering*. 60:26–32. DOI: 10.1016/j.mineng.2014.02.004.

Tadie, M., Corin, K.C., Wiese, J.G., Nicol, M. & O'Connor, C.T. 2015. An investigation into the electrochemical interactions between platinum group minerals and sodium ethyl xanthate and sodium diethyl dithiophosphate collectors: Mixed potential study. *Minerals Engineering*. 83:44–52. DOI: 10.1016/j.mineng.2015.08.003.

Tang, F.Q., Xiao, Z., Tang, J.A. & Jiang, L. 1989. The effect of SiO2 particles upon stabilization of foam. *Journal of Colloid And Interface Science*. 131:498–502. DOI: 10.1016/0021-9797(89)90192-6.

Tangsathitkulchai, C. 2003. The effect of slurry rheology on fine grinding in a laboratory ball mill. *International Journal of Mineral Processing*. 69:29–47. DOI: 10.1016/S0301-7516(02)00061-3.

Tao, D., Luttrell, G.H. & Yoon, R.H. 2000. A parametric study of froth stability and its effect on column flotation of fine particles. *International Journal of Mineral Processing*. 59:25–43. DOI: 10.1016/S0301-7516(99)00033-2.

Tao, D., Chen, G.L., Zhou, X.H., Zhao, C., Fan, M.M., Aron, M. & Wright, J. 2007. Coal and potash flotation enhancement using a clay binder. *Canadian Metallurgical Quarterly*. 46(3):243–250. DOI: 10.1179/cmq.2007.46.3.243.

Tarling, M.S., Rooney, J.S., Viti, C., Smith, S.A.F. & Gordon, K.C. 2018. Distinguishing the Raman spectrum of polygonal serpentine. *Journal of Raman Spectroscopy*. 49:1978–1984. DOI: 10.1002/jrs.5475.

Tartaj, P., Cerpa, A., García-González, M.T. & Serna, C.J. 2000. Surface instability of serpentine in aqueous suspensions. *Journal of Colloid and Interface Science*. 231:176–181. DOI: 10.1006/jcis.2000.7109.

Tohry, A. & Dehghani, A. 2016. Effect of sodium silicate on the reverse anionic flotation of a siliceous-phosphorus iron ore. *Separation and Purification Technology*. 164:28–33. DOI: 10.1016/j.seppur.2016.03.012.

Vergouw, J.M., Difeo, A., Xu, Z. & Finch, J.A. 1998. An agglomeration study of sulphide minerals using zeta potential and settling rate. Part II: Sphalerite/pyrite and sphalerite/galena. *Minerals Engineering*. 11:605–614. DOI: 10.1016/s0892-6875(98)00045-4.

Vermaak, C.F. & Hendriks, L.P. 1976. A review of the mineralogy of the Merensky Reef, with specific reference to new data on the precious metal mineralogy. *Economic Geology*. 71:1244–1269. DOI:

10.2113/gsecongeo.71.7.1244.

Videla, A.R., Morales, R., Saint-Jean, T., Gaete, L., Vargas, Y. & Miller, J.D. 2016. Ultrasound treatment on tailings to enhance copper flotation recovery. *Minerals Engineering*. 99:89–95. DOI: 10.1016/j.mineng.2016.09.019.

Viring, R.G. & Cowell, M.W. 1999. The Merensky Reef on Northam Platinum Limited. *South African Journal of Geology*. 102:192–208.

Viti, C., Mellini, M. & Rumori, C. 2005. Exsolution and hydration of pyroxenes from partially serpentinized harzburgites. *Mineralogical Magazine*. 69:491–507. DOI: 10.1180/0026461056940265.

Viti, C., Collettini, C., Tesei, T., Tarling, M.S. & Smith, S.A.F. 2018. Deformation processes, textural evolution and weakening in retrograde serpentinites. *Minerals*. 8:1–20. DOI: 10.3390/min8060241.

Wang, B. & Peng, Y. 2013. The behaviour of mineral matter in fine coal flotation using saline water. *Fuel*. 109:309–315. DOI: 10.1016/j.fuel.2013.01.030.

Wang, L. & Li, C. 2020. A Brief Review of Pulp and Froth Rheology in Mineral Flotation. *Journal of Chemistry*. 2020:1–16. DOI: 10.1155/2020/3894542.

Wang, B., Peng, Y. & Vink, S. 2013. Diagnosis of the surface chemistry effects on fine coal flotation using saline water. *Energy and Fuels*. 27:4869–4874. DOI: 10.1021/ef400909r.

Wang, L., Peng, Y., Runge, K. & Bradshaw, D. 2015. A review of entrainment: Mechanisms, contributing factors and modelling in flotation. *Minerals Engineering*. 70:77–91. DOI: 10.1016/j.mineng.2014.09.003.

Wang, Y., Peng, Y., Nicholson, T. & Lauten, R.A. 2015. The different effects of bentonite and kaolin on copper flotation. *Applied Clay Science*. 114:48–52. DOI: 10.1016/j.clay.2015.05.008.

Warren, L.J. 1985. Determination of the contributions of true flotation and entrainment in batch flotation tests. *International Journal of Mineral Processing*. 14:33–44.

Wellham, E.J., Elber, L. & Yan, D.S. 1992. The role of carboxy methyl cellulose in the flotation of a nickel sulphide transition ore. *Minerals Engineering*. 5:381–395. DOI: 10.1016/0892-6875(92)90218-X.

Wenner, D.B. & Taylor, H.P. 1973. DOI: 10.2475/ajs.273.3.207.

Wiese, J.G. 2009. Investigating depressant behaviour in the flotation of selected Merensky Ores. MSc Thesis. University of Cape Town.

Wiese, J., Harris, P. & Bradshaw, D. 2005a. Investigation of the role and interactions of a dithiophosphate collector in the flotation of sulphides from the Merensky reef. *Minerals Engineering*. 18:791–800. DOI: 10.1016/j.mineng.2005.01.032.

Wiese, J., Harris, P. & Bradshaw, D. 2005b. The influence of the reagent suite on the flotation of ores

from the Merensky reef. *Minerals Engineering*. 18:189–198. DOI: 10.1016/j.mineng.2004.09.013.

Wiese, J.G., Harris, P.J. & Bradshaw, D.J. 2008. The use of very low molecular weight polysaccharides as depressants in PGM flotation. *Minerals Engineering*. 21:471–482. DOI: 10.1016/j.mineng.2008.02.013.

Wiese, J.G., Harris, P.J. & Bradshaw, D.J. 2010. The effect of increased frother dosage on froth stability at high depressant dosages. *Minerals Engineering*. 23:1010–1017. DOI: 10.1016/j.mineng.2010.04.011.

Wilkens, R.J., Miller, J.D., Plummer, J.R., Dietz, D.C. & Myers, K.J. 2005. New techniques for measuring and modeling cavern dimensions in a Bingham plastic fluid. *Chemical Engineering Science*. 60:5269–5275. DOI: 10.1016/j.ces.2005.04.058.

Wilson, A.H., Lee, C.A. & Brown, R.T. 1999. Geochemistry of the Merensky reef, Rustenburg section, Bushveld complex: Controls on the silicate framework and distribution of trace elements. *Mineralium Deposita*. 34:657–672. DOI: 10.1007/s001260050226.

Witney, J.Y. & Yan, D.S. 1997. Reduction of magnesia in nickel concentrates by modification of th froth zone in column flotation. *Minerals Engineering*. 10:139–154.

Xia, L., Hart, B., Sidorkiewicz, V. & Shaw, D. 2018. The role of soluble sodium silicate for enhancing flotation selectivity of sulphides towards grade and recovery improvements: example from a Cu-sulphide ore. In *Extraction*. Springer International Publishing. 2901–2913. DOI: 10.1007/978-3-319-95022-8.

Xu, Z., Liu, J., Choung, J.W. & Zhou, Z. 2003. Electrokinetic study of clay interactions with coal in flotation. *International Journal of Mineral Processing*. 68:183–196. DOI: 10.1016/S0301-7516(02)00043-1.

Yang, S., Xie, B., Lu, Y. & Li, C. 2018. Role of magnesium-bearing silicates in the flotation of pyrite in the presence of serpentine slimes. *Powder Technology*. 332:1–7. DOI: 10.1016/j.powtec.2018.03.049.

Yang, S., Xu, Y., Liu, C., Ai, G., Huang, L. & Yu, H. 2020. A novel method to achieve the flotation of pyrite from lizardite slime without collector or depressant. *Minerals Engineering*. 157:1–3. DOI: 10.1016/j.mineng.2020.106580.

Yang, X., Roonasi, P. & Holmgren, A. 2008. A study of sodium silicate in aqueous solution and sorbed by synthetic magnetite using in situ ATR-FTIR spectroscopy. *Journal of Colloid and Interface Science*. 328:41–47. DOI: 10.1016/j.jcis.2008.08.061.

Yao, J., Yang, Q., Mao, W., Zhao, Y. & Xu, X. 2016. Precipitation trend-Elevation relationship in arid regions of the China. *Global and Planetary Change*. 143:1–9. DOI: 10.1016/j.gloplacha.2016.05.007.

Ye, H. & Matsuoka, I. 1993. Reverse flotation of fine quartz from dickite with oleate. *International Journal of Mineral Processing*. 40:123–136. DOI: 10.1016/0301-7516(93)90045-C.

Yu, Y., Ma, L., Cao, M. & Liu, Q. 2017. Slime coatings in froth flotation: A review. *Minerals Engineering*. 114:26–36. DOI: 10.1016/j.mineng.2017.09.002.

Yu, Y., Cheng, G., Ma, L., Huang, G., Wu, L. & Xu, H. 2017. Effect of agitation on the interaction of coal and kaolinite in flotation. *Powder Technology*. 313:122–128. DOI: 10.1016/j.powtec.2017.03.002.

Zeng, G., Ou, L., Zhang, W. & Zhu, Y. 2020. Effects of Sodium Alginate on the Flotation Separation of Molybdenite From Chalcopyrite Using Kerosene as Collector. *Frontiers in Chemistry*. 8:1–9. DOI: 10.3389/fchem.2020.00242.

Zhang, M. & Peng, Y. 2015. Effect of clay minerals on pulp rheology and the flotation of copper and gold minerals. *Minerals Engineering*. 70:8–13. DOI: 10.1016/j.mineng.2014.08.014.

Zhang, G., Chen, W. & Liu, D. 2017. The Role of Water Glass in the Flotation Separation of Fine Fluorite from Fine Quartz. *Minerals*. 7:157–171. DOI: 10.3390/min7090157.

Zhou, X. & Feng, B. 2015. The effect of polyether on the separation of pentlandite and serpentine. *Journal of Materials Research and Technology*. 4:429–433. DOI: 10.1016/j.jmrt.2015.02.002.

Zhou, Z., Scales, P.J. & Boger, D. V. 2001. Chemical and physical control of the rheology of concentrated metal oxide suspensions. *Chemical Engineering Science*. 56:2901–2920. DOI: 10.1016/S0009-2509(00)00473-5.

Zingg, A.J. 1996. Recrystallization and the origin of layering in the Bushveld Complex. *Lithos*. 37:15–37. DOI: 10.1016/0024-4937(95)00013-5.

Appendix A

A.1. Batch flotation calculations

Table A.1: Sample densities by pycnometry as determined by a Micromeritics AccuPyc II 1340 Instrument.

	Density (g/ cm³)
PPM – Ore 1	2.940
PPM – Ore 2	2.993

The primary rougher pulp density at PPM was 1.3. This was provided by PPM.

Determining the mass of solids required for flotation experiments using the 8L cell

Based on the densities provided in Table A.1, the mass required for froth flotation using the 8L cell was calculated. The example below shows the mass required for Ore 1:

$$\textbf{Pulp mass} = Pulp\ density \times Cell\ volume \qquad \textit{Equation A.1}$$

$$= 1.3\ \frac{g}{cm^3} \times 8000\ cm^3$$

$$= 10\,400\ g$$

$$\%\ \textbf{solids} = \frac{\frac{1}{\rho_{pulp}} - 1}{\frac{1}{\rho_{ore}} - 1} \times 100 \qquad \textit{Equation A.2}$$

$$= \frac{\frac{1}{1.3} - 1}{\frac{1}{2.9} - 1} \times 100$$

$$= 35.2\%$$

$$\textbf{Mass solids} = \%\ solids \times Pulp\ mass \qquad \textit{Equation A.3}$$

$$= 35.2\% \times 10\,400\ g$$

$$= 3660.8\ g$$

The – 3mm crushed Ore 1 material were representatively split into 3660.8 g bags, ready for the milling experiments. The required mass for Ore 2 milling for the 8L batch flotation experiments is 3598.4 g.

Calculating the volume of water required for milling experiments

Milling experiments were performed at 66% solids. The following calculations determined the amount of water needed for Ore 1 milling:

$$\textbf{Pulp mass} = \frac{Mass\ solids}{\%\ solids} \qquad \textit{Equation A.4}$$

$$= \frac{3660.8\ g}{0.66}$$

$$= 5507.9\ g$$

$$\textbf{Water mass} = Pulp\ mass - Mass\ solids \qquad \textit{Equation A.5}$$

$$= 5507.9\ g - 3660.8\ g$$

$$= 1847.1\ g$$

$$\textbf{Water volume} = 1847.1\ ml$$

The water volume added to the mill was 1847.1 ml. This was calculated to be 1853.1 ml for Ore 2 milling.

Calculating the volume of slurry which needed to be pumped from the flotation cell for solids concentration ***experiments***

The following calculations show the volume of slurry which needed to be pumped from the cell to obtain a 30 wt.% solids concentration. A solids concentration of 30 wt.% serves as an example. The volume of slurry which needed to be drained for the other solids concentrations are shown in **Table A.2**.

1. Calculating the solids concentration of the pulp at a 30 wt.% solids concentration:

$$\%\ \textbf{solids} = \frac{\frac{1}{\rho_{pulp}} - 1}{\frac{1}{\rho_{ore}} - 1} \times 100 \qquad \textit{Equation A.6}$$

$$0.30 = \frac{\frac{1}{\rho_{pulp}} - 1}{\frac{1}{2.9} - 1}$$

$$0.30 \times (-0.66) = \frac{1}{\rho_{pulp}} - 1$$

$$0.80 = \frac{1}{\rho_{pulp}}$$

$$\rho_{pulp} = 1.25$$

2. Calculating the pulp mass at a 30 wt.% solids concentration:

$$\textbf{Pulp mass} = Pulp\ density \times Cell\ volume \qquad \textit{Equation A.7}$$

$$= 1.25\ \frac{g}{cm^3} \times 8000\ cm^3$$

$$= 10\,000\ g$$

3. Calculating the mass of solids within the cell at a 30 wt.% solids concentration:

$$\textbf{Mass solids} = \%\ solids \times Pulp\ mass \qquad \textit{Equation A.8}$$

$$= 0.30 \times 10\,000\ g$$

$$= 3000\ g$$

4. Calculating the pulp mass at 35% solids concentration in a system containing 3000 g solids:

$$\textbf{Pulp mass} = \frac{Mass\ solids}{\%\ solids} \qquad \textit{Equation A.9}$$

$$= \frac{3000\ g}{0.35}$$

$$= 8571.43\ g$$

5. Calculating the pulp volume at a 35% solids concentration in a system where the pulp mass is 8571.43 g:

$$\textbf{Pulp volume} = \frac{Pulp\ mass}{Pulp\ density\ at\ 35\%\ solids} \qquad \textit{Equation A.10}$$

$$= \frac{8571.43\ g}{1.3\ \frac{g}{cm^3}}$$

$$= 8571.43\ cm^3$$

6. Calculating the volume of slurry which needed to be representatively drained and thereafter topped up with synthetic plant water to obtain 30 wt.% solids:

$$\textbf{Drainage volume} = Cell\ volume - Pulp\ volume \qquad \textit{Equation A.11}$$

$$= 8000\ cm^3 - 6593.41\ cm^3$$

$$= 1406.59\ cm^3/ml$$

Table A.2: Volumes of slurry which needed to be representatively drained before being topped with synthetic plant water to achieve the desired solids concentration.

solids concentration **(wt.%)**	**Drainage volume (ml)**
15	5072.85
25	2725.27
30	1406.59
35	None

Determination of mineral masses within the concentrates

This section shows how the mineral masses within the unsized first concentrate samples for the 215 g/t and 2000 g/t SS batch flotation experiments were determined. An example of how the quantity of talc in the 2000 g/t SS first concentrate is provided, and a summary table for other minerals within the 215 g/t and 2000 g/t SS first concentrates are provided in Table A.3. Masses of the first concentrates for the 215 g/t and 2000 g/t SS dosages were required for the calculations (Appendix B) as well as the talc proportions as determined by QEMSCAN (Appendix B).

$$\textbf{Talc mass} = 2000\frac{g}{t}\ first\ concentrate\ mass \times Talc\ proprtion\ \% \qquad \textit{Equation A.12}$$

$$= 72.56 \times 8.39\%$$

$$= 6.09\ g$$

Table A.3: Mineral masses within the 215 g/t and 2000 g/t SS batch flotation first concentrates.

Group minerals for results	Mineral	First concentrate masses (g)	
		215 g/t	2000 g/t
-	BMS	7.14	6.52
	Orthopyroxene	30.87	22.19
	Serpentine	29.21	14.70
	Talc	11.23	6.09
Other silicates	Olivine	2.64	1.65
	Clinopyroxene	5.84	4.45
	Amphibole	2.39	1.57
	Chlorite	4.63	3.15
	Plagioclase	9.40	5.77
	Mica	0.54	0.25
Fe-oxides	Chromite	3.86	1.82
	Magnetite	0.25	0.13
	Fe-To oxides/ hydroxides	1.51	0.79
Other	Other	1.03	0.72
	Total	110.55	69.80

Superficial gas velocity (J_g) calculations

The volume flow during 8L experiments is 11 L/min (183.3 $\frac{cm^3}{s}$).

$$\boldsymbol{J_g \text{ in the } 8L \text{ cell}} = \frac{Volume\ flow}{Cell\ cross\ sectional\ area} \qquad \textit{Equation A.13}$$

$$= \frac{183.3\ \frac{cm^3}{s}}{465.5\ cm^2}$$

$$= 0.4\ \frac{cm}{s}$$

$$\textbf{Volume flow in the 500 ml cell} = J_g \times Cell\ cross\ sectional\ area \qquad \textit{Equation A.14}$$

$$= 0.4\ \frac{cm}{s} \times 76\ cm^2$$

$$= 30.4\ \frac{cm^3}{s}\ (1.82 \frac{L}{min})$$

A.2. PGE distribution calculations

Calculating the PGE distribution within the feed

The PGE and Au grades within the Ore 1 and 2 feeds (by size for Ore 1) are shown in Table A.4.

Table A.4: Unsized and sized PGE grades within the Ore 1 feed.

	Ore 1 grade (g/t)				**Ore 2 grade (g/t)**
PGE (incl. Gold)	**Unsized**	**-10 µm**	**+10/-53 µm**	**+53 µm**	**Unsized**
Pt	1.21	1.00	1.01	0.62	0.30
Pd	0.43	0.66	0.60	0.27	0.15
Rh	0.043	0.054	0.072	0.017	0.048
Ru	0.091	0.14	0.13	0.058	0.054
Ir	0.021	0.028	0.028	0.020	0.055
Au	0.085	0.095	0.096	0.084	0.031
6E PGE	1.88	1.98	1.94	1.06	0.64

The ore was wet screened into various size fractions, dried, and thereafter weighed to determine the size distribution within the feed. These results were not presented within the main body of the thesis because the PSD of the feed was analyzed by the Malvern particle analyzer instead. These masses are very useful when calculating the PGE distribution within the feed and are therefore presented in Table A.5:

Table A.5: Sized mass distribution of the Ore 1 feed.

Size fraction (μm)	Ore mass (g)	Total mass (g)
-10	731.32	731.32
+10/-25	542.10	1063.51
+25/-38	183.11	
+38/-53	338.30	
+53/-75	454.36	1857.44
+75	1403.08	

PGE mass (g) in the – 10 μm size fraction:

The following steps shows how the PGE distribution within the sized samples were calculated. The 6E PGE is the sum of the individual PGE elements together with Au. This section required the grades provided in Table A.4, and the knowledge that a ton is equivalent to 907185 g. An example of the percentage of Pt within the -10 μm sized fraction is given below, and the results for the individual PGE percentages within the rest of the fractions are provided in the tables beneath each calculation step (Table A.6 to Table A.8).

1. Calculating the PGE percentage within the -10 μm size fraction.

$$\textbf{Percentage of Pt \% in the} - \textbf{10 μm size fraction} = \frac{1.00\ g}{907\,185\ g} \times 100$$

$$= 1.10 \times 10^{-4}\%$$

Table A.6: The percentage of PGEs within the Ore 1 sized feed.

	PGE percentage (%)		
PGE (incl. Au)	-10 μm	+10/-53 μm	+53 μm
Pt	1.10×10^{-4}	1.11×10^{-4}	6.83×10^{-5}
Pd	7.28×10^{-5}	6.61×10^{-5}	2.98×10^{-5}
Rh	5.95×10^{-6}	7.94×10^{-6}	1.87×10^{-6}
Ru	1.54×10^{-5}	1.43×10^{-5}	6.39×10^{-6}
Ir	3.09×10^{-6}	3.09×10^{-6}	2.20×10^{-6}
Au	1.05×10^{-5}	1.06×10^{-5}	9.26×10^{-6}
6E PGE	2.18×10^{-4}	2.14×10^{-4}	1.17×10^{-4}

2. Calculating the PGE mass within the -10 μm sized fraction given the mass of the ore within the -10 μm size fraction in Table A.5 and the Pt % in Table A.6.

$$\boldsymbol{Mass\ of\ Pt\ in-10\ \mu m\ fraction} = 1.10 \times 10^{-4}\% \times 731.31\ g$$
$$= 8.06 \times 10^{-4}\ g$$

Table A.7: The masses of PGEs within the Ore 1 sized feed.

	PGE mass (g)		
PGE (incl. Gold)	-10 μm	+10/-53 μm	+53 μm
Pt	8.06×10^{-4}	1.18×10^{-3}	1.27×10^{-3}
Pd	5.32×10^{-4}	7.03×10^{-4}	5.53×10^{-4}
Rh	4.35×10^{-5}	8.44×10^{-5}	3.48×10^{-5}
Ru	1.13×10^{-4}	1.52×10^{-4}	1.19×10^{-4}
Ir	2.26×10^{-5}	3.28×10^{-5}	4.09×10^{-5}
Au	7.66×10^{-5}	1.13×10^{-4}	1.72×10^{-4}
6E PGE	1.60×10^{-3}	2.27×10^{-3}	2.17×10^{-3}

3. Calculating the proportion of Pt in the -10 μm size fraction.

$$\boldsymbol{Total\ PGE\ mass} = (1.60 \times 10^{-3}\ g) + (2.27 \times 10^{-3}\ g) + (2.17 \times 10^{-3}\ g)$$
$$= 6.05 \times 10^{-3}\ g$$

$$\boldsymbol{Pt\ \%\ in\ the-10\ \mu m} = \frac{8.06 \times 10^{4}\ g}{6.05 \times 10^{-3}\ g} \times 100$$
$$= 13.32\%$$

Table A.8: Final proportions of PGEs, per size fraction, within the feed.

	PGE proportions within the ore (%)		
PGE (incl. Gold)	-10 μm	+10/-53 μm	+53 μm
Pt	13.32	19.56	20.98
Pd	8.79	11.62	9.13
Rh	0.72	1.39	0.58
Ru	1.86	2.52	1.96
Ir	0.37	0.54	0.68
Au	1.27	1.86	2.84
6E PGE	26.37	37.58	35.86

A.3. Rheology calculations

Volume percentage of the solids in the pulp

The following calculations determined the solids concentration, vol.%, in the pulp during 8L batch flotation experiments.

$$\boldsymbol{Solids\ volume} = \frac{Mass\ solids}{Ore\ density}$$

$$= \frac{3660.8\ g}{2.9\frac{g}{cm^3}}$$

$$= 1262.3\ cm^3$$

$$\boldsymbol{Solids\ volume\ percent} = \frac{Solids\ volume}{Cell\ volume}$$

$$= \frac{1262.3\ cm^3}{8000\ cm^3} \times 100$$

$$= 15.8\ vol.\%$$

Sample masses, water volumes and depressant volumes required for rheology experiments

Sample masses for rheology experiments were calculated using the densities in Table A.1 and the formulae shown below:

$$\boldsymbol{Rheometer\ pot\ volume} = 50\ ml$$

$$\boldsymbol{Volume\ of\ sample} = Volume\ \% \times Rheometer\ pot\ volume$$

$$\boldsymbol{Sample\ mass} = Sample\ volume \times Sample\ density$$

The following tables show the sample masses and water or reagent volumes required for the 1000 g/t SS (Table A.9) and 2000 g/t SS (Table A.10) rheology experiments. The volumes of water without depressant were used for experiments performed at 0 g/t.

Table A.9: Mass of ore samples, the volume of water and volume of 1000 g/t SS used for the rheology experiments.

% solids by volume	Sample volume (ml)	Sample mass (g)	Volume of water without SS (ml)	Mass of depressant (g)	Volume of depressant (ml)	Volume of water with SS (ml)
10	5.00	14.70	45.00	0.015	1.47	43.53
20	10.00	29.40	40.00	0.029	2.94	37.06
30	15.00	44.10	35.00	0.044	4.41	30.59
35	17.50	51.45	32.50	0.051	5.15	27.36
37.5	18.70	55.13	31.25	0.055	5.51	25.74
40	20.00	58.80	30.00	0.059	5.88	24.12

Table A.10: Mass of ore samples, the volume of water and volume of 2000 g/t SS used for the rheology experiments.

% solids by volume	Sample volume (ml)	Sample mass (g)	Volume of water without SS (ml)	Mass of depressant (g)	Volume of depressant (ml)	Volume of water with SS (ml)
10	5.00	14.70	45.00	0.029	2.94	42.06
20	10.00	29.40	40.00	0.059	5.88	34.12
30	15.00	44.10	35.00	0.088	8.82	26.18
35	17.50	51.45	32.50	0.10	10.29	22.21
37.5	18.75	55.13	31.25	0.11	11.03	20.23
40	20.00	58.80	30.00	0.012	11.76	18.24

A.4. Particle settling calculations

Calculating the particle settling velocities

In order to determine the particle settling velocities at the basline and SS particle settling experiments, the straight line formulae for the trendlines of the steepest slopes were determined. The trendline and formula for each test condition is illustrated in Figure A.1.

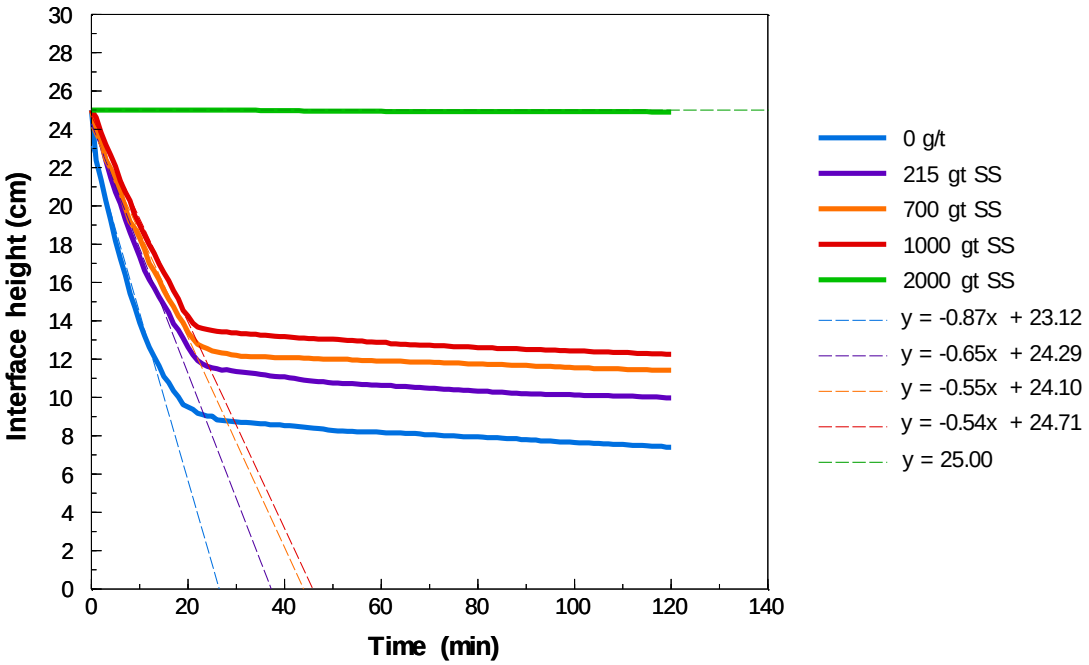

Figure A.1: Evolution of the suspension-liquid interface height over time at the baseline and various SS dosages which includes linear trendlines of the steepest slopes for the experiments.

The example shows how the particle settling velocity for the 215 g/t experiment have been calculated, and the results for the other experiments are summarized in tables beneath each calculation (Table A.11 and Table A.12).

1. Calulating the time where the trendline intersects the x-axis using the straight line formula (y = 0.65× + 24.29).

$$\boldsymbol{X - intercept\ (y = 0)} = \frac{24.29}{0.65}$$

$$= 37.4\ minutes$$

Table A.11: Calculated x-intercept for the particle settling data trendlines for the various SS particle settling experiments.

SS (g/t)	0	215	700	1000	2000
X-intercept (min)	26.57	37.37	43.82	45.76	-

2. Calculating the particle settling velocity:

$$\textbf{\textit{Particle settling velocity}}\ (\mathbf{215}\ {}^{\boldsymbol{g}}/_{\boldsymbol{t}}\ \boldsymbol{SS}) = \frac{y - intercept}{x - intercept}$$

$$= \frac{24.29}{37.37}$$

$$= 0.78 \text{ cm/min}$$

Table A.12: Particle settling velocities for the baseline and various SS conditions.

SS (g/t)	**Particle settling velocity (cm/min)**
0	0.87
215	0.78
700	0.55
1000	0.54
2000	0.00

Appendix B

B.1. Online files

The following files are available online at https://figshare.com/s/2359aa25f154029a1a5c.

1. **Photographs – Samples and Equipment –** A folder of photographs showing the equipment used during this work (flotation cells, froth column, particle settling, QEMSCAN, ultrasonication, zetasizer and rheometer) and the samples used for experiments (ore mining and the serpentine samples).
2. **Raw data – All experiments (excl. rheology) –** An excel workbook containing XRF, XRD, QEMSCAN, PSD, batch flotation, microflotation, particle settling, froth stability and zeta potential raw data.
3. **Raw data – Rheology –** An excel workbook containing all rheology raw data.